Science

In every successful paper you'll find a beginning, middle and

Pure protein is the challenge.
◗ PURE Expertise is the solution.

Imagine having the combined knowledge of hundreds of chromatography experts at your disposal. You'd be able to purify even the most challenging protein and gain the edge in your research. Well now you have it. PURE Expertise is the distillation of 50 years' chromatography experience – available online. Simply put, it's everything you need to gain the best results in protein purification.

Download our purification handbook at **www.gelifesciences.com/pure**

COVER

Depiction of four dinosaurs and dinosaur precursors from fossils found at the Hayden Quarry of northern New Mexico. The dinosaur precursors *Dromomeron romeri* (lower left) and a *Silesaurus*-like animal (bottom center) coexisted during the Late Triassic with the dinosaurs *Chindesaurus bryansmalli* (top center, with crocodylomorph in its mouth) and a coelophysoid theropod (upper right), indicating that the initial rise of dinosaurs was prolonged rather than sudden. See page 358.

Image: Donna Braginetz

DEPARTMENTS

EDITORIAL

NEWS OF THE WEEK

NEWS FOCUS

310

LETTERS

BOOKS *ET AL.*

329 & 376

POLICY FORUM

PERSPECTIVES

Science

SCIENCE EXPRESS

www.scienceexpress.org

345

REPORTS *CONTINUED...*

326
& 384

Wide bands make bad Möbius strips.

SCIENCE**NOW**

www.sciencenow.org DAILY NEWS COVERAGE

What Makes Us Human? Spite.
Chimps will punish one another, but not for the sake of being mean.

A New Twist on the Möbius Strip
Mathematicians can finally predict the shape of the weirdly one-sided object.

Fighting for Flamingos
Conservationists protest Tanzanian industrial plan they say threatens birds.

Dictyostelium on the move.

SCIENCE'S **STKE**

www.stke.org SIGNAL TRANSDUCTION KNOWLEDGE ENVIRONMENT

PERSPECTIVE: Keeping the (Kinase) Party Going— SLP-76 and ITK Dance to the Beat
Q. Qi and A. August
The adaptor protein SLP-76 serves as more than a neutral adaptor during T cell activation.

PERSPECTIVE: Chemotaxis—Navigating by Multiple Signaling Pathways
P. J. M. Van Haastert and D. M. Veltman
Multiple signaling pathways promote cell movement through a chemoattractive gradient.

How to search for an adviser.

SCIENCE **CAREERS**

www.sciencecareers.org CAREER RESOURCES FOR SCIENTISTS

US: To Choose an Adviser, Be an Armchair Anthropologist
S. Carpenter
To choose a research adviser, you'll need to ferret out some scientific and cultural details.

US: Tooling Up—Adding Charisma to Your Toolbox
D. Jensen
What is that ephemeral quality that makes some people stand out in a crowd?

EUROPE: Mastering Your Ph.D.—Playing Well With Other ... Personality Types
B. Noordam and P. Gosling
Acknowledging that other people operate differently than you will make lab life more productive.

US: From the Archives—Writing a Winning Cover Letter
J. Borchardt
Like any good sales pitch, your cover letter should motivate the customer to want to learn more.

Separate individual or institutional subscriptions to these products may be required for full-text access.

Olfactory Neuron Precursor Diversity >>

In the adult mouse, the brain provides a steady supply of newly generated olfactory neurons. These cells are generated in the subventricular zone and migrate to the olfactory bulb. **Merkle** *et al.* (p. 381, published online 5 July) now show that different regions of the subventricular zone give rise to different types of olfactory neurons. Thus, the stem cells of the subventricular zone are not so much individually versatile and are better characterized as a starting point of an already diverse population.
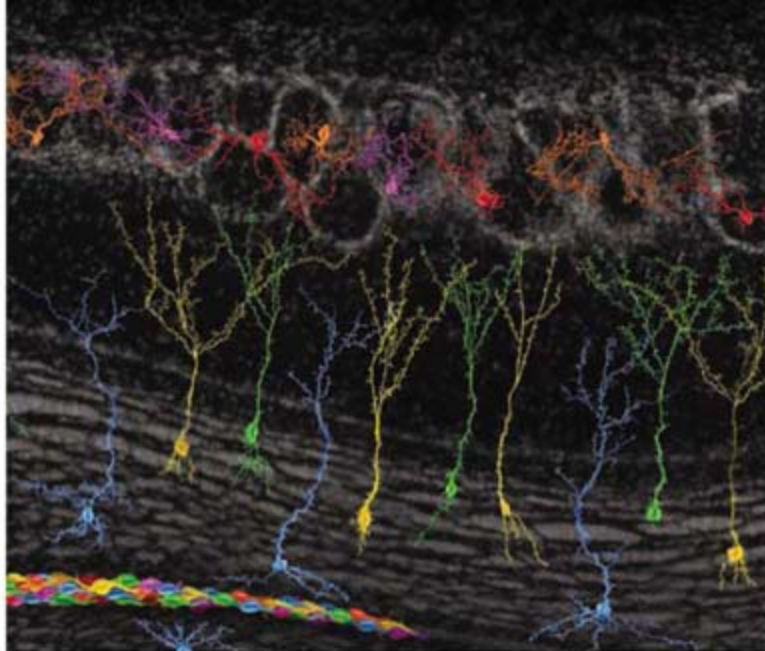
Borrowing Power from Nature

Mechanical tasks are accomplished in the cell through an array of molecular machines and there has been interest in exploiting this machinery in artificial nanoscale structures. **Van den Heuvel and Dekker** (p. 333) review the recent progress on the use of rotary and linear motor proteins for tasks such as facilitating transport or powering a device. Although some clever applications have evolved, the authors note that many uses are still only at the proof-of-principle stage.

Dating Differentiation

Eucrites are meteorites that trace igneous activity on small bodies, similar to the asteroid Vesta, early in the solar system's history. Dating them can tell us about geophysical processes at work when these bodies were differentiating to form a metallic core and silicate mantle. However, such attempts have been difficult because eucrites tend to be changed by later heating and fracturing, and also, the isotopic systems available for dating are hard to calibrate. By analyzing zircons within eucrites, **Srinivasan** *et al.* (p. 345) have dated their crystallization to within 6.8 million years of metal-silicate differentiation on their parent body. They were able to anchor the short-lived Hf-W isotope system with the slower U-Pb system to tie down the timing accurately. Later metamorphism of the eucrites took place after another 9 million years and was likely caused by heating from impacts.

In a Spin

Imaging the surfaces of stars other than the Sun would allow astronomers to map the physical processes at work on them. With advanced optical interferometric techniques. **Monnier** *et al.* (p. 342, published online 31 May; see the Perspective by **Quirrenbach**) have resolved the surface of the main sequence star Altair, one of the brightest stars in the night sky, to a resolution of <1 milliarcsecond. Altair is unusual as it spins very rapidly, fast enough that it appears elongated through centrifugal forces. The amount of distortion and the attendant changes in surface temperatures, characterizing angular momentum transport within the star, diverge from the predictions of standard models, especially around the equator. Thus, extra processes, such as differential rotation and alternative gravity darkening laws, are needed to explain the appearance of rotating stars.

Strained Relations

When films are grown on surfaces through vapor-phase deposition, complex heterostructures can form because of strains that arise through lattice mismatches. **Robinson** *et al.* (p. 355) show in a solution environment that the complex superlattices can form spontaneously in cadmium sulfide nanorods through the controlled introduction of silver cations. Alternating layers of cadmium sulfide and silver sulfide form along the axis of the rod because the lattice-mismatch strain that builds up during silver infiltration limits the growth of the silver sulfide domains. The control over growth achieved by changing the solution parameters and nanowire dimensions was used to tune the near-infrared emission from these nanorods.
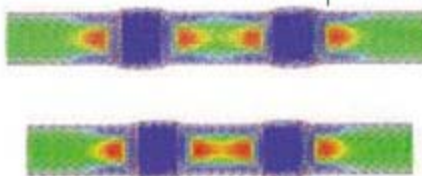
Halogens in Antarctica

Tropospheric halogens affect the concentration of ozone, the oxidizing capacity of the atmosphere, and aerosol formation, all of which are linked to climate. The halogen chemistry of the frozen high latitudes has proven to be particularly interesting, not least because of the role of these regions as harbingers of global climate change, but a better understanding of that chemistry has been hampered by lack of data. **Saiz-Lopez** *et al.* (p. 348) present measurements of BrO and IO in the Antarctic boundary layer from January 2004 to February 2005. They observed high concentrations and persistence of these halogens throughout the sunlit period, contrary to expectations and unlike the situation in the Arctic, where IO has not been detected. The springtime IO levels they found are the highest reported anywhere in the atmosphere, and an apparent synergy between IO and BrO suggests an unknown halogen-activation mechanism. These levels of halogens also cause the rapid oxidation of dimethyl sulfide and mercury in the Antarctic boundary layer.

Gradually Becoming Dominant

Dinosaurs became the dominant land animals by the Jurassic. Whether their early ascension began by way of an extinction that preferentially affected their precursors, including the archeosaurs and amniotes, or through a more gradual replacement of these other groups, is unclear, but the earlier Triassic fossils needed to evaluate these questions have been relatively scarce. **Irmis** *et al.* (p. 358, see the cover) now describe a rich fossil assemblage from New Mexico dating to the Late Triassic that includes both dinosaurs and their reptilian precursors. Thus, some of the precursors persisted much longer than had been thought and existed along with dinosaurs for millions of years. These fossils support a model of a gradual rise of dinosaurs in the Late Triassic that preceded their dominance by the beginning of the Jurassic.

The Same Difference

Recent advances in sequencing technology have increased our power to study variation within a single organism. **Clark *et al.*** (p. 338) resequenced 20 strains of *Arabidopsis thaliana* with high-density nucleotide oligonucleotide arrays and found extensive variation. The comprehensive inventory of genome-wide DNA polymorphisms in *Arabidopsis* illustrates the extent of natural genetic variation, with many genes disabled in different wild strains, as well as high levels of polymorphism among gene family members, including those involved in disease resistance.

What's the Buzz?

The residents of bee hives are well known to be closely related, but hives can often exhibit more genetic diversity than might be anticipated from theories on the benefits of cooperation among closely related individuals. **Mattila and Seeley** (p. 362) show one reason for this is that more genetically diverse hives (those originating from a female mating with multiple males) perform better in the rate of comb building, foraging rates, and honey production than those originating from a single female and male. To advertise her presence in the colony and to exert influence over its members, a honeybee queen produces a complex blend of substances known as queen mandibular pheromone. **Vergoz *et al.*** (p. 384 see the Perspective by **Galizia**) found that exposure to queen pheromone leads to a reduction in aversive learning but not to a reduction in appetitive learning in young honeybees. The queen substance modulates the dopaminergic system of bees, which reduces the capacity of young workers to form aversive memories.
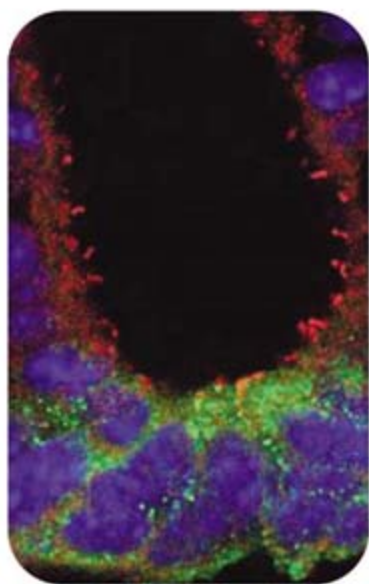
Location, Location, Location

Despite substantial effort, it has remained relatively mysterious how the protein known as Hedgehog (Hh) activates signaling pathways that regulate various biological processes, including stem cell function, development, and cancer. **Rohatgi *et al.*** (p. 372; see the Perspective by **Christensen and Ott**) show that mammalian cells use their primary cilium as an antenna that samples the surrounding environment for the presence of Hh. When Hh bound to its receptor Patched 1 (Ptc1), the receptor left the cilia, where (in the absence of stimulation) it acts to restrain Hh signaling by preventing accumulation of the signaling protein Smoothened (Smo). Accumulation of Smo in the cilia of stimulated cells corresponded to activation of Hh signaling. Further understanding the molecular mechanisms that influence cellular localization of Ptc1 and Smo will improve understanding of the signaling pathway and may lead to new therapeutic targets.

Longevity on the Brain

Several studies show that loss-of-function mutations in the insulin-like signaling cascade extends the life span of worms and flies; however, equivalent mutations are associated with metabolic disease and fatal diabetes in mice. In contrast, calorie restriction or genetic strategies in mice that enhance insulin sensitivity lower the risk of age-related disease and extend life span. **Taguchi *et al.*** (p. 369) resolve these conflicting results by pointing to the brain as the site where reduced insulin-like signaling can extend mouse life span.

Minimal Exposure

The recent discovery that certain viruses express microRNAs (miRNAs) raises the question as to whether these pathogens might use miRNA to evade their hosts. **Stern-Ginossar *et al.*** (p. 376; see the Perspective by **Cullen**) find that for human cytomegalovirus this appears to indeed be the case. One of the virus' miRNAs was predicted to target the 3′ untranslated regions of two immune-related genes, which become activated in response to viral infections. Expression of one of these proteins was indeed dampened by the viral miRNA, which reduced recognition by antiviral natural killer cells. It remains to be seen if miRNA will turn out to be a widespread method exploited by viruses to evade host immunity.

CREDIT: LILJANA MILENKOVIC

AAAS & NPA

How do
Postdocs
Spell
Success?

Here's your link to career advancement

AAAS is at the forefront of advancing early-career researchers
—offering job search, grants and fellowships, skill-building
workshops, and strategic advice through ScienceCareers.org
and our Center for Careers in Science & Technology.

NPA, the National Postdoctoral Association, is providing a
national voice and seeking positive change for postdocs—
partnering with AAAS in career fairs, seminars, and other
events. In fact, AAAS was instrumental in helping the NPA
get started and develop into a growing organization and
a vital link to postdoc success.

If you're a postdoc or grad student, go to the AAAS-NPA link
to find out how to spell career success.

AAAS.org/NPA

NATIONAL
POSTDOCTORAL
ASSOCIATION

Science
AAAS

Colin Challen is a member of Parliament and chair of the All Party Parliamentary Climate Change Group, which has launched an inquiry into the setting of greenhouse gas reduction targets. E-mail: challenc@parliament.uk

Playing Climate Change Poker

TARGETS CAN BE TROUBLESOME THINGS. IF THEY'RE SET FOR SOME DISTANT FUTURE DATE, the target setter may not live long enough to see if they've been met. Interestingly, much discussion about tackling climate change anticipates having achieved something by the middle of this century. What's the target? Both the European Union (EU) and, at a national level, the United Kingdom have focused on a CO_2 emissions cut of at least 60%, which is intended to reduce average global warming by 2°C. (The June G8 summit also spoke of an emissions cut of 50% globally, but only in the context of exploring such a goal and with no greenhouse gas stabilization target in mind.)

What are the chances of meeting the 2° objective? Not likely, according to Malte Meinshausen of the Swiss Federal Institute of Technology, who presented the scientific evidence in a report of the 2005 Exeter climate change conference and who's been quoted since, both by UK government economic advisor Sir Nicholas Stern and the Intergovernmental Panel on Climate Change. His analysis of 11 climate sensitivity studies of the effect of global CO_2 atmospheric concentrations on temperature shows that settling for a 60% cut in atmospheric CO_2 (which corresponds to 550 parts per million by volume) leaves a probability between 63 and 99% of missing the 2°C target. Both the UK and EU proposals indicate that their emissions reduction targets might be toughened. Perhaps, like an athlete attempting the high jump, we are warming up at lower heights first. But scant evidence supports that luxury. Not only must we reduce anthropogenic greenhouse gas emissions, we need a timetable that reduces the risk of positive feedbacks and sink failures that could lead to runaway catastrophic climate change.

In a democracy, it is difficult to convince voters that they should take actions, especially expensive ones, to avoid an as yet largely unseen and unquantifiable danger. How do you base a policy that is likely to have significant economic impacts on model data and forecasts that some might regard as guesswork? We only need to recall the false economy of not spending taxpayers' dollars on building up the New Orleans levees to realize how actions taken today could avert a long-range problem. Delay, combined with the risk that skeptics may accuse the Al Gores of this world of "crying wolf," could make tougher policies harder to adopt later.

In setting a UK target, the government must also ask what the United Kingdom's share of the burden is. Its national target must necessarily relate to reductions in other countries, including the developing world, where industrial growth to alleviate poverty is increasing emissions, as foreshadowed in 1992 by the United Nations Framework Convention on Climate Change. We cannot make a random national calculation and throw it into the global pot of targets; rather, we have to determine what the global need is and figure out how to distribute it—a calculation that must combine science with justice. A successful global climate change framework will have to pay as much attention to the latter as to the former; countries such as China and India will be more inclined to budge if developed countries fully embrace their own responsibilities. Why should anyone sign an agreement that cements their own disadvantage?

The UK government is the first to take on this challenge, with publication of the draft Climate Change Bill in March of this year. Its leadership carries the responsibility to get emissions targets right. The final bill needs to make explicit the formula used to arrive at any target that government sets. That formula should tell us not only the size of the cake but also how we calculate our share of it. The draft bill proposes a figure that cannot be explained in terms of either criterion. If it did, that would surely boost confidence that the result is designed to solve the problem faster than we're creating it. I suspect I have set myself a target of living until I'm 97 to see what transpires.

–Colin Challen

GEOPHYSICS

Electric Aftershocks

Earthquake ruptures are expected to generate electromagnetic activity within the surrounding rocks, but direct evidence for this effect has been lacking. Laboratory experiments on real rocks do generate currents due to fluid movement and piezoelectric effects, but they are weak and in the geological setting it is hard to disentangle them from anthropogenic signals or more ambient electronic noise. Park *et al.* report possible detection of a characteristic electrical signal using an electrode array placed on the San Andreas Fault at Parkfield, California. Electrical distur-

San Andreas Fault.

bances lasting 3 hours were picked up within 250 m of the fault immediately after a magnitude 6.0 earthquake that occurred in September 2004; signals of opposite polarity were subsequently detected after two magnitude 5.0 aftershocks. Although similar electromagnetic changes do occur on a daily basis in this area, the team argue that the localization, timing, and unusual polarity of their signals support association with the earthquake rupture process. They propose fluid movements as the most likely cause of the electrical signals, although they are unable to explain the rapid onset. No precursor signals were observed, so this technique may not ultimately help with earthquake prediction. — JB

J. Geophys. Res. **112**, 10.1029/2005JB004196 (2007).

ECOLOGY/EVOLUTION

Smaller Harvests Than Expected

Leaf-cutting ants of the genus *Atta* are ubiquitous residents of neotropical forests. They construct large subterranean colonies and journey on trails across the forest floor and into the forest canopy, where they harvest leaf fragments that are carried back to the nest. The fragments nourish a mutualistic fungus that in turn provides protein and carbohydrate for the ant colony. Leaf-cutters have been widely assumed to be the dominant herbivores in the forests they inhabit, but supportive quantitative data for this assumption are sparse. Herz *et al.* first used a rapid and nondestructive method, involving the sampling of refuse deposited by ants outside their nests, as a proxy for measuring the daily harvest of leaves. Then they collected data from nearly 50 nests over 15 months in a Panamanian forest and calculated that the ants were actually responsible for only about 0.7% of total leaf consumption by all folivores (insects and vertebrates) in the forest. Even though these results indicate that the defoliation by leaf-cutters is more modest than previously thought, Urbas *et al.* found that herbivory by

Dehydrated (left) and rehydrated larva.

leaf-cutters in a Brazilian forest increased at the margins (versus the interiors) of forests that had been fragmented by human disturbance, thus amplifying environmental change at the forest edge. — AMS

Biotropica **39**, 476; 482; 489 (2007).

BIOCHEMISTRY

Surviving a Dry Spell

Life (as we know it) is based on carbon, and one fortuitous factor is the compatibility of sugars and water. Glucose is readily soluble (at much higher concentrations than the building blocks of other biological polymers), easily handled by enzymes via its chemical functionalities, and benign (and perhaps even beneficial) in its interactions with other biochemicals. In considering the major circulating sugar in insects—trehalose, which is a head-to-head dimer of glucose—the extraordinary tolerance of *Polypedilum vanderplanki* larvae to dessication comes to mind. When the rock pools where these larvae live dry up, the larval fat body synthesizes trehalose and releases it into the hemolymph in order to protect tissue constituents as water is lost. When water becomes available again, dehydrated larvae undergo rehydration and resume their developmental progression into adult midges. Kikawada *et al.* have identified a trehalose transporter (called TRET1) in *P. vanderplanki*. They show that it is specific for trehalose versus maltose, sucrose, and lactose; they also show that it functions as a low-affinity, high-capacity facilitated transporter that can be expressed benignly in mammalian cells. — GJC

Proc. Natl. Acad. Sci. U.S.A. **104**, 11585 (2007).

COMPUTER SCIENCE

Natural and Artificial Flavors

Computer scientists have long worried that their field suffers from split personality disorder: is what they do mathematics or engineering? True, they work on problems such as writing software to carry out calculations on a machine, but they also grapple with the most abstract mathematical properties of computational procedures and the logic of algorithms. So the debate has raged: Is the field a science of the natural world or only a science of the artificial? Denning argues that computer science is decidedly a natural science. Information storage and processing have been found to be fundamental elements of many fields, from the biological data stored in DNA to the quantum information that is transmitted and modified as particles interact. In many areas, principles that transcend com-

puting machines form a set of questions about the deep structure of computation. These questions, in turn, are driving innovative ways to teach computing, sometimes without using sophisticated computer gadgetry at all. The author concludes that the field encompasses a science of information processing in both natural and artificial systems. — DV

Commun. ACM **50**, 13 (2007).

ECOLOGY/EVOLUTION

Eats Roots and Leaves

The understanding of food webs in soil has lagged behind that of above-ground or aquatic systems because of the bewildering complexity of soil organism communities and the sheer intractability of making observations and doing experiments in soil. It has long been thought that invertebrates in forest soils derive most of their carbon from leaf litter that falls from trees. Pollierer *et al.* used a construction crane to alter the isotopic ratio of ^{13}C and ^{12}C supplied (as CO_2) to the canopy of a Swiss forest. They then reciprocally transferred the resultant leaf litter to neighboring forest areas that had experienced a normal isotopic ratio of CO_2, and measured the isotopic ratios in the tissues of soil animals. The carbon isotopic ratio in the invertebrates more closely matched that of the tree roots rather than that of the leaf litter to which they were exposed, indicating that the diet of these animals derived primarily from root tissue and exudates as compared to fallen leaves (which therefore appear to be processed largely by

microorganisms). If this pattern extends to other temperate forests, the configuration of below-ground food webs and patterns of carbon flux might have to be reconsidered. — AMS

Ecol. Lett. **10**, 729 (2007).

CHEMISTRY

Different Routes to a Cluster

In heterogeneous catalysis, the routes whereby molecules come and go from the active sites can substantially affect their reactivity. Röttgen *et al.* have examined a case where direct and indirect adsorption processes compete: the oxidation of CO over Pd clusters supported on MgO films grown on a metal substrate. The Pd clusters (either Pd_8 or Pd_{30}) were mass-selected before deposition, and by changing their surface coverage, the authors could vary the ratio of incoming CO that adsorbed directly on the cluster versus that arriving via diffusion from the support. Data and modeling revealed that for the Pd_8 clusters, the reaction probability was the same whether the CO arrived directly or by diffusion, whereas for the Pd_{30} clusters, the CO supplied by reverse spillover from the support was less reactive than that impinging directly. The results highlight the subtleties of structure-dependent activation energies. — PDS

J. Am. Chem. Soc. **129**, 10.1021/ja068437f (2007).
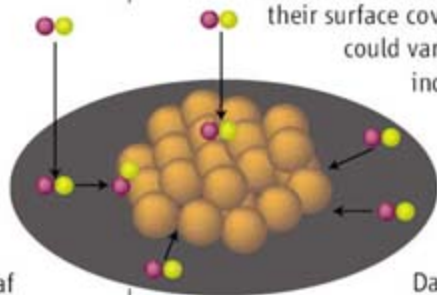
CO arriving at a Pd cluster.

<< Numb Cells Keep Moving

www.stke.org

Integrins are heterodimeric transmembrane receptors that bind to components of the extracellular matrix and are important for both cellular adhesion and migration. The clustering of activated integrins on the substrate-facing surface of the leading edge of a cell results in the recruitment of various proteins, including actin stress fibers, to form a focal adhesion complex (FAC). Cells move, in part, through the coordinated assembly and disassembly of focal adhesions at the leading edge of the cell. Numb is a cargo-specific adaptor protein that binds to several endocytic proteins, and Nishimura *et al.* examined the role of Numb in endothelial and epithelial cell cultures. In a wound-healing assay, Numb polarized toward the leading edge of migrating cells (just behind the lamellipodium), and immunostaining demonstrated that Numb and β-integrin colocalized at focal adhesions. Coimmunoprecipitation experiments revealed that Numb bound to the PAR (for partitioning defective) polarization complex PAR-3. This complex also localizes to the leading edge of polarized migrating cells. One component of this complex, atypical protein kinase C (aPKC) phosphorylated Numb in HeLa cells and, as a consequence, Numb no longer bound to integrins. The authors propose that Numb binds to free integrin molecules (rather than disrupting FACs) and recruits them to clathrin-coated structures to initiate integrin recycling, and that the localization and function of Numb are negatively regulated by aPKC. — JFF

Dev. Cell **13**, 15 (2007).

AAAS
ADVANCING SCIENCE, SERVING SOCIETY

Sick Pictures

A neuroscientist might describe a nightmare differently, but this 1810 image (left) by the English engraver Jean Pierre Simon certainly captures the terror. It's one of thousands of medically themed photos and art housed at Wellcome Images, a new gallery from the British biomedical charity the Wellcome Trust.

The site's contemporary collection is the place to search if you want, say, a spectacular photo of dividing cells caught at the moment of parting or an electron micrograph of influenza viruses barging into tracheal cells. To trace changes in medical knowledge and practice, browse the historical collection, whose holdings include rarities such as 15th century Chinese anatomical drawings and a 1920s Soviet propaganda poster on the dangers of typhus. If your intentions are pure (that is, noncommercial), you can download the images free. >>
images.wellcome.ac.uk

NET WATCH

Multifaceted Menace

Mosquitoes can walk on water as well as any waterbug, or stick to a wall like Spiderman. Now Chinese bioengineers are figuring out what makes them such versatile pests.

A team led by C. W. Wu at the Dalian University of Technology in China mounted a mosquito's leg on a needle and pushed it down onto a tub of water on a digital balance. By varying the angle, they found that a single leg could hold 23 times a mosquito's weight before becoming submerged, they report in July's *Physical Review Letters*.

Scanning electron microscope images revealed that the insect's legs are equipped with tiny scales, each with up to a dozen longitudinal ridges connected by fine transverse ribs. The scientists speculated that air trapped between the ribs may form "nanocushions" that contribute to buoyancy, but their experiments also indicated the importance of the angle of the leg in not breaking through the surface. As the authors note, mosquitoes are equally at home on dry land. It turns out that their feet are equipped with tiny hooks and covered in adhesive hairs similar to those on a fly.
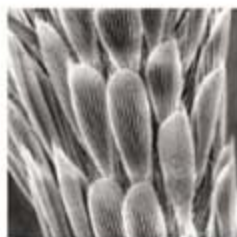
Scales on mosquito leg.

Mathematician David Hu of New York University notes that understanding water-repellent nanostructures will be useful for anyone who wants to make an all-terrain robotic insect. "If it's ever going to fly in the rain, water repellency is going to be important."

Armchair Galaxy-Spotting

If you can tell a star from a galaxy, astronomers at Portsmouth and Oxford universities in the United Kingdom and Johns Hopkins University in the United States would like you and your computer to help classify about a million images from the robotic Sloan Digital Sky Survey telescope at Apache Point Observatory in Sunspot, New Mexico.

Volunteers are invited to go to www.galaxyzoo.org to see pictures of galaxies, "most of which have never been viewed by human eyes before," according to a statement on the Web site. Participants will categorize each image as spiral, elliptical, star/don't know, or mergers. The spiral galaxies are then subdivided into clockwise, anticlockwise, and edge-on.

"The human brain is actually better than a computer at pattern recognition tasks like this," says Oxford astrophysicist Kevin Schawinski. Astrophysicist Bob Nichol of Portsmouth adds that getting the galaxies classified is "as fundamental as knowing if a human is male or female."

VERY OLD WINE

Archaeologists said last week that they had discovered the oldest known winery in France, at a 2000-year-old Roman villa near Béziers in the southern region of Languedoc.

Stephane Mauné, with the French research agency CNRS at Lattes, says the winery was clearly a big business. A 12-by-50-meter building contained 150 huge terra cotta fermentation vessels called "dolia," many smaller amphorae for aging wine, and stone support structures for winepresses. "It was quite a sophisticated enterprise, with running water for cleaning the [jugs]," says Mauné. Dating the establishment was easy thanks to a coin from about 20 C.E. found in the area.

Markings on the wine vessels indicate that a merchant from Puteoli (now Pozzuoli), near Naples, owned the winery. Mauné says workers have found the names of a dozen ceramists among the winery's estimated 80 employees.

Archeologist Jean-Pierre Brun, director of the Jean Bérard Center in Naples, Italy, says the site reflects the enormous growth of commercial wine culture and export during the first and second century C.E. This area "was the 'Far West' for the Romans," he says, noting that they were lured to Gaul by cheaper production costs and land.

Science Alerts in Your Inbox

Get daily and weekly E-alerts on the latest breaking news and research!

This Week in *Science*
Summaries of research content

Science Magazine TOC
Weekly table of contents

Science News This Week
Brief summaries of the journal's news content

Science Posting Notification
Alert when weekly issue is posted

***Science*NOW Daily Alert**
Daily headline summary

***Science*NOW Weekly Alert**
Weekly headline summary

Science Express Notification
Articles published in advance of print

STKE TOC
Weekly table of contents

Editors' Choice
Highlights of the recent literature

Get the latest news and research from *Science* as soon as it is published. Sign up for our e-alert services and you can know when the latest issue of *Science* or *Science* Express has been posted, peruse the latest table of contents for *Science* or *Science*'s Signal Transduction Knowledge Environment, and read summaries of the journal's research, news content, or Editors' Choice column, all from your e-mail inbox. To start receiving e-mail updates, go to:

http://www.sciencemag.org/ema

Science

AAAS

Behind the Scenes

IN THE HINTERLAND. How often does a hog farmer turned government bureaucrat become the toast of a state, all for the greater glory of science? It happened last week in South Dakota, when the National Science Foundation (NSF) chose the Homestake Mine in Lead as the site for a proposed $500 million Deep Underground Science and Engineering Laboratory.

Observers say that Dave Snyder (left), the 62-year-old head of South Dakota's Science and Technology Authority, and his staff worked tirelessly after NSF announced an open site competition in 2004. Last year, Snyder negotiated a deal with the mine's previous owner, Barrick Gold Corporation, for state ownership of the site. "It was a turning point in the project when the state appointed him," says Patrick Garver, executive vice president and general counsel for Barrick. The project also benefited from a $70 million donation from philanthropist T. Denny Sanford.

"Dave has worked miracles," says Kevin Lesko, a physicist from the Lawrence Berkeley National Laboratory, who leads the Homestake scientific collaboration. Snyder says that his role has been simply "to connect the dots." He has a few more to go: The science team must complete a conceptual design, and the NSF has to find the money for the project in a future budget.

AWARDS

PREDICTIVE POWER. Theoretical physicists Makoto Kobayashi of the Japanese accelerator laboratory KEK in Tsukuba and Toshihide Maskawa of Kyoto University have won the European Physical Society's High Energy and Particle Physics Prize for one of the more inspired guesses in the history of science.

In 1973, physicists had only recently discovered that protons and neutrons consist of particles called up quarks and down quarks. A third such particle, the strange quark, was known, and a fourth, the charm quark, predicted. But even before the notion of a quark was entirely accepted, Kobayashi and Maskawa argued that the existence of two more of them would explain a slight asymmetry between matter and antimatter called CP violation, which had been observed in 1964.

Physicists eventually identified six types of quarks, and Kobayashi and Maskawa's theory precisely describes CP violation seen in accelerator experiments. Kudos to them both,

says Helen Quinn, a theorist at Stanford University in Palo Alto, California. "It was a brilliant step to make, but not a difficult one—once you asked the right question," she says.

MOVERS

CHANGE AT HARVARD. Ending a 9-month search, the Harvard Medical School last week picked a new dean from within its ranks: obesity expert Jeffrey Flier. Flier, 58, joined the Harvard faculty in

1978 after studying insulin's role in metabolism and disease at the National Institutes of Health in Bethesda, Maryland. His recent focus has been on how the hormone leptin affects the brain, appetite, and obesity. Flier also has been involved in efforts to make science a bigger part of the undergraduate curriculum. He starts his new job on 1 September.

IN THE COURTS

SPOTTING INFIDELITY. A Michigan state forensic scientist who analyzed DNA samples from her husband's underwear after suspecting him of cheating on her is in hot water for having used government equipment to conduct her investigation.

Ann Chamberlain-Gordon found another female's DNA in the samples and submitted her finding as evidence in a 7 March divorce hearing in Ingham. But after her husband's lawyer informed authorities about the test, the Michigan State Police (MSP), which runs the Lansing lab where Chamberlain-Gordon works, initiated an investigation into whether she had broken department rules. The *Lansing State Journal* quoted her as testifying in a 25 May hearing that she had done the analysis on her own time using chemicals that were slated for disposal.

An MSP spokesperson says the department is investigating the matter.

Got a tip for this page? E-mail people@aaas.org

INSIDE GOVERNMENT

BROADENING OUT. Mark Abbott says a career of exploring the mysteries of ocean life has prepared him to run the $745 million Geosciences Directorate at the National Science Foundation (NSF). "My experience has always been ecological, looking at interactions of natural systems," says the professor of biological oceanography at Oregon State University (OSU) in Corvallis. Now he'll be helping to orchestrate the interactions of an entire scientific community.

Beginning on 1 October, Abbott will be taking on big-science programs involving the solid Earth, deep-sea observing networks, and ocean drilling, another step in the continued broadening of his expertise. His dissertation examined the ecology of Lake Tahoe, but he later tackled satellite observation of ocean biology. And he now oversees what he calls "the whole gamut of earth science" as the dean of OSU's College of Oceanic and Atmospheric Sciences. He'll also be relinquishing his post on NSF's oversight body, the National Science Board.

NEWS>>
THIS WEEK

Checkers
solved
308
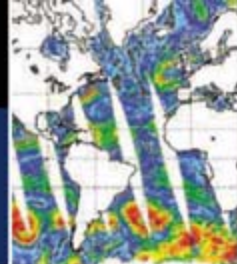
A tempest over
a satellite
309

DEPARTMENT OF ENERGY

Nuclear Weapons Milestone Triggers U.S. Policy Debate

As with high school sweethearts reconnecting at a 25th reunion, U.S. nuclear weapons scientists have found that recapturing the magic of the past takes the right kind of people, a willingness to adapt, and a large capacity for delayed gratification.

In a classified ceremony early this month at Los Alamos National Laboratory (LANL) in New Mexico, Department of Energy (DOE) officials celebrated the belated completion of the plutonium trigger of a nuclear bomb operationally identical to ones last built 18 years ago. The star of the ceremony was the so-called pit—a layered piece of metal the approximate size and shape of a Fabergé egg, with a hollow core—that DOE certified as ready for the nuclear stockpile. The occasion was a milestone for the nuclear weapons program and paves the way for more ambitious work, including building entire weapons from scratch without conducting nuclear tests. It also opens the door for LANL, traditionally a research lab, to consider expanding into manufacturing.

Critics of U.S. nuclear policy, however, say that building new pits contradicts the country's stated intention to reduce its nuclear arsenal. They also believe that the $1.4 billion spent on the project shows that the cost of manufacturing weapons parts, in the words of activist Greg Mello of the Los Alamos Study Group in Albuquerque, New Mexico, could be "toxic to science" by diverting funds from research.

In 1989, the government found environmental and other violations at the nation's only source of building plutonium pits, a DOE facility at Rocky Flats, Colorado. It was later shut down, halting work on a batch of pits for the W88, a 475-kiloton submarine-fired warhead. In 1996, the government asked LANL to build a set of replacements within 5 years, with one caveat: A 1993 ban on nuclear tests meant that the scientists wouldn't be able to test their version.

That restriction stiffened the already-imposing technical challenges of matching the Rocky Flats specifications. The relatively small plutonium research facility at Los Alamos had the requisite ventilation and glove boxes, for example, but its foundation would not support the heavy-duty plutonium forming tools used at Rocky Flats. Instead, workers had to pour molten plutonium into shaped molds and weld pieces together. To conform to new environmental rules, engineers cut down on the use of lubricants and used new solvents to clean metal surfaces.

Even so, in 2001, DOE auditors con-

Boxed in. Los Alamos scientists worked extensively with glove boxes to develop a new plutonium trigger.

cluded that the program was "at risk." They cited delays in half of the roughly 40 nuclear manufacturing procedures to be finalized. "Everyone underestimated how hard it was going to be," says former DOE official Madelyn Creedon, now a Senate aide.

In response, then–lab director John Browne replaced the head of the program with co-leaders, one overseeing physics and the other, weapons manufacturing and engineering. In addition, says Richard Mah, a former Rocky Flats metallurgist who led the revamped manufacturing effort from 2001 to 2004, the lab brought in "some old hands who had done some of this stuff." By 2003, researchers had matched the physical specifications of the Rocky Flats design.

The parallel management structure helped the lab verify that the new pit would work, says Mah. For example, fears that a different metallic grain size could hamper performance dissolved after verification experiments—which included non-nuclear explosions, numerical simulations, and materials science studies—showed physicists that the difference wouldn't degrade pit performance. It took until this year for LANL to certify the pit as stockpile-ready, meeting a goal set in 2001.

Although the Rocky Flats pits had been proven to work in underground tests, LANL researchers realized they weren't perfect. Layered metal surrounds their hollow plutonium shell, which undergoes fission when crushed by conventional explosives. Studies at Los Alamos found that the original pits contained "impurities that can affect mechanical properties," says DOE weapons official David Crandall. At first, "there was an attempt to make plutonium in pits as pure as possible," he says. But weapons scientists made more credible progress when they decided the pits "needed to be as much as possible like those [previously] tested, including any impurities in plutonium."

Crandall says the new W88 pits show that the country's nuclear weapons complex can both monitor current bombs and build new ones without testing them: "This was a valuable initiation into the processes we'll need for RRW [the Reliable Replacement Warhead]." The RRW program seeks to build new bombs from scratch to replace aging warheads (*Science*, 9 March, p. 1348). Planetary geophysicist Ray Jeanloz of the ▶

CREDIT: LANL

FOCUS

Zapping the
tsetse fly
310

Taming China's
dust storms
314
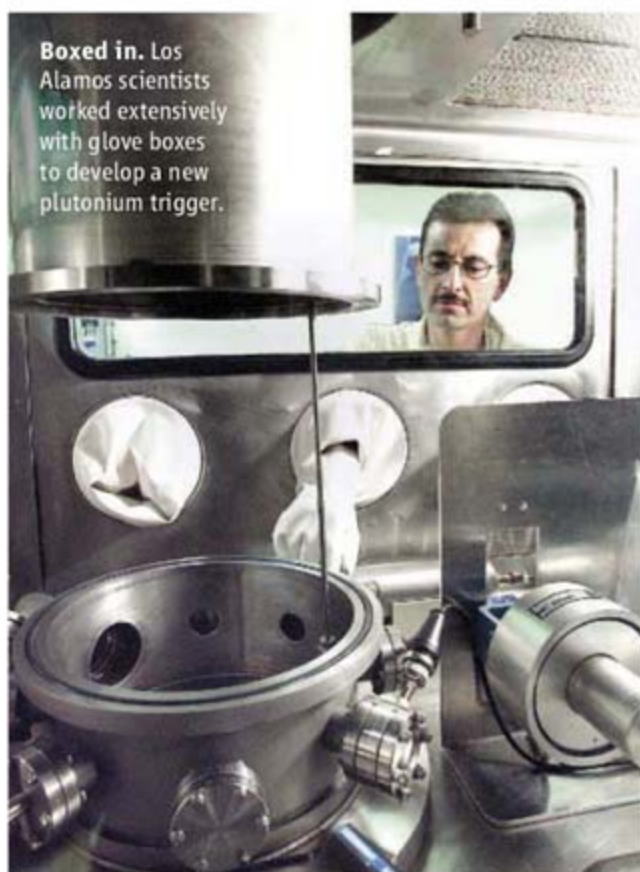
University of California, Berkeley, says that the struggle to make the new pits highlights the importance of maintaining a well-funded and experienced talent pool that can respond quickly to emergencies or new developments.

Senator Pete Domenici (R–NM), speaking at the 2 July celebration, used the milestone to attack some $600 million in cuts to the weapons program by House appropriators in DOE's upcoming 2008 budget, several of which would affect planned expansion of plutonium science at Los Alamos. The fate of the cuts is uncertain, however, given different versions of the spending bill that must be reconciled and a White House threat to veto the overall bill.

In the meantime, Mah, who last year worked directly for the new Bechtel–University of California lab management partnership, says that building more pits could become an additional business for the lab. His fear is that government officials might value manufacturing more highly than science. But a lab spokesperson says "there's no plan to make [manufacturing] the primary role of Los Alamos."
                                    –ELI KINTISCH

BIOTECHNOLOGY

Singapore Firm Abandons Plans for Stem Cell Therapies

In a sign that hopes for quick medical benefits from stem cells are fading, ES Cell International (ESI)—a company established with fanfare in Singapore 7 years ago—is halting work on human embryonic stem (hES) cell therapies. Investors lost interest because "the likelihood of having products in the clinic in the short term was vanishingly small," says Alan Colman, a stem cell pioneer who until last month was ESI's chief executive.

ESI's setback may dampen investors' enthusiasm for stem cell therapies, says Robert Lanza, vice president for R&D at Advanced Cell Technology in Worcester, Massachusetts: "What the field badly needs is one or two success stories."

Colman, a member of the team that cloned the sheep Dolly, will become head of the Singapore Stem Cell Consortium, which funds research at institutes affiliated with Singapore's Agency for Science, Technology and Research (A*STAR) and also offers grants. He will also set up a lab at A*STAR's Institute of Molecular and Cell Biology. Most of the 24 scientists working on hES cell therapies at ESI will continue their research with "more secure government funding" at A*STAR's new Institute of Medical Biology, Colman says. A*STAR announced Colman's move on 9 July.

ESI was set up in 2000 to commercialize hES cell findings produced by a collaboration involving Monash University in Clayton, Australia; National University of Singapore; Hadassah Medical Organization in Jerusalem; and the Hubrecht Laboratory in

From bedside to bench. Sagging investor confidence in stem cells has prompted Alan Colman to leave the corporate world for a basic research lab.

Utrecht, Netherlands. Australian investors and an investment arm of Singapore's government put up seed funding, and ESI had raised $24 million as of last October, according to the company. ESI hired Colman as chief scientist in April 2002; he became CEO in 2005.

The company was attempting to turn hES cells into insulin-producing cells to treat diabetes and cardiac muscle cells to counter congestive heart failure. Both conditions represent major markets with unmet clinical needs, but making well-functioning insulin-producing cells "proved really difficult," Colman says. Both envisioned therapies would need at least a billion cells for each human dose. Producing such numbers at the required purity "becomes very expensive," Colman says, and meeting these challenges would have taken longer than investors have patience for.

ESI's setback need not cast a pall on the field,

researchers say. Alan Trounson, a Monash University stem cell scientist who contributed to the research ESI was trying to take to market, says he is "profoundly disappointed" that the company is giving up. But he says that ESI pursued "a high-risk strategy" in focusing narrowly on two potential applications. With the field still young, Trounson says, "the primary aim should be to establish a broad platform of robust and reliable science that can underpin translation to clinical applications."

Irving Weissman, a stem cell researcher at Stanford University in Palo Alto, California, agrees: "ES cell research is, for the most part, still scientific discovery research."

Although ESI is out of the game, at least two companies say they have hES cell therapies in the pipeline. Geron Corporation in Menlo Park, California, expects to start clinical trials of a therapy for spinal cord injury early in 2008, according to spokesperson David Schull. And by early next year, Advanced Cell Technology hopes to file a new drug application for a treatment for macular degeneration, Lanza says.

ESI, under new leadership, will now focus on providing hES cells and derived cells for basic research and drug development, Colman says. He admits to a "tinge of disappointment that the field is moving more slowly than I had hoped." Colman hopes to spur the field along with his own research, although he declines to discuss details.
                                    –DENNIS NORMILE

Recipe for recovery. Rebuilding fish stocks will require putting at least a fifth of Hawaii's waters under protection like Hanauma Bay, says Alan Friedlander.

FISHERIES MANAGEMENT

Conservationists and Fishers Face Off Over Hawaii's Marine Riches

HANAUMA BAY, HAWAII—The school of big-eye jacks was right where Alan Friedlander of the National Oceanic and Atmospheric Administration's biogeography branch said it would be, circling slowly at the mouth of Hanauma Bay, a protected area just 15 kilometers from the skyscrapers of downtown Honolulu. There must have been close to 200 fish, each about 50 centimeters long and utterly unafraid as Friedlander, a marine biologist, glided through them.

"You hardly ever see this anymore in Hawaii," Friedlander said after surfacing. Jacks are prized by anglers, and such large schools have become rare in inhabited parts of the archipelago, he says.

Friedlander knows the bay better than most. He published a study in the April issue of *Ecological Applications* showing that total fish biomass in Hanauma and 11 other protected areas was 2.7 times greater than the biomass in comparable unprotected areas. And in the uninhabited 2000-kilometer-long Northwestern Hawaiian Islands chain, a national monument since 2006, there is 6.7 times more fish biomass on average than in comparable habitats—an indication that humans have reduced fish stocks in the main Hawaiian islands to about 15% of what they once were.

To Friedlander, the message is simple: The main Hawaiian Islands' reserves, which protect only 0.3% of the coastline, are too small. "If you want to rebuild fish stocks, you need to stop fishing in at least 20% of Hawaii's waters and regulate fishing in the rest," Friedlander says. Increasing the protected areas, therefore, would result in a larger fish catch.

The appeal for new conservation areas prompted a reaction. In March, the state's House of Representatives approved a "right-to-fish" bill that would require the state to provide unattainable data, such as stock assessments throughout species' entire ranges, before any new protected area is created. The bill "would tie up all fishing regulations, not just marine reserves, in endless studies and red tape, making it impossible for the state to properly manage the public's marine assets," says William Chandler, director of ocean policy at the Marine Conservation Biology Institute in Bellevue, Washington. To his relief, Hawaii's Senate significantly modified the bill. But scientists and state officials expect the fight to continue in the next legislative session, which starts in January.

Although similar right-to-fish bills have been approved in Rhode Island and Maryland, they have not impeded the creation of protected areas in those states, says Sarah Clark Stuart of the Coastal Ocean Coalition in Atlantic Highlands, New Jersey. Because the Hawaii legislation would effectively end all fishing restrictions, she says it "is far more anticonservation than any of the other bills that were introduced in the U.S."

Hawaii's right-to-fish bill got further than a conservation bill in the House. In 2003, Friedlander helped draft legislation that would have set aside 20% of state waters for conservation. Like other states, Hawaii controls the first 3 nautical miles (6 kilometers) off its coasts, and the federal government controls the rest, up to 200 miles (370 kilometers). The Marine Reserve Network Act would have made Hawaii the leader in marine conservation in the United States, where less than 1% of coastal waters are protected. But the bill drew the ire of Hawaii's fishing lobby and was scuttled.

The loss, conservationists say, is a cautionary tale of how science sometimes is no match for a powerful bureaucracy tied to fishing interests.

As Hawaii's tourism grew, and cost of living skyrocketed—the state has the nation's highest average rents—fishing became an important supplement for poorer residents. The use of gillnets, which snare turtles, seals, and nonfood fish in addition to target species, is widespread. Trolling, shore casting, and spearfishing are unregulated, and the state's estimated 260,000 anglers are not licensed. Only this year were restrictions put on gillnets, including a ban on their use on Maui Island and overnight elsewhere.

Opponents of the Marine Reserve Network Act gained momemtum earlier this year in a series of meetings designed to increase input from native Hawaiian communities. The meetings were organized by the Western Pacific Regional Fishery Management Council (Wespac), one of eight such regional councils that advise the U.S. Commerce Department. Wespac's chair is Sean Martin, president of the Hawaii Longliners Association. State officials and environmentalists have long accused Wespac of defending narrow fishing industry interests.

Wespac's influence is supposed to be limited to federal waters, but activists and state officials contend that the organization lobbied illegally for the right-to-fish bill. "Numerous times during the process that produced the bill, I saw Wespac employees openly talking to legislators about it," asserts Keiko Bonk of the Northwest Hawaiian Islands Network, which campaigns for marine conservation. The bill

CREDIT: C. PALA/SCIENCE

passed the House, but a Senate draft now awaiting action would encourage community-led protection efforts.

In May, Bonk filed a complaint with the Commerce Department's Inspector General, claiming that Wespac had violated statutes that prohibit federal employees from lobbying state legislatures. Bonk called for an investigation and congressional hearings. Wespac denies it engaged in lobbying. The right-to-fish bill "has nothing to do with us," says Paul Dalzell, Wespac's senior scientist, adding, "All I know is that it was drafted by fishermen."

"The scary thing is that the bill could pass next year," says Peter Young, who recently completed a term as director of Hawaii's Department of Land and Natural Resources, which manages the state's waters.

"If it passes," adds William Aila, an active Hawaiian fisher and harbormaster, "it's going to further deplete our marine resources. That's unacceptable for our future generations."

–CHRISTOPHER PALA

Christopher Pala is a writer based in Honolulu.

PALEOHYDROLOGY

Did a Megaflood Slice Off Britain?

Britain as an ungainly peninsula of France? It might have been. At some time in the geologic past, it almost certainly was. But long ago, some force somehow lowered a high-standing ridge from Dover to France that would be dry land today. A group of geoscientists has new evidence of the culprit: A huge gushing of lake water, they suggest, cut down into solid rock to form the Dover Strait before rushing down the then-dry English Channel.

The strait-cutting megaflood, if it happened, would not have been the first or the last of its kind. The classic example broke out of ancient Lake Missoula about 15,000 years ago to ravage eastern Washington state and create the tortured terrain of the Channeled Scablands. That required a flow of 10 million to 20 million cubic meters of the lake's glacial meltwater each second, or 50 to 100 times the flow of the Amazon River.

Geologist Sanjeev Gupta of Imperial College London and his colleagues present evidence in this week's issue of *Nature* for scablandlike terrain downstream of the Dover Strait. Gupta and colleagues had to look for their evidence at the bottom of the English Channel, which melting ice sheets filled with water at the end of the last ice age. Using depth-finder data collected for navigational charting, they mapped the bottom in new detail. They found kilometer-scale, flat-topped islands in the same distinctive elongated shapes as the erosional remnants of the Channeled Scablands. They also saw broadly sweeping streamlined valley edges, "braided" channels, ridges and grooves pointing downstream, and crescentlike scours. All these features speak of extreme flows, the group says.

Gupta and his colleagues envision a lake hemmed in by glacial ice where the southern North Sea is today. The lake's waters could have overtopped the Dover ridge a few hundred thousand years ago, lowering the ridge and increasing the flow until 200,000 to 1 million cubic meters per second were streaming over the ridge. The megaflood would have cut loose the peninsula during times of high sea level like the present, the group suggests. Island Britain would have been born.
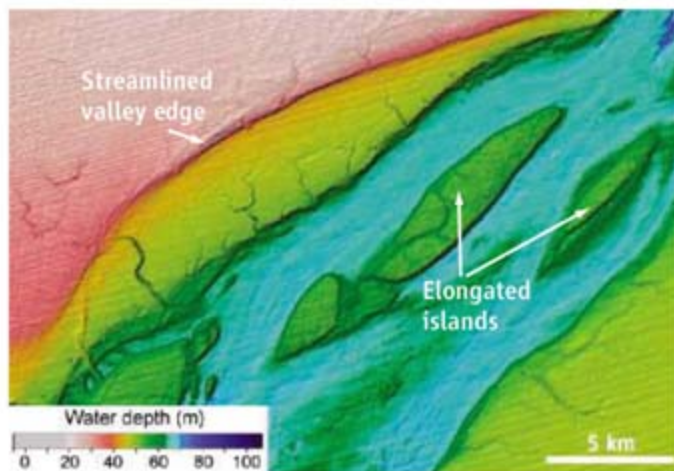
A day's work? The elongated "islands" and streamlined edge of this submarine valley on the floor of the English Channel suggest that a huge but brief flood gushed between Britain and France.

"When you put the association of landforms together, it is very similar to what Victor Baker has described in the Scablands," says geologist Philip Gibbard of the University of Cambridge. "I'm persuaded by it." But Baker, of the University of Arizona in Tucson, says "it's not a smoking gun, but this is a very productive idea that deserves more attention."

–RICHARD A. KERR

Spaced Out

The United Kingdom risks lagging behind in space studies if the government does not increase space spending, the House of Commons science and technology committee warns in a report this week. The parliamentarians suggest setting up the National Space Technology Programme to provide seedcorn funding, although no total is suggested.

The U.K. spent just $425 million on space during 2005–06, substantially less than its European counterparts. The report recommends bolstering British strengths such as planetary exploration and earth observation while considering new efforts in human space flight and launchers. The committee also calls on the European Space Agency to locate one of its facilities in the U.K., a topic of ongoing negotiations with ESA, says Richard Holdaway of the Rutherford Appleton Laboratory in Chilton.

–DANIEL CLERY

Biologists Going Down Under ...

Last week, the European Molecular Biology Laboratory (EMBL) spread to the antipodes when delegates from the group's 19 member nations voted to extend an associate membership to Australia. The 7-year initial term starts next year, when Australia will begin sending faculty members and research fellows to EMBL's five European basic research laboratories while receiving EMBL research support. Sponsors include several Australian universities and the government, which will spend a combined $7.2 million to fund the initial term. "With [Australia's] special expertise, for example, in the fields of medical epidemiology and stem cell research, it will be an excellent complement to EMBL's focus on basic research in molecular biology," says Iain Mattaj, EMBL's director general.

–BENJAMIN LESTER

... Heat Rising

The world can't afford to stall on confronting climate change, says a resolution passed last week by the International Union of Geodesy and Geophysics, and scientists shouldn't let it. The 58-nation scientific umbrella organization, which includes seven international bodies, passed the nine-point resolution focusing on the inevitable consequences of warming and urging nations to "promote adaptation." In addition to pushing for more climate-monitoring research funds, the union's members promise more "outreach," which its outgoing president Michael MacCracken says includes getting the word out about impending warming-related floods or droughts.

–MARISSA CEVALLOS

COMPUTER SCIENCE

Program Proves That Checkers, Perfectly Played, Is a No-Win Situation

If two players face off at checkers and neither makes a wrong move, then the game will inevitably end in a draw. That's the result of a proof executed by hundreds of computers over nearly 2 decades and reported online by *Science* this week (www.sciencemag.org/cgi/content/abstract/1144079). The finding guarantees that an appropriately programmed machine will never lose to a human. It also marks a personal victory for Jonathan Schaeffer, a computer scientist at the University of Alberta in Edmonton, Canada, who set out to "solve" checkers in 1989.

Hopeless. Unable to beat the computer program, a human will eventually make a mistake that leads to a win for the machine.

"It's a huge accomplishment," says David Levy, president of the International Computer Games Association in London and an expert on chess-playing machines. "It's by far the most complex game ever solved." The tools and strategies developed for the problem might prove useful for analyzing genetic code or computerized translation, he says.

The point of checkers, or draughts as the game is also known, is to get the jump on your opponent. The game is played on an eight-by-eight grid of red and black squares. The check-

ers are black and red disks that can slide forward diagonally from black square to black square. The players, call them Bob and Rita, start with 12 checkers each in the rows closest to their sides of the board. Players move in turn, and Bob can capture one of Rita's checkers by hopping over it into an empty space just beyond, and vice versa. Checkers that cross the board become "kings" that can move backward. The game continues until one player captures all of the other's pieces.

Schaeffer and his team have shown that if

Bob and Rita have perfect foresight, they will always reach a stalemate in which neither can finish the other off. So checkers resembles tick-tack-toe (known as "noughts and crosses" in Britain), the game in which players fill a three-by-three grid with X's and O's in hopes of getting three in a row. Given that there are roughly 500 billion billion possible arrangements of checkers on the board, proving checkers is a guaranteed draw is far harder than proving that tick-tack-toe can't be won.

The researchers began by constructing a database of all 39,000 billion arrangements with 10 or fewer pieces on the board. In the process, they determined whether each one led to a win for black, a win for red, or a draw. They then considered the very beginning of the game, opened with a move by black, and then used a specialized search algorithm to trace out subsequent moves and show that, as the two players try to maximize their advantage, they inevitably steer the game to one of the 10-checker configurations that leads to a draw.

Schaeffer credits improvements in computers for making the result possible. In fact, he suspended work from 1997 to 2001 to wait for a particular technology—the 64-bit processor—to mature. But Murray Campbell, a computer scientist at IBM's Thomas J. Watson Research Center in Hawthorne, New York, says that the researchers' ingenuity was key, too. "Without a lot of the clever ideas behind what they did, I think it would have been a number of years before technology alone could have solved checkers," says ▶

U.S. SCIENCE FUNDING

Pentagon Is Looking for a Few Good Scientists

Topflight researchers at U.S. universities, the nation needs you.

This fall, the U.S. Department of Defense (DOD) will launch a grants program to fund researchers with innovative ideas for tackling important security challenges. It will be modeled on the National Institutes of Health Director's Pioneer Awards, which support blue-sky, interdisciplinary research in biomedicine. DOD plans to make about 10 awards, each good for $3 million over 5 years. Applicants for the National Security Science and Engineering Faculty Fellowships must be U.S. citizens, and preference will be given to early-career researchers.

Agency officials hope the program will foster research outside the bounds of predetermined research questions. "We do not have specific areas in mind; rather, we have

challenges that cut across several disciplines," says William Rees, DOD's deputy under secretary of defense for laboratories and basic science. Although the research performed under the program would be unclassified, awardees would need a security clearance to be briefed on the challenges they are supposed to address.

The challenges, not yet chosen, are likely to be similar to those identified last year by DOD's Quadrennial Defense Review. Its list of priorities includes biometrics; social, cultural, and behavioral modeling; tracking of enemy targets; countering improvised explosive devices; and extracting information about suspicious activities and events from large data sets. Agency officials plan to invite about 20 applicants who survive an initial cut to make presentations at the Pentagon. The

first class of winners will be announced next spring.

V. S. Subrahmanian, a computer scientist at the University of Maryland, College Park, whose research is partly funded by DOD, says allowing researchers to come up with proposals in response to agency-designated challenges is an "outstanding" idea. "We are used to having research topics defined top-down by DOD," says Subrahmanian, who plans to apply. "While that usually works well, researchers know best what their field has to offer." He also thinks the fellowships will create a "corps of academic researchers dedicated to defense and national security."

If the first round goes well, DOD officials hope to eventually support as many as 50 researchers.

–YUDHIJIT BHATTACHARJEE

Campbell, who co-wrote the Deep Blue program that defeated chess champion Garry Kasparov in 1997.

Most experts expected that checkers would eventually be proved a draw, says Jaap van den Herik, a computer scientist at Maastricht University in the Netherlands, if only because grandmaster players routinely play each other to a draw. But, he says, "if you have not proved the result, then every expectation is worth nothing."

Schaeffer says he feels vindicated by the proof. In 1994, a program he developed called Chinook played the then-reigning world champion, Marion Tinsley, to a series of draws before Tinsley withdrew because of health problems and conceded. Tinsley, who is considered the best player ever and who lost only three tournament games from 1951 to 1991, died of cancer 8 months later. Some players scorned Schaeffer, he says, and even charged that the stress of the special title match had killed Tinsley. Chinook defended its crown in two subsequent matches against the next-highest-ranked player. "To this day, I still get people saying that you would never have beaten Tinsley," Schaeffer says. "The program today would never lose to Tinsley or anyone else, period." And because humans eventually make mistakes, the program should inevitably prevail in a series of games against any person, even Tinsley, for whom Schaeffer says he has "great respect."

Van den Herik worries that Schaeffer's solution will accelerate the decades-long decline of tournament checkers. Meanwhile, Schaeffer is turning his computers to poker. In principle, that game can't be solved—but it can make you a lot of money. **–ADRIAN CHO**

U.S. WEATHER FORECASTING

Satellite Kicks Up a Storm Looking Out for Hurricanes

An 8-year-old NASA weather satellite sits improbably at the center of the latest scientific storm raging in Washington, D.C.

In the last 2 weeks, two congressional panels have held hearings on events surrounding the ouster of William Proenza as director of the National Hurricane Center (NHC) on 9 July. Proenza had repeatedly criticized his employer, the National Oceanic and Atmospheric Administration (NOAA), for failing to plan for the impending failure of QuikSCAT, a satellite launched in 1999 and 3 years past its design life. Proenza, a 35-year NOAA forecaster who became NHC head in January, says loss of the craft's sensors could degrade 3-day hurricane track forecasts by 16%, citing a study in press that analyzed forecasts for six 2003 storms. Scientists familiar with QuikSCAT's capabilities say Proenza was both "right and wrong" in his acerbic charges.

To predict coming hurricanes, forecasters rely most heavily on radar or visual cloud data from satellites, typically NOAA's Geostationary Operational Environmental Satellite. Its information is bolstered by a network of buoys, hurricane-hunting planes, and coastal radar units to help modelers make computer simulations of developing storms. QuikSCAT added to that ensemble by bouncing microwave signals off ocean waters over a 1800-kilometer swath, reporting surface wind speeds by analyzing the reflections. By following a polar orbit, QuikSCAT covers 90% of the oceans, in many areas twice a day.

NOAA researchers have lauded its data, which is particularly useful for detecting tropical Atlantic storms early and providing vital coverage over colder waters, including the Pacific. A Hawaii-based U.S. Navy official said last year it plays a "critical role" in Pacific forecasting. NHC forecasters most treasure the craft's ability to see developing tropical depressions long before they're otherwise detected. Last year, NOAA forecaster Hugh Cobb called

It's a breeze. NASA's QuikSCAT satellite measures global ocean surface winds, including speed and direction (*inset*).

QuikSCAT, now operating on its backup transmitter, "our bread and butter."

But forecasters don't live on bread alone. Last week, at a Senate hearing in which NOAA officials were lambasted for not preparing adequately for QuikSCAT's demise, NOAA satellite branch chief Mary Ellen Kicza tried to poke holes in Proenza's arguments. The satellite's sensors don't

quantify hurricane wind speeds greater than 105 km, can't see well through rain, and its polar orbit means QuikSCAT "may not be at the right place at the right time," she said. European and U.S. Navy satellites provide data "not quite as good" as QuikSCAT but could plug holes if the NASA craft fails, she said, adding that NOAA's other tools pick up storms once they seem headed for a landfall. "We are not blind" if QuikSCAT dies, Kicza asserted.

Meteorologist and respected weather blogger Jeff Masters agrees, noting that the unpublished study Proenza cited involved only one of roughly seven active forecasting models. Folding in all the simulations, plus the rest of the data sources, creates a "global system" of which QuikSCAT is but one element, says hurricane expert Greg Holland of the National Center for Atmospheric Research in Boulder, Colorado. So Proenza "was right and wrong," Holland explains.

A joint NASA-NOAA study, due next year, will spell out the next options. But lawmakers want to push NOAA along. In May, Representative Ron Klein (D–FL) and co-sponsors proposed a bill to authorize $375 million to build a QuikSCAT replacement. "The loss of this data—whether minute or significant—could cause dire consequences," Klein told the committee. Those funds, however, have not been included in appropriations bills moving through Congress that otherwise provide generous increases to NOAA's 2008 budget.

–ELI KINTISCH

Welcome to Ethiopia's Fly Factory

One of the poorest countries in the world has an ambitious plan to eliminate the tsetse fly. But some scientists say it's a waste of money

KALITI, ETHIOPIA—Noisy, multicolored trucks lumber along the busy main road in this far suburb of Addis Abeba, belching clouds of smoke and honking at the pedestrians that crowd the road. A muddy, bumpy side road leads past a row of shacks to an industrial area that's home to a factory for pots and pans. Then a gate slides open, and a brand-new gray building the size of a soccer field emerges, surrounded by a sea of smooth asphalt. It's almost too clean and organized for its chaotic surroundings.

In a matter of months, the vast building will be buzzing with activity—literally. Here, Ethiopia is developing a sophisticated weapon against an age-old scourge: the tsetse fly, which transmits a parasitic livestock disease called nagana that has long crippled the country's rural economy.

The scheme sounds simple. Produce as many as a million male flies a week, make them sterile by blasting them with radiation for a couple of seconds, then release them in tsetse-infested areas, making sure they outnumber wild males 10 to 1. Hapless females will mate with the lab critters, but their rendezvous will produce no offspring. Repeat the procedure several times, and the tsetse population will die out.

It's an elegant and environmentally friendly method; birth control for insects, some call it. The sterile insect technique (SIT), as it's officially known, has a long and solid track record (see sidebar, p. 312). Over the course of 50 years, it helped sweep the screwworm fly, which feeds on open wounds in livestock, from half the Western Hemisphere, and it's being used to protect everything from Chilean apples to Dutch onions to Japanese melons from voracious pests.

Perhaps more important, it helped wipe out the entire tsetse fly population on Zanzibar's main island in the 1990s, a project hailed as an important proof of principle. Now, Ethiopia hopes it can become a model itself by showing that the same is possible on the African mainland. More than 35 countries have tsetse, and in many, they transmit not just nagana but also sleeping sickness, a devastating human disease.

And yet, the Ethiopian project is at the center of a divisive, often caustic, debate among entomologists. Critics believe that for a variety of reasons—such as the fact that there are five tsetse species in Ethiopia—it is likely to fail. And besides, it's not a sustainable solution, they say, because flies may reinfest the country. The money—Ethiopia's government spent $12 million on the factory

alone—would have been much better spent on cheaper and simpler ways to fight tsetse, such as insecticide spraying, says Glyn Vale, a former head of tsetse research in Zimbabwe. "I hate to see a poor country waste so much money," Vale adds.

Veterinary entomologist Ian Maudlin of the University of Edinburgh, U.K., calls SIT Ethiopia's "man-on-the-moon project."

These critics blast the International Atomic Energy Agency (IAEA), which is supporting the project, for seducing Ethiopia into trying sterile insects—and they're even more dismayed that other African countries are following suit. Best known for its wrangling with aspiring nuclear powers, the U.N. agency, headquartered in Vienna, Austria, also promotes the peaceful use of atomic energy, including the creation of sterile insects, and its lab in Seibersdorf, outside Vienna, is the world's premier SIT research center.

Green Desert

Opinions differ about the solution but not about the problem. Almost a quarter-million square kilometers of mostly fertile valley land in western and southwestern Ethiopia is infested with tsetse flies. Nagana, caused by a unicellular parasite of the *Trypanosoma*

Fly belt. An area of about 10 million square kilometers—including one-fifth of Ethiopia—is home to dozens of species of tsetse flies.

Tsetse fly region

Ethiopia

AFRICA

INDIAN OCEAN

genus, makes keeping livestock difficult. That means fewer animals to plow the land, less milk, and less manure—in short, poverty. A large swath of Africa has the same problem. The U.N.'s Food and Agriculture Organization puts the bill for missed farming revenues in this "Green Desert" across Africa at about $4.5 billion annually.

Then there's the human cost: Sleeping sickness, or human trypanosomiasis, is believed to infect some 50,000 to 70,000 people a year, although hard data are not available. No vaccine exists, and drugs—most more than 50 years old—are toxic and decreasingly effective. Melarsoprol, an arsenic-based drug, kills between 3% and 10% of patients.

For colonial powers, tsetse posed a formidable barrier to the development of their African assets, and they all started programs to deal with the problem. They did have some early successes. Most famously, the Portuguese rid the small West African island of Principe of tsetse in 1905, largely by equipping plantation workers with sticky backpacks.

Colonial concerns also inspired one of the earliest but least known studies of SIT. In the 1940s, in what was then Tanganyika and is now Tanzania, British entomologist F. L. Vanderplank discovered that crossing two different species of tsetse flies resulted in hybrids with very low fertility. This gave him the idea for a trial in which the pupae of one tsetse species were collected and transported by train to an area occupied by another species, in hope of creating sterile offspring. Vanderplank never published the results, but before his

death he gave the raw data to entomologist Chris Curtis of the London School of Hygiene and Tropical Medicine, who published them in a 2005 book. The trial was a success.

But SIT didn't really take off until after the successful U.S. fight in the 1950s against the screwworm, which was subsequently rolled back all the way down to Panama. As it turned out, it wasn't hybridization but radiation that proved the most effective way to create sterile insects.

So far, the majority of SIT programs have addressed agricultural pests in richer countries. The projects can cost tens of millions of dollars, but those costs are often quickly recovered. The screwworm eradication, for instance, saves U.S. livestock

Source of pride. Project coordinator Temesgen Alemu (*right*) and insect facility manager Solomon Mekonnen—posing with a gamma ray source used to sterilize flies—hope Ethiopia's tsetse fight will serve as an example for Africa.

producers $900 million a year, according to the U.S. Department of Agriculture.

Yet by the 1970s, IAEA had also set its sights on tsetse. The Seibersdorf lab refined the technology of rearing tsetse flies. Whereas at first they were fed on live rabbits and guinea pigs, cow blood is used today.

In the mid-1980s, the agency and the Tanzanian government picked Unguja, the main island of Zanzibar, for a test site. It took almost 10 years to build a fly-rearing facility and train local staff, says Andrew Parker, a tsetse expert at IAEA. After the flies had first been attacked using insecticides, planes started delivering weekly loads of male flies across the island in August 1994. By 1997, Zanzibar was declared tsetse-free, at an estimated total cost of $5.7 million. It still is today.

The example piqued the interest of the Ethiopian government, says Temesgen Alemu of the Southern Tsetse Eradication Project, a program of the Ethiopian Science and Technology Organization that IAEA supports with scientific expertise and technical advice. And 10 years later, thanks in part to funding from the U.N., the African Development Bank, and the government of Japan, things are well under way. Workers are busy unloading new racks and installing an automated feeding system in sparkling clean rearing halls. An old building on the same grounds now houses a colony of about 100,000 breeding females that produce a weekly harvest of 10,000 males. In the new building, those numbers should go up by a factor of 70 to 100, Alemu explains.

The project involves much more than SIT, Alemu says. Conventional techniques such as traps and so-called targets—blue or black sheets sprayed with insecticide and baited with cow urine or artificial attractants—are currently used to drive down the population to less than 5% of its original level. SIT's role will be to finish it off, Alemu says, because sexual attraction can do what insecticides can't: reach and kill even the very last fly. The 25,000-km^2 valley that has been selected as a first target is protected by mountains, reducing chances of reinfestation. It has only one species, *Glossina pallidipes*, which is what the factory is churning out at the moment.

Later, it will have to start producing the country's four other *Glossina* species as well, because the goal is to rid all of Ethiopia—which is right on the northeastern edge of Africa's tsetse belt—of the flies. To prevent them from coming back, neighboring countries will have to adopt aggressive control programs as well, Alemu says.

Proven Technology May Get a Makeover

The sterile insect technique (SIT) being tested in Ethiopia relies on two of the most formidable forces in the world: atomic energy and sex. Gamma radiation helps make male insects sterile, and sexual attraction ensures that released en masse, they will find females even in the most remote hideouts.

Although its use in tsetse and malaria control is highly controversial, SIT has allowed several triumphs in insect control over the past 50 years, and its range of applications is expanding even today. Still, some believe the future may be a new, genetic version of SIT—one that keeps the sex but eliminates the radiation. One advantage is that it does not require the use of gamma ray sources, which terrorists could use to make dirty bombs.

Scientists knew as early as the 1920s that x-rays and ionizing radiation produce dominant lethal mutations in male insects that effectively make them sterile. The idea to use sterility to control populations was developed independently in the 1930s and 1940s in the British colony of Tanganyika, the Soviet Union, and the United States.

In the 1950s, U.S. pioneers Edward Knipling and Raymond Bushland put the idea in practice to fight the screwworm fly, a major pest whose larvae feed on the flesh of livestock and other animals. After a successful test run on the island of Curaçao, they took on Florida, and later, all of the U.S. states where the screwworm reigned. After victory was declared in 1966, the battle moved south, where through international cooperation, the flies were rolled back all the way through Mexico and Central America. Last year, a new screwworm-rearing plant was opened in Panama that produces 150 million flies weekly to guard the current frontier, close to the Colombian border.

SIT is also widely used to prevent or suppress infestations of the Mediterranean fruit fly. A global pest, Medfly is a threat to everything from apples to tomatoes and pomegranates; being "Medfly-free" brings countries important trade benefits. Medfly factories have sprung up around the world. The largest, in Guatemala, produces more than 125 billion flies a year for several countries; huge numbers are dropped every week over the port cities of Los Angeles, Tampa, and Miami to prevent stowaways from causing outbreaks.

Two months ago, a new Medfly-rearing plant was opened in the Spanish province of Valencia, a major citrus-exporting region. Meanwhile, a SIT program also helped eliminate the melon fly from islands in southern Japan between 1972 and 1993; and in the Netherlands, a company called The Green Fly sells environmentally conscious

High costs, uncertain outcome

The critics barely know where to begin.

A technique that can drive down a population by 95% or 99% can also get rid of the remaining flies, says Stephen Torr of the University of Greenwich in the U.K. "There's nothing magical about that level," he says, and past experience proves it.

Tsetse were wiped out of an 11,500-km^2 area in the western province of Zambia using odor-baited targets; Botswana got rid of tsetse flies in the 16,000-km^2 Okavango Delta in 2 years by aerial spraying of very low amounts of insecticides, to which tsetse are extremely sensitive. ("They only have to look at it to drop dead," Edinburgh's Maudlin says.)

And there are many other reasons why SIT cannot work and is the wrong thing to try in Africa, critics say. Approximately 10 million km^2 are infested, and there are 29 species and subspecies, of which at least seven are important from an economic or public health standpoint. Extrapolating from the experience in Zanzibar's 1600 square kilometers, infested by just one species, it would take 3500 centuries and $67 billion to do the same in all of Africa, David Molyneux of the Liverpool School of Tropical Medicine sneered in a 2001 commentary. What's more, experience shows that as a result of political instability, poor infrastructure, and bad governance, such complex operations aren't sustainable in Africa, says Maudlin.

Finally, some say, the investments needed are too high given the uncertain outcome. IAEA doesn't fund SIT projects; however, it provides technical assistance, with countries picking up most of the tab. "Can you ask Ethiopia to spend $12 million on a factory if you're not even sure the technique will work on mainland Africa?" asks Bart Knols, a former IAEA staffer who's now at Wageningen University in the Netherlands. "To me, that's an ethical question." (The total cost is unknown but will be much higher than $12 million, because the project is expected to take decades.)

Zimbabwe's Vale says that IAEA, in its zeal to promote nuclear technology, has lost sight of all these problems.

"Nonsense," answers Assefa Mebrate, an Ethiopian ecologist and one of the founding fathers of the country's SIT project. IAEA didn't sell the country on anything, he says; it was Ethiopian scientists who saw SIT's potential and convinced the government to invest in it. And the expense is well worth it if it can bring about a permanent reduction in poverty. Mebrate deplores the fact that the

Will it fly? A worker in the mass-rearing facility outside Addis Abeba looks at a cage of tsetse flies.

Fruitful fight. Factories around the world produce billions of sterile Mediterranean fruit flies every week to protect the global fruit industry.

onion farmers sterile male onion flies.

But lately, the spread of gamma ray sources such as cobalt-60 and cesium-130 to politically volatile countries has sparked concern. That's one reason the SIT lab at the International Atomic Energy Agency (IAEA) near Vienna, Austria, is now experimenting with x-rays as a way to sterilize males.

A new method called "Release of Insects Carrying a Dominant Lethal" (RIDL) may provide another solution. Developed by Oxford University entomologist Luke Alphey and colleagues (*Science*, 31 March 2000, p. 2474), the technique doesn't actually sterilize released males but instead equips them with a gene that is lethal when expressed in females. As a result, they can only have male offspring, which in turn can only produce males, and so on. Models show that this can wipe out a population just as quickly as SIT, Alphey says.

The technology, now in development at a company called Oxitech in Oxford, U.K., has already been used to create RIDL Medflies, Mexican fruit flies, and *Aedes aegypti* mosquitoes, which transmit the dengue virus. Entomologist Paul Reiter, who's currently testing the behavior and fitness of Alphey's *Aedes* mosquitoes at his Pasteur Institute lab in Paris, calls RIDL "very promising." Many other entomologists are now using genetic tricks to make mosquitoes unable to transmit disease that could "replace" natural populations (*Science*, 30 March, p. 1777), but Reiter believes wiping out populations, as RIDL does, is more likely to work. However, RIDL comes with some of the same problems (see main text) as classical SIT.

For the IAEA insect lab, a driving force behind many of the breakthroughs, radiation-free techniques would spell the end of its raison d'être: promoting peaceful cooperation in nuclear technology. But Jorge Hendrichs, who heads the section, is not worrying yet, because RIDL still has to prove its mettle. "The proponents of these molecular approaches underestimate the step from a small-scale lab experiment to an operational program," he wrote in an e-mail to *Science*. **–M.E.**

vocal opposition, which he describes as a "cult," has made donors shy of funding SIT in Africa.

The head of IAEA's Insect Pest Control Section, Jorge Hendrichs, declined to be interviewed about tsetse and urged *Science* to instead write about SIT's success in the fight against the codling moth, a pest of pome fruit and walnut trees. But he did send a nine-page response to a list of e-mailed questions. "The IAEA is pushing nothing, but responds to demands from its member states," Hendrichs wrote. "This is an Ethiopian project under the **COMPLETE** control of the Ethiopians." It's a "fallacy" to think that conventional techniques can always kill off a population, he wrote, and IAEA believes in a role for SIT where they can't. "It is morally detestable," he added, to claim that Africans should learn to live with the … problem because they are not capable of making projects sustainable."

Pie in the sky?
The debate has also engulfed Africa's larger project, the Pan African Tsetse and Trypanosomiasis Eradication Campaign (PATTEC). Called into life by African leaders at a meeting in Togo in 2000, PATTEC advocates SIT as one tool in the continent-wide battle. Indeed, SIT is part of tsetse programs coordinated by PATTEC in Tanzania—which still has the fly factory from the Zanzibar campaign—and in Uganda and in Kenya, both of whom plan to build one. But even Mebrate, who firmly believes in the Ethiopian project, has doubts

that Tanzania and Uganda can succeed with SIT, because they are targeting areas that are surrounded by infested areas and are thus much more prone to reinvasion.

PATTEC head John Kabayo, a Ugandan biochemist who spent 6 years as a researcher at the IAEA lab, says, "People like to debate this issue until the cows come home." He tries to avoid it, he says, because it's diverting attention from the real work. Insecticide spraying and targets will remain PATTEC's main tools, Kabayo says, and SIT is "a backup option."

Blood bank. To feed tsetse flies, cow blood, provided for free by a local slaughterhouse, is sterilized, frozen, and stored in a freezer.

Meanwhile, a similar controversy is simmering over SIT's usefulness in combating malaria. With IAEA support, Sudan has just embarked on a project to fight the *Anopheles arabiensis* mosquito from the Nile valley in its Northern State; construction of a special mosquito factory is planned for Khartoum.

Knols, who works as a consultant on the project, says that at IAEA, he repeatedly questioned whether Sudan, too poor to buy malaria drugs and bed nets, should pay for a SIT feasibility study. Given the lack of qualified staff, logistical nightmares, and the strained tensions with the Sudanese government as a result of the Darfur crisis, the country "probably wasn't the best place" to study the approach either, he adds.

Paul Reiter of the Pasteur Institute in Paris calls the idea to tackle malaria in Africa with SIT "complete pie in the sky."

In Kaliti, the debate does not seem to bother the team managing the fly factory too much. They're mainly eager to get on with the project. Just recently, they have started releasing small numbers of sterile males in the project area, a day's drive from Kaliti. They are testing whether the sterile males can survive in nature and are still attractive to wild females—neither of which is guaranteed after 50 generations of lab life.

The first results are very promising, says Alemu, who is convinced that the project—which he hopes will become a source of national pride—will eventually bear fruit. "We are very confident that we can do it, and we must succeed," he says. "Ethiopia cannot live with the tsetse fly." **–MARTIN ENSERINK**

ECOLOGY

Getting at the Roots of Killer Dust Storms

East Asia's dust storms are growing in number and ferocity. A simple experiment to wean villagers off destructive land practices suggests a way to tame the yellow blizzard

BAYINHUSHU, CHINA—When Nasen Wuritu was a boy in this village in Inner Mongolia, "the grass grew as tall as an adult," he says. In the 1960s, cows grazed year-round and never went hungry. After Nasen Wuritu reached adulthood, however, throngs of livestock had denuded the land, forcing him and other herders to spend precious cash on animal feed. Hand in hand with this crisis was a rising frequency and intensity of dust storms. "People couldn't go outside, and we had to light candles in the middle of the afternoon," says Nasen Wuritu, now 50.

In Bayinhushu, those hard times have passed. On a late spring day here, lush hills roll toward the horizon and the air is clear despite a steady wind. After a 5-year effort, the people of Bayinhushu—with help from officials and an army of ecologists, botanists, and economists—have restored the pastures. And dust storms here have abated.

Bayinhushu is a rare bright spot in a bleak landscape. In the arid grasslands of northern China and Mongolia, overgrazing, over-cultivating, and squandering of scarce water resources have created a massive dust bowl where winds sweep topsoil away. Dust storms regularly blight eastern China, Korea, and Japan, closing schools, damaging jet engines, and triggering respiratory ailments as far away as California. A particularly nasty storm in May 1993 resulted in 85 deaths, the

loss of 120,000 head of livestock, and the destruction of more than 4400 houses and 2.3 million hectares of crops, according to the Chinese Academy of Forestry Sciences. The economic toll in China alone is approximately $650 million a year, says Wang Tao, a physical geographer who heads a national project to combat desertification.

Things are likely to get worse before they get better. Wang, who is based at the Cold and Arid Regions Environmental and Engineering Research Institute of the Chinese Acad-

Taking root. Jiang Gaoming shows how dense grass roots hold soil in place.

emy of Sciences (CAS) in Lanzhou, estimates that northern China's arid grasslands are being degraded at a rate of 3600 square kilometers—an area bigger than the U.S. state of Rhode Island—every year. Wang predicts that as a result, dust storms, which have increased in number nearly sixfold over the past 20 years, will become more frequent, more intense, and more deadly.

If the lessons of Bayinhushu can be applied across the vast steppes once ruled by Genghis Khan, dust storms should diminish. But there are challenges to implementing sustainable land practices in China's northern provinces. "Ecologically, it is easy to control dust storms. Economically, it is difficult," says Bayinhushu project leader Jiang Gaoming, a plant ecologist at the CAS Institute of Botany in Beijing. Solutions must be tailored to the needs of local residents and ecological conditions in each region. Complicating the picture, top Chinese officials still hew to discredited policies that aim to subdue dust storms by conquering the deserts. "We have a lot of convincing to do," Jiang says.

The perfect dust storm

The basic anatomy of East Asia's dust storms is fairly well established. For starters, the common term "sand storms" is a misnomer. Sand particles are too heavy to get lifted high into the atmosphere. Thus, little of the dust

A green revolution. Restricting grazing (*inset*) allowed this pasture in Inner Mongolia to recover naturally.

that blights East Asia comes from deserts, where erosion over the millennia has carried away most of the smaller particles. Studies indicate that the dust originates in dry lakebeds and arid lands on desert fringes. In these regions, a crust forms on undisturbed soil, giving some resistance to wind erosion. But in springtime, that crust is broken up by plowing and livestock, which also strip the land of new growth and pound soil into dust.

Meanwhile, the temperature difference between a chilly atmosphere and a surface warmed by intensifying spring sunlight creates updrafts that lift dust into the air. As air streams south and east from Siberia, the winds bump up against the mountain ranges that ring northern China and Mongolia, forming low-pressure pockets that suck airborne dust into the upper atmosphere. Easterly winds sweep the particulate matter to Beijing, Seoul, Tokyo, and sometimes across the Pacific Ocean to North America.

There are good years and bad years. Heavy snows add moisture to the soil, dampening dust in early spring. Conversely, without snow cover, soil dries out during winter and is more prone to wind erosion.

This dynamic has persisted for centuries, as have dust storms. But the storms have been worsening. Seoul, which bears the brunt of East Asia's dust storms, suffered "dust events" on 23 days during the 1970s, 41 days in the 1980s, 70 days in the 1990s, and 96 days so far this decade, according to the Korea Meteorological Administration.

The primary reason for this onslaught, most scientists believe, is degradation of fragile ecosystems. The population of Xilingol League, the district that includes Bayinhushu, increased from about 200,000 in the late 1940s to more than 950,000 in 2000, Jiang says. Over that period, herds of grazing animals skyrocketed from around 1 million head to more than 24 million, while the grazing area shrank from 5 hectares per animal to about one-tenth of a hectare.

Staggering growth such as this occurred all across northern China. The national government encouraged nomadic herders to settle in villages and multiply herds to boost incomes, says Jiang. Livestock created an

CREDIT: JEFF SCHMALTZ/MODIS RAPID RESPONSE TEAM/NASA

ever-widening ring of denuded land around settlements. The government also encouraged Han Chinese farmers to migrate to northern regions to "tame the deserts" with artificial oases and irrigation. The migrants cleared land for farms and cut brush for fuel. Irrigation gradually dried up many lakes and rivers. The result, Jiang says, is that 90% of China's grasslands, an area encompassing 4 million square kilometers, are degraded.

Authorities have long recognized the problem, but attempted fixes have been futile if not counterproductive. Since 1978, China has spent at least $1 billion planting trees in arid and semiarid regions to combat desertification, says Luo Yiqi, an ecologist at the University of Oklahoma in Norman, who with colleagues at the Cold and Arid
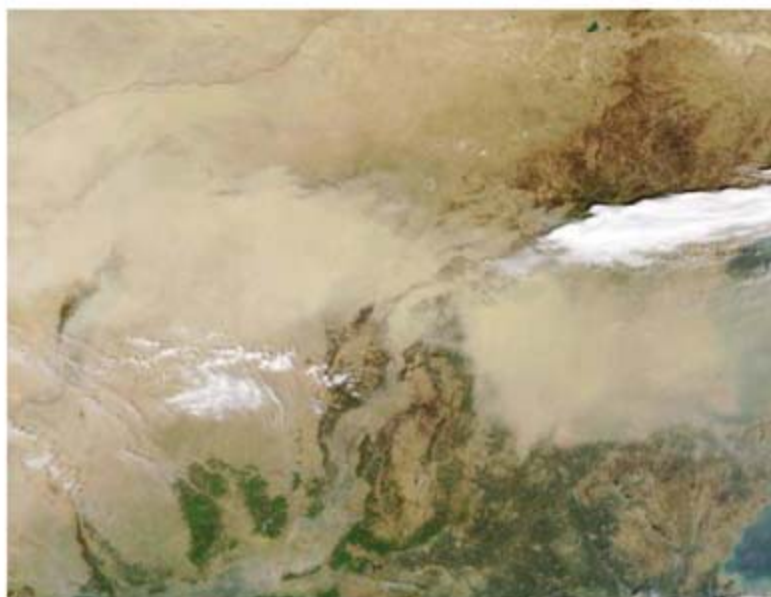
Don your masks! Beijing gets battered by dust in this 28 April 2005 image captured by NASA's Terra satellite.

Regions Institute has studied such afforestation efforts.

Afforestation is misguided, Luo asserts. "People proposed the idea without considering ecological principles," he says. "They set out to create forests in regions where forests naturally do not grow due to limited precipitation." The tree of choice has been the poplar. If watered, poplars grow rapidly, but without intensive care, they die. Sticks protruding from barren earth—dead poplar saplings—line roads in Inner Mongolia. Where poplar groves become established, Luo says, the deeply rooted trees hemorrhage water through transpiration, lowering the water table and making it harder for native grasses and shrubs to survive.

China's tree-planting campaign has successfully reforested areas with ample rain, says Luo. But planting poplars in arid

regions, he says, "does not help combat desertification." The government continues to pour money into afforestation, regardless of water resources, through a bureaucracy whose mission is to plant trees. "It is time for the Chinese government … to scientifically evaluate long-term policies," Luo says.

Sustainable living

In 2000, CAS applied a scientific approach to dust storms by funding five grassland-restoration pilot projects, including Jiang's. Jiang headed for Zhenglan County, a subdivision of Xilingol League, partly because the Institute of Botany has a research station there that had documented the loss of 12 centimeters of topsoil to wind erosion in the past 24 years. Another reason: Beijing is only 180 kilometers south. "If [the land] is degraded here, the dust will affect Beijing," Jiang says.

Realizing that the key to solving the dust problem is involving the people who live on the land—a big task given, Jiang says, "their poverty and their level of education"—he invited onto his team social scientists and economists as well as ecologists and animal husbandry specialists. The goal was to improve the lives of villagers while reducing environmental degradation. At the start of the 5-year, $600,000 project, Bayinhushu consisted of 72 households with 316 people and 11,560 head of livestock—75% sheep and goats, the rest cattle. The village manages 7330 hectares of land, much of it communal pasture.

Jiang's team calculated that villagers could boost incomes if they reduced sheep and goat numbers and introduced an improved breed of dairy cattle, while curtailing open grazing. It was not easy to convince them, however. Mongols consider the size of the herd a measure of wealth. To help overcome doubts, local authorities chipped in additional incentives: They dug wells and extended the power grid to Bayinhushu to run pumps and electrify houses. The county also improved the dirt track connecting the village to a paved road.

The villagers agreed to ban grazing on 2670 hectares of communal rangeland to allow vegetation to recover. Harvesting hay from this land in autumn provided enough forage for a smaller number of livestock during a typical winter, eliminating the expense of commercial feed. To tide the villagers over while the land recovered, Jiang's team planted corn on several dozen hectares.

Less is more. Nasen Wuritu saw his income increase after raising fewer animals.
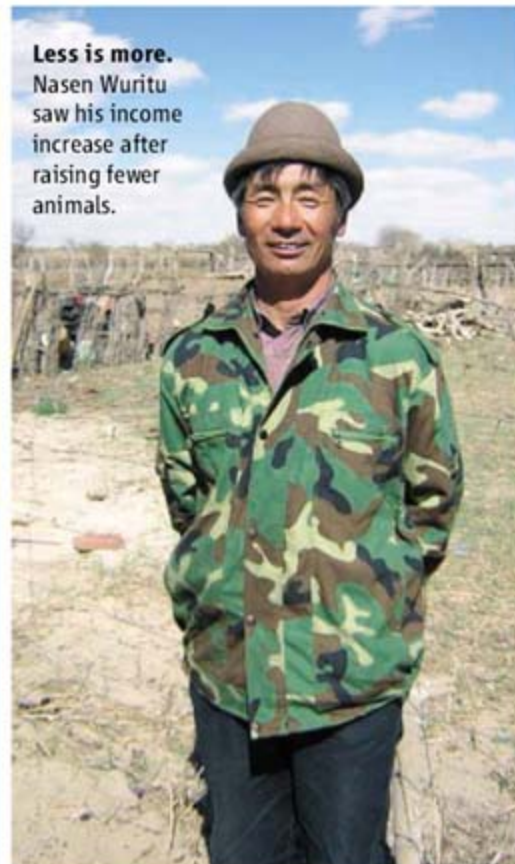
Jiang's team made some mistakes along the way. More than half of the initial budget went to aerial grass seeding and planting trees to form windbreaks. Both proved "a waste of money," Jiang says. The trees died, and sown plots fared no better than those left to recover naturally.

By and large, however, the simple plan worked. The villagers grew enough corn to feed animals without grazing in the common pasture. Herds were reduced to 5783 head, a little over half of which were sheep and goats. Milk production doubled per head. By the end of the third summer, the grass had recovered to provide more than enough hay for the village's needs.

Five years later, Jiang says, the land looks much as it probably did a century ago. Annual incomes have increased 46%, from $315 to $460 per capita. In Nasen Wuritu's living room, a framed ceramic relief of Genghis Khan hangs on the wall. A large-screen TV and a satellite dish in the front yard pipe in previously unimagined entertainment. "We used to joke that there was nothing for Mongols to do at night but sleep and make babies," Nasen Wuritu says. And the dust storms, which used to drive people indoors once or twice a month, are now occasional nuisances.

Bayinhushu is a "good example" of grassland restoration, Wang says. In an encouraging sign, herders in nearby villages are restricting grazing on communal pastures. Still, the Bayinhushu experience may not be easy to replicate in places with less favorable ecological conditions. Jiang notes that Bayinhushu had sufficient topsoil replete with seeds, and groundwater levels had not been affected by excessive irrigation.

Severe degradation may require "human facilitation of the restoration process," says Lu Qi, a desertification specialist at the Institute of Forestry in Beijing. After studying restoration projects on the Tibetan Plateau, where extreme degradation has created shifting sand dunes, Lu found that a hands-off approach led to a slow and spotty revegetation and little stabilization of the dunes. In contrast, erecting sand barriers and planting soil-stabilizing shrubs promoted the healthy recovery of native plants. Because shifting dunes smother new vegetation before it can take root, Lu argues that active intervention is needed to reverse desertification.

The toughest task may be to undo the harm wrought by artificially expanding oases, like one at Minqin, between the Tengger Desert and the Badain Jaran Desert in Gansu Province, west of Inner Mongolia. Beginning in the 1950s, irrigation on a massive scale helped establish thousands of farms but eventually dried up natural rivers and depleted groundwater, fueling the expansion of the two deserts. Earlier this year, provincial authorities ordered 10,500 people to vacate farms in a 1000-km^2 area surrounding Minqin within 3 1/2 years.

Wang says that resettling the farmers elsewhere "may relieve some problems in this area but cause new problems in another area." It would be better, he argues, to introduce water-conservation techniques, such as those pioneered in Israel, which might allow sustainable farming in the area.

At Bayinhushu, Jiang continues to measure the experiment's results and explore ways to further raise village incomes. The project is leaving an unexpected legacy. Before the project began, Nasen Wuritu says, village youngsters typically dropped out of school after the compulsory 9 years. But the scientists who spent time in the village exposed the youngsters to the Internet and text messaging. "Many young people realized the importance of an education," he says. Exhibit A is Nasen Wuritu's eldest son, now studying to be a veterinarian at Inner Mongolia University in Hohhot. "He wants to stay in the city to pursue a better life," Nasen Wuritu says. That would mean one less person eking out a living on the grasslands—and a greater chance of enjoying an environment increasingly liberated from dust.

–DENNIS NORMILE

With reporting by Gong Yidong of *China Features*.

GENOME SEQUENCING

The Greening of Plant Genomics

As the National Plant Genome Initiative turns 10, it is beefing up its bioinformatics and its portfolio of sequenced crop and noncrop genomes

In the genomics world, plants are second-class citizens. Researchers have sequenced the DNA of hundreds of microbes and dozens of animals, yet they have deciphered the genomes of just three plants, *Arabidopsis*, rice, and poplar—four, if you count *Chlamydomonas*, an alga. Comparisons between finned, legged, and feathered species have yielded tremendous insights into the evolution of these organisms. Yet plant biologists still lack the ability to compare the genomes of their favorite species, let alone begin to construct a coherent history of plants. No wonder plant researchers are complaining.

At a 6 July workshop to evaluate the 10-year-old National Plant Genome Initiative (NPGI), experts in bioinformatics, plant breeding, and biotechnology called for more plant genomes to be sequenced and lamented the dearth of computational and analytical tools to evaluate genomes. Yet, at the same time, they praised the program for its progress to date. Over the past decade, NPGI has spent $780 million finding genes and sequencing plant DNA. That's a drop in the bucket, compared to more than $3 billion available from the National Human Genome Research Institute for decoding the genomes of humans and other animals, notes Jeff Dangl of the University of North Carolina, Chapel Hill. "Plant genomics research is a huge bang for the buck," argues Dangl, who chairs the National Research Council panel charged with reviewing NPGI and recommending future directions.

Congress kicked off this multi-agency program in 1998. With prompting from U.S. corn growers, it earmarked $40 million for the National Science Foundation (NSF) to usher plants, in particular corn and other crops, into the genomics era. Now 10 years later, NSF, with additional support from the U.S. departments of Agriculture and Energy (DOE) and other federal agencies, has sponsored hundreds of genome-related projects.

But researchers are clamoring for more DNA. At the meeting, Erik Legg of Syngenta, which is based in Research Triangle Park, North Carolina, called for more crop genomes. Eric Ward of the Two Blades Foundation in Durham, North Carolina, which supports the development of disease-resistant crops, cited the need for species that represent all the plant groups. Others argued for "resequencing" species from different places whose genomes are already known—say, *Arabidopsis*—to get a sense of the natural variation.

Workshop participants also decried the genome initiative's lack of progress in bioinformatics. Funding agencies supported the sequencing of many animal species to help interpret the human genome. Toward that end, centralized databases, such as Ensembl, developed ways to compare genomes and look for conserved genes and pathways. That hasn't happened in the plant world. As a result, "data resources are balkanized," complains Lincoln Stein, a bioinformaticist at Cold Spring Harbor Laboratory in New York state. For *Arabidopsis* sequence information, researchers go to a database called TAIR, but for corn, they head to MaizeGDB. "[You] can't go and see a comprehensive comparison between *Arabidopsis* and rice," notes Ward. "It's frustrating."

Stein and others called for the integration of the various plant genome databases and for the establishment of uniform standards for characterizing genes and other DNA. "If you don't do this, your comparisons between genomes are utterly meaningless," says Suzanna Lewis, a bioinformaticist at Lawrence Berkeley National Laboratory in California.

NSF, DOE, and its collaborating agencies are taking steps to address these complaints. In late 2005, NSF awarded Washington University in St. Louis, Missouri, $29.5 million to sequence corn. Potato, tomato, and soybean sequencing is also under way. DOE's Joint Genome Institute in Walnut Creek, California, plans to devote increasingly more of its sequencing capacity to plants and microbes, curtailing its work with animals, says JGI's Daniel Rokhsar. All told, about two dozen species are in the sequencing hopper.

NSF is pushing for better bioinformatics as well. It is reviewing proposals for a "plant cyberinfrastructure," which will have the computers and know-how to meld the various sequence, gene-expression, functional genomics, and mutant databases to make possible one-stop shopping for genomics. NSF plans to spend up to $10 million a year for 5 years—10 years at most—to make these genomic resources accessible and to train researchers how to use them. Training is key, says Dangl. NPGI has "brought the mind frame of genomics to plant systems where there wasn't much before," he notes.

Indeed, NPGI has become "the major basic science program for plants," says Jeffrey Bennetzen of the University of Georgia, Athens. The initiative will never have the resources of the National Human Genome Research Institute, but it is slowly lifting plants from second-class status.

–ELIZABETH PENNISI

Plants in Sequencing Pipeline

Common Name	Scientific Name	Genome Size
Club Moss	*Selaginella moellendorffii*	88 Mb
Thale Cress*	*Arabidopsis thaliana*	130 Mb
Pink Purse	*Arabidopsis lyrata*	230 Mb
Shepherd's Purse	*Capsella rubella*	250 Mb
Peach	*Prunus persica*	270 Mb
Purple False Brome	*Brachypodium distachyon*	355 Mb
Monkey Flower	*Mimulus guttatus*	430 Mb
Rice*	*Oryza sativa*	430 Mb
Poplar*	*Populus trichocarpa*	480 Mb
Grape	*Vitis vinifera*	500 Mb
Barrel Medic	*Medicago truncatula*	550 Mb
Sorghum	*Sorghum bicolor*	736 Mb
Cassava	*Manihot esculenta*	760 Mb
Potato	*Solanum tuberosum*	840 Mb
Cotton	*Gossypium raimondii*	880 Mb
Tomato	*Solanum lycopersicum*	950 Mb
Soybean	*Glycine max*	1115 Mb
Maize	*Zea mays*	2600 Mb

* Published sequences.

LETTERS

edited by Etta Kavanagh

Reminding Scientists of Their Civic Duties

THE VERY WISE FORMER CONGRESSMAN SHERWOOD BOEHLERT OF THE HOUSE SCIENCE Committee said, "If scientists are going to be more effective participants in the policy arena, they have to … learn more about the policy work" ("S&T Forum: States, industry play key role in U.S. innovation drive," AAAS News and Notes, 25 May, p. 1140). For over 40 years, I have been urging the scientific societies (like AAAS, American Chemical Society, American Physical Society, and Materials Research Society, to which I belong) to stop merely, again and again, berating the public's "scientific illiteracy" and turn all that energy to fixing the unbelievable policy illiteracy of scientists. For years I have tested this, in talks at largish audiences in society meetings. Over 90% typically admitted to not being able to name their two senators and congressperson. Very, very few recognized what the "House Science Committee" was or did.

"Physician (or physicist, chemist, biologist), heal thyself!" A regular clever quarter-page lesson on contemporary "civics" in *Science* might be a start and a recurring reminder of scientists' responsibilities as citizens.

RUSTUM ROY

Evan Pugh Professor of the Solid State Emeritus and Professor of Science, Technology, and Society Emeritus, The Pennsylvania State University, University Park, PA 16802, USA; Visiting Professor of Medicine, University of Arizona; Distinguished Professor of Materials, Arizona State University. E-mail: rroy@psu.edu

Insula Damage and Quitting Smoking

IN THEIR REPORT "DAMAGE TO THE INSULA disrupts addiction to cigarette smoking" (26 Jan., p. 531), which is based on a retrospective study of patients who had brain lesions, N. H. Naqvi et al. conclude that damage to the insula was responsible for the disruption of nicotine dependence in some cases. The claim is consistent with an earlier report describing a young man who lost interest in abuse of substances after a selective bilateral stroke of the globus pallidus (1), which is an important neural target of the insula (2). However, methodological limitations inherent in brain lesion studies undermine the validity of conclusions derived from this study.

The main outcome measure is a recall of smoking behavior, especially the differentiation of "quitting smoking with difficulty" from "quitting smoking." In the present sample, smoking cessation took place on average 8 years earlier, which introduces the probability of a major recall bias, especially when studying damage to brain areas with memory function, including the insula (3). In addition, retrospective assessment of the interval between the occurrence of the actual brain lesion and its detection on a diagnostic scan is difficult. The nonselectivity of brain lesions makes the interpretation of brain site–related loss of function particularly difficult. The authors used MRI and CT scans that may not be sensitive enough to detect potentially relevant brain lesions.

We suggest that before any firm conclusions about the insula's involvement in nicotine dependence are established, the results of this retrospective study need to be verified using prospective studies and a more rigorous methodology. Validated human behavioral laboratory techniques could be used to measure craving as well as subjective and reinforcing effects of cigarettes (4) in stroke patients or in surgical patients before and after planned resections of the insula. One could study patients with seizure-recording electrodes along the insular surface. Individual electrodes can be stimulated to transiently block the function of the area of interest, and the impact of focal disruption can then be assessed. Anatomical information (MRI, CT) should be supplemented with an assessment of functional integrity through imaging (PET, functional MRI) and neuropsychological testing (1).

The history of addiction treatment is plagued with examples of scientific evidence misused to justify treatments without appropriate safety and efficacy testing. Premature conclusions based on unconfirmed data lead to unfounded hope and bitter disappointments for desperate patients and their families. More than 1000 patients in China and Russia reportedly underwent brain surgery for addiction before the procedure was stopped by the respective governments (5, 6). Although Naqvi et al. do not advocate surgery, we caution that the study should not be (mis)taken as evidence justifying insula surgery to cure addiction. The study has too many methodological flaws that make a firm conclusion or even enthusiasm premature. We are hoping that future controlled prospective studies and application of human laboratory techniques can improve the validity of derived conclusions.

STANISLAV R. VOREL,[1] ADAM BISAGA,[1] GUY MCKHANN,[2] HERBERT D. KLEBER[1]

[1]Department of Psychiatry, Division on Substance Abuse, Columbia University/New York State Psychiatric Institute, New York, NY 10032, USA. [2]Department of Neurological Surgery, Columbia University/New York State Psychiatric Institute, New York, NY 10032, USA.

References
1. J. M. Miller et al., Am. J. Psychiatry **163**, 786 (2006).
2. S. M. Reynolds, D. S. Zahm, J. Neurosci. **25**, 11757 (2005).
3. T. Fujii et al., Neuroimage **15**, 501 (2002).
4. K. A. Perkins, M. Stitzer, C. Lerman, Psychopharmacology (Berl.) **184**, 628 (2006).
5. C. Orellana, Lancet Neurol. **1**, 333 (2002).
6. W. Hall, Addiction **101**, 1 (2006).

Response

WE SHOWED THAT SMOKERS WITH DAMAGE to the insula were more likely than smokers with damage in other brain regions to be able to quit smoking easily, immediately, without

[1]Division of Cognitive Neuroscience, Department of Neurology, University of Iowa Carver College of Medicine, Iowa City, IA 52242, USA. [2]Laboratory of Computational Neuroimaging, Department of Neurology, University of Iowa Carver College of Medicine, Iowa City, IA 52242, USA. [3]Dornsife Cognitive Neuroscience Imaging Center, University of Southern California, Los Angeles, CA 90089, USA. [4]Brain and Creativity Institute, University of Southern California, Los Angeles, CA 90089, USA.

*To whom correspondence should be addressed. E-mail: bechara@usc.edu

relapsing, and without a persistent urge to smoke. Our conclusion from this result, combined with the results of previous functional imaging studies (1–3) and an established theoretical framework for insula function (4, 5), was that insula damage interferes with a specific psychological process that makes it difficult to quit smoking and that promotes relapse, namely, the conscious urge to smoke. We are confident that the anatomical and behavioral techniques we used were appropriate for our data and adequate to support this conclusion.

We entirely agree with Vorel et al. that our findings do not justify invasive treatments for smoking addiction. We never suggested in our Report or anywhere else that surgically damaging the insula would be a viable therapy for smoking addiction. Indeed, we join Vorel et al. in strongly condemning any surgical manipulation of the insula to achieve a therapeutic aim. Apart from the historical excesses of psychosurgery, there is clinical evidence that insula damage can impair a variety of functions, such as language (6), attention (7), and mood (8), and can cause significant cardiovascular morbidity (9). Although our results do have therapeutic implications—for example, the development of drugs that target insula functions, behavioral therapies that address the bodily/visceral components of smoking, and functional imaging of insula activity to monitor the progress of treatments—we never used the term "cure" to describe any aspect of our findings.

The fact that our study was retrospective raises a valid concern about recall bias. This is why we excluded patients who had impairments of long-term memory and obtained information from collaterals whenever it was available. The possibility

still exists, however, that insula damage disrupted memory for the emotional experience of quitting, such as memory for how difficult it was to quit and for urges that were felt after quitting. This possibility seems unlikely, especially given the vivid descriptions of the experience of quitting provided by some of our patients. Also, we found a strong trend for patients with insula damage to be more likely than patients with damage in other regions to be abstinent at the time of the study (i.e., to have quit smoking after lesion onset), a finding that was not susceptible to recall bias. Nonetheless, we agree with the need for prospective studies and have already begun such studies.

Vorel et al. point out certain technical limitations that are inherent to all human lesion studies, most notably the problem of nonselectivity of lesions. We addressed this problem through an analysis that looked at effects in regions surrounding the insula. Through this analysis, we found that the insula was the only region in which lesions had a significant effect on smoking addiction. By including a larger number of subjects and employing more precise voxel-based lesion mapping techniques, future studies may be able to detect effects of lesions in other regions that possibly play a role in addiction and may be able to trace effects within subregions of the insula.

Our goal in performing this study was not the immediate discovery of a "cure" for smoking addiction, but rather to shed light on a brain region that has been largely ignored in the drug addiction literature. We hope that our findings spur further research on this topic, which ultimately could lead to better treatments for smoking addiction.

NASIR H. NAQVI,[1] DAVID RUDRAUF,[1,2] HANNA DAMASIO,[3,4] ANTOINE BECHARA[1,3,4]*

References
1. G. J. Wang et al., Life Sci. **64**, 775 (1999).
2. K. R. Bonson et al., Neuropsychopharmacology **26**, 376 (2002).
3. A. L. Brody et al., Arch. Gen. Psychiatry **59**, 1162 (2002).
4. A. R. Damasio, The Feeling of What Happens: Body and Emotion in the Making of Consciousness (Harcourt, Chicago, 2000).
5. A. D. Craig, Nat. Rev. Neurosci. **3**, 655 (2002).
6. A. Ardila, Aphasiology **13**, 79 (1999).
7. F. Manes, S. Paradiso, J. A. Springer, G. Lamberty, R. G. Robinson, Stroke **30**, 946 (1999).
8. F. Manes, S. Paradiso, R. G. Robinson, J. Nerv. Ment. Dis. **187**, 707 (1999).
9. H. Ay et al., Neurology **66**, 1325 (2006).

Not Necessarily the First

THE NEWSMAKERS ITEM "OPENING UP" (11 May, p. 811) states that "German physicist Romano Rupp of the University of Vienna in Austria has become the first non-Chinese person to be named science dean at a Chinese university." In fact, George W. Groff, a Penn State graduate in horticulture, was dean of the College of Agriculture at Canton Christian College in Guangzhou, China, from 1922 to 1941 (1). Canton Christian College became Lingnan University, whose College of Agriculture merged with that of Sun Yat Sen University in 1952 to form South China Agricultural College, now South China Agricultural University, with a current enrollment of 36,000 students. Groff began teaching horticulture in China in 1907, beginning a century of partnership between Penn State and South China Agricultural University that is still thriving in the form of training and research collaboration in plant biology, including a joint Laboratory of Root Biology inaugurated by the presidents of South China Agricultural University and Penn State on May 29 of this year. Rupp appears to be (at least) 85 years late to merit the title of "first non-Chinese science dean at a Chinese university."

JONATHAN P. LYNCH

Department of Horticulture, College of Agricultural Sciences, Pennsylvania State University, University Park, PA 16802–4201, USA.

Reference
1. Lingnaam Agric. Rev. **1**, 1 (1922).

CREDIT: PHOTOS.COM

CORRECTIONS AND CLARIFICATIONS

News Focus: "Population geneticists move beyond the single gene" by E. Pennisi (22 June, p. 1690). The individuals pictured on page 1691 are from Siberia, not North and South America.

This Week in Science: "The root of the problem" (8 June, p. 1391). The first sentence of this item was incorrect. Although mosses do exhibit a relatively primitive life-style, mosses have both haploid gametophyte and diploid sporophyte phases.

News Focus: "A new twist on training teachers" by J. Mervis (1 June, p. 1270). The article misspelled the name of Jason Ermer, a master teacher in the UTeach program at the University of Texas, Austin.

Random Samples: "Country cooking" (25 May, p. 1105). The last sentence is incorrect. It should read, "The device may not cut down on wood consumption, but tests suggest it will make use of up to 30% of a wood fire's energy, much more than an open fire's 7% efficiency."

News Focus: "Putting the brakes on psychosis" by C. Schmidt (18 May, p. 976). The brain scans of schizophrenic patients shown on page 976 were meant to illustrate that the brains were changing rapidly, not to suggest that the therapy described in the article could prevent such changes. The patients received medication before and during the period when scans were taken.
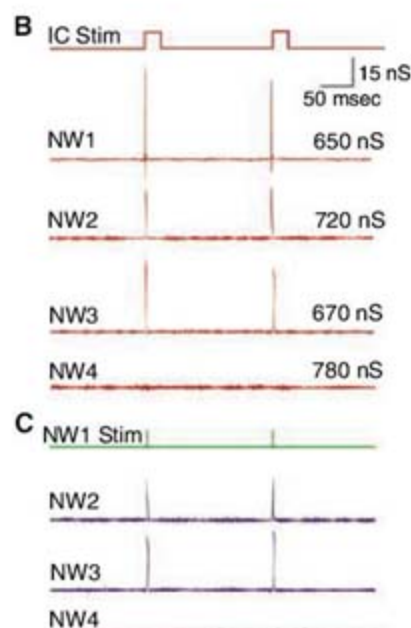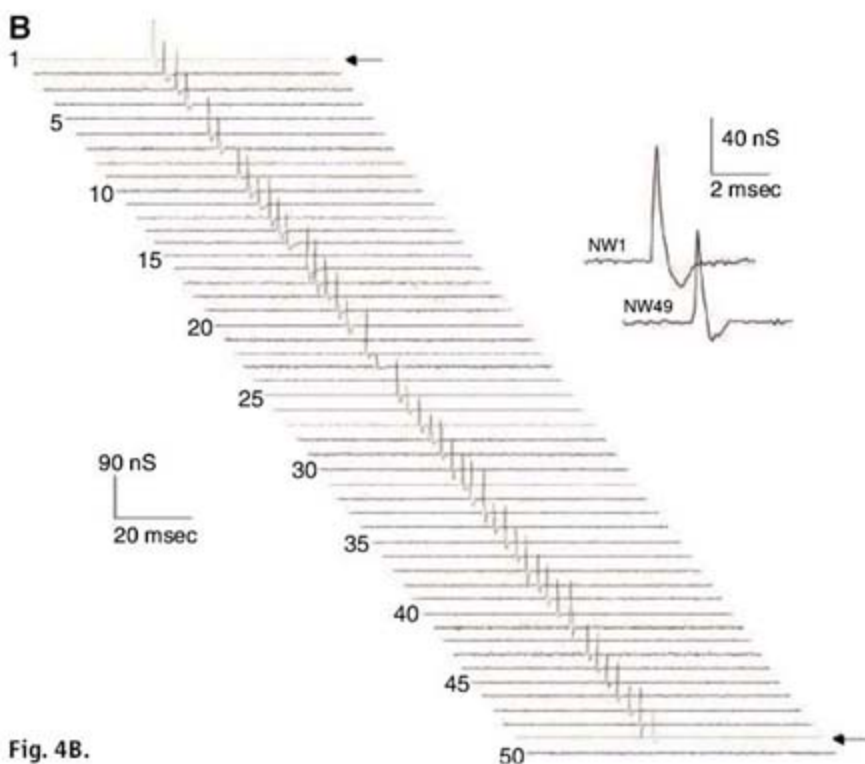
News Focus: "Closing the net on common disease genes" by J. Couzin and J. Kaiser (11 May, p. 820). The table on page 822 incorrectly listed the sample size of a 2005 genome-wide association study in macular degeneration. The study included 146 people, not 1700.

News Focus: "Thymosins: clinical promise after a decades-long search" by J. Marx (4 May, p. 682). Hynda Kleinman was incorrectly identified in the article. She is a former intramural scientist at the National Institute of Dental and Craniofacial Research.

Editors' Choice: "Reducing together" (27 April, p. 516). The paper covered in this item [C. W. Kim et al., J. Am. Chem. Soc. 129, 10.1021/ja0706347 (2007)] has now been retracted by the editor of that journal.

Reports: "Detection, stimulation, and inhibition of neuronal signals with high-density nanowire transistor arrays" by F. Patolsky et al. (25 Aug. 2006, p. 1100). The trace for NW2 in Fig. 2C and the inset for NW49 in Fig. 4B were incorrect. Additionally, the IC trace in Fig. S4A was improperly plotted on the time axis. The corrected Fig. 2C is shown to the left with the replotted Fig. 2B. There are minor differences between the original and replotted versions of Fig. 2B due to export settings in the plotting software. Fig. 4B is shown below with the corrected inset. The replotted trace for Fig. S4A is now available in the Supporting Online Material for the Report. In the original Fig. S4A, the arrows showing current injection were misplaced; in the corrected version, injection is indicated by the region of more positive membrane potential. These errors occurred during the final production of the figures, and none of the results or conclusions of the paper are affected. The authors apologize for these errors in the published paper. In addition, the authors would like to clarify several points. (i) Detailed timing analysis was done from data files in IGOR Pro (WaveMetrics, Inc., Portland, OR) and not from composed figures. (ii) In Fig. 1D, the intracellular and nanowire signals were measured on different computers with small timing offsets between the data sets and were not intended to show precise relative timing. (iii) In Fig. 2F, the published scale bar refers to the scale of each individual trace; however, they are arbitrarily offset relative to each other for clarity. (iv) In Fig. 4B, data were measured sequentially after multiple stimulations, not simultaneously. (v) In Fig. S2, the baseline similarities between NW3 and NW5 are real and most likely caused by coupling to ground noise fluctuations and the use of similar lock-in amplifier parameters for data acquisition. (vi) In Fig. S6A, the neuron was stimulated over the course of four hours. However, the cell was impaled with the IC pipette only during the first and last several minutes of the experiment to confirm neuronal response and viability.

Reports: "Optical signatures of the Aharonov-Bohm phase in single-walled carbon nanotubes" by S. Zaric et al. (21 May 2004, p. 1129). Some of the data and conclusions presented as novel in the Report were previously presented in S. Zaric et al., Superlattices Microstructures **34**, 413 (2004), which was part of a proceedings volume from the 6th International Conference on New Phenomena in Mesoscopic Structures and the 4th International Conference on Surfaces and Interfaces of Mesoscopic Devices. The authors now realize that this reference should have been indicated.

Fig. 2B and C.

Fig. 4B.

TECHNICAL COMMENT ABSTRACTS

COMMENT ON "Redefining the Age of Clovis: Implications for the Peopling of the Americas"

Gary Haynes, David G. Anderson, C. Reid Ferring, Stuart J. Fiedel, Donald K. Grayson, C. Vance Haynes Jr., Vance T. Holliday, Bruce B. Huckell, Marcel Kornfeld, David J. Meltzer, Julie Morrow, Todd Surovell, Nicole M. Waguespack, Peter Wigand, Robert M. Yohe II

Waters and Stafford (Reports, 23 February 2007, p. 1122) provided useful information about the age of some Clovis sites but have not definitively established the temporal span of this cultural complex in the Americas. Only a continuing program of radiometric dating and careful stratigraphic correlations can address the lingering ambiguity about the emergence and spread of Clovis culture.

Full text at www.sciencemag.org/cgi/content/full/317/5836/320b

RESPONSE TO COMMENT on "Redefining the Age of Clovis: Implications for the Peopling of the Americas"

Michael R. Waters and Thomas W. Stafford Jr.

Haynes et al. misrepresent several aspects of our study. Our revised dates and other archaeological data imply that Clovis does not represent the earliest occupation of the Americas, and we offered both human migration and technology diffusion as hypotheses to explain the expansion of Clovis. We stand by the data and conclusions presented in our original report.

Full text at www.sciencemag.org/cgi/content/full/317/5836/320c

OCEANS

Fragile Frontiers in the Abyss

Cindy Lee Van Dover

Accounts of the biology of the deep sea tend to focus on the epic efforts undertaken to gain access to this humanly inhospitable environment and on the strange animals that live there. *The Silent Deep* pays homage to these same themes but stands apart from other books about life in the abyss due to Tony Koslow's thoughtful accounts of deep-water fisheries, mineral exploitation, habitat destruction, and contamination of the deep-ocean wilderness and his call for new strategies for managing ocean resources. Although his prose lacks the poetry that Rachel Carson brought to her books about marine life at the edge of the sea, Koslow succeeds in painting a picture of the deep sea as an environment with inherent and threatened value.

> **The Silent Deep**
> The Discovery, Ecology, and Conservation of the Deep Sea
>
> *by Tony Koslow*
>
> University of Chicago Press, Chicago, 2007. 292 pp. $35, £22.50. ISBN 9780226451251. University of New South Wales Press, Sydney, Australia. Aus $49.95. ISBN 9780868404158.

The author's credentials as a proponent of deep-ocean conservation efforts are impeccable. For a decade, Koslow led the deep-water ecology program at the Australian Commonwealth Scientific and Industrial Research Organization in studies of biodiversity associated with seamount coral reefs that are threatened by the effects of commercial trawling. He has lately been engaged in using our limited knowledge of ocean ecosystems to inform international policy-makers as they prescribe laws to manage the seas for the benefit of humankind.

The deep ocean represents the largest volume of richly inhabited biosphere on our planet. As Koslow relates, at present it can be a tricky business to offer informed science of such an expansive system. We have only the barest skeleton of baseline knowledge and an incomplete understanding of components, processes, and dynamics in deep-sea systems. Deep-sea scientists work in an environment where each day of effort using a submersible or tethered vehicle can cost more than $50,000. Although we have become efficient at extracting the most information possible

from each visit to the seafloor, the cumulative precious minutes of submersible research add up to a pitifully small record of observation on an annual basis, myopically centered on pinpoint locales in a literal sea of habitat.

Our dilemma is squarely before us in Koslow's chapter on climate change and the deep sea. As the climate warms, deepwater circulation patterns change, increased carbon dioxide levels acidify the ocean, patterns of primary productivity at the surface reorganize, and methane-hydrate deposits shift to new equilibrium states. There is little doubt that these and other climate-induced changes will affect deep-ocean life, but the manners in which effects will be expressed are nearly impossible to predict or to document because we have scant understanding of how deep-sea ecosystems operate in the first place. While we have all but abandoned the view that deep-sea organisms are exquisitely adapted to a stable and unvarying environment, we have only a modest understanding of physiological tolerances of organisms and ecological responses of populations and ecosystems to changes in basic parameters like temperature, oxygen content, pH, current regimes, and food supply. We wonder at the strange animals captured

in deep-sea trawls, revel in the unsuspected diversity of life dwelling in the cold muds of the seafloor, and celebrate the beauty of deep-sea hot springs and cold-water coral reefs. Dramatic deep-sea discoveries unfold year after year, but Koslow reminds us that this "pristine" ocean wilderness is being trampled by the insidious "human footprint across the deep sea": the seabed suffers a nightmarish legacy of tens of thousands of merchant ships sunk and rotting on the seabed, hundreds of thousands of tons of military ordnance scuttled in deep water, millions of curies of radioactive waste and 17 nuclear reactors dumped at depth with no attempt at containment, and residual DDT and PCBs accumulating in deep-sea food chains.

Koslow offers a litany of new ventures with the potential to challenge and insult the deep sea even as they reap economic and societal benefits: Just three decades after the first discovery of hot springs on the seafloor there is a rush to strip-mine their gold-rich ores. Fields of manganese nodules on abyssal plains and cobalt-rich crusts on the sides of seamounts inspire capacity building in nation states with strategic as well as economic interests in exploitation of deep-ocean resources. Pharmaceutical companies prospect for new drugs and genetic resources from the sea. A burgeoning carbon economy provides incentive for commercial interests to experiment with unchecked schemes to fertilize ocean meadows and to develop deep-water carbon lakes. Commercial ventures such as these will have uncertain consequences on deep-sea biodiversity and the sustainability of deep-ocean ecosystem services.

Koslow closes *The Silent Deep* with a

BROWSINGS

The Deep. The Extraordinary Creatures of the Abyss. Claire Nouvian. University of Chicago Press, Chicago, 2007. 256 pp. $45. ISBN 9780226595665.
Abysses. Fayard, Paris, 2006. €40. ISBN 9782213625737.
Weirdness and beauty are often paired in the 170 species portrayed in this visual survey of deep-sea diversity. Nouvian provides the color photos, most taken by researchers, with extended captions that describe the animals' lifestyles and habitats. For example, the swimming sea cucumber *Enypniastes eximia* "undulates slowly and gracefully through the water, sometimes even rather far from the bottom." Short topical essays from eminent deep-sea biologists (including Koslow and Van Dover) cover related aspects of marine science, history, and conservation.

The reviewer is at the Division of Marine Science and Conservation, Nicholas School of the Environment and Earth Sciences, Duke University, 135 Duke Marine Lab Road, Beaufort, NC 28516, USA. E-mail: clv3@duke.edu

chapter on "the way forward," written with Kristina Gjerde, a respected expert on international ocean governance, and Craig Smith, a preeminent deep-sea biologist. The authors focus on policy and conservation options that address threats posed by high-seas bottom trawling, including a global moratorium on deep-sea trawling, regulation of demersal fisheries, and establishment of marine protected areas. They briefly tackle the broader policy needs for sustainable use and conservation of the global deep ocean in national and international waters.

We are on the cusp of engaging in commercial activities that have the potential of exerting substantial impacts on the quality of deep-ocean ecosystems; there is only a brief window of opportunity for setting policy in place before habitats are compromised. Such policy, internationally sponsored and international in scope, can be holistic and precautionary, rather than a reaction to environmental catastrophe.

A forward-thinking approach has immense advantage over negotiating and implementing policy after financial capital is invested, wilderness resources consumed, and habitats destroyed. Koslow provides us with a report on the current status of the ocean depths. Now is the time to chart a path toward rational conservation strategies and sustainable resource uses that acknowledge and accommodate the many gaps in our understanding of the deep ocean.

DEVELOPMENTAL BIOLOGY

Passage to Global Stem Cells

M. Ian Phillips

When President George W. Bush took office in January 2001, he quickly made it clear that he was not in favor of research on human embryonic stem cells. That August he sealed off access to federal funds for research on all but a few (now suboptimal) lines of human embryonic stem cells. His action not only caused stem cells to become a national political issue but also emboldened any country that wanted to compete with the United States in this research. The global race to establish dominance in a field with enormous scientific, health, and commercial possibilities was on, but with U.S. participants denied federal funding.

In *Cell of Cells*, Cynthia Fox brings her impressive talent as a science writer and journalist to telling the story of this race. The hefty book offers a great read for anyone interested in the topic. Fox makes the story an adventure. She carries us to unlikely places, beginning with a camel ride to the Pyramids with an Egyptian stem cell researcher. She then flies to Israel to meet the scientist with whom the Egyptian wanted to collaborate (politics made it impossible). Israel's Joseph Itskovitz-Eldor provided four of the five lines to Jamie Thomson for their seminal paper on the first human embryonic stem cells (*1*).

With a journalist's eye, Fox details her interviewees' offices, labs, mannerisms, and habits—even the views they see each day. Those details, impossible to obtain from a scientific paper, make the researchers come alive. Moving on to Singapore to describe stem cell work in the lavish research city of Biopolis and then on to Australia, Japan, China, and Korea, Fox accurately reveals the sociological and technical issues that stem cell research involves. For nonscientists, she gives pithy but effective explanations without disturbing the flow; for scientists, the book is a smooth read because Fox does not dumb down scientific terminology. The knowledge she acquired in her journeys is astonishing in range and depth, and she cites papers from the primary literature as rungs on the ladder to her overview. (The book includes 43 pages of references and interview notes.)

Fox creates indelible images. Her fly-on-the-wall description of a kidney transplant and chimeric stem cell operation at Massachusetts General Hospital is riveting, as is the almost smelly account of extracting oocytes for tissue cloning from pigs. In Jerry Yang's lab, she witnesses the Star Wars–like drama of remotely controlling pipettes to enucleate oocytes for somatic cell nuclear transfer. She tells the desperate stories of patients with heart failure, autoimmune disease, kidney failure, and Duchenne's dystrophy. She also warns of the trap of unethical, unscientific stem cell treatments in locations such as Moscow, Ukraine, and the Caribbean.

This is not a book to be read while multitasking. Fox explains complex concepts and introduces numerous places and people. There are plenty of main characters—including Irv Weissman, Ron McKay, Shimon Slavin, Alan Colman, Ian Wilmut, Steve Minger, Wise Young, Doug Melton, Mahendra Rao, and the now disgraced Woo Suk Hwang—and some appear repeatedly.

The author's fascination with "science trouncing science fiction," the potential of stem cells, and our desire to learn what happens next make this a rare can't-put-it-down science book. It reminds me of the fun of first reading *The Double Helix* (*2*). There are fights between and within labs, gossip, and different cultures, but there are also knowledge and exhilarating progress. *Cell of Cells* is a serious book, spiced up by Fox's wit and storytelling.

Cell of Cells
The Global Race to Capture and Control the Stem Cell

by Cynthia Fox

Norton, New York, 2007. 558 pp. $26.95, C$35.50. ISBN 9780393058772.

What might have originally been the climax of the book occurred when Hwang became the first to publish work claiming the generation of a human embryonic stem cell line from a cloned blastocyst (*3*). South Korea seemed poised to win the race to therapeutic cloning, but the tale became a Greek tragedy of hubris and downright lies. It was as if in the space race Neil Armstrong had faked the Moon landings. Hwang's seeming triumph unraveled, slowly at first and ever faster as many of his claims were undermined. Because Fox wrote the book between 2003 and 2005, she probably had to go back and add "appeared to" or "apparently" to every reference to Hwang's results and then create a new last chapter, "The Fall of Seoul and the Rise of San Francisco." She writes, "the Woo Suk Hwang fraud is the biggest in science history in terms of the number of guilty parties."

Bush has twice vetoed congressional bills to increase federal funding for human embryonic stem cell research. *Cell of Cells* illustrates the consequences for global science, states that fund their own researchers, and the dashed hopes of those who need potential treatments. Fox eloquently chronicles the consequences of this isolationist policy and squarely advocates a rational approach to funding research on both adult and embryonic stem cells.

References
1. J. A. Thomson *et al.*, *Science* **282**, 1145 (1998).
2. J. D. Watson, *The Double Helix: A Personal Account of the Discovery of the Structure of DNA* (Atheneum, New York, 1968).
3. W. S. Hwang *et al.*, *Science* **308**, 1777 (2005).

The reviewer is at the Keck Graduate Institute, 535 Watson Drive, Claremont, CA 91711, USA. E-mail: ian_phillips@kgi.edu

SUSTAINABILITY

Education for a Sustainable Future

Debra Rowe

Sustainability is being integrated into higher-education institutions' mission and planning, curricula, research, student life, and operations.

S ustainability is a lens through which increasing numbers of individual colleges and universities, as well as national organizations, are collectively examining and acting upon our shared world systems (*1*, *2*). In the United States, a national trend has begun, but much more needs to be done.

College and University Actions

Sustainability is being integrated into U.S. institutions' mission and planning, curricula, research, student life, operations and purchasing, and community partnerships. Students and staff at hundreds of campuses are engaged in sustainability committees and actions, including the following: learning to focus on acquiring sustainability knowledge and application skills; sustainability-oriented film festivals, speakers, and other campus events; socially and environmentally responsible criteria for purchasing and endowments; infusion of sustainability into the general education core requirements, courses, disciplines, whole colleges, and specialized degrees; and regional and global approaches to sustainability in collaboration with businesses, government, nongovernmental organizations (NGOs), and kindergarten through high school (K–12) education.

Core requirements at many universities and colleges (e.g., Portland State University, Miami Dade Community College, University of Minnesota) include the components of sustainability education, even if the word sustainability is not specifically used. Degrees in sustainability have sprouted up at dozens of institutions [see (*3*) for a listing]. In the Campus Climate Challenge, students on over 400 campuses are working with administrators and staff to measure and reduce greenhouse gas emissions (*4*) and are voluntarily raising student fees and changing energy policies to move to renewable sources.

U.S. business, architecture, and engineering schools are in the forefront of sustainability education. Architecture and engineering schools have criteria for accreditation that require students to be able to understand and implement sustainable design. Nonprofit organizations such as Engineers for a

California students working to save energy on campuses.

Sustainable World and Engineers without Borders have developed. The World Resources Institute and the Aspen Institute have worked with business schools to develop case studies and business curricula that include sustainability principles and practices (*5*). Increasingly, interdisciplinary learning experiences focus on our sustainability challenges.

The purchasing power alone of colleges and universities, as they demand more environmentally and socially responsible products and processes, can help move sustainability from its present niche markets to become the standard in product and process design. This can be expressed through commitments to sustainable behaviors and policies in institutional mission and planning; more energy-efficient and greener buildings and operations; substantial purchases and installations of renewable energies and commitments to carbon emissions reductions and neutrality; sustainability audits and reporting; and sustainable living campaigns in the residential halls. For example, over 300 presidents have signed commitments and taken action to move toward carbon neutrality and to eliminate greenhouse gas emissions. Michigan State University, NYU (New York University), University of California at Berkeley, the Pennsylvania State University, and others have conducted sustainability audits and reports. Sustainability-oriented residential living practices are in place at Bowdoin, Carnegie Mellon, Dartmouth, Harvard, Tufts, University of Vermont, and Yale. Rutgers and the National Association for Educational Procurement have focused on developing resources for the purchasing side

of sustainability (*6*, *7*). Stanford University has developed both environmental and social screens for their endowments.

A statement drafted by the Business Sector Team of the U.S. Partnership calls upon higher education to make sustainability education a requirement for all undergraduates. Participating members came from both small and large corporations—from media conglomerates to energy companies such as Duke Energy and consumer products such as Burt's Bees. "All students need to learn, through an interdisciplinary approach, not only the specifics of our sustainability challenges and the possible solutions, but also the interpersonal skills, the systems thinking skills, and the change agent skills to effectively help to create a more sustainable future. We are looking for these sustainability educated students as future business people, as employees, as consumers, innovators, government leaders and investors" (*8*).

Activities of National Organizations

After the United Nations declared a Decade of Education for Sustainable Development (2005–14), a grassroots effort from higher education developed in the United States in the absence of a federal government response. The National Council for Science and the Environment hosted its annual conference in 2003 on Education for a Sustainable and Secure Future. Out of that meeting, the U.S. Partnership for Education for Sustainable Development (*9*) was created to catalyze a U.S. response for this decade and beyond. This national network of over 300 organizations has sector teams in Faith, Business, Communities,

President of the U.S. Partnership for Education for Sustainable Development, Washington, DC 20037, USA; E-mail: dgrowe@oaklandcc.edu

Higher Education, K–12 schooling, and Youth. The U.S. Partnership convenes mainstream leaders and catalyzes their commitment to educating for a sustainable future. With impetus from multiple sources interested in sustainability, three major efforts emerged in the higher-education sector: the Higher Education Associations Sustainability Consortium (HEASC), the Disciplinary Associations Network for Sustainability (DANS), and the Association for the Advancement of Sustainability in Higher Education (AASHE).

The HEASC (*10*) was formed to advance sustainability in the mainstream higher education associations and in the system of higher education itself. HEASC members currently represent about half of the U.S. college and university presidents; about half of all of the boards of trustees, and many, if not most, facilities directors, business officers, college and university planners; purchasers; and staffs of residential housing, student affairs, and campus activities. Projects include the Higher Education Climate Action Partnership (*11*) to measure and reduce greenhouse gas emissions, support for the American College and University Presidents' Climate Commitment for clean energy, carbon-neutral campuses (*12*), and professional development initiatives on sustainability.

DANS (*13*) was formed after the U.S. Partnership asked the Association of American Colleges and Universities (*14*), the AASHE (*15*), and the Association of University Leaders for a Sustainable Future (*16*) to cohost meetings of more than 20 disciplinary associations to discuss each discipline's potential contributions to a more sustainable future. These meetings included national associations for psychology, sociology, philosophy, religion, biology, chemistry, engineering, anthropology, political science, math, broadcasting, architecture, women's studies, and others. Working groups are focusing on infusing sustainability into curricula, professional development, standards (including tenure, promotion, and accreditation criteria that value sustainability research and action), cross-disciplinary projects, legislative briefings, and ways to educate the public about how to help create a sustainable future (*17*).

AASHE (*15*) serves colleges and universities in the United States and Canada. It offers an extensive resource center of sustainability initiatives and policies, discussion lists, sample syllabi showing how sustainability can be infused into various courses, a biennial conference, and professional development opportunities. AASHE also publishes an electronic-mail bulletin and an annual digest with campus sustainability news stories, resources, events, and job opportunities.

Moving Forward

For real progress, the implementation has to be broad (across all higher education institutions) and thorough. We need to make sure that none of the courses currently being taught in the United States reflect the old, inaccurate paradigms such as "endless resources" and "man conquers nature." Textbooks need to describe our sustainability challenges and the contributions each discipline can make to the solutions. Funders have to support such work. The National Science Foundation should encourage a sustainability focus in its grants to STEM (projects to increase students' interest in science, technology, engineering, and mathematics) and other areas and should fund interdisciplinary coursework and research. Other governmental funding sources, foundations, and corporations need to understand and support this trend.

Through sharing stories of how people have made a difference in society and by providing assignments that focus on solving real sustainability issues, educators can engage students and help institutions and the larger society turn toward more sustainable behavioral and policy norms. Students can learn and practice via such assignments how to be more environmentally, economically, and socially responsible and how to support policies and legislation that support a sustainable future. Imagine what might happen if students were regularly assigned actual sustainability problems that were brought to higher education by cities, businesses, nonprofit organizations, and other institutions. If classroom exercises produced workable contributions to solutions, students would understand they can have a positive impact on the world through their academic learning. Most of our higher education institutions include somewhere in their mission statements goals for preparing students to help create a better society, yet this ideal is often not fully implemented. Given the challenges of sustainability and the need for policy and behavioral modifications, we need to change our emphasis from critical thinking alone to the inclusion of effective change-agent skills and opportunities to take action on campus and off. A matchmaking Web site listing real-world sustainability projects from business, government, and nonprofit organizations available to students, faculty, and volunteers has just been launched (*18*).

To have a sustainable future, sustainability education has to be implemented at the K–12 levels as well. There are examples of innovation, including the Sustainable Schools Project sponsored by Shelburne Farms in Vermont (*19*); the Educating for Sustainability master's of education program at Antioch University training teachers for the K–12 level (*20*); and the global sustainability resources produced by Facing the Future (*21*), including K–12 curricula, community service activities, and teacher preparation programs.

However, state standards and assessments primarily emphasize writing, reading, and math, often do not relate to societal problems and solutions, and create barriers to learning about sustainability. The K–12 sector team of the U.S. Partnership has created draft sustainability education standards, has compiled resources for K–12 teachers, and has just begun a process similar to what was done in higher education to convene the national leaders in K–12 education and to share information to catalyze their commitment to sustainability.

Right now, sustainability is treated by many as an add-on, as another item on an already full plate. Sustainability needs to be a main focus of our efforts in education. Given the educational and research capacity, the external partnerships, and the position of higher education as an influential voice in society, there is ample opportunity for higher education to help shift societal norms toward a healthier environmental, social, and economic sustainability.

References and Notes

1. A. Cortese, Higher Education Associations Sustainability Consortium (HEASC) presentation, 12 January 2007.
2. For additional information regarding available resources, see the supporting online material.
3. For a listing, see Association of University Leaders for a Sustainable Future (ULSF), www.ulsf.org/resources_sust_degrees.htm.
4. Campus Climate Challenge, www.climatechallenge.org.
5. Beyond Grey Pinstripes, www.beyondgreypinstripes.org.
6. Rutgers, http://purchasing.rutgers.edu/ green/index.html.
7. National Association of Educational Procurement (NAEP) www.naepnet.org/Microsites/sustainability/sustainability.html.
8. Minutes of 30 April 2007 meeting, Business Sector Team, U.S. Partnership for Education for Sustainable Development, Washington, DC, Appendix A.
9. The U.S. Partnership, www.uspartnership.org.
10. HEASC, www.aashe.org/heasc.
11. Higher Education Climate Action Partnership, www.hecap.org.
12. University President's Climate Commitment, www.presidentsclimatecommitment.org.
13. Disciplinary Associations Network for Sustainability, www.aashe.net/dans.
14. Association of American Colleges and Universities, www.aacu.org.
15. Association for the Advancement of Sustainability in Higher Education, www.aashe.org.
16. ULSF, www.ulsf.org/.
17. AAAS is part of this network. Contact Sarah Banas at sbanas@aaas.org to participate.
18. Play a Greater Part, www.playagreaterpart.org.
19. Sustainable Schools Project, www.sustainableschoolsproject.org/index.html.
20. Antioch University, www.antiochne.edu/ed/exed/ss_edforsustainability.cfm.
21. Facing the Future, www.facingthefuture.org/.

ASTRONOMY

Seeing the Surfaces of Stars

Rapidly rotating stars are flattened spheres with poles that are hotter than the equator.

Andreas Quirrenbach

Just as carousel riders would slide away from the center if not held in place, the mass in rotating celestial bodies tends to move toward the equator, giving them an ellipsoidal bulge. This effect is well known for Earth, which has an equatorial radius some 20 km larger than the polar radius. The Sun is only slightly flattened because of its slow rotation rate, with an equatorial radius exceeding the polar radius by only one part in 10^5.

Other stars, however, rotate very rapidly. On page 342 of this issue, Monnier et al. (1) present images of Altair, also known as α Aquilae, one of the three stars of the Summer Triangle. These images clearly show that

still limited by diffraction at the telescope's aperture. Even the largest current telescopes see all but a handful of the very largest cool stars as mere points of light.

To obtain images of Altair's surface, Monnier et al. had to combine the light from four telescopes of a six-element array located on Mt. Wilson near Los Angeles. In such interferometric arrays, the resolution is given by the separation between the individual telescopes, not their sizes; Monnier et al. could thus use a "telescope" with an effective size of 265 m by 195 m. There is, however, a price to

the rotation rate and viewing geometry of Vega, it will be possible to improve instrument calibrations.

Stellar rotation also has strong implications for our understanding of the formation and evolution of galaxies. Because distant galaxies cannot be resolved into individual stars, their observed properties cannot be interpreted without the use of stellar population models. These models assume that these galaxies contain a certain mix of stars with a prescribed distribution of masses and ages; these stars are collectively responsible for the light emitted by the distant galaxy. Rotation affects the outward appearance
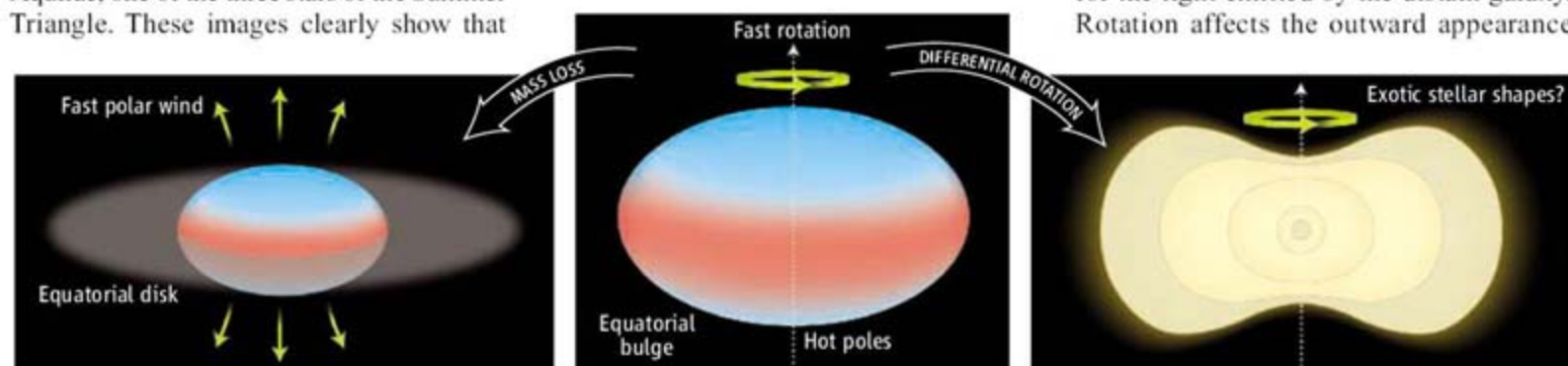
Stellar shapes. (Center) Rapidly rotating stars develop an equatorial bulge, which is cooler (and thus redder) than the polar regions, as seen by Monnier et al. **(Left)** Radiation pressure drives a fast wind from the polar regions if they are sufficiently hot, whereas disks are frequently formed in the equatorial plane. **(Right)** Stars in which the rotation rate decreases strongly with distance from the axis may have unusual shapes (with convective regions shaded) [diagram adapted from (8)].

Altair is flattened by more than 20% and that the polar region is much brighter than the equatorial zone. This agrees with the theory of stellar structure, which holds that variations of the gravity across a stellar surface must be accompanied by variations in temperature (2). For Altair, the centrifugal force counteracting the gravitational attraction near the equator therefore causes cooling—and thus reduced brightness—with respect to the poles (see the figure, center panel). Not only does the work of Monnier et al. tell us something new about this particular object, it also shows that detailed imaging of other unusual stars will be possible.

Astronomical images taken by ground-based telescopes are normally degraded by turbulence in Earth's atmosphere. Researchers have recently developed ways to compensate this atmospheric blurring with adaptive optical systems, but the resolution achievable is

pay for substituting a huge telescope with a small number of meter-sized ones: Instead of getting an instant detailed image, one obtains a set of rather abstract data that do not easily lend themselves to intuitive interpretation. Monnier et al. have now succeeded in producing synthetic images of Altair through computer processing of these interferometric data.

Such methods are causing astronomers to reassess some of the conventional wisdom. Interferometric observations of Vega (α Lyrae, also in the Summer Triangle) have recently shown that this star is a rapid rotator, too (3, 4). Unlike Altair, however, we see this star nearly pole-on. Vega had long been used as a standard star for the calibration of ground-based and spaceborne telescopes and instruments. Some of the assumptions underlying these calibrations now appear to be on shaky ground, as they were based on spherically symmetric stellar models. Such models do not take into account the influence of rotation on the structure of the star, or whether one sees predominantly the equatorial or polar regions. Now that we know

and emitted spectrum of stars, the rate at which they lose mass, and their interior structure, which in turn determines how fast the stars burn their hydrogen supply and how they evolve over time. To avoid misinterpreting galactic spectra, the assumed stellar population must therefore contain the correct mix of stars with different rotation rates, as well as the correct recipes for their structure and evolution.

For individual stars, rotation has a dramatic influence on mass loss and winds (see the figure, left panel). Imagine spinning up a star; the centrifugal forces would rise until at some point they overwhelm the gravitational attraction and the star flies apart. We do not know how closely stars can approach this critical rotation rate, but it appears that centrifugal forces can facilitate the loss of mass and the formation of disks in the equatorial plane. On the other hand, the fact that the poles can be substantially hotter than the equatorial regions can give rise to a separate mass-loss mechanism, namely the generation of a fast wind through radiation pressure. It is likely

The author is at the Landessternwarte Königstuhl, University of Heidelberg, D-69117 Heidelberg, Germany. E-mail: a.quirrenbach@lsw.uni-heidelberg.de

that equatorial disks and polar winds can coexist in single objects; both phenomena lend themselves to imaging studies with interferometer arrays (5, 6).

A solid body like Earth must rotate uniformly, with all parts completing a revolution in the same time. This is not true for gaseous bodies. We have long known that the equatorial regions of the Sun need about 25 days for one revolution, whereas the polar regions take several days longer. Through the analysis of tiny oscillations of the Sun with methods analogous to those used to infer the structure of Earth from seismic events, astronomers have determined the rotation rate for the interior of the Sun (7).

Monnier et al. compared their observations to the simplest possible model, which assumes uniform rotation. They found subtle discrepancies, which could well be explained by a modest amount of nonuniform rotation. Models of stars with strong differential rotation predict not-so-subtle modifications of the overall stellar structure; in extreme cases the stars might have nonconvex shapes halfway between a sphere and a donut (8). It is not known whether such "exotic" stars exist, but they could be discovered with present-day interferometers.

Elucidating the dramatic effects of rotation is but one of the contributions that interferometry can make to stellar astrophysics. With telescopes separated by several hundred meters, current facilities are well suited to measuring the "global" properties of stars. A future array with 20 to 30 telescopes on kilometric baselines could produce much more detailed images of stellar surfaces, revealing star spots, eruptions, and convection patterns, and enabling studies of complex phenomena that today can be measured only in the Sun.

References

1. J. D. Monnier et al., Science 317, 342 (2007); published online 31 May 2007 (10.1126/science.1143205).
2. H. von Zeipel, Mon. Not. R. Astron. Soc. 84, 665 (1924).
3. J. P. Aufdenberg et al., Astrophys. J. 645, 664 (2006).
4. D. M. Peterson et al., Nature 440, 896 (2006).
5. A. Quirrenbach et al., Astrophys. J. 479, 477 (1997).
6. F. Malbet et al., Messenger 127, 37 (2007).
7. M. J. Thompson, Astron. Geophys. 45, 21 (2004).
8. K. B. MacGregor, S. Jackson, A. Skumanich, T. S. Metcalfe, Astrophys. J. 663, 560 (2007).

NEUROSCIENCE

Brainwashing, Honeybee Style

Queen bee pheromones prevent young bees from learning to sting until they leave the hive, which makes the hive safer.

C. Giovanni Galizia

In the 1932 novel *Brave New World*, Aldous Huxley created a society where fetuses develop in bottles and are treated with chemicals to modify their bodies and mentalities (1). Later, children are sleep-conditioned to their future task in society. This procedure creates people who have clear roles, putting them in castes, ranging from alphas (the leaders) to epsilons (the drones). Among other things, lower castes are programmed not to be aggressive against higher caste members. A treatment with neurotoxic chemicals (including alcohol) during development leads to the appropriate brain changes. On page 384 of this issue, Vergoz et al. (2) elucidate some of the chemical cues that influence learning and development in an actual animal caste system—the honeybees.

Within the animal kingdom, social insects have evolved the most stable caste societies. Many ant species have a wide range of castes, from workers to foragers, from groomers to soldiers (3). Individuals all develop from eggs laid by the same mother—the colony's queen. Generally, the food supplied to each egg is the biological signal that leads the embryo to develop into one caste or another, a situation reminiscent of Huxley's fictional world. Thus, if we take as an example the leaf-cutter ant *Atta texana*, small individuals tend to the fungus garden within the nest, intermediate-sized individuals search and collect leaves from the forest to feed the fungus, and large individuals with strong mandibles defend the colony.

Honeybees have evolved a different caste system: The individual worker bees (always females, because male drones do not contribute to social life apart from mating with queens during nuptial flights) perform different tasks in the course of their lives. The workers start off as nurses tending to the hive right after emergence, continue with tasks such as nest-building and hive defense, and then end their lives as foragers by collecting nectar and pollen to make honey and feed their sisters.

How is this developmental polyethism organized? Age is the main factor that determines the task that an individual will perform, mediated by regulation with juvenile hormone (4), but feedback from the hive is also important. Much information is delivered by pheromones. For example, when a hive loses the queen, her queen mandibular pheromone (QMP) will also disappear, leading to rapid changes in behavior among the worker bees, who start raising new queens to replace her.

However, the life of a honeybee is not hardwired. Bees are amazingly intelligent animals and learn a lot about their environment. In particular, forager bees learn color, odor, and position of nectar-rich flowers and use this information to optimize their harvest. This capacity has been used for many years to learn more about the basic mechanisms underlying appetitive (i.e., food-related) learning and memory, and the honeybee has become an important model animal to this end (5).

Chemical control. Nurse bees surround the queen (identified by the mark) and groom her. This behavior is important for distributing the queen's pheromone, QMP, within the entire hive.

CREDIT: DONALD FERNS/DEPARTMENT OF ZOOLOGY, UNIVERSITY OF OTAGO, NEW ZEALAND

The author is in the Department of Neurobiology, University of Konstanz, D-78457 Konstanz, Germany. E-mail: Galizia@uni-konstanz.de

Recently, it has been shown that bees also learn to associate noxious stimuli, and an experimental paradigm has been developed whereby an odor can be associated with the sting reflex (6). In associative learning, a stimulus without meaning [a conditioned stimulus (CS) such as an odor] is associated with a reinforcer stimulus [an unconditioned stimulus (US) such as sweet nectar or a noxious electric shock]. The US elicits a response, for example, the extension of the tongue to lick the nectar or the extension of the sting for defense. After conditioning, the CS alone (e.g., the odor) will elicit the conditioned response. The neural substrates for an aversive US and for a positive US differ in bee brains, both in terms of the neurons involved and in terms of the neurotransmitter they use. The appetitive US channel uses octopamine as a transmitter (7), whereas the aversive US uses dopamine (6).

Is the learning capacity of a bee related to her developmental succession of tasks? Recent results have created an unprecedented link from molecules all the way to complex behavior, and some of the molecular effects of QMP are now understood. It turns out that QMP directly influences the chemistry of the brain in an age-dependent manner, contributing to developmental polyethism. One major component of QMP is homovanillyl alcohol (HVA), a substance with a striking chemical similarity to the biogenic amine dopamine, the neurotransmitter that mediates aversive learning. Indeed, QMP acts directly on the dopamine pathway: Levels of dopamine in the brain are reduced in young bees exposed to QMP, and this effect is amplified by a concurrent reduction in the levels of dopamine-sensitive receptors (8). Thus, exposure of a nurse bee to the queen's odor down-regulates the brain's dopamine networks and reduces activity levels.

What is the biological consequence of this down-regulation? Vergoz et al. now show that young bees exposed to QMP are not able to learn noxious stimuli. This defect is not a general learning deficit, because appetitive learning is not affected. Furthermore, the deficit is limited to young bees. Specifically, the authors show with aversive conditioning that young bees exposed to QMP cannot learn to extend their sting to an odor that has been presented together with an electric shock, whereas young bees not exposed to QMP are very good at this task. Aversive learning in older bees is also intact.

Thus, the presence of the queen, through her pheromone, influences the behavior, and indeed the brain pharmacology, of her hive. Young workers remain in the hive, are docile, and display less motor activity, whereas older guards and foragers leave the

hive and become more motile and aggressive. Why would aversive learning be blocked in a young nurse bee? Within the hive, the sting reflex can only have negative effects. Thus, preventing nurse bees from developing aversive memories against the odors in the hive, which include the queen's own odor, makes the colony more secure. With increasing age, bees start to leave the colony, fly to distant foraging sites, and perform tasks outside the hive where they need to learn not only about sweet nectar but also about nasty dangers. It is useful, under these circumstances, that the effect of QMP to block aversive learning wanes. This is a wonderful example in which the effect of a releaser pheromone can be followed all the way to the neurons that are being modulated, and then to behavioral modifications.

Thus, honeybees differ substantially from the beings in Huxley's world, because individuals are not trapped within their castes for

their entire life span. The manipulation of brain activity by the queen, modulating learning capacity in young bees to make them more docile, is a different view of parenthood. As the saying goes: When children are young, give them roots; when they grow, give them wings. The bee mother seems to have evolved exactly this strategy for her family.

References
1. A. Huxley, *Brave New World* (Doubleday Doran, Garden City, NY, 1932).
2. V. Vergoz, H. A. Schreurs, A. R. Mercer, *Science* **317**, 384 (2007).
3. B. Hölldobler, E. O. Wilson, *The Ants* (Belknap Press of Harvard Univ. Press, Cambridge, MA, 1990).
4. S. E. Fahrbach, G. E. Robinson, *Dev. Neurosci.* **18**, 102 (1996).
5. R. Menzel, M. Giurfa, *Trends Cogn. Sci.* **5**, 62 (2001).
6. V. Vergoz, E. Roussel, J. C. Sandoz, M. Giurfa, *PLoS ONE* **2**, e288 (2007).
7. M. Hammer, *Trends Neurosci.* **20**, 245 (1997).
8. K. T. Beggs *et al.*, *Proc. Natl. Acad. Sci. U.S.A.* **104**, 2460 (2007).

MICROBIOLOGY

Life on the Thermodynamic Edge

Edward F. DeLong

Metabolic cooperation enables some microbial partners to thrive on low-energy carbon sources that neither partner could utilize on its own.

Microbial life can persist under physicochemical conditions that challenge the very fabric of biological structure and function. In habitats of extreme temperatures, pH's, and salinities, microbes are often the sole inhabitants. But microbial life also exists at another type of extreme: under conditions that yield barely enough free energy for cell maintenance, much less growth. In a recent study of the full genome sequence of the anaerobic bacterium *Syntrophus aciditrophicus*, McInerney et al. (1) reported new insights into some of the fundamental machinery required for living at life's thermodynamic edge.

S. aciditrophicus grows mainly by a symbiotic process known as syntrophy—a metabolic cooperation usually involving two anaerobic microbes, in which each partner depends on the other for growth on a specific substrate (2). For example, *S. aciditrophicus* can efficiently degrade fatty acids or benzoate in the absence of oxygen, but only when a syntrophic partner (typically a hydrogen-con-

suming methanogen or sulfate-reducing bacterium) is around to consume its metabolic waste products (3). Symbiotic hydrogen removal shifts the chemical equilibria, thereby yielding sufficient metabolic free energy for *S. aciditrophicus* to grow while simultaneously feeding its syntrophic partner with energy-rich growth substrates like hydrogen or formate (see the figure). Alone, neither partner can grow well on benzoate anaerobically; the thermodynamics for growth are favorable only when the partners engage in metabolic cooperation (4, 5).

The genome sequence of *S. aciditrophicus* (1) provides new insight into the details of this unusual anaerobic life-style. As expected, the genome encodes little potential for a respiratory metabolism using external terminal electron acceptors like oxygen, nitrate, fumarate, sulfate, or iron. It also lacks many of the genes required for fermentation, the other main pathway for balancing oxidizing and reducing potential in the absence of oxygen. Instead, *S. aciditrophicus* is dependent on the electron-consuming activities of its partners as its primary terminal electron sink.

Although *S. aciditrophicus* cannot grow

The author is at the Massachusetts Institute of Technology, Cambridge, MA 02139, USA. E-mail: delong@mit.edu

on compounds like starch or sugars, it contains four different α-amylase genes encoding proteins that hydrolyze starch. Perhaps it not only feeds hydrogen to other downstream syntrophic partners, but also assists its fermentative neighbors further up the anaerobic food chain in the initial steps of polysaccharide hydrolysis. This could help to ensure that fatty acids—the preferred growth substrate of *S. aciditrophicus*—are supplied as the waste products of its sugar-fermenting cohorts. Such potential for metabolic cooperation both upstream and downstream in the anaerobic food chain emphasizes the fact that many (and perhaps most) microbial metabolic and biogeochemical transformations in nature require coordinated, synergistic interactions within microbial communities.

Adenosine triphosphate (ATP) is the common energy currency of all cellular life. One of the functions of energy metabolism is to ensure an adequate supply of this biochemical fuel. Surprisingly, *S. aciditrophicus* lacks the genes for acetate kinase, one of the central enzymes anaerobes typically use to produce ATP via a substrate-level phosphorylation. However, the presence of nine genes that code for the enzyme acetyl–coenzyme A synthetase suggests that *S. aciditrophicus* employs an alternative reaction also used by acetate-forming Archaea and by anaerobic Eukarya to produce ATP.

The *S. aciditrophicus* genome sequence also provides evidence for various mechanisms to generate cellular energy potential via different types of ion-translocating pumps. Of special interest is the presence of a membrane-bound ion-translocating complex (called Rnf-type) that is unlike those found in most microbes, with the exception of other syntrophic microorganisms. McInerney *et al.* propose (*1*) that this complex uses the potential energy stored in ion gradients to couple the oxidation of NADH (nicotinamide adenine dinucleotide, reduced) to the reduction of ferredoxins, which are required for critical biosynthetic reactions.

The characterization of microbial syntrophic interactions has provided important clues about the metabolic interactions that drive matter and energy cycling, especially in anaerobic habitats. One take-home lesson has been the importance of studying microbial interactions in mixed cultures and in the environment, in addition to pure cultures. Many metabolic and biogeochemical transformations will only occur in the context of the interspecies interactions.

In syntrophic interactions between marine archaeal methanotrophs and sulfate-reducing bacteria, the anaerobic oxidation of methane
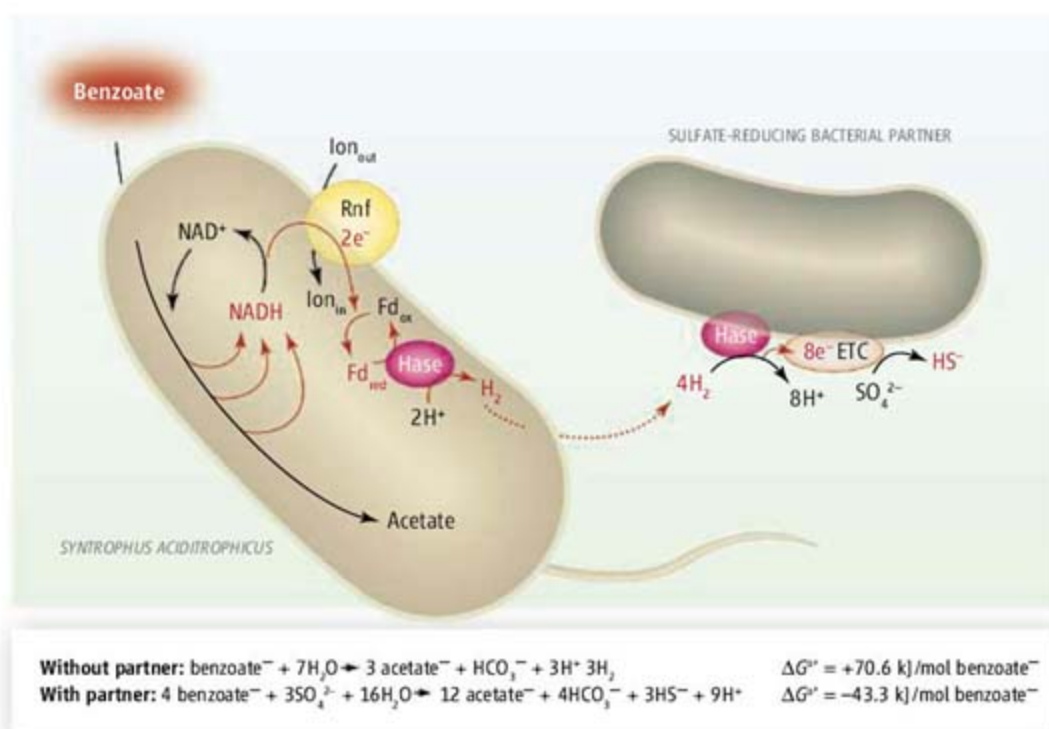
Metabolic cooperation. Hypothetical electron transfer between *S. aciditrophicus* and a sulfate-reducing bacterial partner during the anaerobic oxidation of benzoate. The schematic traces the interspecies transfer of electrons (red) from the source reductant (benzoate) to the terminal oxidant (sulfate). Efficient removal of hydrogen by the sulfate-reducing bacterial partner increases the amount of free energy available in the anaerobic oxidation of benzoate to acetate. Rnf, ion-translocating electron transport complex; Fd, ferredoxin; Hase, hydrogenase; ETC, electron transport chain; $\Delta G^{\circ\prime}$, Gibbs free energy under physiological standard state conditions. [Adapted from (*1, 3*)]

can be coupled to the reduction of sulfate (*6–9*), a reaction that no single species can perform alone. Although these associations depend on interactions that occur on microscopic scales, they drive teragram (10^{12} g) fluxes of methane annually on a global scale (*10*). Such global transformations depend on microbial community interactions, including syntrophy. Ultimately, these interactions provide the checks and balances that sustain global biogeochemical cycles.

Another important aspect of microbial syntrophy is the possibilities afforded by its inherent modularity. For example, many syntrophic hydrogen producers can partner with either hydrogen-consuming methanogens or sulfate reducers, depending on the environmental context. Another example is provided by the anaerobic oxidation of methane in freshwater sediments, which appears to be coupled to nitrate reduction (*11*). Very close relatives of marine methanotrophic Archaea oxidize methane in these habitats, but instead of teaming up with sulfate reducers, they have completely different syntrophic partners that reduce nitrate (*11*). This flexibility with respect to who partners with whom opens up a wide range of possible reductants and oxidants that can be metabolized, and of environments in which these interactions can occur. The central drivers are the overall thermodynamic constraints, the availability of the terminal oxidants (like sulfate and nitrate), and the indigenous diversity of microbial physiologies.

Microbial energetic interactions are providing important insights into how microbes can extract and grow using vanishingly small amounts of free energy. The details of these reactions, and how they are optimized for efficiency through interspecies interactions, are well worth understanding. As our own species takes a sober look at dwindling hydrocarbon energy supplies, we may well have a few lessons in energy efficiency to learn from microbial syntrophic processes.

References
1. M. J. McInerney *et al.*, *Proc. Natl. Acad. Sci. U.S.A.* **104**, 7600 (2007).
2. B. Schink, *Antonie Van Leeuwenhoek* **81**, 257 (2002).
3. B. E. Jackson, V. K. Bhupathiraju, R. S. Tanner, C. R. Woese, M. J. McInerney, *Arch. Microbiol.* **171**, 107 (1999).
4. B. E. Jackson, M. J. McInerney, *Nature* **415**, 454 (2002).
5. B. Schink, *Microbiol. Mol. Biol. Rev.* **61**, 262 (1997).
6. A. Boetius *et al.*, *Nature* **407**, 623 (2000).
7. K. U. Hinrichs, J. M. Hayes, S. P. Sylva, P. G. Brewer, E. F. DeLong, *Nature* **398**, 802 (1999).
8. V. J. Orphan, C. H. House, K.-U. Hinrichs, K. D. McKeegan, E. F. DeLong, *Science* **293**, 484 (2001).
9. V. J. Orphan, C. H. House, K. U. Hinrichs, K. D. McKeegan, E. F. DeLong, *Proc. Natl. Acad. Sci. U.S.A.* **99**, 7663 (2002).
10. W. S. Reeburgh, *Chem. Rev.* **107**, 486 (2007).
11. A. A. Raghoebarsing *et al.*, *Nature* **440**, 918 (2006).

IMMUNOLOGY

Outwitted by Viral RNAs

Human cytomegalovirus expresses noncoding RNAs that repress host immune responses during infection.

Bryan R. Cullen

Herpesviruses are pathogenic DNA viruses that can establish long-term latent or persistent infections. After infecting a host cell, a herpesviral DNA genome enters the nucleus where it is transcribed to make both messenger RNAs (mRNAs), which encode proteins, and noncoding RNAs (ncRNAs) (*1*) (see the figure). Some of these viral ncRNAs are long [more than 100 nucleotides (nt)], whereas others, called microRNAs (miRNAs), are short (~22 nt). Although miRNAs can selectively

Mammals are armed with a range of innate and adaptive antiviral defense mechanisms. Innate responses, such as the programmed death (apoptosis) of infected cells or the production of interferons that activate immune responses, are often triggered by molecular determinants that are invariant characteristics of particular pathogens. Adaptive immune responses, in contrast, recognize novel viral antigens, generally proteins, that are not invariant but nevertheless are foreign to the infected organism. Innate responses are rapid and can

death is induced early in the virus life cycle.

Despite these insights, we are left with numerous herpesviral ncRNAs, including miRNAs, for which no functions are known. Do these ncRNAs promote viral replication and/or pathogenesis? HCMV, a herpesvirus that can cause severe disease in newborn infants and in immunocompromised individuals, encodes at least two long ncRNAs and 11 miRNAs. Reeves *et al*. and Stern-Ginossar *et al*. suggest that two of these HCMV ncRNAs are indeed

Shutting down the immune response. Infection by HCMV induces a state of metabolic stress that would normally trigger host immune responses, including cell lysis or apoptosis. HCMV prevents these immune responses using two viral ncRNAs. The β2.7 ncRNA binds MRCC-I components and stabilizes mitochondrial energy production; miR-UL112 miRNA blocks the expression of cell surface MICB, and hence prevents lysis by immune cells that recognize MICB.

inhibit gene expression (*2*, *3*), the function of most viral ncRNAs has been unclear. It has been suggested that viral ncRNAs might inhibit host immune responses (*3*). Evidence supporting this hypothesis is now provided by Reeves *et al*. in a recent issue of *Science* (*4*) and by Stern-Ginossar on page 376 in this issue (*5*). Both studies show that human cytomegalovirus (HCMV) expresses ncRNAs that allow infected cells to evade innate immune responses.

Whereas the function of most cellular regulatory ncRNAs is poorly understood, long ncRNAs are known to direct chromosome silencing, regulate gene expression, or maintain chromosome integrity. In addition, eukaryotic cells express numerous miRNAs that guide a ribonucleoprotein complex [the RNA induced silencing complex (RISC)] to mRNAs that display sequence complementarity (*3*). RISC recruitment can inhibit mRNA translation or induce mRNA degradation.

reduce virus spread while the slower, but often more effective, adaptive responses are mounted. Successful pathogens have often evolved mechanisms that attenuate these host immune responses.

Although numerous virally encoded immunosuppressive proteins are known, regulatory ncRNAs offer viruses several potential advantages. ncRNAs do not need to be translated and can therefore act rapidly. They can also be quite small, which may be important given the compact size of viral genomes. RNAs are also poor targets for adaptive immune responses. Given the precedent of cellular regulatory ncRNAs, it is therefore not surprising that herpesviruses encode both long ncRNAs and miRNAs (*1*, *2*). For example, Epstein-Barr virus expresses two long ncRNAs that inhibit cellular interferon responses, although the underlying mechanism remains unclear (*6*). A miRNA encoded by herpes simplex virus 1 (HSV-1) prevents apoptosis by blocking the expression of two cellular proteins, SMAD3 and transforming growth factor–β, which can trigger apoptosis (*7*). Apoptosis can be an important innate defense mechanism if cell

acting as immune-response inhibitors.

Within hours of HCMV infection, a ~2.7-kb viral ncRNA (aptly called β2.7) accumulates, reaching ~20% of total viral RNA (*8*). Reeves *et al*. report that β2.7 binds to components of mitochondrial respiratory chain complex I (MRCC-I) and thereby stabilizes MRCC-I function. Infection of cells with an HCMV mutant lacking β2.7 induces the relocalization of MRCC-I components away from the mitochondrial membrane, resulting in reduced energy [in the form of adenosine triphosphate (ATP)] production and the induction of apoptosis. Strikingly, a similar effect is seen when cells are treated with rotenone, a compound that inhibits MRCC-I (*9*). Expression of β2.7 by wild-type HCMV prevents the relocalization of MRCC-I by either HCMV infection or rotenone treatment. As a result, β2.7 not only prevents the premature death of infected cells, but also ensures the stable production of ATP during the HCMV life cycle.

Members of the herpesvirus family encode

The author is in the Center for Virology and Department of Molecular Genetics and Microbiology, Duke University Medical Center, Durham, NC 27707, USA. E-mail: culle002@mc.duke.edu

CREDIT: P. HUEY/SCIENCE

numerous miRNAs but, with the exception of one HSV-1 miRNA (7), no functions have been described. Stern-Ginossar et al. noted that one HCMV miRNA, miR-UL112, displays sequence complementarity to the 3′-untranslated region of cellular mRNA encoding MHC class I–related chain B (MICB), a ligand for a receptor found on natural killer cells of the immune system. MICB expression is normally activated when cells are subjected to severe stress, including virus infection. Cell-surface MICB marks these cells for destruction by natural killer cells (10). The authors show that HCMV miR-UL112 inhibits the translation of MICB mRNA. The resulting absence of MICB protein protects HCMV-infected cells against

lysis by natural killer cells. This finding is surprising because the HCMV UL16 glycoprotein also inhibits MICB cell-surface expression by causing its intracellular sequestration (11). It therefore appears that HCMV has evolved two distinct mechanisms to prevent cell-surface MICB expression—one mediated by a protein and the other by a miRNA.

Together, these two studies suggest that many of the long ncRNAs and miRNAs encoded by human herpesviruses may share the ability of certain herpesvirus nonstructural proteins to inhibit host immune responses and, hence, act as pathogenicity factors. Viral ncRNAs therefore clearly merit serious consideration as potentially attractive

targets for chemotherapeutic intervention in herpesvirus-induced diseases.

References

1. N. K. Conrad et al., Cold Spring Harbor Symp. Quant. Biol. **71**, 337 (2006).
2. B. R. Cullen, Nat. Genet. **38**, 525 (2006).
3. D. P. Bartel, Cell **116**, 281 (2004).
4. M. B. Reeves, A. A. Davies, B. P. McSharry, G. W. Wilkinson, J. H. Sinclair, Science **316**, 1345 (2007).
5. N. Stern-Ginossar et al., Science **317**, 376 (2007).
6. M. J. Clemens, Int. J. Biochem. Cell Biol. **38**, 164 (2006).
7. A. Gupta et al., Nature **442**, 82 (2006).
8. B. P. McSharry et al., J. Gen. Virol. **84**, 2511 (2003).
9. N. Li et al., J. Biol. Chem. **278**, 8516 (2003).
10. S. Bauer et al., Science **285**, 727 (1999).
11. C. Dunn et al., J. Exp. Med. **197**, 1427 (2003).

CELL SIGNALING

A Ciliary Signaling Switch

Søren Tvorup Christensen and Carolyn Marie Ott

Primary cilia contain the receptor for a secreted protein crucial for cell regulation, strengthening their potential as signaling centers in the cell.

Many people are familiar with motile cilia, the cellular, hairlike projections whose beating generates fluid flow that removes particles from our respiratory tract or help oocytes pass through the fallopian tube. Appreciation is now growing for primary cilia, the nonmotile counterparts, present as a single copy on the surface of most cell types in our body. Defects in primary cilia have been linked to disease, and we now know that they function as unique antenna-like structures, probing the extracellular environment for molecules that are recognized by the receptors they bear. This sensory function allows primary cilia to coordinate numerous intercellular signaling pathways that regulate growth, survival, and differentiation of cells during embryonic development and maintenance of healthy tissues (1). On page 372 of this issue, Rohatgi et al. (2) further define the role of primary cilia in regulating the response of cells to Sonic hedgehog (Shh), a secreted protein that constitutes one of the most fundamental and highly conserved signaling systems in vertebrate development (3). Regulated movement of key proteins into and out of the cilium creates a sophisticated switch by which cells can turn this powerful signaling on and off.

Shh is one of three paralogous vertebrate

proteins [related to the invertebrate Hedgehog (Hh) protein] that binds to the transmembrane protein Patched (Ptc) at the cell surface. Upon binding, Shh abolishes the inhibitory effect of Ptc on another transmembrane protein, Smoothened (Smo). This relief from inhibition allows Smo to transduce a signal to the nucleus via glioma (Gli) transcription factors, trigger-

ing the expression of specific genes. This general scheme is well established; however, there are many unresolved questions about the regulated interaction between separate components of the pathway, and it is unclear how Shh-Ptc interaction increases Smo signaling activity.

Previous work has shown that primary cilia are essential for Shh signaling. Mutations in
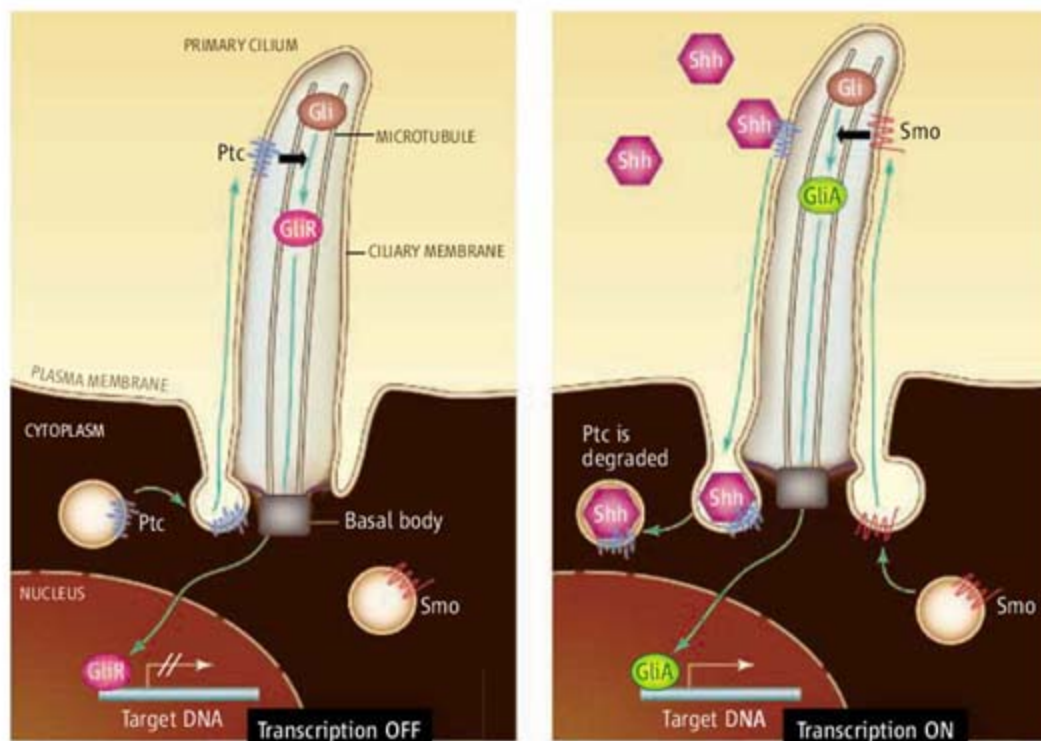
A ciliary switch. The primary cilium emanates as a solitary organelle from most cells in our body. (**Left**) In the absence of Shh, Ptc translocates to the primary cilium and blocks ciliary localization of Smo. Transcription factors (Gli) are degraded or processed to repressors (GliR). (**Right**) Upon binding of Shh to Ptc in the cilium, Ptc leaves, and Smo enters, the cilium. This switch may be controlled by oxysterols released from the cilium membrane by Ptc. Gli is processed to an activator form (GliA).

S. T. Christensen is at the Department of Molecular Biology, University of Copenhagen, Copenhagen DK-2100, Denmark. E-mail: stchristensen@aki.ku.dk C. M. Ott is in the Cell Biology and Metabolism Branch, National Institute of Child Health and Human Development, Bethesda, MD 20892, USA. E-mail: ottcarol@mail.nih.gov

genes encoding proteins essential for cilia assembly, such as the intraflagellar transport proteins (4), result in dysfunctional Shh signaling and severe developmental disorders in mammals (5). Further, several components of the Shh pathway specifically localize to the tip or base of the primary cilium (6–9), including Gli transcription factors and proteins that regulate Gli activity at the cilium tip. Localization of Smo to the primary cilium increases when a cell is stimulated with Shh (7), indicating that Shh-mediated generation of active forms of the Gli transcription factors takes place in the cilium. Rohatgi et al. now show that Ptc localizes to the primary cilium and that Shh binds to Ptc when it is in this location. In addition, the authors show that the unique and concerted movement of Ptc out of, and Smo into, the primary cilium constitutes a cellular signaling switch responsive to Shh (see the figure).

Why does Ptc localize to the primary cilium? There are several obvious advantages. The cilium provides a much smaller surface area over which to integrate a signal. Because the cilium protrudes from the main cell body, Ptc has a greater opportunity to sense gradients of Shh molecules in areas further removed from the general cell surface. For example, during early embryonic development, the directed movement of Shh-containing lipoprotein particles is thought to break left-right body symmetry in vertebrates (10). In this scenario, rotating cilia, present on cells in a region called the embryonic node, generate a leftward flow of fluid that directs movement of the particles to the left side of the developing embryo. The particles subsequently fragment, and released Shh molecules are sensed by primary cilia, which activates a signaling cascade in the appropriate tissue that helps define the left-right body plan.

Another important question concerns how the regulated trafficking of Ptc and Smo in primarily cilia is achieved. For Ptc, the answer is still unclear, but Rohatgi et al. demonstrate that addition of oxysterols, which regulate responsiveness to Shh and activate Hh signaling (3), cause Smo (harbored in intracellular vesicles) to move into the cilium and activate Shh signal transduction, while Ptc also remains in the cilium. This finding supports their conclusions that oxysterols make Smo insensitive to the inhibitory effects of Ptc, and that release of oxysterols from the cell membrane regulates Smo trafficking. Ciliary membranes are rich in cholesterol, the precursor of oxysterols. Ptc may control the release of oxysterols from the cholesterol-rich membrane of the primary cilium. The receptor contains a sterol-sensing domain and is highly homologous to Niemann-Pick C1 protein, which is important for cellular cholesterol trafficking (11). Oxysterols may affect Smo localization, directly or indirectly, by masking or unmasking a ciliary targeting motif in the cytoplasmic domain of Smo. One mutation in this domain prevents cilia localization and thus Shh signaling, whereas another mutation increases ciliary localization of Smo and supports constitutive activation of the Shh signaling pathway (7, 9). Moreover, lipid rafts—membrane regions enriched in sterols—may promote the continuous ciliary targeting and/or retention of specific signal components (1), such as Ptc and Smo, in response to Shh signaling.

The concerted action of Shh molecules and oxysterols in the primary cilium may constitute a unique cellular switch between activation and inactivation of the Shh pathway during development and control of tissue homeostasis. Analogously, the protein inversin, which also localizes to primary cilia, functions as a molecular switch between two signaling pathways controlled by the secreted protein Wnt, another fundamental and conserved system that controls development (12). The next challenges are to define the precise molecular mechanisms that underlie the Shh cellular switch, to determine how primary cilia function as specialized organelles that integrate positive and negative inputs on transcription factor (Gli) activity, and to discover how these mechanisms may interact with other signaling events, such as Wnt signaling, in human health and disease.

References and Notes
1. S. T. Christensen, L. B. Pedersen, L. Schneider, P. Satir, *Traffic* **8**, 97 (2007).
2. R. Rohatgi, L. Milenkovic, M. P. Scott, *Science* **317**, 372 (2007).
3. Y. Wang, A. P. McMahon, B. L. Allen, *Curr. Opin. Cell Biol.* **19**, 159 (2007).
4. J. L. Rosenbaum, G. B. Witman, *Nat. Rev. Mol. Cell Biol.* **3**, 813 (2002).
5. J. M. Scholey, K. V. Anderson, *Cell* **125**, 439 (2006).
6. T. Caspary, C. E. Larkins, K. V. Anderson, *Dev. Cell* **12**, 767 (2007).
7. K. C. Corbit et al., *Nature* **437**, 1018 (2005).
8. C. J. Haycraft et al., *PLoS Genet.* **1**, e53 (2005).
9. S. R. May et al., *Dev. Biol.* **287**, 378 (2005).
10. Y. Tanaka, Y. Okada, N. Hirokawa, *Nature* **435**, 172 (2005).
11. T. Y. Chang, C. C. Chang, N. Ohgami, Y. Yamauchi, *Annu. Rev. Cell Dev. Biol.* **22**, 129 (2006).
12. M. Simons et al., *Nat. Genet.* **37**, 537 (2005).
13. We thank L. B. Pedersen and P. Satir for helpful comments on the manuscript.

CHEMISTRY

Learning Nature's Way: Biosensing with Synthetic Nanopores

Charles R. Martin and Zuzanna S. Siwy

Synthetic sensors use molecular recognition events in nanometer-scale pores for selective detection of proteins, nucleotides, and drugs.

Living systems use nanometer-scale pores called protein channels as biosensors. For example, the ligand-gated ion channels in the human brain (1) span the membranes of nerve cells and are closed in their resting state. But when a specific neurotransmitter binds to molecular-recognition sites on the channel, it opens, allowing an ionic current to flow. This process—molecular-recognition chemistry followed by transduction of that chemistry into a measurable current—is the essence of biosensing. In recent years, scientists have used these ideas to make artificial ion-channel sensors for analytes including drugs, proteins, and oligonucleotides. They have done so by attaching molecular-recognition agents (MRAs) that bind these species to synthetic or biological nanopores.

This sensing concept was first used in the Coulter counter, which uses a micrometer-sized pore to count and size particles (2). To do the same for molecules required a much smaller pore, and biology provided an ideal candidate: the α-hemolysin (α-HL) nanopore. α-HL is a protein that forms a nanopore through lipid-bilayer membranes (see the figure, top panel). To act as a sensor, the membrane is placed between two salt solutions, and an ionic current is passed through the electrolyte-filled nanopore (3, 4). When an analyte such as a drug molecule enters the nanopore, it transiently blocks this current; the current is restored when the drug exits. As a result, a string of current pulses is obtained, with each pulse corresponding to a single

C. R. Martin is in the Department of Chemistry and the Center for Research at the Bio/Nano Interface, University of Florida, Gainesville, FL 32611, USA. E-mail: crmartin@chem.ufl.edu Z. S. Siwy is in the Department of Physics and Astronomy, University of California, Irvine, Irvine, CA 92697, USA.

molecular-translocation event. Thus, analyte molecules are counted one at a time as they pass through the nanopore (*3*).

However, a sensor based on the native α-HL nanopore would count any molecule that can enter and pass through. To make the pore selective, an MRA that binds the target analyte has been attached to the inside surface of the nanopore (*3*). Now, when the analyte enters, it binds to the MRA and blocks the ion current for a period of time determined by the chemistry of the MRA/analyte interaction. The resulting current pulses can be distinguished from those produced by molecules that do not bind to the MRA, and a selective sensor is obtained.

This approach has been used to make α-HL–based sensors that are selective to metal ions, drugs, proteins, and oligonucleotides (*3*). However, the lipid membrane that houses the nanopore is very fragile, diminishing the prospects for developing practical sensors from this technology. Synthetic-nanopore sensors, in which the pore is bored into a chemically and mechanically stable membrane material (*5–10*), offer a possible solution. Current research in this area focuses on two key questions: How can synthetic pores with inside diameters approaching molecular dimensions (nanometers) be prepared? And how can MRAs be attached so that selective sensors are obtained?

Two technologies are emerging as the front runners for preparing synthetic-nanopore sensors. The first derives from microlithography and entails using a beam of electrons (*5*) or ions (*6*) to bore a hole through a thin membrane of an inorganic material such as silicon dioxide. The electron-beam method uses a transmission electron microscope, allowing the pore to be imaged during preparation (see the figure, middle panel). Pores with diameters as small as 1 nm have been prepared (*5*).

In the second technology, a thin plastic membrane is bombarded with a beam of high-energy particles to create damage tracks through the membrane, followed by chemical etching of these tracks to make the nanopores (*11*). This method has been used commercially for decades to prepare nanopore filters. More recently, GSI in Darmstadt, Germany, has developed simple

A peptide analyte passes through the α-HL nanopore (*4*).
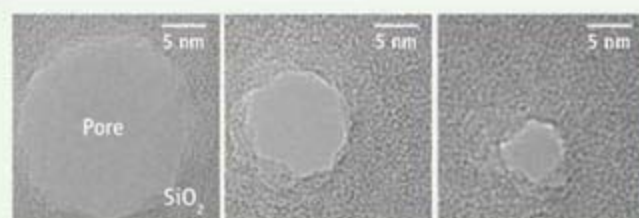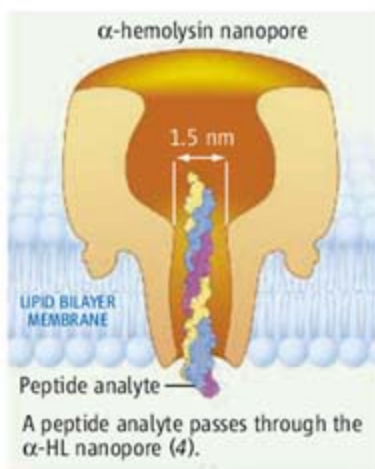
Electron micrograph of three nanopores with different diameters in silicon dioxide membranes (*5*).
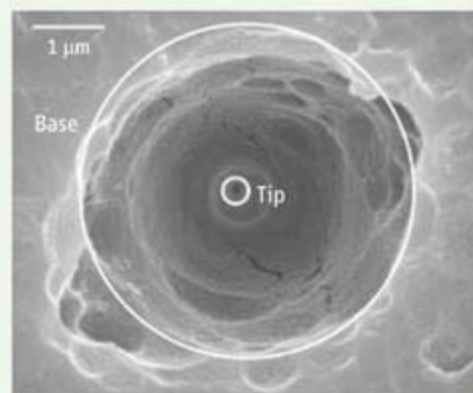
Electron micrograph looking down a conical nanopore in a polycarbonate membrane.

Both microfabricated and track-etched nanopores have been used as sensors to count analyte species, including large DNAs, proteins, and small molecules (*5–10*). However, in most of these studies, the nanopore was not selective. The final challenge is to attach MRAs to create analyte-selective sensors.

There have been two reports of making MRA-functionalized sensors. In the first, protein binding MRAs (such as an antibody to the protein toxin ricin) were attached to track-etch protein sensors based on conical gold nanotubes (*8*). The MRAs were attached to the gold through simple thiol-based chemistry. The sensor was mounted between two salt solutions, and an ionic current was passed through the nanotube. The diameter of the nanotube tip was fine-tuned to match the size of the analyte protein (~5 nm) bound by the MRA. As a result, the tip became occluded upon protein binding, shutting off the ion current—an "inverse" ligand-gated ion channel.

methods for preparing single-nanopore membranes of this type (*12*), and for etching conical pores (see the figure, lower panel) (*13*). Analyte species can be counted one at a time as they traverse the narrow opening (or tip) of a conical nanopore (*7*). Sensors with tip openings of 2 nm have been described (*7*).

The second MRA synthetic-nanopore sensor (*10*) derives from an MRA-based oligonucleotide-transport membrane (*14*). The pore was microfabricated in silicon dioxide, which is easy to functionalize using siloxane chemistry. An oligonucleotide served as the attached MRA, and the target analyte was the oligonucleotide sequence that is complimentary to the bound sequence. The current pulses for the analyte oligonucleotide could be distinguished from pulses produced by oligonucleotides that did not bind to the attached MRA (*10*).

Reliable methods are now available for preparing synthetic nanopores, and methods for attaching the MRAs are known, but several challenges remain. First, because the α-HL nanopore is prepared by protein self-assembly, pore fabrication is very reproducible. It must be demonstrated that synthetic nanopores can also be prepared reproducibly. Second, their long-term stability (over months) must be explored. Finally, with α-HL, genetic engineering can be used to attach the MRA at any desired location along the inside walls of the nanopore. A step toward such point-selective MRA functionalization has recently been demonstrated with a synthetic nanopore by depositing a material that binds the MRA at only one opening of the pore (*15*). Synthetic nanopore sensors could revolutionize biosensing, but much basic science remains to be done before this promise is realized.

The sensor could detect subpicomolar protein concentrations (*8*).

References

1. B. Hille, *Ion Channels of Excitable Membranes* (Sinauer, Sunderland, MA, 3rd ed., 2001).
2. R. W. Lines, in *Particle Size Analysis*, N. G. Stanley-Wood, R. W. Lines, Eds. (Royal Society of Chemistry, Cambridge, UK, 1992), pp. 350–373.
3. H. Bayley, P. S. Cremer, *Nature* **413**, 226 (2001).
4. T. D. Sutherland et al., *Nano Lett.* **4**, 1273 (2004).
5. A. J. Storm, J. H. Chen, X. S. Ling, H. W. Zandbergen, C. Dekker, *Nat. Mater.* **2**, 537 (2003).
6. J. Li et al., *Nature* **412**, 166 (2001).
7. E. A. Heins, Z. S. Siwy, L. A. Baker, C. R. Martin, *Nano Lett.* **5**, 1824 (2005).
8. Z. Siwy et al., *J. Am. Chem. Soc.* **127**, 5000 (2005).
9. C. Dekker, *Nat. Nanotech.* **2**, 209 (2007).
10. S. M. Iqbal, D. Akin, R. Bashir, *Nat. Nanotech.* **2**, 243 (2007).
11. R. L. Fleischer, P. B. Price, R. M. Walker, *Nuclear Tracks in Solids: Principles and Application* (Univ. California Press, Berkeley, 1975).
12. R. Spohr, German Patent No. DE 2951376 C2 (1983); United States Patent No. 4369370 (1983).
13. P. Yu Apel, Yu. E. Korchev, Z. Siwy, R. Spohr, M. Yoshida, *Nucl. Instrum. Methods Phys. Res. Sect. B* **184**, 337 (2001).
14. P. Kohli et al., *Science* **305**, 984 (2004).
15. J. Nilsson, J. R. I. Lee, T. V. Ratto, S. E. Letant, *Advanced Mater.* **18**, 427 (2006).

Motor Proteins at Work for Nanotechnology

Martin G. L. van den Heuvel and Cees Dekker*

The biological cell is equipped with a variety of molecular machines that perform complex mechanical tasks such as cell division or intracellular transport. One can envision employing these biological motors in artificial environments. We review the progress that has been made in using motor proteins for powering or manipulating nanoscale components. In particular, kinesin and myosin biomotors that move along linear biofilaments have been widely explored as active components. Currently realized applications are merely proof-of-principle demonstrations. Yet, the sheer availability of an entire ready-to-use toolbox of nanosized biological motors is a great opportunity that calls for exploration.

A huge amount of biological research in recent decades has spurred the realization that the living cell can be viewed as a miniature factory that contains a large collection of dedicated protein machines (1). Consider the complicated tasks that a single cell can perform: It can create a full copy of itself in less than an hour; it can proofread and repair errors in its own DNA, sense its environment and respond to it, change its shape and morphology, and obtain energy from photosynthesis or metabolism, using principles that are similar to solar cells or batteries. All this functionality derives from thousands of sophisticated proteins, optimized by billions of years of evolution. At the moment, we can only dream of constructing machines of similar size that possess just a fraction of the functionality of these natural wonders.

One particular class of proteins is formed by molecular motor enzymes, which are catalytic proteins that contain moving parts and use a source of free energy to direct their motion. Upon studying these motors, their resemblance to machines becomes more and more clear. We find rotary motors that comprise shafts and bearings, as well as linear motors that move along tracks in a step-by-step fashion.

Kavli Institute of Nanoscience, Delft University of Technology, Lorentzweg 1, 2628 CJ Delft, Netherlands.

*To whom correspondence should be addressed. E-mail: c.dekker@tudelft.nl

We find motors that are powered by chemical energy, derived from hydrolyzing adenosine triphosphate (ATP) molecules (the cell's major energy currency), and motors that employ a gradient of ions, using both electric and entropic forces.

It is of interest to ponder whether we can employ these biological nanomachines in artificial environments outside the cell to perform tasks that we design to our benefit (2, 3). Or, at the very least, can these proteins provide us with the inspiration to mimic biocomponents or design artificial motors on comparable scales?

Nature's Workhorses in the Cell

In contrast to macroscopic machines, motor proteins operate in a world where Brownian motion and viscous forces dominate. The relevant energy scale here is k_BT, the product of Boltzmann's constant and temperature, which amounts to 4 pN·nm. This may be compared to the ~80 pN·nm of energy derived from hydrolysis of a single ATP molecule at physiological conditions. Thermal, nondeterministic motion is thus an important aspect of the dynamics of motor proteins.

Let's briefly consider some examples of biomotors. The rotary engine F_OF_1-ATP synthase (Fig. 1A) synthesizes ATP from adenosine diphosphate (ADP) and phosphate (4). The flow of protons along an electrochemical gradient through the membrane-bound F_O motor drives rotation of the F_O ring and the central stalk connecting the F_O and F_1 motors. This induces conformational changes of the F_1 motor that drives the catalytic formation of ATP. Remarkably, the complex can also work in reverse, using the energy of ATP hydrolysis to drive the reverse rotation of the F_1 motor and subsequently pump protons against their electrochemical gradient.

The rotary bacterial flagellar motor (Fig. 1B) is used by bacteria such as *Escherichia coli* as a propulsion mechanism by spinning a helical flagellum (5). This powerful motor, assembled from more than 20 different proteins, is driven by an inward proton flux that is converted by several torque-generating stators into a rotary motion of the cylindrical rings and central shaft. The motor generates torques of more than 10^3 pN·nm (250 k_BT) and rotates at speeds of over 100 Hz (5).

Linear-motion motors are found among the members of the super families of kinesin, dynein, and myosin proteins (6) (Fig. 1, C to E). These motors move in discrete steps along tracks made of long protein polymers (actin filaments for myosin, microtubules for kinesin and dynein) that form

Fig. 1. Motor proteins in the cell. (**A**) Representation of F_OF_1-ATPase [reprinted with permission from (45); copyright 2006, Wiley-VCH]. (**B**) Representation of the bacterial flagellar motor (image courtesy of Keïichi Namba, Osaka University). Inset shows an electron microscopy image of the motor [reprinted with permission from (46); copyright 2001, Elsevier]. (**C**) Conventional kinesin and dynein transport cargo in opposite directions along microtubules [adapted from (7)]. (**D**) Kinesin is a processive motor, consisting of two heads, that walks in alternate steps of 8 nm along the microtubule [adapted from (6)]. (**E**) Muscle contraction is caused by the sliding of interdigitated actin and myosin filaments in a sarcomere unit. The nonprocessive myosin II motor detaches after each power stroke so as not to impede the further sliding of the actin filament caused by other myosins [adapted from (6)]. (**F**) RNA polymerase moves along a double-stranded DNA template, transcribing a RNA copy (image courtesy of D. S. Goodsell, Scripps Research Institute).

the cytoskeleton that extends throughout the cell. The structural polarity of these filaments (denoted by a plus and minus end) allows unidirectional movement of motors along their tracks. Cytoskeletal motors are involved in almost every aspect of controlled motion and force generation within cells, such as intracellular transport of materials (Fig. 1C) (7), cell division, or powering eukaryotic flagella and cilia. The contraction of a muscle is driven by the orchestrated sliding of series of actin filaments with respect to arrays of myosin motors (Fig. 1E). Typically, a linear motor can generate forces of up to ~10 pN.

Many other proteins exist that can use energy to perform work, such as ion channels, DNA- or RNA-processing enzymes (Fig. 1F), ribosomes, or light-powered electron pumps, but these fall outside the scope of this review.

Muscle Power for Nanotechnology

One striking demonstration of a biomolecule-powered nanostructure is the construction of a nickel nanopropeller that rotates through the action of an engineered F_1-ATPase motor (8) (Fig. 2A). The directed assembly of the devices was controlled through genetic engineering of histidine tags that stuck the F_1-ATPase onto nickel posts, with its central stalk protruding upwards. This connected to a nickel propeller of ~1 μm length through biotin-streptavidin bonds. Addition of ATP caused rotation of the propeller. A metal-binding site was engineered into the motor and acted as a reversible on-off switch by obstructing the rotation upon binding of a zinc ion (9), similar to the action of putting a stick between two cogwheels.

On a larger scale, gliding bacteria have been used to power a micromechanical device comprising a cogwheel-shaped rotor of 20-μm diameter rotating in a silicon track (10). Bacteria adhered to the rotor, turning it with ~2 rpm (Fig. 2B). The increase in size (cells compared with individual proteins) is accompanied with larger torques, together with self-repairing properties. Cardiomyocytes (heart muscle) have been used to drive a self-assembled microwalker (11). The coordinated contraction of muscle bundles, which were assembled onto a ~0.1-mm large two-legged SiO_2 structure, drove its stepwise movement with a speed of 38 μm/s.

Linear cytoskeletal kinesin and myosin motors have dominated the emerging field of protein-powered devices because they are relatively robust and readily available. Actin and tubulin can be commercially purchased, whereas the motor proteins can be purified from cells or expressed in recombinant bacterial systems and harvested in large quantities. In their most basic geometry, these motor systems are employed in a so-called gliding assay, in which the cytoskeletal filaments (usually about 1 to 20 μm in length) are propelled by surface-bound motors (Fig. 2C). The rotational flexibility of the motor stalks is high enough to rotate the randomly bound motors into the correct orientation for binding onto the microtubule or actin filament. Plus-end–directed motors will then propel the filaments with their minus end leading.
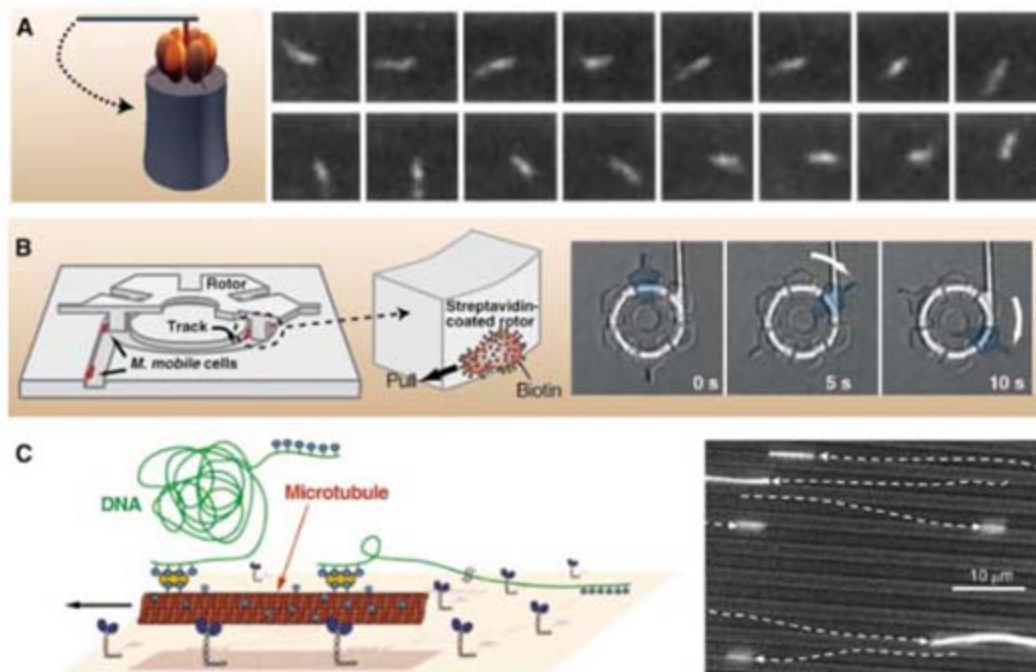
Fig. 2. Motor proteins in nanotechnology. (**A**) An F_1-ATPase–powered nanopropeller [adapted from (8)]. Fluorescence images (133-ms interval) are from the earlier experiment (47) that first demonstrated the rotary motion of the F_1-ATPase motor by using a fluorescent actin filament connected to the stalk [adapted with permission from (47); copyright 1997, Macmillan Publishers Ltd: Nature]. (**B**) A microrotor (20-μm diameter) powered by bacteria that adhere to the rotor and glide unidirectionally through the track. Photo images show the clockwise rotation of the rotor [adapted with permission from (10); copyright 2006, National Academy of Sciences USA]. (**C**) Schematic of kinesin motor proteins adsorbed to a surface propelling a microtubule shuttle, which binds cargo such as a DNA molecules [reprinted with permission from (12); copyright 2003, American Chemical Society (ACS)]. The fluorescence image shows kinesin-propelled microtubules moving through open polyurethane channels [reprinted with permission from (16); copyright 2003, ACS]. The velocity of microtubules is typically about 1 μm/s, whereas actin motility can reach speeds up to 10 μm/s.

Like nanoscale trucks, the microtubules or actin filaments can act as shuttles that transport an attached cargo such as nanoparticles or DNA (12) (Fig. 2C).

In an alternative geometry, motor-coated cargo can move along cytoskeletal filaments that are adsorbed onto a substrate. This requires the controlled placement of filaments onto a substrate and precoating of the cargo with motors. The inverted gliding geometry offers better opportunities, however, for actuation, functionalization, assembly, and control and is thus preferred. In general, multiple motors attach to a single filament shuttle, so that large forces (>>10 pN) can be generated. Another advantage is that the shuttles can routinely be interfaced to a variety of cargo using the biotin-streptavidin linkage or through antibodies.

Kinesin- and Myosin-Driven Transport on Chips

One vision is that motor proteins will be used for controlled cargo manipulation on a chip, with applications in sorting, separation, purification, or assembly of materials (2, 13). To reach this goal, one needs to develop controlled motion along specific routes, directionality, coupling to cargo, external control, and steering.

A prerequisite of any useful transport system is that motion and transport can be (uni-) directionally guided along predesigned pathways. When filaments are absorbed randomly onto a substrate, the direction of cargo transport is random as well (Fig.

3A-I). Therefore, considerable effort has been directed at creating confined motility by employing either chemical patterning of active motor proteins (14) or fabricated topographical patterns (Fig. 3A-II) (15, 16). A disadvantage of purely chemical patterns is that filaments easily derail from their tracks, which occurs when the leading end of the filament cannot find a new motor to bind to, whereas in purely topographically structured surfaces the selectivity of functional motor absorption is lost.

A combination of topographical and chemical patterning (17), with the motor proteins only at the bottom of the trenches (Fig. 3A-III), has proven to combine the best of both approaches with respect to guiding and confinement of microtubules (18) and actin (19). The recent use of enclosed fluidic channels (20, 21) can be considered as a logical final step in the development toward confinement, offering much better perspectives for packaging (20), and for the addressability of individual filaments through electric fields or flows (21).

For sorting applications, it is desirable that motion occur unidirectionally. Because the motors bound to a surface are rotationally flexible, unidirectional motion in gliding geometries can only be achieved through reorientation of the filaments. One method exploits asymmetrical arrow-shaped structures (17) (Fig. 3B) that rely on the principle that the probability to traverse the rectifier structure depends on the direction from which the filament enters. This hands-off method can achieve up to

92% efficient rectification per arrow (22). A different, active-control method is to use external force fields that bend and align the leading end of the motor-propelled filaments parallel to the field, which can be electric (15), magnetic (23), or flow fields (24). By subsequent fixation of the filaments to the underlying motors (using a chemical such as gluteraldehyde), the carpet can serve as a directionally aligned surface for motor-protein–coated cargoes (25, 26).

The coupling of cargo to protein shuttles is relatively straightforward. The simplest configuration relies on the nonspecific electrostatic or hydrophobic adsorption of cargo onto kinesin, which was used for unidirectional transport of materials such as gold, polystyrene, and glass (25). Biotin-

in sensing applications. A similar example is the use of microtubules coated with single-stranded DNA oligonucleotides, which could hybridize very specifically with its target DNA in solution, with sensitivity for a single-basepair mismatch (31). Another interesting approach is the report on myosin-driven transport of gold nanowires (32). The nanowires were created by catalytic enlargement of gold nanoparticles bound to actin filaments, while leaving some actin free to interact with the myosin-coated surface. This method could offer a way of assembling small electrical circuits.

One way to achieve reversible starting and stopping of the motility is to control the concentration of ATP or other necessary cofactors in solution. Light-controlled switching of the mo-

velocity of actin filaments (34), although the motion could not be entirely stopped. Another method exploits thermo-responsive polymers on a surface to control the motility of microtubules (35). The polymers, absorbed between the kinesin molecules, are in an extended configuration at low temperatures, which then sterically prevent gliding of the microtubules (Fig. 3D). Increasing the temperature shrinks the polymers and allows the microtubules to interact with the motors. By spatial patterning of these polymers, this technique can be of use for gating the density of motile microtubules. Another method of locally gating the microtubule density has exploited electric fields to attract microtubules onto a kinesin-coated gold surface (36).

Control of the direction of individual microtubules has recently become possible through the use of electric or magnetic forces. By using enclosed fluidic channels, one can apply strong electric fields very locally that act on the leading tip of a microtubule (which is electrically charged). In this way, individual microtubules approaching a Y junction can be steered into the desired direction by an electric field that is applied through a channel perpendicular to the junction (Fig. 3E) (21). The combination of electric and fluidic technologies is advantageous for on-chip integration. Magnetic fields have been used to direct the motility of microtubules that were functionalized with small magnetic particles (23).

The latest advances in the field of biomolecular motors in nanotechnology have made it clear that we can use motor proteins to drive nanoscale components and that we can interface proteins selectively to different materials. We can control the placement of motor proteins through self-assembly, confine their motion, and exert electrical, chemical, or physical control, sometimes even over single proteins. These isolated demonstrations have, however, not yet been integrated into functional and useful devices. Currently, denaturation of proteins limits the lifetime of a regular gliding assay to several days, although separation between fabrication and use of assembled devices can be achieved through freezing and lyophilization (37).

Fig. 3. Biomotor-driven transport. (**A**) Evolution in the confinement of motility. (I) On flat surfaces, the motion of filaments is in random directions (fluorescence image at bottom). (II) To confine the motion, people initially used (top) chemical patterning of motors (as indicated by red x's) or (middle) topographical structuring of the substrates. (Bottom) Scanning electron microscopy (SEM) image shows microfabricated channels in SiO₂. (III) A combination of both methods proved more effective. Bottom image shows time-integrated fluorescence of actin filaments, which are mobile exclusively in the letter-shaped tracks [reprinted with permission from (19); copyright 2004, Institute of Physics Publishing]. (IV) The use of submicrometer fluidic channels offers three-dimensional (3D) confinement. (Bottom) SEM image of a closed channel. (**B**) Arrow-shaped structures rectify the motility. Initially, the amount of microtubules is equal in both reservoirs, but after 18 min most microtubules have collected in the left reservoir [reprinted with permission from (17); copyright 2001, Biophysical Society]. (**C**) A kinesin-propelled microtubule binds to and stretches a DNA molecule attached to a gold post [reprinted with permission from (27); copyright 2006, Wiley-VCH]. (**D**) Thermoresponsive polymers form a clever way of switching the motility on and off [reprinted with permission from (35); copyright 2006, ACS] (**E**) An electric force is used to steer individual kinesin-propelled microtubules within an enclosed fluidic channel.

functionalized microtubules and actin filaments can be interfaced to any cargo with streptavidin groups. Using the inverted assay, transport of polystyrene beads (16), DNA molecules (12, 27) (Fig. 3C), and quantum dots (28) has been demonstrated.

A disadvantage of these methods is that the cargo has to be prefunctionalized. Therefore, a promising and versatile method is the use of microtubules that are coated with antibodies to the cargo that needs to be transported (29, 30). This technique was used to pick up tobacco mosaic virus particles (29) and specific proteins (30) from solution, which can be advantageous, for example,

tility was achieved using caged ATP, an inactive form of ATP, in conjunction with hexokinase, an ATP-consuming enzyme. Flashes of ultraviolet (UV) light liberated the ATP, which was concurrently depleted by the hexokinase, creating spikes in the motility that lasted several minutes (16). A faster time response of about 10 s was obtained through simply flushing hexokinase or ATP into the flow cell (33), but this requires more elaborate handling.

Temperature modulation in a flow cell, as through the fabrication of an electrical heater on a cover slip, allowed for reversible control of the

Outlook: Will Biomotors Make Their Way?

When people think of molecular motors and areas for their applications, they initially come up with scaled-down extensions of macroscopic systems: rotary motors to drive a propeller, and linear motors as locomotives pulling cargo. A recurring theme is the building of a molecular transport system or assembly line using kinesin or myosin motors (Fig. 4A). Indeed, applications can be imagined along these lines, where antibody-functionalized shuttles capture and separate target molecules that are present in otherwise undetectably low quantities in an analyte. Such a motor-assisted nanotechnology can be used for concentration of molecules and more sensitive detection.

Other areas where a role for motor proteins is envisioned include the use of motors to drive and accelerate self-assembly processes of nano-

Fig. 4. Prospects and future directions. (**A**) Fictitious motor-protein–powered device that performs on-chip sorting of materials, assembly of different components, and concentrating another component for enhanced detection. (**B**) Polymer vesicles containing bacteriorhodopsin and F_OF_1-ATP synthase create ATP from the light-driven proton gradient established over the membrane [reprinted with permission from (48); copyright 2005, ACS]. (**C**) 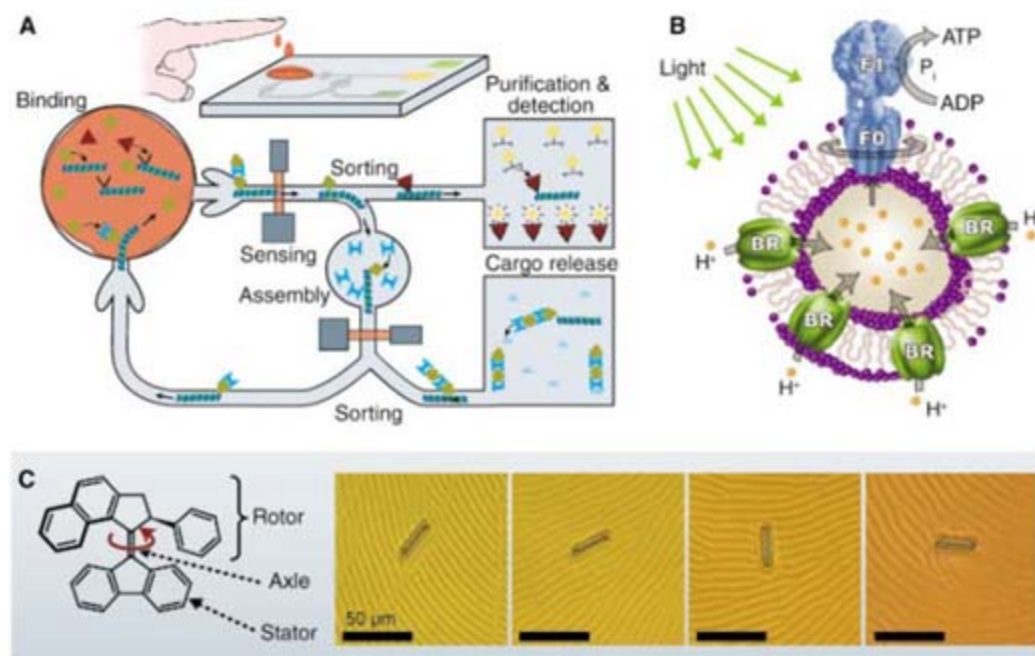Artificial molecular motors are a new development. Upon illumination with UV light, organic molecules embedded in a liquid-crystal film induce a reorganization of the film texture, driving the rotation of a glass particle. Photo images taken with 15-s intervals [adapted with permission from (44); copyright 2006, Macmillan Publishers Ltd: Nature].

structures (*13*), to power nanoscale mechanical elements [e.g, a nanoscale version of the bacteria-powered cogwheel (Fig. 2B)], or to drive small fluidic pumps (*38*). Ideas for applications that employ the massively parallel nature of autonomous molecular motors include the use of kinesin-propelled microtubules as a probe for surface topography (*39*) or for biocomputational maze-solving, where a large number of motile probes find different ways through a microfabricated maze (*40*).

Many of these applications are little more than proof-of-principle examples, for which more developed alternative technologies exist. For example, a biomolecular transport system should be gauged against lab-on-a-chip or micro-total-analysis systems, which are fairly well established technologies. Perhaps, though, the applicability of biomotors is merely limited by the imagination and creativity of researchers (including us). Progress in the field will likely come from integration of achievements of the past few years into more complete and functional devices. Promising in this respect is the sol-gel packaging of vesicles containing bacteriorhodopsin, a light-driven proton pump, and F_OF_1-ATP synthase (*41*) (Fig. 4B). Upon illumination of these sol gels, protons are pumped into the vesicles and ATP is created outside the vesicle by the ATP synthase. Besides the excellent stability of these gels (bacteriorhodopsin continued functioning for a month), this technology provides a convenient packaging method and a way to use light energy for fueling devices. Another interesting development is the engineering of polypeptides

that can specifically bind to inorganic materials (*42*). When engineered into motor proteins, this technology could provide new opportunities for motor-driven nanoscale assembly of different materials.

A related but even more futuristic field is the development of artificial molecular machines by bottom-up organic chemistry (*43*). Artificial molecular machines are synthesized molecules that can switch between different shapes upon illumination with light or through electrochemical reactions. An illustrative example is shown in Fig. 4C. The molecular motor molecules, embedded within the surface of a textured liquid crystal film, induce the rotation of a macroscopic glass particle through a continuous reorganization of the film texture (*44*). Although the stability of these molecular machines is probably superior to proteins, their control, directionality, and interface to the outside world are yet far less developed (*43*).

The small size and force-exerting capabilities of motor proteins and the range of opportunities for specific engineering give them unique advantages over current human-made motors. Upon studying and using biomotors, we will gather a lot of knowledge that is of interest to biology, material science, and chemistry, and it is reasonable to expect spin-offs for medicine, sensors, electronics, or engineering. The exploration of biomotors in technology will thus remain an interdisciplinary playground for many years to come.

References and Notes
1. B. Alberts, *Cell* **92**, 291 (1998).
2. H. Hess, G. D. Bachand, V. Vogel, *Chem. Eur. J.* **10**, 2110 (2004).
3. K. Kinbara, T. Aida, *Chem. Rev.* **105**, 1377 (2005).
4. M. Yoshida, E. Muneyuki, T. Hisabori, *Nat. Rev. Mol. Cell Biol.* **2**, 669 (2001).
5. H. C. Berg, *Annu. Rev. Biochem.* **72**, 19 (2003).
6. R. D. Vale, R. A. Milligan, *Science* **288**, 88 (2000).
7. R. D. Vale, *Cell* **112**, 467 (2003).
8. R. K. Soong *et al.*, *Science* **290**, 1555 (2000).
9. H. Liu *et al.*, *Nat. Mater.* **1**, 173 (2002).
10. Y. Hiratsuka, M. Miyata, T. Tada, T. Q. P. Uyeda, *Proc. Natl. Acad. Sci. U.S.A.* **103**, 13618 (2006).
11. J. Xi, J. J. Schmidt, C. D. Montemagno, *Nat. Mater.* **4**, 180 (2005).
12. S. Diez *et al.*, *Nano Lett.* **3**, 1251 (2003).
13. H. Hess, *Soft Matter* **2**, 669 (2006).
14. H. Suzuki, A. Yamada, K. Oiwa, H. Nakayama, S. Mashiko, *Biophys. J.* **72**, 1997 (1997).
15. D. Riveline *et al.*, *Eur. Biophys. J.* **27**, 403 (1998).
16. H. Hess, J. Clemmens, D. Qin, J. Howard, V. Vogel, *Nano Lett.* **1**, 235 (2001).
17. Y. Hiratsuka, T. Tada, K. Oiwa, T. Kanayama, T. Q. P. Uyeda, *Biophys. J.* **81**, 1555 (2001).
18. J. Clemmens *et al.*, *Langmuir* **19**, 10967 (2003).
19. R. Bunk *et al.*, *Nanotechnology* **16**, 710 (2005).
20. Y. M. Huang, M. Uppalapati, W. O. Hancock, T. N. Jackson, *IEEE Trans. Adv. Packag.* **28**, 564 (2005).
21. M. G. L. van den Heuvel, M. P. de Graaff, C. Dekker, *Science* **312**, 910 (2006).
22. M. G. L. van den Heuvel, C. T. Butcher, R. M. M. Smeets, S. Diez, C. Dekker, *Nano Lett.* **5**, 1117 (2005).
23. B. M. Hutchins, M. Platt, W. O. Hancock, M. E. Williams, *Small* **3**, 126 (2007).
24. R. Stracke, K. J. Bohm, J. Burgold, H. J. Schacht, E. Unger, *Nanotechnology* **11**, 52 (2000).
25. K. J. Bohm, R. Stracke, P. Muhlig, E. Unger, *Nanotechnology* **12**, 238 (2001).
26. L. Limberis, J. J. Magda, R. J. Stewart, *Nano Lett.* **1**, 277 (2001).
27. C. Z. Dinu *et al.*, *Small* **2**, 1090 (2006).
28. G. D. Bachand *et al.*, *Nano Lett.* **4**, 817 (2004).
29. G. D. Bachand, S. B. Rivera, A. Carroll-Portillo, H. Hess, M. Bachand, *Small* **2**, 381 (2006).
30. S. Ramachandran, K. H. Ernst, G. D. Bachand, V. Vogel, H. Hess, *Small* **2**, 330 (2006).
31. S. Taira *et al.*, *Biotechnol. Bioeng.* **95**, 533 (2006).
32. F. Patolsky, Y. Weizmann, I. Willner, *Nat. Mater.* **3**, 692 (2004).
33. R. Yokokawa *et al.*, *J. Microelectromech. Syst.* **13**, 612 (2004).
34. G. Mihajlovic *et al.*, *Appl. Phys. Lett.* **85**, 1060 (2004).
35. L. Ionov, M. Stamm, S. Diez, *Nano Lett.* **6**, 1982 (2006).
36. M. G. L. van den Heuvel, C. T. Butcher, S. G. Lemay, S. Diez, C. Dekker, *Nano Lett.* **5**, 235 (2005).
37. R. Seetharam, Y. Wada, S. Ramachandran, H. Hess, P. Satir, *Lab Chip* **6**, 1239 (2006).
38. J. L. Bull, A. J. Hunt, E. Meyhofer, *Biomed. Microdev.* **7**, 21 (2005).
39. H. Hess, J. Clemmens, J. Howard, V. Vogel, *Nano Lett.* **2**, 113 (2002).
40. D. V. Nicolau *et al.*, *Microelectron. Eng.* **83**, 1582 (2006).
41. T. J. M. Luo, R. Soong, E. Lan, B. Dunn, C. Montemagno, *Nat. Mater.* **4**, 220 (2005).
42. M. Sarikaya, C. Tamerler, A. K. Y. Jen, K. Schulten, F. Baneyx, *Nat. Mater.* **2**, 577 (2003).
43. W. R. Browne, B. L. Feringa, *Nat. Nanotechnol.* **1**, 25 (2006).
44. R. Eelkema *et al.*, *Nature* **440**, 163 (2006).
45. D. W. Wendell, J. Patti, C. D. Montemagno, *Small* **2**, 1324 (2006).
46. D. Thomas, D. G. Morgan, D. J. DeRosier, *J. Bacteriol.* **183**, 6404 (2001).
47. H. Noji, R. Yasuda, M. Yoshida, K. Kinosita, *Nature* **386**, 299 (1997).
48. H. J. Choi, C. D. Montemagno, *Nano Lett.* **5**, 2538 (2005).
49. We acknowledge the involvement of and discussions with C. Butcher, I. Dujovne, M. de Graaff, S. Lemay, Y. Shen, R. Smeets, and with collaborators S. Diez, M. Dogterom, and J. Howard. We acknowledge financial support from the Foundation for Fundamental Research on Matter (FOM), NanoNed, the Dutch Organization for Scientific Research (NWO), and Biomach.

10.1126/science.1139570

Tumor Growth Need Not Be Driven by Rare Cancer Stem Cells

Priscilla N. Kelly,[1,2] Aleksandar Dakic,[1,2] Jerry M. Adams,[1]* Stephen L. Nutt,[1]* Andreas Strasser[1]*†

Cancer biologists are intrigued by the hypothesis that tumor growth may be sustained by a rare subpopulation of the cells, termed cancer stem cells. Supporting this concept are the heterogeneous cellular composition of certain tumors and the finding that only a minute proportion of the cells (~1/10[6]) in some human acute myeloid leukemia (AML) samples can seed tumor growth when transplanted into sublethally irradiated nonobese diabetic (NOD) severe combined immunodeficient (scid) mice (1). The interpretation of such xenotransplantation studies, however, is complicated by the critical role in tumor growth of interactions with the microenvironment, which are mediated by both soluble and membrane-bound factors (2). Notably, many such mouse factors cannot engage the cognate human receptor and vice versa (3). Thus, the low frequency of human AML cells producing tumors in NOD/scid mice might reflect in part the rarity of human tumor cells that can readily adapt to growth in a foreign (mouse) milieu.

In our view, the frequency of cells that can sustain tumor growth, and thus the generality of the cancer stem cell hypothesis, can best be tested by transfer of titrated numbers of mouse tumor cells into nonirradiated histocompatible recipient mice. We isolated primary pre-B/B lymphoma cells from three independent Eμ-myc transgenic mice and injected 10 to 10[5] cells into nonirradiated congenic animals. Regardless of the cell number injected, all recipients became moribund with disseminated lymphoma within 35 days (Table 1). Although the number of injected cells did not noticeably affect tumor burden, organ infiltration, or disease severity, recipients of 10 or 100 lymphoma cells usually developed tumors more slowly than those receiving 10[5] cells. Importantly, even transfer of a single cell elicited fatal lymphoma in three of eight recipients within 33 to 76 days (case 2).

A small fraction (~2 to 5%) of the cells in primary Eμ-myc lymphomas displayed the characteristic stem cell markers Sca-1 and/or AA4.1. However, when sorted Sca-1^{+} AA4.1[hi] or Sca-1^{+} AA4.1^{lo} lymphoma cells were transplanted, as few as 10 cells of each population elicited fatal lymphoma within 17 to 40 days (Table 1). Similarly, with Eμ-N-RAS thymic lymphomas and four independent cases of AML caused by PU.1 deficiency, recipients transplanted with as few as 10 cells developed tumors, although onset was delayed in mice receiving only 10 or 100 AML cells (Table 1). For all three malignancies, the cell surface marker phenotype (fig. S1), the gene expression profile (fig. S2), and the invasiveness of the transplanted tumors mirrored that of the primary tumor.

These observations challenge the concept that growth of AML, and possibly other malignancies, are always sustained by a rare cancer stem cell (1). Although cancer stem cells may well drive the growth of many cancers, particularly those displaying extensive differentiation, our studies of mouse lymphomas and leukemias indicate that at least certain malignancies (particularly those with substantial homogeneity) can be maintained by a relatively large proportion (>10%) of tumor cells, perhaps even the majority. Although mouse and human tumors differ in notable respects, the marked disparity with results from human AML cells (1) suggests that xenotransplantation may underestimate the percentage of tumor-sustaining cells. With common human solid tumors (for example, brain, colon, and breast), transplantation places the tumor growth–sustaining cells within subpopulations (for example, CD133^{+}) that compose up to 20% of the cells (4–6), and most of the remaining cells might be at differentiation stages unsupportable by the mouse microenvironment. The reported rarity of cancer stem cells in AML (1) and colon cancer (4) might reflect the need to cotransfer an essential human accessory cell (we note that endothelial cell progenitors are also CD133^{+}).

Determining whether the growth of various tumors is sustained by most of the tumor cells or by a rare subpopulation has important ramifications for the design of novel therapies. Therefore, the cancer stem cell hypothesis merits more rigorous tests. For human tumors, ultimately this will require transfer of tumor cells into mice installed with all the requisite human support cells. Lastly, because the term "cancer stem cell" also currently designates the normal cell that founded the tumor, we suggest that the cells sustaining growth of an established tumor be referred to as "tumor-propagating cells."

Table 1. A large proportion of tumor cells can sustain the growth of murine lymphoid and myeloid malignancies. Cells from primary Eμ-myc pre-B/B lymphomas, Eμ-N-RAS thymic lymphomas, or PU.1[−/−] AML, all from mice on a C57BL/6 (Ly5.2[+]) background (>15 backcrosses), were transplanted into nonirradiated congenic C57BL/6 (Ly5.1[+]) recipient mice. To circumvent problems associated with injection of low cell numbers, we mixed the tumor cells with 10[6] congenic (C57BL/6-Ly5.1^{+}) spleen cells as carriers. Shown are the fraction of recipients that developed tumors and the average time from transplantation to tumor development. No mice (0/24) injected with carrier spleen cells alone developed any tumor over a 100-day period. ND, not determined.

	Recipients that developed tumors (days to kill)			
	10[5] cells	10[3] cells	10[2] cells	10 cells
Eμ-myc B lymphoma				
Case 1	3/3 (25)	3/3 (25)	3/3 (32)	2/2 (35)
Case 2	3/3 (21)	3/3 (23)	3/3 (24)	3/3 (24)
Case 3 Sca-1^{+} AA4.1[hi]	3/3 (21)	3/3 (21)	ND	3/3 (17)
Sca-1[+] AA4.1[lo]	2/2 (17)	2/2 (28)	2/2 (28)	2/2 (40)
Eμ-N-RAS T lymphoma				
Case 1	3/3 (28)	3/3 (42)	3/3 (28)	3/3 (28)
PU.1[−/−] AML				
Case 1	1/1 (54)	2/2 (168)	1/2 (192)	0/2
Case 2	2/2 (84)	2/2 (85)	2/2 (224)	1/2 (114)
Case 3	1/1 (85)	2/2 (62)	2/2 (69)	2/2 (90)
Case 4	1/1 (30)	1/1 (37)	2/2 (79)	2/2 (88)

References

1. K. J. Hope, L. Jin, J. E. Dick, *Nat. Immunol.* **5**, 738 (2004).
2. D. Hanahan, R. A. Weinberg, *Cell* **100**, 57 (2000).
3. K. I. Arai *et al.*, *Annu. Rev. Biochem.* **59**, 783 (1990).
4. C. A. O'Brien, A. Pollett, S. Gallinger, J. E. Dick, *Nature* **445**, 106 (2007).
5. S. K. Singh *et al.*, *Nature* **432**, 396 (2004).
6. M. Al-Hajj, M. S. Wicha, A. Benito-Hernandez, S. J. Morrison, M. F. Clarke, *Proc. Natl. Acad. Sci. U.S.A.* **100**, 3983 (2003).

[1]Walter and Eliza Hall Institute of Medical Research, Melbourne 3050, Australia. [2]Department of Medical Biology, University of Melbourne, Melbourne 3050, Australia.

*These authors contributed equally to this study.
†To whom correspondence should be addressed. E-mail: strasser@wehi.edu.au

Common Sequence Polymorphisms Shaping Genetic Diversity in *Arabidopsis thaliana*

Richard M. Clark,[1] Gabriele Schweikert,[1,2,3]* Christopher Toomajian,[4]* Stephan Ossowski,[1]* Georg Zeller,[1,2,5]* Paul Shinn,[6] Norman Warthmann,[1] Tina T. Hu,[4] Glenn Fu,[7] David A. Hinds,[7] Huaming Chen,[6] Kelly A. Frazer,[7] Daniel H. Huson,[5] Bernhard Schölkopf,[3] Magnus Nordborg,[4] Gunnar Rätsch,[2] Joseph R. Ecker,[6,8] Detlef Weigel[1,8]†

The genomes of individuals from the same species vary in sequence as a result of different evolutionary processes. To examine the patterns of, and the forces shaping, sequence variation in *Arabidopsis thaliana*, we performed high-density array resequencing of 20 diverse strains (accessions). More than 1 million nonredundant single-nucleotide polymorphisms (SNPs) were identified at moderate false discovery rates (FDRs), and ~4% of the genome was identified as being highly dissimilar or deleted relative to the reference genome sequence. Patterns of polymorphism are highly nonrandom among gene families, with genes mediating interaction with the biotic environment having exceptional polymorphism levels. At the chromosomal scale, regional variation in polymorphism was readily apparent. A scan for recent selective sweeps revealed several candidate regions, including a notable example in which almost all variation was removed in a 500-kilobase window. Analyzing the polymorphisms we describe in larger sets of accessions will enable a detailed understanding of forces shaping population-wide sequence variation in *A. thaliana*.

Comprehensive polymorphism data are essential for the systematic identification of sequence variants affecting phenotypes (*1*). Despite progress with new technologies, direct resequencing of individual genomes is not yet cost effective for most organisms (*2*). High-density oligonucleotide arrays provide an alternative approach for polymorphism detection and have been used to identify a large fraction of the SNP variation in the human and the mouse (*3, 4*). We applied this technology to 20 wild accessions of *A. thaliana*, for which a genome sequence from a single accession was generated in the year 2000 (*5*). The resulting polymorphism data set captures much of the common sequence variation in the worldwide *A. thaliana* population. We used this information to systematically determine the types of sequences and genes that differ between accessions and to provide a high-resolution description of the genome-wide distribution of polymorphisms in this multicellular reference organism.

Sample selection, array design, and polymorphism detection. For polymorphism discovery, we selected accessions with maximal genetic diversity (*6, 7*). In addition, we chose several commonly used strains, such as L*er*-1 (table S1). Col-0, the reference accession, was included as a control. For 19 of the 20 accessions (*7*), 1213 fragments of ~500 base pairs (bp) in length, which were spaced throughout the genome, had previously been sampled by dideoxy sequencing; between 2266 and 3949 nucleotide substitutions per accession relative to Col-0 had been identified (*6*). This data set, called "2010," allowed us to assess the quality of our polymorphism predictions.

Whole-genome amplified DNA from each accession was hybridized to resequencing microarrays interrogating >99.99% of bases in the 119-Mb reference genome sequence (*7*). Each position was queried with forward- and reverse-strand probe quartets consisting of oligonucleotides of length 25 (fig. S1). Within a probe quartet, all four nucleotides were represented at the central position, and differences in relative intensities across probe quartets indicated potential SNPs. For tightly linked SNPs, however, all probes harbor at least one mismatch, hybridization is suppressed, and SNP detection is confounded (fig. S1).

We used two computational methods to detect SNPs at 105,920,272 positions that were not highly repetitive (*7*) (table S2 and fig. S2). In *A. thaliana*, the sequence composition (i.e., GC content) and low polymorphism levels typical for coding sequences are favorable for hybridization-based SNP detection (*7*). Accordingly, recovery of SNPs with a model-based (MB) algorithm (*3, 4*) was higher for coding than for noncoding regions (36 versus 15%) at a corresponding FDR that was only one-third as high (Fig. 1A). An average of 96,814 SNPs were identified per accession by the MB method, for a total of 456,956 nonredundant SNPs (Fig. 1B and table S3).

We also developed a machine learning (ML) method with support vector machines (*8, 9*) for SNP identification (*7*) (figs. S3 to S8). The training step exploited the 2010 data, and as input we used information for all oligonucleotide probes corresponding to positions within a 9-bp window centered on candidate polymorphisms (*7*). In addition to hybridization data, we included as inputs sequence characteristics and genome-wide repetitiveness of probes (tables S5 and S6). The ML method assigns a probability to each prediction, and we generated 440,657 to 1,074,055 nonredundant SNP predictions over a corresponding range of FDRs from 2 to 10% (*7, 10*). Performance of the ML method was inferior to the MB method for coding sequences but superior for noncoding sequences (Fig. 1, A and B, and table S3).

When the FDR for the ML method was at 2%, the FDR and recovery for the ML and MB methods were similar; however, the two methods were complementary, with 60% of predictions made with only one of the methods (Fig. 1C). This resulted, in part, from differing performance in polymorphic regions (Fig. 1D). Recall for SNPs more than ~30 bp from another SNP or insertion or deletion (indel) was higher for the MB method, whereas recall for SNPs separated by 7 to 30 bp from a nearby polymorphism was about two times as high for the ML method. For very closely linked SNPs (<7 bp), recovery was low with both methods (~3%). FDRs for both methods peaked in regions of low hybridization quality (Fig. 1E), an effect of sequence divergence but also of other factors (*7*).

For subsequent analyses, we combined all MB predictions with ML predictions supported at a 2% FDR. The resulting data set, "MBML2," consisted of 648,570 nonredundant SNPs (*7, 10*) (Fig. 2), an average of one polymorphic site per 166 nonrepetitive positions in the genome. Within MBML2, SNPs supported by both methods have a very low FDR of ~0.2%, whereas SNPs supported by only one method have correspondingly higher FDRs (Table 1 and table S3). A caveat for our error estimates is that 2010 data, which we used for specificity and sensitivity assessment of the two prediction methods, are underrepresented for noncoding sequences, repeats, and sequences not similar to the reference (*6, 7*).

Apart from SNPs, deletions or sequences highly dissimilar to the reference are detectable on high-density arrays as regions of reduced hybridization (*11*) (fig. S1). We developed a heuristic algorithm to identify tracts of reduced hybridization extending over more than ~200 bp (*7*) (figs. S9 and S10). The median length of 13,470 polymorphic region predictions (PRPs) generated across all accessions with this algorithm was 589 bp; the longest was 41.2 kb (*10*). In the 2010 data set, which was ascertained by polymerase chain reaction (PCR), missing data correspond in part to highly polymorphic or deleted regions. Consistent with high specificity for PRPs, a 162-fold overrepresentation was observed between PRPs and absent data in 2010. We also attempted validation of 382 PRPs by PCR and sequencing, ob-

[1]Department of Molecular Biology, Max Planck Institute for Developmental Biology, 72076 Tübingen, Germany. [2]Friedrich Miescher Laboratory of the Max Planck Society, 72076 Tübingen, Germany. [3]Department of Empirical Inference, Max Planck Institute for Biological Cybernetics, 72076 Tübingen, Germany. [4]Molecular and Computational Biology, University of Southern California, Los Angeles, CA 90089, USA. [5]Center for Bioinformatics Tübingen, Tübingen University, 72076 Tübingen, Germany. [6]Genomic Analysis Laboratory, The Salk Institute for Biological Studies, La Jolla, CA 92037, USA. [7]Perlegen Sciences, 2021 Stierlin Court, Mountain View, CA 94043, USA. [8]Plant Biology Laboratory, The Salk Institute for Biological Studies, La Jolla, CA 92037, USA.

*These authors contributed equally to this work.

†To whom correspondence should be addressed. E-mail: weigel@weigelworld.org

tained complete or partial sequence data for 171 products, and identified 124 deletions ranging from 50 bp to more than 10 kb. In all other cases, PRPs corresponded to clusters of SNPs or small indels (table S11). Many deletions or clusters of polymorphisms extended beyond PRP boundaries, potentially contributing to the high failure rate for validation attempts (~55%). Where sequence data were available, 98.6% of bases in PRPs were either deleted or within 6 bp of a SNP or indel polymorphism (7). Nearly 4.1% of the reference genome sequence was included in PRPs, with transposon and pseudogene sequences overrepresented 3.5-fold (Fig. 2).

To complement polymorphism predictions, we developed a base-calling algorithm to identify positions identical to the reference at low FDRs (7). Between 80.3 and 92.3% of coding positions and between 39.7 and 61.2% of intergenic posi-

tions were predicted to be the same as the reference in the different accessions (table S8). We combined these reference base calls with MBML2 to generate pseudochromosome sequences for each of the 20 accessions (10).

Effects of polymorphisms on genes. To characterize genome evolution in *A. thaliana*, we assessed effects of the nonredundant MBML2 SNPs on the 26,541 annotated protein-coding genes (12). In addition to SNPs resulting in 109,979 amino acid changes, we identified many SNPs with large effects on gene integrity. In this class, 1227 introduce premature stop codons, 156 alter initiation methionine residues, and 435 lead to nonfunctional splice donor or acceptor sites (10) (table S9). Also, 198 SNPs remove annotated stop codons, resulting in longer open reading frames. Given that large-effect SNPs are expected to be uncommon in the genome

relative to all SNPs, FDRs for this SNP subclass might differ from that for MBML2 as a whole. To rule out the possibility that large-effect SNPs resulted predominantly from false SNP calls, we assayed 701 of these predictions directly (table S9). Dideoxy-sequencing validated 650 SNPs, including 413 resulting in premature stop codons (table S10). At 7.3%, the FDR for large-effect SNPs is moderately higher than for an average SNP in MBML2 (7). In total, 1614 genes harbor at least one large-effect SNP. In addition, the coding regions of 1191 genes are at least partially included in PRPs; that is, they are highly polymorphic or deleted. The overlap between the two classes is greater than expected by chance ($\chi^2 = 186.1$, df = 2, $P < 10^{-20}$). Together, large-effect SNPs and PRPs, hereafter referred to simply as "major-effect changes," affected 2495, or 9.4%, of *A. thaliana* protein-coding genes.

The number of genes harboring major-effect changes varies significantly according to annotation support ($\chi^2 = 239.2$, df = 2, $P < 10^{-20}$), duplication status ($\chi^2 = 256.4$, df = 2, $P < 10^{-20}$), and gene family ($\chi^2 = 311.6$, df = 12, $P < 10^{-20}$) (Fig. 3A). Correction for gene size and repetitive content does not appreciably change the observed patterns (fig. S11). By annotation, genes known to be expressed but lacking functional support or high homology ("Expressed unknown"), as well as genes without expression support ("Not expressed"), are over-represented. In addition, of 836 *A. thaliana* genes that either lack or have only moderate similarity
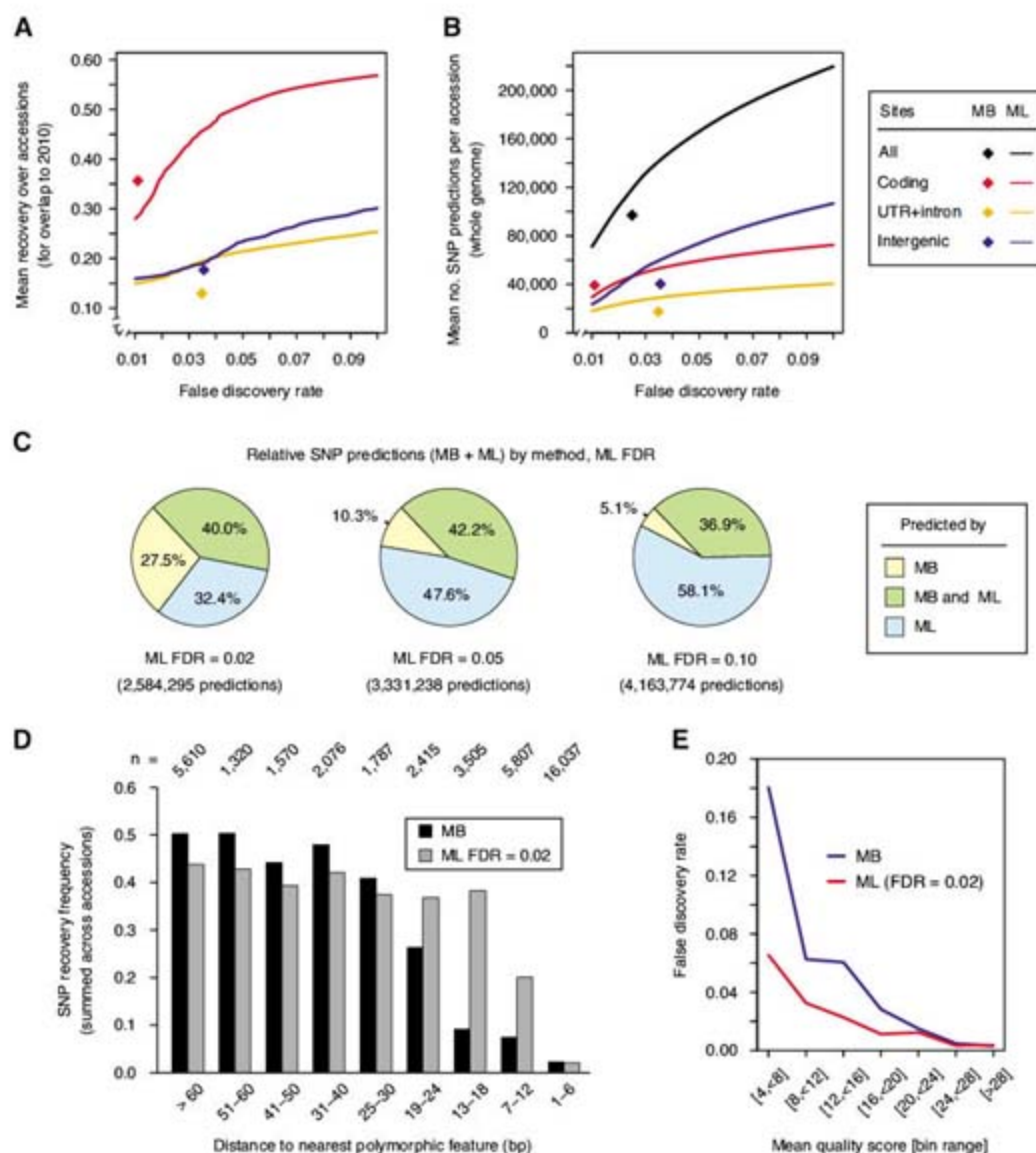
Fig. 1. Comparison of SNP detection methods. (**A**) FDR-dependent recovery of 48,700 known SNPs in 2010 fragments by the MB and ML methods. Because of small sample size for untranslated region (UTR) SNPs in 2010, this group was combined with intron sequences. (**B**) FDR-dependent recovery across the entire genome by both methods with precision estimates from 2010. The FDR for all SNPs is also given with a correction for both methods to account for the different sequence composition of 2010 and the whole genome. (**C**) Overlap between genome-wide MB and ML calls across all accessions. (**D**) Recovery frequency for SNPs as a function of distance to the nearest polymorphic feature. Analysis was based on 2010 sites with sufficient flanking information to assign bin membership. Sample sizes per bin are shown at the top. (**E**) FDRs for MB and ML predictions as a function of the mean quality score for the forward- and reverse-strand probe quartets.
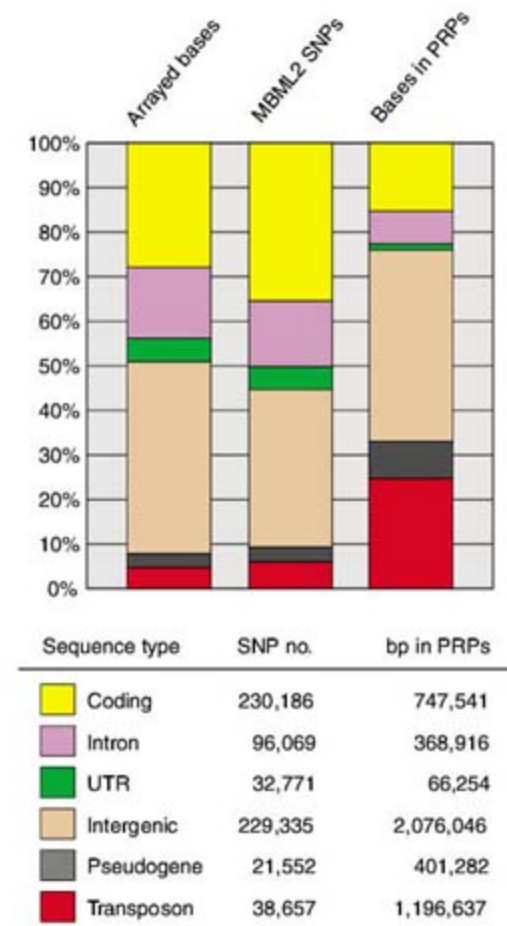

Fig. 2. Distribution of SNPs in MBML2 and positions included in PRPs compared with sequences tiled on arrays.

Sequence type	SNP no.	bp in PRPs
Coding	230,186	747,541
Intron	96,069	368,916
UTR	32,771	66,254
Intergenic	229,335	2,076,046
Pseudogene	21,552	401,282
Transposon	38,657	1,196,637

to genes in *Populus trichocarpa* (*7*), the closest sequenced genome to *A. thaliana* (*13*), 26.0% harbor major-effect changes, compared with 8.9% of all other genes. Poor gene annotation likely contributes to this effect, but rapid gene evolution may also play a part.

Table 1. SNPs identified per accession in MBML2 with FDR and recovery assessed against 2010.

SNP type	Mean no. SNPs per accession by method [Mean FDR (%): Mean recovery (%)]			
	Total	MB only	MB ∩ ML	ML only
Coding	53,700 [2.0: 48.0]	11,379 [3.2: 11.3]	27,833 [0.1: 24.6]	14,488 [4.8: 12.1]
Intron+UTR	29,395 [3.1: 20.5]	5,762 [9.6: 4.3]	11,652 [0.4: 8.8]	11,981 [2.6: 7.5]
Intergenic	60,478 [3.5: 24.4]	22,395 [7.3: 7.7]	17,976 [0.3: 10.2]	20,107 [3.6: 6.5]
All	143,572 [2.8: 27.7]	39,536 [6.5: 7.0]	57,461 [0.2: 13.7]	46,575 [3.7: 7.8]
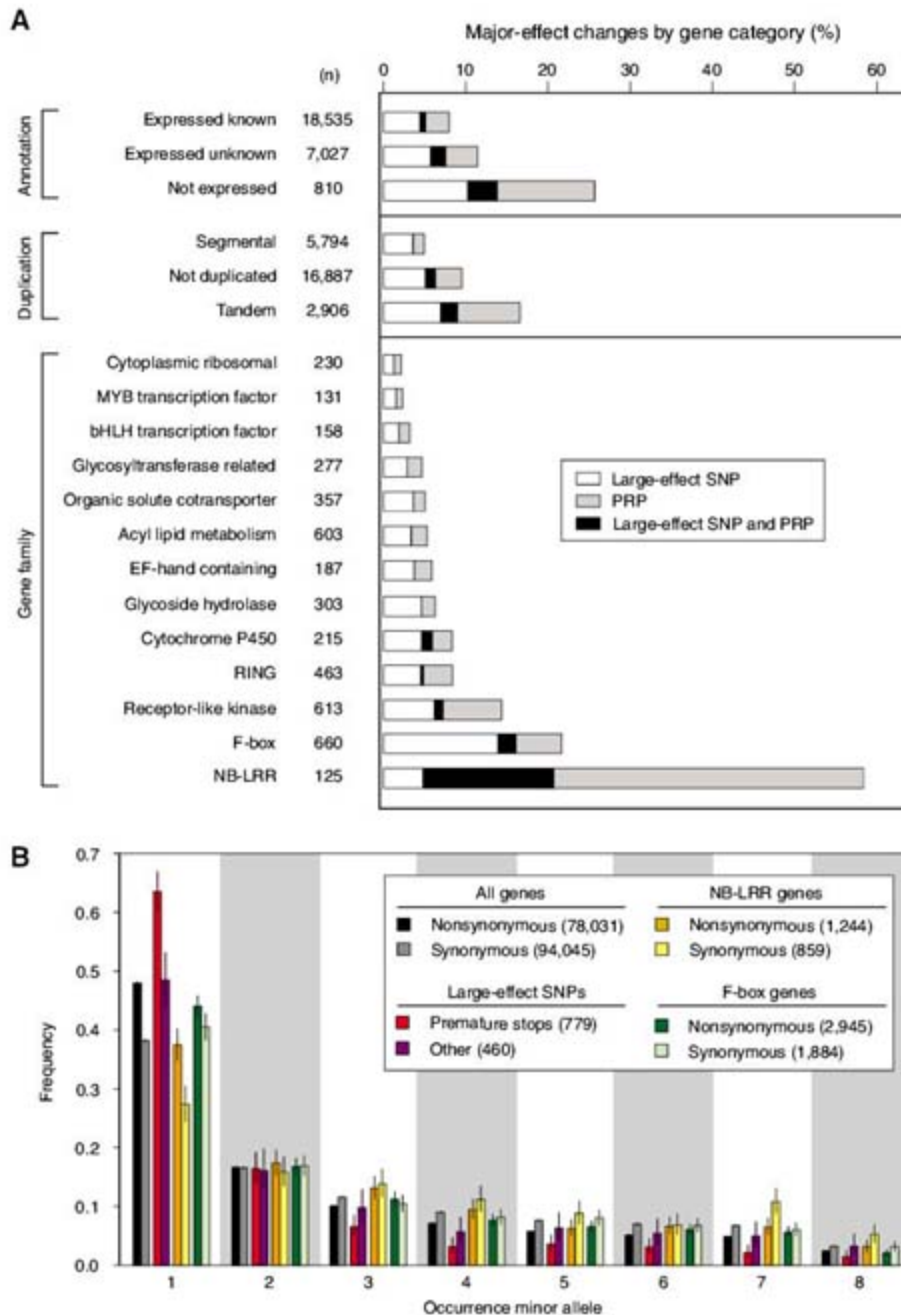
Fig. 3. Distribution of major-effect changes and allele frequencies. (**A**) Fraction of genes affected by large-effect SNPs or PRPs by gene category. "Large-effect SNP and PRP" (black) denotes a gene harboring both types of polymorphism, either within the same accession or in different accessions. Genes that were entirely masked as repetitive, and for which no SNPs could be predicted, were excluded from analysis. RING, Really Interesting New Gene. (**B**) Minor allele frequency by SNP type and gene family. Only positions with complete data for at least 16 of the 20 accessions were assessed. The number of polymorphic positions included in the analysis is shown in the inset. For large-effect SNPs, "Other" includes nonfunctional splice site changes, substitutions in initiation methionine codons, and substitutions that remove termination codons. Error bars denote 95% confidence intervals for binomial expectations.

Consistent with relaxed purifying selection following recent gene duplication (*14*), tandem duplicates are 3.4- and 1.7-fold overrepresented for major-effect changes relative to segmentally duplicated and nonduplicated genes, respectively (Fig. 3A). Segmentally duplicated genes in *A. thaliana* resulted from ancient genome-wide duplications (*5, 15*); these genes harbor relatively few major-effect changes, which is consistent with earlier work suggesting that duplicates persisting over long evolutionary time frames are under strong purifying selection (*13, 14*).

Analysis of individual gene families provided additional insights. Families involved in basic biological processes (such as ribosomal function), as well as families involved in transcriptional regulation [such as MYB and basic helix-loop-helix (bHLH) transcription factors], harbor relatively few major-effect changes (Fig. 3A). In contrast, nearly 60% of nucleotide-binding leucine-rich repeat (NB-LRR) genes (*7*) and 15% of receptor-like kinase (RLK) genes harbor at least one major-effect change. The only function assigned to members of the NB-LRR gene family is in strain-specific resistance to pathogens (*16*), and receptors of this class can be exceedingly variable, as presence and absence polymorphisms are common in *A. thaliana* and other plants (*17–19*). Our data indicate that this extends to the majority of NB-LRR genes in the *A. thaliana* genome. Although they have diverse functions (*20*), RLK genes have also been implicated in race-specific pathogen defense (*21*). Thus, the finding that RLK genes are overrepresented for major-effect changes raises the possibility that this is, similar to NB-LRR genes, a consequence of fitness trade-offs between pathogen defense and growth (*22*).

We found major-effect changes in 143 members of the F-box superfamily, which comprises more than 660 genes in *A. thaliana* (*23*) (Fig. 3A). This finding, in combination with other data (*13, 24*), shows that F-box genes have undergone rapid birth and death in the *A. thaliana* genome. Although F-box genes have been proposed to evolve quickly in response to pathogen pressure (*24*), experimental support for this hypothesis is lacking. The polymorphisms we describe provide a resource for ascribing biological roles to members of this large, yet not well-characterized, gene family.

Signatures of selection by SNP type and gene family. To assess the extent to which the variation we observed has been shaped by selection, we examined allele frequency distributions for different classes of polymorphisms. Consistent with general expectations for selective constraints in coding sequences, there is a skew toward low-frequency variants at nonsynonymous relative to synonymous sites (*6*) (Fig. 3B). This skew is most notable for SNPs that introduce premature stop codons and less extreme for other large-effect SNPs. The tendency of SNPs causing premature stops to be rare suggests that, at least under natural settings, these changes are often associated with fitness costs.

Although allele frequency distributions across gene families are broadly similar, NB-LRR genes are an exception (Fig. 3B and fig. S12). Here,

both nonsynonymous and synonymous variants are strongly skewed toward high frequency compared with the genome average (Fig. 3B). This shift is a hallmark of some type of balancing selection (perhaps in the form of regional adaptation), and agrees with earlier work, on the basis of fewer family members, that suggested this mode of selection to be not uncommon for NB-LRR genes in *A. thaliana* (17, 19, 22). An additional prediction of balancing selection is a higher-than-average level of polymorphism because of the maintenance of relatively ancient, highly diverged alleles. Consistent with this expectation, more than 50% of NB-LRR genes are at least partially included in PRPs (Fig. 3A), many of which correspond to highly dissimilar sequences. Although less extreme, a similar allele frequency skew and high number of PRPs were observed for RLK genes (Fig. 3A and fig. S12). Although F-box genes harbor the second-highest occurrence of major-effect changes, allele frequency distributions are similar to the average (Fig. 3B).

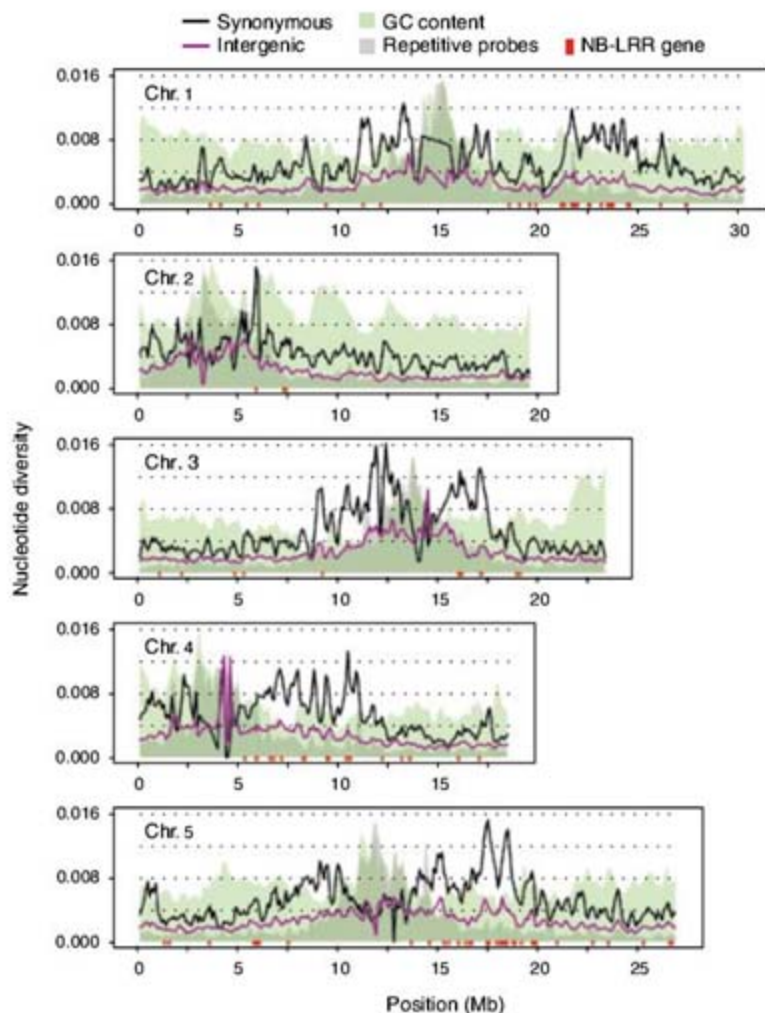**Genome-wide patterns of polymorphism.** Turning to broader patterns of variation, we found a markedly nonrandom distribution of polymorphism levels across the genome (Fig. 4). Regions of high polymorphism extend from the centromeres to beyond the pericentromeric regions. Similarly, clusters of NB-LRR genes (7, 25) are associated

with high levels of polymorphism (e.g., between 21 and 25 Mb on chromosome 1).

It is difficult to determine the reasons for these patterns. Given that they are evident for both synonymous and intergenic polymorphism, direct selection on the polymorphic sites seems unlikely, although selection on linked sites may either increase or decrease variation (6). Mutation rates may also differ between chromosomal regions because of differences in base composition. Finally, there are almost certainly biases in the array-based resequencing—e.g., due to regional differences in repeat content (7).
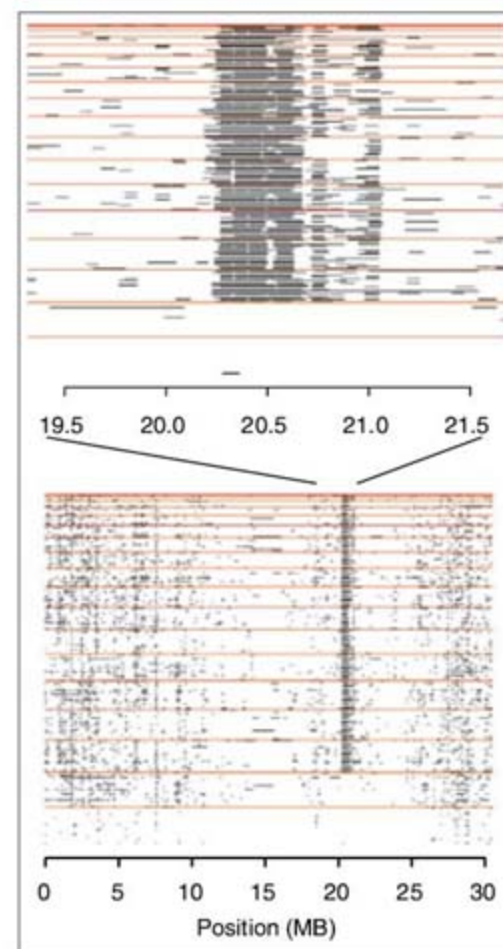
We believe that all three explanations contribute to the observed patterns. In a multiple regression, the estimated polymorphism levels are significantly correlated with several variables, including repeat density, GC content, fraction of missing data, distance from the centromere, and density of NB-LRR genes (table S12). The patterns are, however, not simply an artifact of the resequencing technology; they are also evident in resequencing data obtained with other techniques (6, 26) (fig. S13). For the regions around NB-LRR gene clusters, polymorphism was elevated even when the NB-LRR genes themselves were excluded (fig. S14), and polymorphism was also elevated in intergenic DNA. Pervasive balancing selection acting on these genes, as suggested by the results in Fig. 3B and other studies (17), is a

likely explanation. Balancing selection can increase coalescence times for regions linked to selectively maintained polymorphisms (27), a phenomenon that should be more easily detected in selfing organisms (28) and that has been reported for *A. thaliana* (22, 29, 30). Clusters of tightly linked genes subject to balancing selection, such as NB-LRR genes (25) (Fig. 4), may give rise to regions of high polymorphism similar to what has been observed for the vertebrate major histocompatibility complex genes (31, 32). The forthcoming *A. lyrata* genome sequence (33) will be instrumental in analyzing these data further, because it will allow divergence to be estimated between these two closely related species. This will be essential for determining the relative importance of selection versus mutation-rate variation.

In contrast, regions of low polymorphism might reflect recent positive selection, or "selective sweeps" (34, 35) characterized by extensive haplotype sharing. A study with 2010 data found strong evidence for two separate partial sweeps involving inactivation of *FRI*, a major determinant of flowering time in natural populations of *A. thaliana* (36). The

Fig. 4. Genome-wide pattern of nucleotide diversity. Average pairwise nucleotide diversity is plotted for both fourfold degenerate synonymous and intergenic sites along each chromosome with sliding windows of 250 kb (counted from all sites) with an offset of 100 kb (7). GC content in each window was calculated from sites called in the Col-0 sample and has been rescaled so 35% is at the bottom of each plot and 47.5% is at the top. The broad peaks of repetitive probe density on each chromosome correspond to the centromeric and pericentromeric regions. Repeat content has been rescaled so 100% is at the top of each plot and 0% is at the bottom. Levels of polymorphism for both fourfold degenerate and intergenic sites are significantly negatively correlated with the distance to the centromere and positively correlated with the number of NB-LRR genes in nonoverlapping 50-kb windows (table S12). Polymorphism is reduced at intergenic relative to synonymous sites, which is partly due to lower recovery of SNPs in intergenic regions (e.g., Fig. 1A).

Fig. 5. Regions of extensive pairwise haplotype sharing along chromosome 1. Accession pairs are sorted along the *y* axis. Horizontal red lines demarcate comparisons using one accession. Each possible pairwise comparison is shown only once. Black lines indicate regions of very high similarity between a pair of accessions. The region between 20 and 21 Mb exhibits extensive haplotype sharing over nearly 500 kb in all but two accessions, Cvi-0 and Lov-5, which are shown at the bottom.

current data set confirmed extensive haplotype sharing of up to 600 kb around *FRI* (fig. S15), as well as haplotype sharing around other low-frequency candidate alleles (*36*) (fig. S16).

We looked for evidence of additional sweeps in the form of extensive haplotype sharing across at least 50 kb (Fig. 5 and figs. S17 to S19). Because of its composition and size, our sample is only suited for discovering species-wide sweeps. We did not find evidence of a recent sweep affecting all accessions. However, on chromosome 1 all but two accessions were nearly identical for approximately 500 kb (Fig. 5). The two unaffected accessions, Cvi-0 and Lov-5, are from the periphery of the *A. thaliana* range and may have escaped the sweep because of different selective environments or geographic isolation. The region of most extreme haplotype sharing extends from 20.34 to 20.49 Mb and contains 50 annotated genes (table S13). There are several additional candidates for sweeps affecting a smaller number of accessions (figs. S17 to S20). With the SNPs identified in this project and the ability to determine their frequencies in hundreds to thousands of accessions (*37*), the goal of understanding the forces shaping diversity at global, regional, and local scales will soon be within reach.

Conclusions. We used array-based methods to generate a comprehensive polymorphism resource for *A. thaliana*. Our SNP data set is highly applicable for linkage disequilibrium mapping studies. In addition, we identified hundreds of thousands of polymorphisms in both coding and noncoding regions, providing an important resource for both evolutionary genetic and functional studies. Recently, studies in plants with large, repetitive genomes, like maize (genome size ~2.5 Gb), have shown that as much as 50% of sequences can differ between strains (*38*). In contrast to these plants, *A. thaliana* has a compact genome consisting largely of unique sequences. Nevertheless, our data highlight that even for species with streamlined genomes, individuals can differ substantially in genic content.

Mutations identified in laboratory phenotypic screens typically have marked phenotypic effects that are likely detrimental in the wild. The genes segregating for major-effect changes in our population have few known mutant phenotypes (tables S10 and S11), but nonetheless, allele frequency patterns suggest functional constraints under natural conditions. Variation in copy number for genic sequences may explain this observation; in a given accession, higher constraint may be observed if a paralog is absent. Nevertheless, as highlighted by the current study, many genes harboring major-effect changes in wild populations are likely to mediate interactions with the environment. Ultimately, experiments under more natural conditions will be required to fully appreciate the functional relevance of such sequence variation.

References and Notes

1. The International HapMap Consortium, *Nature* **437**, 1299 (2005).
2. J. Kling, *Nat. Biotechnol.* **23**, 1333 (2005).
3. D. A. Hinds *et al.*, *Science* **307**, 1072 (2005).
4. N. Patil *et al.*, *Science* **294**, 1719 (2001).
5. The Arabidopsis Genome Initiative, *Nature* **408**, 796 (2000).
6. M. Nordborg *et al.*, *PLoS Biol.* **3**, e196 (2005).
7. Materials and methods are available as supporting material on *Science* Online.
8. B. Schölkopf, A. Smola, *Learning with Kernels* (MIT Press, Cambridge, MA, 2002).
9. V. N. Vapnik, *Estimation of Dependences Based on Emperical Data* (Springer, New York, 1982; reprinted by Springer, New York, 2006).
10. SNP and PRP data sets along with effects on genes and pseudochromosome sequences are hosted at The *Arabidopsis* Information Resource (TAIR) (www.arabidopsis.org/).
11. D. A. Hinds, A. P. Kloek, M. Jen, X. Chen, K. A. Frazer, *Nat. Genet.* **38**, 82 (2006).
12. TAIR annotation Version 6 (www.ncbi.nlm.nih.gov/mapview/map_search.cgi?taxid=3702).
13. G. A. Tuskan *et al.*, *Science* **313**, 1596 (2006).
14. M. Lynch, J. S. Conery, *Science* **290**, 1151 (2000).
15. G. Blanc, K. Hokamp, K. H. Wolfe, *Genome Res.* **13**, 137 (2003).
16. J. D. Jones, J. L. Dangl, *Nature* **444**, 323 (2006).
17. E. G. Bakker, C. Toomajian, M. Kreitman, J. Bergelson, *Plant Cell* **18**, 1803 (2006).
18. M. R. Grant *et al.*, *Proc. Natl. Acad. Sci. U.S.A.* **95**, 15843 (1998).
19. J. Shen, H. Araki, L. Chen, J. Q. Chen, D. Tian, *Genetics* **172**, 1243 (2006).
20. S. H. Shiu, A. B. Bleecker, *Sci. STKE* **2001**, RE22 (2001).
21. W. Y. Song *et al.*, *Science* **270**, 1804 (1995).
22. E. A. Stahl, G. Dwyer, R. Mauricio, M. Kreitman, J. Bergelson, *Nature* **400**, 667 (1999).
23. E. Lechner, P. Achard, A. Vansiri, T. Potuschak, P. Genschik, *Curr. Opin. Plant Biol.* **9**, 631 (2006).
24. J. H. Thomas, *Genome Res.* **16**, 1017 (2006).
25. B. C. Meyers, A. Kozik, A. Griego, H. Kuang, R. W. Michelmore, *Plant Cell* **15**, 809 (2003).
26. K. J. Schmid, S. Ramos-Onsins, H. Ringys-Beckstein, B. Weisshaar, T. Mitchell-Olds, *Genetics* **169**, 1601 (2005).
27. R. R. Hudson, N. L. Kaplan, *Genetics* **120**, 831 (1988).
28. M. Nordborg, *Genetics* **146**, 1501 (1997).
29. J. Kroymann, T. Mitchell-Olds, *Nature* **435**, 95 (2005).
30. D. Tian, H. Araki, E. Stahl, J. Bergelson, M. Kreitman, *Proc. Natl. Acad. Sci. U.S.A.* **99**, 11525 (2002).
31. A. L. Hughes, M. Nei, *Nature* **335**, 167 (1988).
32. M. Nordborg, H. Innan, *Genetics* **163**, 1201 (2003).
33. Eightfold coverage for *A. lyrata* and *Capsella rubella* is being generated by the Joint Genome Institute (www.jgi.doe.gov/).
34. N. L. Kaplan, R. R. Hudson, C. H. Langley, *Genetics* **123**, 887 (1989).
35. J. M. Smith, J. Haigh, *Genet. Res.* **23**, 23 (1974).
36. C. Toomajian *et al.*, *PLoS Biol.* **4**, e137 (2006).
37. A. C. Syvanen, *Nat. Genet.* **37** (Suppl.), S5 (2005).
38. M. Morgante, *Curr. Opin. Biotechnol.* **17**, 168 (2006).
39. We thank G. Nielson and H. Huang for bioinformatics support; R. Gupta and M. Morenzoni for information management; T. Altman, J. Borevitz, C. Dean, and C. Shindo for seed stocks; J. Gagne, D. Gingerich, R. Vierstra, L. Sterck, and Y. van de Peer for providing gene family or homology information; and K. Schneeberger for helpful discussions. Supported by Innovation Funds of the Max Planck Society, NIH (HG002790 to M. Waterman, and GM62932 to J. Chory and D.W.), NSF (DEB-0115062 to M.N., and DBI-0520253 to J.R.E.), an NIH National Research Service Award fellowship to C.T., and core funding from the Max Planck Society. D.W. is a director of the Max Planck Institute. Sequence data have been deposited in GenBank (accession codes EI100660 to EI102044).

REPORTS

Imaging the Surface of Altair

John D. Monnier,[1*] M. Zhao,[1] E. Pedretti,[2] N. Thureau,[3] M. Ireland,[4] P. Muirhead,[5] J.-P. Berger,[6] R. Millan-Gabet,[7] G. Van Belle,[7] T. ten Brummelaar,[8] H. McAlister,[8] S. Ridgway,[9] N. Turner,[8] L. Sturmann,[8] J. Sturmann,[8] D. Berger[1]

Spatially resolving the surfaces of nearby stars promises to advance our knowledge of stellar physics. Using optical long-baseline interferometry, we constructed a near-infrared image of the rapidly rotating hot star Altair with a resolution of <1 milliarcsecond. The image clearly reveals the strong effect of gravity darkening on the highly distorted stellar photosphere. Standard models for a uniformly rotating star cannot explain our findings, which appear to result from differential rotation, alternative gravity-darkening laws, or both.

Whereas solar astronomers can take advantage of high-resolution, multi-wavelength, real-time imaging of the Sun's surface, stellar astronomers know most stars—whether located parsecs or kiloparsecs away—as simple points of light. To discover and understand the processes around stars unlike the Sun, we must rely on stellar spectra averaged over the entire photosphere. Despite their enormous value, spectra alone have been inadequate to resolve central questions in stellar astronomy, such as the role of angular momentum in stellar evolution (*1*), the production and maintenance of magnetic fields (*2*), the launching of massive stellar winds (*3*), and the interactions between very close binary companions (*4*).

Fortunately, solar astronomers no longer hold a monopoly on stellar imaging. Long-baseline visible and infrared interferometers have enabled the cataloging of photospheric diameters of hundreds of stars and high-precision dynamical masses for dozens of binaries, offering exacting constraints for theories of stellar evolution and stellar atmospheres (*5*). This work requires an angular resolution of ~1 milliarcsecond (mas) (1 part in 2×10^8, or 5 nanoradians) for resolving even nearby stars, which is more than an order of

magnitude better than that achievable with the Hubble Space Telescope or ground-based 8-m telescopes equipped with adaptive optics.

Stellar imaging can be used to investigate the rapid rotation of hot, massive stars. A large fraction of hot stars are rapid rotators with surface rotational velocities of more than 100 km/s (6, 7). These rapid rotators are expected to traverse evolutionary paths very different from those of their slowly rotating kin (1), and rotation-induced mixing alters stellar abundances (8). Although hot stars are relatively rare by number in the Milky Way Galaxy, they have a disproportionate effect on galactic evolution due to their high luminosities, their strong winds, and their final end as supernovae (for the most massive stars). Recently, rapid rotation in single stars has been invoked to explain at least one major type of gamma-ray bursts (9) and binary coalescence of massive stars or remnants (10).

The distinctive observational signatures of rapid rotation were first described by von Zeipel (11), beginning with the expectation that centrifugal forces would distort the photospheric shape and that the resulting oblateness would induce lower effective temperatures at the equator. This latter effect, known as gravity darkening, will cause distortions in the observed line profiles as well as the overall spectral energy distribution. Precise predictions can be made, but these rely on uncertain assumptions, in particular the distribution of angular momentum in the star; uniform rotation is often assumed for simplicity.

The most basic predictions of von Zeipel theory—centrifugal distortion and gravity darkening—have been confirmed to some extent. The Palomar Testbed Interferometer (PTI), the first instrument to measure photospheric elongation in a rapid rotator, found the diameter of the nearby A-type star Altair to be ~14% larger in one dimension than the other (12). The Navy Prototype Optical Interferometer (NPOI) and the Center for High Angular Resolution Astronomy (CHARA) interferometric array both measured strong limb-darkening profiles for the photometric standard Vega (13, 14), consistent with a rapid rotator viewed nearly pole-on. A brightness asymmetry for Altair was also reported by NPOI

(15, 16), suggestive of the expected pole-to-equator temperature difference from gravity darkening. In recent years, a total of five rapid rotators have been measured to be elongated by interferometers (17–19).
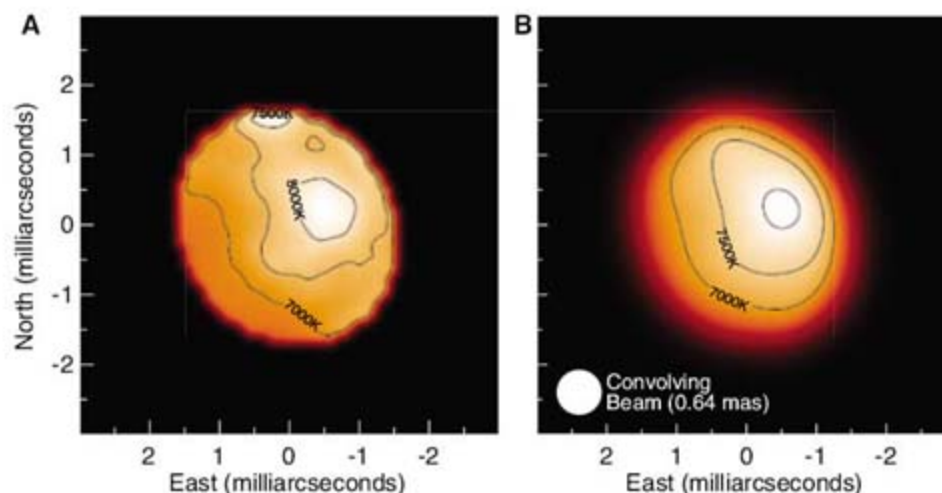
Although von Zeipel theory appears to work at a basic level, serious discrepancies between theory and observations have emerged. Most notably, the diameter of the B3V-type star Achernar (17) was measured to be ~56% longer in one dimension than the other, a discrepancy too large to be explained by von Zeipel theory. Explanations for this include strong differential rotation of the star (20) or the presence of a polar wind (3), either of which have far-reaching consequences for our understanding of stellar evolution. To address these issues, we must move beyond the simplest models for rapidly rotating stars, and this will require a corresponding jump in the quality and quantity of interferometry data. Indeed, all previous results were based on limited interferometer baselines that lacked the capability to form model-independent images, and relied entirely on model fitting for interpretation. Thus, previous confirmations of von Zeipel theory, although suggestive, were incomplete.

Here we report a development in imaging capabilities that enables a test of von Zeipel theory, both through basic imaging and precise model-fitting. By combining near-infrared light from four telescopes of the CHARA interferometric array, we have synthesized an elliptical aperture with dimensions 265 m by 195 m (Fig. 1), allowing us to reconstruct images of the prototypical rapid rotator Altair (spectral type A7V) with an angular resolution of ~0.64 mas, the diffraction limit defined by $\lambda/2D$, the observing wavelength divided by twice the longest interferometer baseline. The recently commissioned Michigan Infrared Combiner (MIRC) (21) was essential for this work, allowing the light from the CHARA telescopes to be combined simultaneously into eight spectral channels spanning the astronomical H band
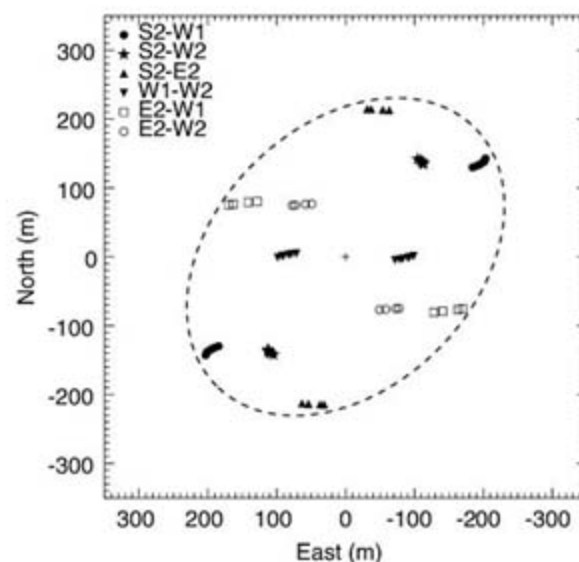
Fig. 1. Fourier (u, v) coverage for the Altair observations, where each point represents the projected separation between one pair of the four CHARA telescopes S2, E2, W1, and W2 (31). The dashed ellipse shows the equivalent coverage for an elliptical aperture of 265 m by 195 m oriented along a position angle of 135° east of north.

[1]Department of Astronomy, University of Michigan, Ann Arbor, MI 48109, USA. [2]School of Physics and Astronomy, University of St. Andrews, Fife KY16 9AJ, Scotland, UK. [3]Astrophysics Group, Covendish Laboratory, Cambridge University, Cambridge CB3 0HA, UK. [4]Division of Geological and Planetary Sciences, California Institute of Technology, Pasadena, CA 91125, USA. [5]Astronomy Department, Cornell University, Ithaca, NY 14850, USA. [6]Laboratoire d'Astrophysique de Grenoble, Observatoire de Grenoble, F-38041 Grenoble Cédex 9, France. [7]Michelson Science Center, California Institute of Technology, Pasadena, CA 91125, USA. [8]Center for High Angular Resolution Astronomy, Georgia State University, Atlanta, GA 30302, USA. [9]National Optical Astronomy Observatory, Tucson, AZ 85719, USA.

*To whom correspondence should be addressed. E-mail: monnier@umich.edu

Fig. 2. (**A**) Intensity image of the surface of Altair ($\lambda = 1.65$ μm) created with the MACIM/MEM imaging method using a uniform brightness elliptical prior ($\chi_\nu^2 = 0.98$). Typical photometric errors in the image correspond to ±4% in intensity. (**B**) Reconstructed image convolved with a Gaussian beam of 0.64 mas, corresponding to the diffraction limit of CHARA for these observations. For both panels, the specific intensities at 1.65 μm were converted into the corresponding blackbody temperatures; contours for 7000, 7500, and 8000 K are shown. North is up and east is left.

(λ = 1.50 to 1.74 μm). The Altair data presented here were collected on 31 August and 1 September 2006 (UT); complete observational information is available (22). In addition, we used some K-band (λ = 2.2 μm) observations by the PTI to constrain the short-baseline visibilities in subsequent analysis.

With the use of four CHARA telescopes, interferometric imaging of Altair is now possible, although this requires specialized image reconstruction techniques. We used the publicly available application MACIM (Markov-Chain Imager for Optical Interferometry) (23) in this work, applying the maximum entropy method (MEM) (24). We restricted the stellar image to fall within an elliptical boundary, similar in principle to limiting the field of view in standard aperture synthesis procedures. This restriction biases our imaging against faint emission features arising outside the photosphere; however, we do not expect any circumstellar emission in Altair, which is relatively cool, lacking signs of gas emission or strong winds. Further details of our imaging procedures, along with results from validation tests, can be found in (22). Our image shows the stellar photosphere of Altair to be

well resolved (Fig. 2A), appearing elongated in the northeast-southwest direction with a bright dominant feature covering the northwest quadrant of the star. To reduce the influence of possible low-level artifacts that are beyond the diffraction limit of our interferometer, we have followed the standard procedure (25) of convolving the reconstructed image with a Gaussian beam matching the resolution of the interferometer (Fig. 2B).

These images confirm the basic picture of gravity darkening induced by rapid rotation. We see Altair's photosphere to be oblate with a bright region identifiable as the stellar polar region. The intensity of the dark equatorial band is about 60 to 70% of the brightness at the pole, broadly consistent with expectations for the near-infrared from previous models. Although we see some evidence for deviations from axisymmetry (small excess emission on the northern limb), this feature is at the limit of our image fidelity and will require additional Fourier coverage to investigate further. We have also fitted our data set with a rapid rotator model, following the prescription set out in Aufdenberg et al. (14) and references therein, assuming a Roche potential (central point mass) and solid-body rotation. The main parameters of the model are the stellar radius and temperature at the pole, the angular rotation rate as a fraction of breakup (ω), the gravity darkening coefficient (β), and the viewing angles (inclination and position angle). We used the stellar atmosphere models of Kurucz (26) to determine the specific intensity of each point on the surface as a function of local gravity, effective temperature, and limb darkening. In addition to matching the new MIRC/CHARA data, we forced the model to match the measured V- and H-band photometric magnitudes (0.765 ± 0.015 and 0.235 ± 0.043, respectively) derived from a broad literature

survey. When fixing the gravity-darkening coefficient to β = 0.25 appropriate for radiative envelopes, our derived parameters (Table 1) agree well with the best-fit parameters of Peterson et al. (15) on the basis of visible data. However, our best-fit model reached only a reduced χ^2 of 1.79, which suggests a need for additional degrees of freedom in our model. To improve our fits, we explored an extension to the von Zeipel model, allowing the gravity-darkening coefficient β to be a free parameter. We found that a model with β = 0.190 significantly improved the goodness of fit (Table 1), and this improvement is visually apparent when comparing synthetic model images to the Altair image from CHARA (Fig. 3). In addition to a lower β, the new model prefers a slightly less inclined orientation, a cooler polar temperature, and a faster rotation rate.

Both our imaging and modeling results point to important deficiencies in the currently popular models for rapid rotators. Previous workers have also encountered problems explaining high-resolution interferometry data with standard prescriptions for rotating stars. In addition to the Achernar case previously cited, Peterson et al. (15) were unable to find a satisfactory fit for Altair assuming a standard Roche–von Zeipel model (χ^2_ν = 3.8), consistent with the need for additional stellar physics. Recent results for Alderamin (19) also specifically favor models with smaller βs, in line with our findings. Although model fitting has revealed deviations from standard theory, our model-independent imaging allows new features to be discovered outside current model paradigms. The most striking difference between our CHARA image and the synthetic model images (Fig. 3) is that our image shows stronger darkening along the equator, inconsistent with any von Zeipel–like gravity-darkening prescription assuming uniform

Table 1. Best-fit parameters for Roche–von Zeipel models of Altair. Parameter descriptions: Inclination (0° is pole-on, 90° is edge-on) and position angle (degrees east of north) describe our viewing angle, T_{pole} and R_{pole} describe the temperature and radii of the pole (alternatively, one can describe the temperature and radii at the equator as T_{eq} and R_{eq}), ω is the angular rotation rate as a fraction of critical breakup rate, and β is the gravity-darkening coefficient. Models assumed stellar mass = 1.791 $M_\odot$ (15), metallicity [Fe/H] = −0.2 (32), and distance = 5.14 pc (33).
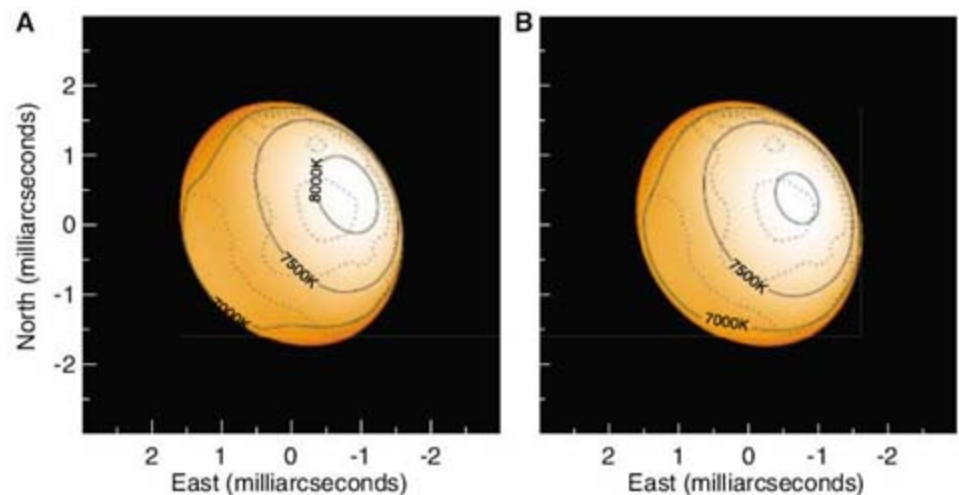
Parameter	β fixed	β free
Inclination	62.7° ± 1.5°	57.2° ± 1.9°
Position angle	−61.7° ± 0.9°	−61.8° ± 0.8°
T_{pole} (K)	8710 ± 160	8450 ± 140
R_{pole} (R_*)	1.661 ± 0.004	1.634 ± 0.011
(mas)	1.503 ± 0.004	1.479 ± 0.010
T_{eq} (K)	6850 ± 120	6860 ± 150
R_{eq} (R_*)	2.022 ± 0.009	2.029 ± 0.007
(mas)	1.830 ± 0.008	1.835 ± 0.007
ω	0.902 ± 0.005	0.923 ± 0.006
β	0.25 (Fixed)	0.190 ± 0.012
Model V-band photometric magnitude	0.765	0.765
Model H-band photometric magnitude	0.225	0.220
Model v sin i (km/s)	241	240
Reduced χ^2:		
Total	1.79	1.37
Closure phase	2.08	1.73
Vis^2	1.48	1.10
Triple amp	2.14	1.58

Fig. 3. Synthetic images of Altair (λ = 1.65 μm) adopting conventional rapid-rotation models. (**A**) The best-fit model assuming standard gravity-darkening coefficient for radiative envelopes (β = 0.25, χ^2_ν = 1.79). (**B**) The result when β is a free parameter (β = 0.190, χ^2_ν = 1.37). For both panels, the specific intensities at 1.65 μm were converted into the corresponding blackbody temperatures; contours for 7000, 7500, and 8000 K are shown. We have overplotted the contours from the CHARA image (Fig. 2A) as dotted lines to facilitate intercomparison.

rotation. Lower equatorial surface temperatures could naturally arise if the equatorial rotation rate were higher than the rest of the star (differential rotation), reducing the effective gravity at the surface (27). Another possibility is that the cooler equatorial layers could be unstable to convection (28, 29), invalidating a single gravity-darkening "law" applicable to all stellar latitudes. Other studies (30) have found further faults with simple application of the von Zeipel law due to opacity effects in the surface layers. Even though it is difficult to isolate or untangle these various effects from one another, the new interferometric results and our modeling convincingly establish the case for stellar physics beyond the standard models used today to describe rotating stars. A path forward is clear: Differential rotation will leave both geometric and kinematic signatures different from opacity or convection-related phenomena. Observers must be armed with a new generation of models incorporating these physical processes in order to exploit the powerful combination of detailed line profile analysis and multiwavelength interferometric imaging now available.

References and Notes

1. A. Maeder, G. Meynet, *Annu. Rev. Astron. Astrophys.* **38**, 143 (2000).
2. J. D. Landstreet, *Astron. Astrophys. Rev.* **4**, 35 (1992).
3. P. Kervella, A. Domiciano de Souza, *Astron. Astrophys.* **453**, 1059 (2006).
4. P. Barai et al., *Astrophys. J.* **608**, 989 (2004).
5. J. D. Monnier, *Rep. Prog. Phys.* **66**, 789 (2003).
6. H. A. Abt, N. I. Morrell, *Astrophys. J. Suppl. Ser.* **99**, 135 (1995).
7. H. A. Abt, H. Levato, M. Grosso, *Astrophys. J.* **573**, 359 (2002).
8. M. Pinsonneault, *Annu. Rev. Astron. Astrophys.* **35**, 557 (1997).
9. G. E. Brown et al., *N. Astron.* **5**, 191 (2000).
10. N. Gehrels et al., *Nature* **437**, 851 (2005).
11. H. von Zeipel, *Mon. Not. R. Astron. Soc.* **84**, 684 (1924).
12. G. T. van Belle, D. R. Ciardi, R. R. Thompson, R. L. Akeson, E. A. Lada, *Astrophys. J.* **559**, 1155 (2001).
13. D. M. Peterson et al., *Nature* **440**, 896 (2006).
14. J. P. Aufdenberg et al., *Astrophys. J.* **645**, 664 (2006).
15. D. M. Peterson et al., *Astrophys. J.* **636**, 1087 (2006).
16. N. Ohishi, T. E. Nordgren, D. J. Hutter, *Astrophys. J.* **612**, 463 (2004).
17. A. Domiciano de Souza et al., *Astron. Astrophys.* **407**, L47 (2003).
18. H. A. McAlister et al., *Astrophys. J.* **628**, 439 (2005).
19. G. T. van Belle et al., *Astrophys. J.* **637**, 494 (2006).
20. S. Jackson, K. B. MacGregor, A. Skumanich, *Astrophys. J.* **606**, 1196 (2004).
21. J. D. Monnier, J.-P. Berger, R. Millan-Gabet, T. A. Ten Brummelaar, *Proc. SPIE* **5491**, 1370 (2004).
22. See supporting material on *Science* Online.
23. M. J. Ireland, J. D. Monnier, N. Thureau, *Proc. SPIE* **6268**, 62681T (2006).
24. R. Narayan, R. Nityananda, *Annu. Rev. Astron. Astrophys.* **24**, 127 (1986).
25. J. A. Högbom, *Astron. Astrophys.* **15** (suppl.), 417 (1974).
26. R. Kurucz, *ATLAS9 Stellar Atmosphere Programs and 2 km/s Grid* (Smithsonian Astrophysical Observatory, Cambridge, MA, 1993).
27. S. Jackson, K. B. MacGregor, A. Skumanich, *Astrophys. J. Suppl. Ser.* **156**, 245 (2005).
28. A. Claret, *Astron. Astrophys.* **359**, 289 (2000).
29. F. Espinosa Lara, M. Rieutord, http://arxiv.org/abs/astro-ph/0702255 (2007).
30. C. Lovekin, R. G. Deupree, C. I. Short, *Astrophys. J. Suppl. Ser.* **643**, 460 (2006).
31. T. A. ten Brummelaar et al., *Astrophys. J.* **628**, 453 (2005).
32. D. Erspamer, P. North, *Astron. Astrophys.* **398**, 1121 (2003).
33. European Space Agency, *The Hipparcos and Tycho Catalogues* (1997) (www.rssd.esa.int/Hipparcos/catalog.html).
34. We thank A. Tannirkulam, S. Webster, A. Boden, B. Zavala, C. Tycner, C. Hummel, D. Peterson, J. Aufdenberg, PJ Goldfinger, and S. Golden for their contributions. Research at the CHARA Array is supported by NSF grants AST 06-06958 and AST 03-52723 and by the offices of the Dean of the College of the Arts and Sciences and the Vice President for Research, Georgia State University.

The Crystallization Age of Eucrite Zircon

G. Srinivasan,[1]* M. J. Whitehouse,[2] I. Weber,[3] A. Yamaguchi[4]

Eucrites are a group of meteorites that represent the first planetary igneous activity following metal-silicate differentiation on an early planetesimal, similar to Asteroid 4 Vesta, and, thus, help date geophysical processes occurring on such bodies in the early solar system. Using the short-lived radionuclide ^{182}Hf as a relative chronometer, we demonstrate that eucrite zircon crystallized quickly within 6.8 million years of metal-silicate differentiation. This implies that mantle differentiation on the eucrite parent body occurred during a period when internal heat from the decay of ^{26}Al and ^{60}Fe was still available. Later metamorphism of eucrites took place at least 8.9 million years after the zircons crystallized and was likely caused by heating from impacts, or by burial under hot material excavated by impacts, rather than from lava flows. Thus, the timing of eucrite formation and of mantle differentiation is constrained.

The accretion of the parent bodies of differentiated meteorites (e.g., eucrites), Mars, Moon, and Earth was quickly followed by large-scale melting and metal-silicate differentiation, resulting in core-mantle formation. Basaltic eucrites are a group of differentiated meteorites that formed as lava flows or as shallow intrusions following metal-silicate differentiation on the eucrite parent body (EPB). Asteroid 4 Vesta is identified as a plausible eucrite parent body (1). Time constraints on the processes of melting, metal-silicate separation leading to core formation, and subsequent mantle differentiation that produced precursors to basaltic eucrites are critical to models of the thermal evolution of EPB. To constrain precisely the time of eruption and crystallization of basalts on EPB, we report high-precision measurements of the Hf-W composition of zircon from three eucrites and explore the use of ^{182}Hf as a relative chronometer.

Eucrites are composed primarily of pyroxene; plagioclase; minor chromite; ilmenite; and trace quantities of zircon, metal, and quartz. The presence of decay products of short-lived radio-

nuclides. ^{26}Al [half-life ($T_{1/2}$) $\approx$ 0.7 million years (My)], ^{53}Mn ($T_{1/2} \approx$ 3.5 My) and ^{182}Hf ($T_{1/2} \approx$ 8.9 My) (2–5), in eucrites requires their formation within a few million years of formation of the solar system. An age of 4555 ± 9 My is inferred from the ^{207}Pb/^{206}Pb composition of eucrite zircons (6). This age spans the entire time window when the eucrite parent body (EPB) was undergoing extensive igneous activity fuelled by heat produced from the decay of short-lived radionuclides ^{26}Al and ^{60}Fe ($T_{1/2} \approx$ 1.5 My).

Eucrites are extensively metamorphosed and extremely brecciated as a result of impacts. Related thermal disturbance of parent-daughter isotopic systematics of radiometric chronometers can potentially obscure crystallization records. Therefore, the eucrite crystallization ages determined from long-lived chronometers, e.g., ^{147}Sm ($T_{1/2} \approx$ 103 Gy) and short-lived chronometers (e.g., ^{26}Al) are poorly constrained (7), as are models of the thermal evolution of EPB.

When planets containing bulk solar proportions of elements are melted and differentiated, lithophile Hf and siderophile W are chemically fractionated and redistributed into the silicate mantle and metallic core, respectively (8). Therefore, the decay of ^{182}Hf to ^{182}W has been used to determine time scales of metal-silicate differentiation leading to core formation of planets (5) and mantle differentiation resulting in eruption of basalts on EPB (4, 5). However, Hf-W compositions of bulk silicate mineral and metal separates in eucrites reflect meta-

[1]Department of Geology, University of Toronto, Toronto, ON, Canada, M5S 3B1. [2]Laboratory for Isotope Geology, Swedish Museum of Natural History, SE-104 05 Stockholm, Sweden. [3]Institute for Planetology, Department of Geosciences, University of Münster, D-48149 Münster, Germany. [4]National Institute of Polar Research, Tokyo 173-8515, Japan.

*To whom correspondence should be addressed. E-mail: srini@geology.utoronto.ca

morphic reequilibration of W between these phases at 4547 ± 2 My (9). The Hf-W mineral isochron is therefore not useful for determining the primary igneous crystallization chronology of eucrites.

The high Hf (1 to 2%) and very low W concentration (ppm to subppm) in zircon make it an ideal mineral for determining the ^{182}Hf abundance. The record of primary igneous crystallization should also be better preserved in zircon, which is resistant to resetting of U-Pb isotopic systematics up to metamorphic temperatures of ~1000°C (10). The ion microprobe is ideally suited for in situ microanalysis of small (several 10s of micrometers or less) phases present in trace abundance. Using this method (11), we determined the Hf-W composition of individual eucrite zircons in polished thin sections in order to constrain the chronology of igneous crystallization of eucrites and impact-induced partial melting.

The three basaltic eucrites chosen for this study are the Asuka meteorites A-881467 and A-881388 and Elephant Moraine meteorite EET90020 from the Antarctic meteorite collection. The Asuka meteorites are unbrecciated and have a recrystallized rock texture (12, 13). Plagioclase crystals are mostly anhedral (size: about 0.05 mm to 1.1 mm) (Fig. 1), with a few lath-shaped crystals (about 1 mm × 0.15 mm). Pigeonite and augite grains up to 0.4 mm are present. Exsolution lamellae were found in both pyroxenes, although augite lamellae in host pigeonite are more common (Fig. 1, bottom). Minor phases, ilmenite and chromite, occur as 20- to 50-μm grains, whereas the trace phases zircon, sulfides, and silica are smaller. Zircon grains are typically associated with ilmenite and chromite, are triangular in shape, and resemble broken fragments. A few zircon grains appear to border ilmenite-chromite mineral assemblage; however, unlike high-grade metamorphic rocks (14), they do not have a flat base in direct contact with ilmenite. EET90020 (polished thin section no. 28) has granulitic texture and a minor amount of coarse-grained area (15). The granulitic portion is composed of anhedral pyroxene (~250 μm) enclosed by lathlike and stubby plagioclase (~60 μm). Minor oxides, tridymite and troilite, also occur in this section. The estimated metamorphic temperature based on the Ca thermometer is ~800°C (16).

The Hf-W composition of W-metal; NIST610 silicate glass standard; terrestrial zircons (91500, 97SU-51, and G-Zircon); A-881388, A-881467, and EET90020 zircon; and pyroxene are reported in table S2 (11), and Fig. 2. All analyzed terrestrial zircon grains over a wide range of ^{180}Hf/^{186}W ratios (≈ 10³ to 2.4 × 10⁵) have normal ^{182}W/^{186}W and ^{183}W/^{186}W isotopic composition. The analyzed Asuka meteorite zircon grains have excess δ^{182}W and normal δ^{183}W (17, 18). EET90020 zircon with high ^{180}Hf/^{186}W ≈ 1 × 10⁵ shows very low excess δ^{182}W compared with Asuka zircon. Pyroxenes from A-881467 and

A-881388 with low ^{180}Hf/^{186}W values have normal W isotopic composition. If one assumes a typical Hf concentration of ~1% for zircon, the estimated W abundance in terrestrial zircon is about 760 ppb to 9.8 ppm, whereas meteoritic zircon has about 100 to 760 ppb. In A-881467, the highest excess δ^{182}W value of 9.1 (±4.2) × 10³‰ (2σ$_m$ confidence level) is observed in Z2 with a corresponding ^{180}Hf/^{186}W ratio of ~1.29 × 10⁵, and the lowest δ^{182}W value of 1.1 (±0.6) × 10³‰ (2σ$_m$) is observed in Z4 with a ^{180}Hf/^{186}W

ratio of ~1.7 × 10⁴. In A-881388, the highest excess δ^{182}W value of 17.0 (±9.5) × 10³‰ (2σ$_m$) is observed in Z3 with a ^{180}Hf/^{186}W ratio of ~2.2 × 10⁵, and the lowest δ^{182}W value of 3.4 (±2.2) × 10³ (2σ$_m$) is observed in Z2 with a ^{180}Hf/^{186}W ratio of ~9.5 × 10⁴.

The observed excess δ^{182}W is correlated linearly with the Hf/W values in zircon and is attributed to the in situ decay of ^{182}Hf in the host phase. The inferred ^{182}Hf abundance [table S3 (11) and Fig. 2] at the time of crystallization of

Fig. 1. Backscattered electron (BSE) image of a typical granulitic region in A-881467 (**top**) and enlarged BSE image of another typical area in A-881467 (**bottom**). All minerals meet in triple junctions. Anhedral plagioclase of variable size (from about 0.05 mm up to 1.1 mm), as well as pyroxene grains up to 0.4 mm, is present. Minerals listed from dark to lighter gray/white BSE response: SiO$_2$, SiO$_2$-phase; Plag, Plagioclase; Cpx, Ca-rich pyroxene; Lpx, Ca-poor pyroxene; Ilm, Ilmenite; and Chr, Chromite). (Bottom) Zircon (Zir) indicated by arrow with a bright BSE response in association with an ilmenite (lighter gray BSE) and chromite (darker gray BSE) grain. The individually photodocumented meteorite zircons are labeled, e.g., A-881467-Z3, for identification, and the isotopic data (table S2) for each grain are reported as A-881467-Z3 and repeat analyses on the same as A-881467-Z3 repeat.
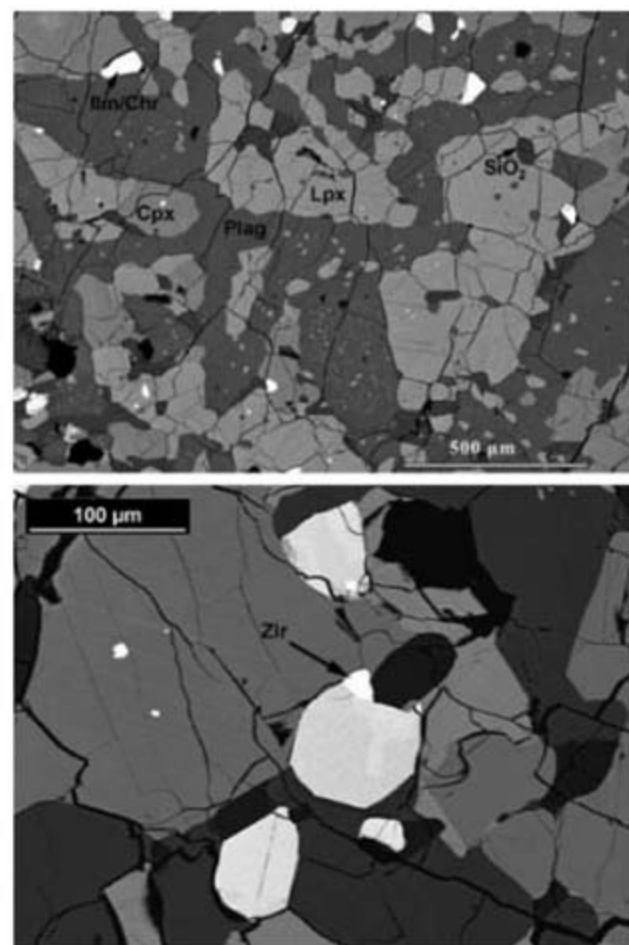
Fig. 2. The ^{182}W/^{186}W values are plotted against ^{180}Hf/^{186}W values with correlated 1σ$_{mean}$ error ellipses for terrestrial and meteorite mineral phases. The dashed line (in the main figure and inset) represents the EWR correlation line with initial ^{182}Hf/^{180}Hf = 7.25 (±0.5) × 10⁻⁵ (2σ$_m$), as reported by (5). The horizontal solid line representing normal W isotopic composition with δ^{182}W = 0 (17) is shown in the main figure and inset. The terrestrial zircons (G-zircon, 91500, and 97-SU51-2) have normal δ^{182}W values. Meteorite zircons in A-881467, A-881388, and EET90020 with high ^{180}Hf/^{186}W have correlated excess δ^{182}W, which is attributed to the decay of the short-lived radionuclide ^{182}Hf. The data are regressed using Isoplot (28) to determine the initial ^{182}Hf at the time of formation of these zircons [table S3 (11)].
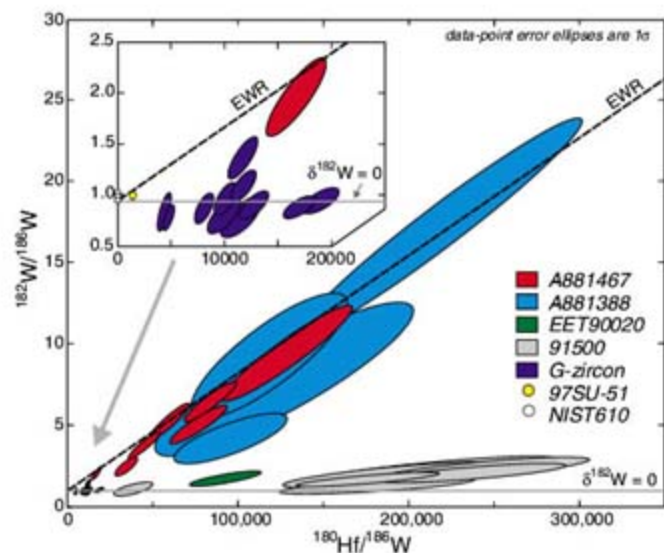
A-881388 zircons is $^{182}Hf/^{180}Hf = 7.5\ (\pm0.9) \times 10^{-5}$ [$2\sigma_m$; mean square of weighted deviates (MSWD) = 1.5] and, for A-881467 zircons, is $^{182}Hf/^{180}Hf = 6.0\ (\pm1.4) \times 10^{-5}$ ($2\sigma_m$; MSWD = 1.8). The model upper limit for ^{182}Hf abundance at the time of crystallization of EET90020 zircon is $^{182}Hf/^{180}Hf \leq 7 \times 10^{-6}$. The initial ($^{182}W/^{186}W$) values determined from all the eucrite regressions are close to the initial values determined from eucrite whole-rock (EWR) samples [5].

We used ^{182}Hf as a relative chronometer on the assumption that it was uniformly distributed in the reservoir from which constituents of primitive meteorite and EPB were derived. The ($^{182}Hf/^{180}Hf$)$_{SSI}$ (SSI, solar system initial) as determined from primitive meteorites is $1.07\ (\pm0.10) \times 10^{-4}$ [19]. The abundance of ^{182}Hf inferred from EWR samples is [$^{182}Hf/^{180}Hf$]$_{EWR} = 7.25\ (\pm0.50) \times 10^{-5}$ [5]. The time difference between solar system formation and metal-silicate differentiation on the EPB is 3.8 ± 1.3 My, and the model Hf-W age for this event is 4563.4 ± 1.5 My [5].

The difference in ^{182}Hf abundance between Asuka zircons and the EWR [5] suggests that, relative to the time of metal-silicate differentiation (table S4) on EPB, A-881388 crystallized -0.4 ± 3.5 My and A-881467 2.4 ± 4.4 My. Because eucrites formed as a result of mantle differentiation following metal-silicate separation, relative ages of zircons predating metal-silicate differentiation on EPB are physically implausible. Therefore, the ^{182}Hf abundance indicates that A-881388 zircon formed in <3.1 My and A-881467 zircon formed in <6.8 My after metal-silicate differentiation on EPB. If zircons are primary crystallization products as observed in unmetamorphosed eucrites [6], then mantle differentiation on EPB lasted for a maximum of 6.8 million years after metal-silicate differentiation. If they are secondary metamorphic products, then duration of igneous activity on EPB was even shorter. By using the model Hf-W absolute age for mantle differentiation of 4563.4 ± 1.5 My [5], we show that the zircon ^{182}Hf abundance model age of A-881388 is 4563.8 ± 3.8 My and that of A-881467 is 4561.0 ± 4.6 My.

The Hf-W model ages of A-881388 and A-881467 overlap within errors, and they formed when ^{26}Al abundance ranged from $^{26}Al/^{27}Al \approx 1 \times 10^{-6}$ in eucrites Piplia Kalan and A-881394 [2, 20, 21] to a significantly lower abundance of $<2 \times 10^{-7}$. The model $^{26}Al-^{26}Mg$ ages of A-881467 and A-881388 of <4561 My [20] are not sufficiently well constrained to distinguish between time of crystallization and metamorphic overprints. The model Mn-Cr ages of 4546 to 4556 My for A-881467 and <4548 My for A-881388 are younger [20] and poorly constrained because of metamorphic resetting. The Hf-W data from zircon and Mn-Cr ages of mineral separates show that zircon crystallization preceded metamorphism of A-881388 by

a minimum of 12.0 My and that of A-881467 by a minimum of 0.5 My. The Mn-Cr ages determined from whole rock, pyroxene, and ilmenite mineral separates reflect resetting of isotopic signatures by the metamorphic event that produced the granulitic texture of these meteorites.

The EET90020 zircon with an extremely low ^{182}W excess has $^{182}Hf/^{180}Hf$ of $\leq7 \times 10^{-6}$, and its model Hf-W age is <4533.3 My. The formation time of 4483 ± 26 My inferred from ^{146}Sm abundance [15] and the low ^{182}Hf abundance of EET90020 suggest zircon crystallization in a melting event when ^{26}Al and ^{60}Fe had completely decayed and ceased to be heat sources. Zircon in EET90020 is more likely a product of late partial melting on EPB [15] as a result of an impact-related heating event.

Basaltic eucrites formed as a result of some of the first planetary scale igneous processes. Their textures suggest that they are products of lava flows or shallow intrusions. They experienced prolonged metamorphism and impact, which disturbed their mineralogy, texture, isotopic composition, and radiometric ages. Thermal metamorphism may result from burial under successive lava flows or impact. One possibility is that brecciated and thermally metamorphosed eucrites formed at the contact zones between crater walls and hot impact–melt sheets [22]. Alternatively, eucrites crystallized early and were metamorphosed during formation of crust on the parent body [23, 24]. If eucrites formed by partial melting, melts would migrate to the surface of the parent body and so produce a basaltic crust that could grow to a thickness of 10 km [25] or up to 25 km [26]. Later eruptions would bury the earlier layers, which could then be thermally metamorphosed from internal heat. Hot lava flows will cease when heat-producing short-lived radionuclides (^{26}Al and ^{60}Fe) are depleted significantly within the first few million years after metal-silicate differentiation of the EPB. The zircon of Asuka eucrites, which formed in <6.8 My after metal-silicate differentiation on EPB, constrains the maximum duration of mantle differentiation on EPB, which results in the formation of eucrites. Therefore, thermal metamorphism due to direct contact with hot lava flows will cease once ^{26}Al and ^{60}Fe are exhausted as heat sources. Thermal evolution models for EPB [27] suggest layers >10 km beneath the surface are at temperatures >1000 K at least 16 My after metal-silicate differentiation on EPB. Thermal metamorphism leading to reequilibration of Hf-W isotopes between bulk metal and silicate phases in eucrites (e.g., Camel Donga) at 4547 ± 2 My [9] postdates crystallization of Asuka zircon by at least ~8.9 My. If Asuka zircons represent the last vestiges of igneous crystallization on the surface of EPB, then the metamorphic event resulting in Hf-W reequilibration of Camel Donga at 4547 ± 2 My cannot be due to lava flow on the surface energized by heat-producing ^{26}Al and ^{60}Fe. Heating

that was directly due to impact or to burial under hot material excavated by impact is considered to be the most plausible mechanism for eucrite metamorphism.

References and Notes

1. R. Binzel, S. Xu, *Science* **260**, 186 (1993).
2. G. Srinivasan, J. N. Goswami, N. Bhandari, *Science* **284**, 1348 (1999).
3. G. Lugmair, A. Shukolyukov, *Geochim. Cosmochim. Acta* **62**, 2863 (1998).
4. G. Quitte, J. L. Birck, C. J. Allegre, *Earth Planet. Sci. Lett.* **184**, 83 (2000).
5. T. Kleine, K. Mezgar, C. Münker, H. Palme, A. Bischoff, *Geochim. Cosmochim. Acta* **68**, 2935 (2004).
6. K. Misawa, A. Yamaguchi, H. Kaiden, *Geochim. Cosmochim. Acta* **69**, 5847 (2005).
7. R. W. Carlson, G. W. Lugmair, in *Origin of Earth and Moon*, K. Righter and R. Canup, Eds. (Univ. of Arizona Press, Tucson, AZ, 2000), pp. 25–44.
8. H. Palme, W. Ramanesse, *Proc. Lunar Sci. Conf.* **12**, 949 (1981).
9. T. Kleine, K. Mezgar, H. Palme, E. Scherer, C. Münker, *Earth Planet. Sci. Lett.* **231**, 41 (2005).
10. J. K. W. Lee, I. S. Williams, D. J. Ellis, *Nature* **390**, 159 (1997).
11. Materials and methods are available as supporting material on *Science* online.
12. H. Takeda, T. Ishi, T. Arai, M. Miyamoto, *Antarctic Meteorite Res.* **10**, 401 (1997).
13. A. Yamaguchi, G. J. Taylor, K. Keil, *Anatarctic Meteorite Res.* **10**, 415 (1997).
14. B. Bingen, H. Austrheim, M. Whitehouse, *J. Petrol.* **42**, 355 (2001).
15. A. Yamaguchi et al., Shih Chi-Y. *Geochim. Cosmochim. Acta* **65**, 3577 (2001).
16. D. H. Lindsley, *Am. Mineral.* **68**, 477 (1983).
17. $\delta^{182}W$ and $\delta^{183}W$ are defined by the equations $[(^{182}W/^{186}W)_{sample}/(^{183}W/^{186}W)_{standard}) -1] \times 1000$ and $[(^{183}W/^{186}W)_{sample}/(^{183}W/^{186}W)_{standard}) -1] \times 1000$. The standard values for $^{182}W/^{186}W = 0.934382$ and $^{183}W/^{186}W = 0.50439$ were recalculated from [18].
18. R. Schoenberg, B. S. Kamber, K. D. Collerson, O. Eugster, *Geochim. Cosmochim. Acta* **66**, 3151 (2002).
19. T. Kleine, K. Mezgar, H. Palme, E. Scherer, C. Münker, *Geochim. Cosmochim. Acta* **69**, 5805 (2005).
20. L. E. Nyquist, Y. Reese, H. Weismann, C.-Y. Shih, H. Takeda, *Earth Planet. Sci. Lett.* **214**, 11 (2003).
21. G. Srinivasan, *Lunar Planet Sci* **XXXIII**, 1489 (abstr.) (2002).
22. K. Metzler, K. D. Bobe, H. Palme, B. Spettel, D. Stoffler, *Planet. Space Sci.* **43**, 499 (1995).
23. E. Stolper, *Geochim. Cosmochim. Acta* **41**, 587 (1977).
24. A. Yamaguchi, G. J. Taylor, K. Keil, *Icarus* **124**, 97 (1996).
25. M. Miyamoto, H. Takeda, *Earth Planet. Sci. Lett.* **122**, 343 (1994).
26. J. S. Delaney, *Lunar Planet Sci.* **XXVI**, 329 (1995).
27. A. Ghosh, H. Y. McSween Jr., *Icarus* **134**, 187 (1998).
28. K. R. Ludwig, Isoplot version 2.6, Special Publication 1a, 1991 (Berkeley Geochronology Center, 1991).
29. Supported by a Natural Sciences and Engineering Research Council of Canada grant to G.S. Cosmochemistry Laboratory Contribution no. 5. The Nordsim facility in Stockholm is operated under an agreement among the Nordic Research Councils, the Geological Survey of Finland, and the Swedish Museum of Natural History. This is Nordsim contribution no. 184. Discussions (G.S.) with A. Bischoff and comments from referees helped to improve this manuscript.

Boundary Layer Halogens in Coastal Antarctica

Alfonso Saiz-Lopez,[1,2]* Anoop S. Mahajan,[1] Rhian A. Salmon,[3] Stephane J.-B. Bauguitte,[3] Anna E. Jones,[3] Howard K. Roscoe,[3] John M. C. Plane[1,2]†

Halogens influence the oxidizing capacity of Earth's troposphere, and iodine oxides form ultrafine aerosols, which may have an impact on climate. We report year-round measurements of boundary layer iodine oxide and bromine oxide at the near-coastal site of Halley Station, Antarctica. Surprisingly, both species are present throughout the sunlit period and exhibit similar seasonal cycles and concentrations. The springtime peak of iodine oxide (20 parts per trillion) is the highest concentration recorded anywhere in the atmosphere. These levels of halogens cause substantial ozone depletion, as well as the rapid oxidation of dimethyl sulfide and mercury in the Antarctic boundary layer.

For the past 2 decades, considerable attention has been given to the role of bromine chemistry in causing rapid surface ozone depletion events (ODEs) in the Arctic springtime (1). Two sources of reactive halogens have been proposed: acidified sea-salt surfaces such as aerosol, frost flowers, or sea salt in surface snow accumulated through horizontal drifting from refrozen lead areas and photodegradable halocarbon compounds from anthropogenic and natural origins (2). Halogens are also involved in the oxidation of oceanic dimethyl sulfide (DMS), which may influence formation of cloud condensation nuclei (3), and the oxidation of gaseous elemental Hg in the Arctic troposphere (4). Recently, it was shown that condensable iodine oxide vapors can nucleate very efficiently to form particles, which may have an impact on cloud cover and hence on climate (5, 6).

In the Antarctic, work on bromine species has been mainly concerned with the halogen-catalyzed removal of ozone in the stratosphere (7). Observations over Antarctica of the integrated tropospheric column densities of bromine oxide (BrO) and iodine oxide (IO) have been reported at a coastal site (8, 9) and, in the case of BrO only, from space (10). However, these are integrated measurements: There have been no direct measurements of IO or BrO within the boundary layer above the snowpack. It is also noteworthy that in several Arctic locations, even when elevated BrO was present in the boundary layer during an ODE, IO was not observed (11, 12), although aerosol measurements of filterable iodine have been reported (13).

A field campaign was performed from January 2004 to February 2005 at Halley Station (75°35'S, 26°30'W), which is situated on the Brunt Ice Shelf, Antarctica, about 35 m above sea level (fig. S1). The ice edge is some 12 km north and 30 km west of the station; 20 km southwest is Precious Bay, a semipermanently open patch of water with large areas of fresh sea ice where frost flowers grow in winter and spring. Sea-salt ion concentrations on frost flowers and nearby surface snow are at least three times greater than those in seawater, and this has been linked to the

enhanced release of photolabile bromine compounds into the gas phase (14).

The concentrations of IO and BrO were measured with the long-path differential optical absorption spectroscopy technique (LP-DOAS) (15). A folded optical path of 4 km (total path = 8 km) was set up at a height of 4 to 5 m above the snowpack (varying through the year as a result of snow accumulation). The light source was a xenon lamp, whose beam was folded back to a Newtonian telescope receiver by an array of quartz corner-cube reflectors. The path-averaged concentrations of IO and BrO were obtained by fitting laboratory-measured cross sections of the molecules to atmospheric spectra recorded in the visible and near-ultraviolet (UV), respectively (15) (Fig. 1). Between January 2004 and February 2005, IO was measured on 41 days and BrO on 125 days. The two species were not measured simultaneously because they absorb in different spectral regions (Fig. 1).

IO and BrO were detected above the detection limit whenever the solar zenith angle was less than ~92° (i.e., twilight and full daylight). The peak concentrations of both species were about 5×10^8 molecules cm^{-3} or 20 parts per trillion by volume (pptv), observed during austral spring (October). For BrO, this concentration is similar to the levels observed in the springtime Arctic (16). In contrast, the IO concentration is an order of magnitude larger than the upper limit reported from the Arctic (11, 12) and is actually the highest concentration reported anywhere in the atmosphere. One impact of such high levels of iodine oxides is the formation of ultrafine aerosol from the polymerization of IO and OIO (6) (OIO forms from the reaction of IO with itself or with BrO), which might explain particle nucleation events observed in summer over sea ice near Antarctica (17).

The concentrations of both IO and BrO exhibited a diurnal cycle, essentially tracking the solar radiation (Figs. 2 and 3). This indicates that both species are produced photochemically and have a boundary layer lifetime of less than 2 hours against nonphotochemical loss processes. The concentrations of IO and BrO were strongly correlated with the local wind direction as well as

[1]School of Chemistry, University of Leeds, Leeds, LS2 9JT, UK. [2]School of Environmental Sciences, University of East Anglia, Norwich, NR4 7TJ, UK. [3]British Antarctic Survey, National Environment Research Council, Cambridge, CB3 0ET, UK.

*Present address: Earth and Space Science Division, Jet Propulsion Laboratory, California Institute of Technology, Pasadena, CA 91109, USA.
†To whom correspondence should be addressed. E-mail: J.M.C.Plane@leeds.ac.uk

Fig. 1. Examples of atmospheric spectral fits. The solid line corresponds to the atmospheric spectrum after removing all known absorbers, except the species of interest, with the overlying reference spectrum (dotted line) calculated from literature absorption cross sections measured at 298 K (27, 28). The fitting procedure yields (**A**) [IO] = 20.5 ± 1.2 ppt and (**B**) [BrO] = 18.8 ± 1.0 ppt.
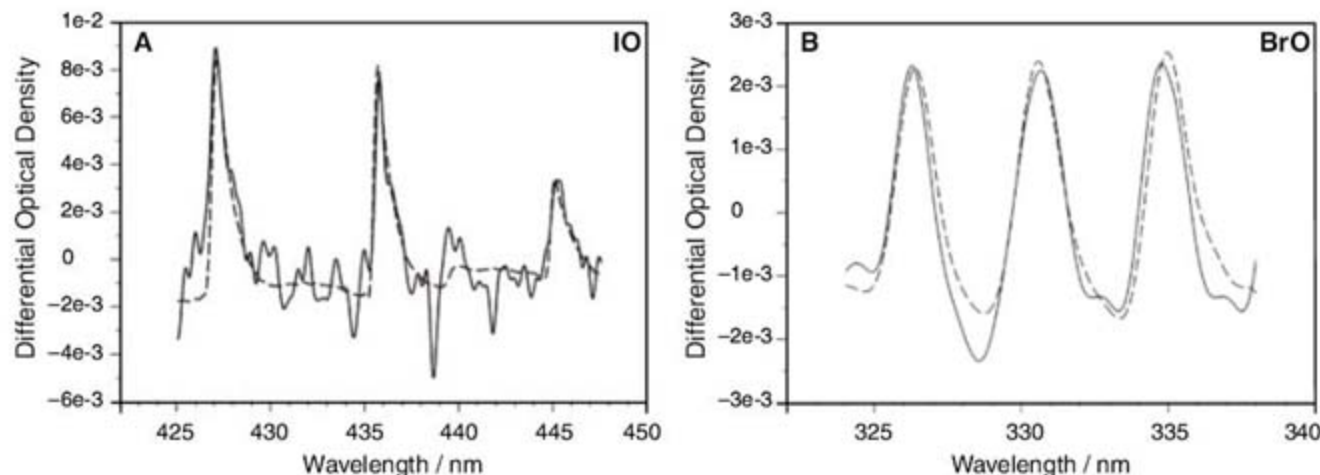
the air mass origin predicted by back trajectory calculations (Fig. 2 and 3). Enhanced concentrations of both radicals were observed when the wind was from the open ice front sector (~200° to 45°), in air masses that had been over sea ice within the previous 24 hours. Although the levels of halogen oxides were lower in continental air that had not been over sea ice for at least 3 days, IO and BrO were often still observed at mixing ratios up to ~6 ppt during sunlit periods, clearly above the instrumental detection limit of 1 to 2 ppt (Figs. 2 and 3). This strongly suggests that halogen activation in sunlight is widespread in the coastal Antarctic boundary layer and not restricted to close proximity to the ice front. This inference is supported by satellite observations of the BrO tropospheric column density over Antarctica (10), which showed that large column abundances are present above all coastal areas of Antarctica between August and November, with smaller amounts between December and April (10).

The record of IO and BrO concentrations over the entire year is displayed in Fig. 4. The day-to-day concentrations are quite scattered as a result of differences in solar radiation and wind direction. However, the 10-day running average concentrations (solid lines in Fig. 4) show that the seasonal cycles of IO and BrO are remarkably similar, both in timing and absolute concentration. This is quite unexpected, given the different sources of the two halogens (see below). There is a distinct maximum in spring [also seen in the integrated tropospheric column measurements of IO (9), which are consistent with our measurements if all the IO was in the boundary layer]. This is followed by a decrease toward the summer and a possible secondary maximum in autumn. The smaller levels in autumn could be a consequence of lower rates of halogen activation or could result from a less-stable boundary layer allowing faster mixing into the free troposphere. During the polar night, the halogen oxides were never observed above the detection limit of the instrument. However, the first appearance of IO and BrO occurs very early in the Antarctic spring, during twilight: Mixing ratios up to 4 ppt were detected as early as 9 August. This indicates an activation mechanism that is efficient in the absence of direct sunlight or where the activation occurred further north in direct sunlight, with the halogen oxides then persisting for at least 10 hours while being transported to Halley.

We used a photochemical box model (Materials and Methods) to estimate the contributions of halogen chemistry to boundary layer ozone loss in the polar spring. With use of the observed BrO diurnal profile, we estimated the diurnally averaged rate of O_3 loss because of bromine chemistry alone to be 0.14 parts per billion (ppb) hour^{-1}. A similar calculation for iodine chemistry alone yields a rate of O_3 removal of 0.31 ppb hour^{-1}. However, when iodine and bromine chemistry act together, the modeled loss rate increases to 0.55 ppb hour^{-1} because the reaction IO + BrO → Br + OIO increases the rate at which BrO is converted back to Br (18) (fig. S2). This fourfold increase in

the depletion rate resulting from bromine and iodine chemistry, compared with bromine alone, has not been considered previously in simulations of O_3 depletion in the Antarctic troposphere.

The O_3 record during the campaign shows three substantial depletion events in September and October 2004. During two of these ODEs, there were no halogen oxide measurements, because of bad visibility in one case and in the other because the DOAS was being used to observe a different species. However, during the third ODE there were IO measurements that appear to be anticorrelated with O_3 (fig. S3A). Interestingly, however, plots of the deviation of [O_3] from its long-term mean against [IO] or [BrO] do not show a significant correlation (fig. S4). Indeed, the highest IO concentration during
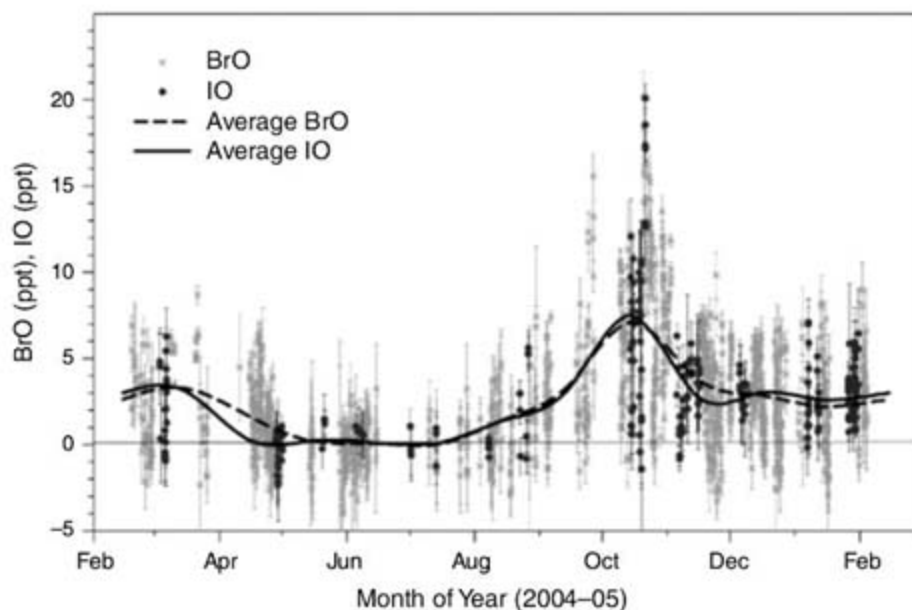
the campaign was observed in the presence of 18 ppb of O_3 (close to the October average of 19 ppb). Because there is insufficient NO_x in the boundary layer to promote photochemical production of O_3, there are two possible explanations: Either the halogens were freshly injected into the boundary layer air less than 6 hours before reaching Halley, so that only a small quantity of O_3 (less than ~ 2 ppb) was depleted (which is consistent with trajectories crossing the ice-front sector such as shown in Figs. 2 and 3, top), or O_3 was entrained from the free troposphere rapidly enough to offset significant boundary layer depletion (this would require a strong halogen source to offset the simultaneous dilution of IO and BrO). Indeed, the boundary layer at Halley during the sunlit period often
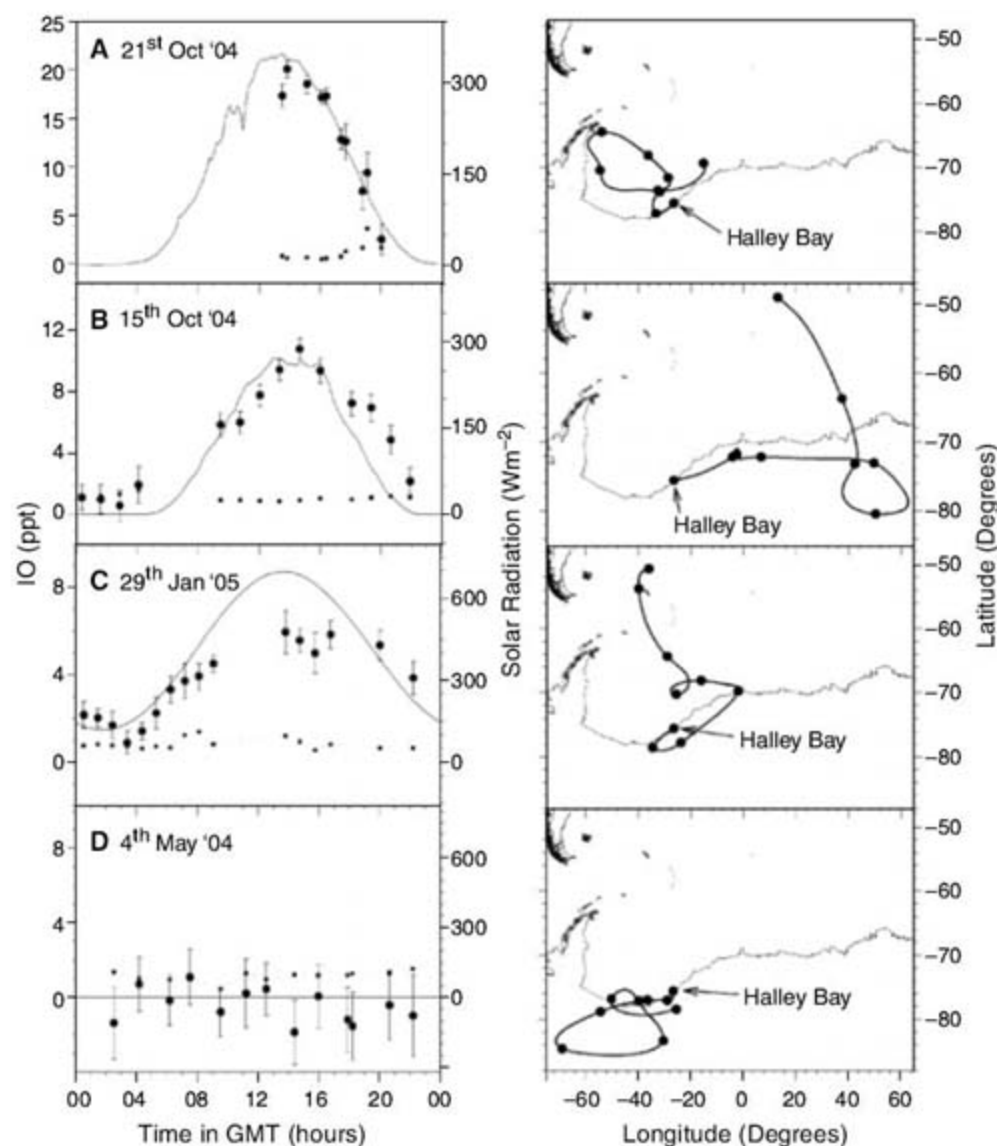
Fig. 2. The diurnal variation of the IO mixing ratio (black points with 2σ error bars), the DOAS detection limit for IO (black squares with a dotted line), which varied depending on visibility, and the solar irradiance (black line). The corresponding 8-day air mass back trajectory arriving at Halley (250 m above sea level) is shown adjacent to each diurnal plot. Each circle on the trajectory indicates 24 hours. Trajectories were calculated from the British Atmospheric Data Centre Web service, which uses the European Centre for Medium-Range Weather Forecasts archive. (**A**) A day in spring (21 October 2004) displaying the highest IO mixing ratio of 20.5 ± 1.2 ppt observed during the campaign; the air mass trajectory indicates a strong oceanic influence. (**B**) A day in spring (15 October 2004) when the air mass had not been over the ocean for at least 3 days. (**C**) A day in summer (29 January 2005) with an oceanic air mass. (**D**) A day in winter (4 May 2004) when IO was below the detection limit of about 2 ppt.
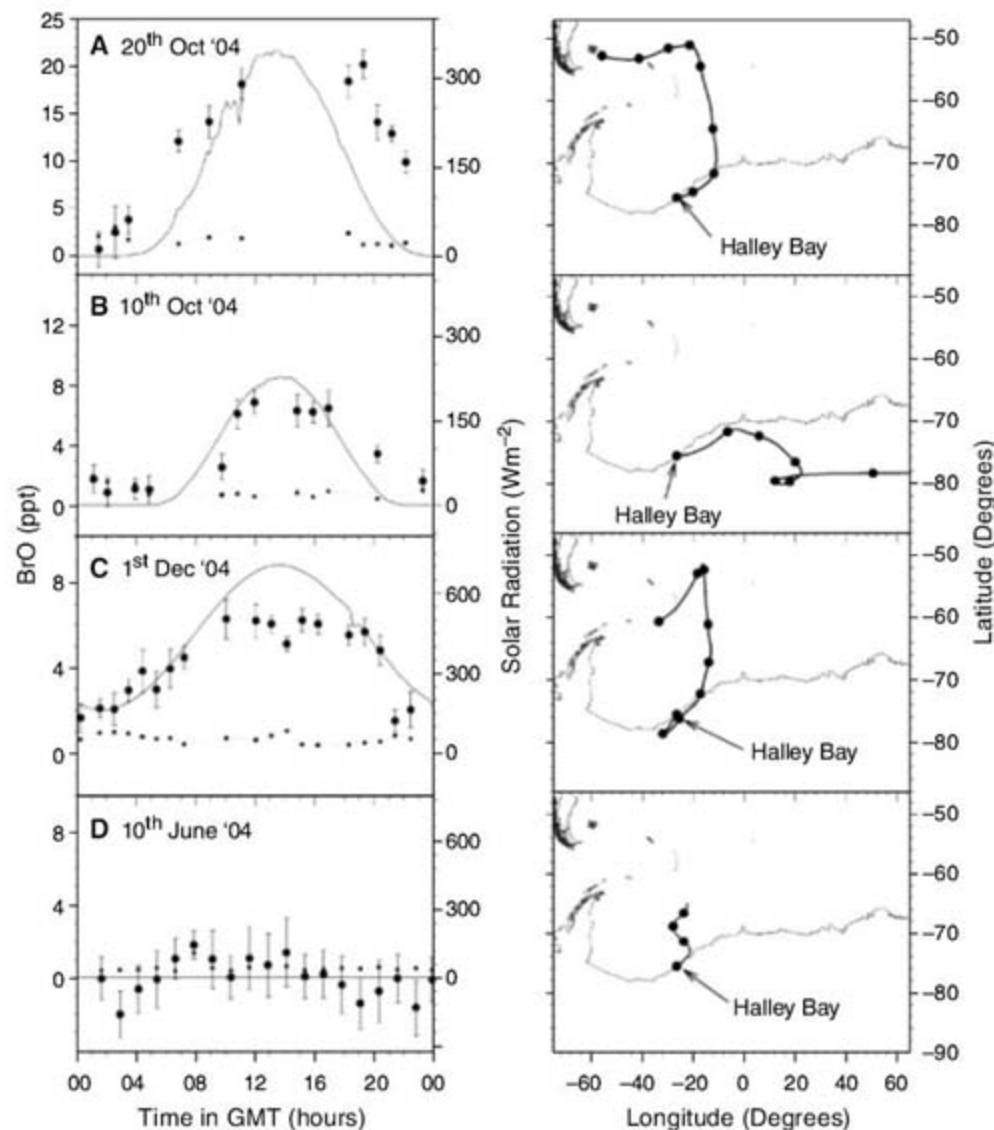
Fig. 3. Diurnal variation of the BrO mixing ratio and solar irradiance (notation as in Fig. 2). (**A**) A day in spring (20 October 2004) with the highest mixing ratio of 20.2 ± 1.1 ppt for the campaign. The air mass originated from the ocean. (**B**) A day in spring (10 October 2004) with a continental air mass. (**C**) A day in summer (1 December 2004) with an oceanic air mass. (**D**) A day in winter (10 June 2004) when BrO was not detected above the detection limit of about 2 ppt.

exhibits extreme variability and is not strongly capped (19). Thus, although elevated halogen oxides are almost certainly a prerequisite for an ODE, the degree of O_3 depletion appears to be controlled by the boundary layer meteorology.

These high levels of halogen oxides will change the oxidizing capacity of the Antarctic boundary layer by increasing the NO_2/NO ratio (e.g., via $IO + NO \rightarrow NO_2 + I$) and by decreasing the HO_2/OH ratio (e.g., via $HO_2 + IO \rightarrow HOI + O_2$; HOI subsequently undergoes loss in aerosol or photolysis to OH). The formation of gas-phase $BrONO_2$ and $IONO_2$, followed by fast deposition to the snowpack or aerosol, will remove NO_2 and accelerate the activation of bromide and chloride from sea-salt surfaces (20). The rate of DMS oxidation by BrO will be an order of magnitude faster than that by OH at average mixing ratios of 4 ppt and 0.01 ppt, respectively, making BrO the most important oxidant of DMS around coastal Antarctica. Atomic Br is also highly reactive toward certain organic compounds (21) and elemental Hg at low temperatures (22). The removal of Hg should be further enhanced by the atomic iodine that must exist in steady state with the observed IO (23).

A final point to consider is the source of iodine. High concentrations of phytoplankton, which colonize the underside of sea ice, extend over large areas of the Weddell Sea (24, 25). Phytoplankton produce iodocarbons such as CH_2I_2 and CH_2IBr and probably I_2. These photolabile species (compared with the much less photolabile biogenic bromocarbons) then provide a source of inorganic iodine in the boundary layer. The high levels of IO in the boundary layer must then be sustained either through the photolysis of the higher iodine oxides (e.g., OIO, I_2O_3, I_2O_4, and I_2O_5), which likely form from IO (26), or the recycling of these species through aerosols or the snowpack. The uptake of species such as HOI on halide-rich surfaces will also trigger the release of bromine in the form of IBr. Such a coupling may explain the strikingly sim-

Fig. 4. Annual variation of the halogen oxides measured at Halley Station. The 10-day moving averages of BrO and IO are indicated by a dashed line and a solid line, respectively. The maximum IO and BrO mixing ratios occurred in spring (October), whereas during winter (May to August) the radicals were consistently below the detection limit. A second smaller peak in the annual halogen mixing ratio cycle may also be present during autumn (March to April).

ilar seasonal variations of IO and BrO (Fig. 4). The observations of notable IO and BrO levels in continental air masses indicate that halogen activation is not limited to coastal sea ice. Sea-salt aerosol and frost flower fragments coated with sea salt will be wind-borne from the ice front into the interior of the continent and deposited on the snowpack; subsequent heterogeneous reactions will then recycle photolabile halogens to the gas phase. It is therefore very likely that IO is as widespread around coastal Antarctica as satellite measurements show to be the case for BrO (10).

Our results indicate that these high and sustained levels of halogen oxides should have a profound impact on the chemistry of the Antarctic boundary layer. Further observations and laboratory work are needed to confirm the processes that lead to the formation of such a large burden of reactive iodine and bromine and to establish the overall influence of the chemistry on the Antarctic troposphere.

References and Notes

1. L. A. Barrie, J. W. Bottenheim, R. C. Schnell, P. J. Crutzen, R. A. Rasmussen, *Nature* **334**, 138 (1988).
2. R. von Glasow, P. J. Crutzen, *Treatise on Geochemistry*, K. K. Turekian, H. D. Holland, Eds. (Elsevier, Amsterdam, 2003), vol. 4, pp. 21–64.
3. R. J. Charlson, J. E. Lovelock, M. O. Andreae, S. G. Warren, *Nature* **326**, 655 (1987).
4. S. E. Lindberg et al., *Environ. Sci. Technol.* **36**, 1245 (2002).
5. C. D. O'Dowd et al., *Nature* **417**, 632 (2002).
6. Research front: Iodine and marine aerosols, R. von Glasow, Ed., *Environ. Chem.* **2** (no. 4), 243–337 (2005).
7. S. Solomon, *Nature* **347**, 347 (1990).
8. K. Kreher, P. V. Johnston, S. W. Wood, B. Nardi, U. Platt, *Geophys. Res. Lett.* **24**, 3021 (1997).
9. U. Frieß, T. Wagner, I. Pundt, K. Pfeilsticker, U. Platt, *Geophys. Res. Lett.* **28**, 1941 (2001).
10. J. Hollwedel et al., *Adv. Space Res.* **34**, 804 (2004).
11. G. Honninger, H. Leser, O. Sebastian, U. Platt, *Geophys. Res. Lett.* **31**, L04111 (2004).
12. M. Tuckermann et al., *Tellus* **49B**, 533 (1997).
13. A. Sirois, L. A. Barrie, *J. Geophys. Res.* **104**, 11599 (1999).
14. A. M. Rankin, E. W. Wolff, S. Martin, *J. Geophys. Res.* **107**, 4683 10.1029/2002JD002492 (2002).
15. J. M. C. Plane, A. Saiz-Lopez, in *Analytical Techniques for Atmospheric Measurement*, D. E. Heard, Ed. (Blackwell, Oxford, 2006), ch. 3.
16. M. Hausmann, U. Platt, *J. Geophys. Res.* **99**, 25399 (1994).
17. B. Davison et al., *J. Geophys. Res.* **101**, 22855 (1996).
18. M. K. Gilles, A. A. Turnipseed, J. B. Burkholder, A. R. Ravishankara, S. Solomon, *J. Phys. Chem. A* **101**, 5526 (1997).
19. P. S. Anderson, *Boundary-Layer Meteorol.* **107**, 323 (2003).
20. R. Sander, Y. Rudich, R. von Glasow, P. J. Crutzen, *Geophys. Res. Lett.* **26**, 2857 (1999).
21. B. T. Jobson et al., *J. Geophys. Res.* **99**, 25355 (1994).
22. M. E. Goodsite, J. M. C. Plane, H. Skov, *Environ. Sci. Technol.* **38**, 1772 (2004).
23. J. G. Calvert, S. E. Lindberg, *Atmos. Environ.* **38**, 5105 (2004).
24. D. N. Thomas, G. S. Dieckmann, *Sea Ice: An Introduction to Its Physics, Chemistry, Biology, and Geology* (Blackwell, Oxford, 2003).
25. J. K. Moore, M. R. Abbott, *J. Geophys. Res.* **105**, 28709 (2000).
26. R. W. Saunders, J. M. C. Plane, *Environ. Chem.* **2**, 299 (2005).
27. P. Spietz, J. C. Gomez-Martin, J. P. Burrows, *J. Photochem. Photobiol. A* **176**, 50 (2005).
28. O. C. Fleischmann, J. P. Burrows, J. Orphal, *J. Photochem. Photobiol. A* **157**, 127 (2003).
29. This work was supported by the UK Natural Environment Research Council's Antarctic Funding Initiative. We are grateful to the University of Leeds for a research fellowship (A.S.-L.) and a research studentship (A.S.M.).

Intra- and Intermolecular Band Dispersion in an Organic Crystal

G. Koller,[1]*† S. Berkebile,[1]* M. Oehzelt,[1] P. Puschnig,[2]* C. Ambrosch-Draxl,[2] F. P. Netzer,[1] M. G. Ramsey[1]*†

The high crystallinity of many inorganic materials allows their band structures to be determined through angle-resolved photoemission spectroscopy (ARPES). Similar studies of conjugated organic molecules of interest in optoelectronics are often hampered by difficulties in growing well-ordered and well-oriented crystals or films. We have grown crystalline films of uniaxially oriented sexiphenyl molecules and obtained ARPES data. Supported by density-functional calculations, we show that, in the direction parallel to the principal molecular axis, a quasi–one-dimensional band structure of a system of well-defined finite size develops out of individual molecular orbitals. In contrast, perpendicular to the molecules, the band structure reflects the periodicity of the molecular crystal, and continuous bands with a large dispersion were observed.

The bulk band structures of many crystalline inorganic materials have been determined experimentally with methods such as angle-resolved valence band photoemission spectroscopy (ARPES), in part because single crystals with almost any desired orientation are available and well-defined surface terminations can be prepared in situ. For their organic counterparts, this situation is not the case because single crystals of organics generally face three basic problems: Their small size limits signal, these materials are not highly conductive and thus charging, and the orientations available are limited to their cleavage planes. Numerous attempts to measure band structures on in situ grown organic films have had limited success because of inherent disorder in these films. The propensity of the molecules to crystallize leads to a multiplicity of crystallite orientations and morphologies unless great care is taken. The challenge lies in growing thin films on conducting substrates with a single unique crystallite orientation (1–7).

Although thin films of conjugated organic molecules are entering the marketplace as the active elements in various optoelectronic devices, the basic understanding of their electronic structure, crucial to their function, is lacking. The electronic band structure, electron energy versus momentum $E(k)$, of the conjugated π system defines both the electronic properties and the optical properties of the so-called organic semiconductors.

Here we report the electronic π band structure of sexiphenyl (6P), a rodlike molecule with six phenyl rings linked together in the para-position, obtained with ARPES from a (20-3) oriented crystalline film and compare the results with ab initio calculations (8). This orientation can be grown on weakly interacting anisotropic substrates, such as Cu(110)-p(2x1)O or TiO$_2$(110), which uniaxially align the molecules parallel to the atomic corrugation of the substrate (9–13). The band dispersions were measured parallel to the long molecular axis and in two directions perpendicular to the molecule. In the direction parallel to the molecules, the observed dispersion, that is, the energy spread of related orbitals constituting a band, is determined by the molecule itself. This so-called intramolecular dispersion provides a textbook example of the formation of the band structure from discrete orbitals of a quasi–one-dimensional system of well-defined finite size. Perpendicular to the molecules' long axis, continuous bands reflecting the crystal lattice periodicity were observed. This anisotropy, together with the contribution from the various π orbitals with different intermolecular overlap, is discussed in light of band structure calculations (14, 15).

The 200 Å–thick films investigated consisted of rectangular 6P(20-3) crystallites (~200 nm by 500 nm), which completely tiled the p(2x1)oxygen-reconstructed Cu(110) sub-

[1]Institute of Physics, Surface and Interface Physics, Karl-Franzens University Graz, 8010 Graz, Austria. [2]Chair of Atomistic Modeling and Design of Materials, University of Leoben, 8700 Leoben, Austria.

*These authors contributed equally to this work.
†To whom correspondence should be addressed. E-mail: georg.koller@uni-graz.at (G.K.); michael.ramsey@uni-graz.at (M.G.R.)

strate. The schematic of Fig. 1A shows a 6P(20-3) oriented crystallite with the relevant dimensions and directions indicated. The (20-3) planes, parallel to the substrate, have a rectangular unit cell of 54.6 Å by 11.1 Å and consist of uniaxially oriented molecules whose aromatic planes are tilted at ±35° to the substrate. A scanning tunneling microscopy (STM) image of the 6P monolayer, on which the crystallites grow, with the two-dimensional (2D) unit cell indicated, is shown in Fig. 1B. The molecules in the y direction are close-packed in columns, with their tilt angle alternating between columns. In the crystallite, perpendicular to the surface (z direction), the molecules also have alternating tilt directions, leading to a periodicity of 7.7 Å or twice the interplanar distance.

Sexiphenyl consists of six phenyl rings with an inter-ring spacing of ~4.35 Å. In the gas phase, steric hindrance of the hydrogen atoms of neighboring rings leads to a torsional angle of ~30° between adjacent phenyl units. Structural studies have concluded that this twist in the molecule is removed on packing in the crystal, and the rings become co-planar (16). The electronic structure of the upper π bands of 6P can be best conceptualized by considering the molecule as a chain of benzene rings, each contributing two degenerate π orbitals. On building the 12 π orbitals of the seximer, the two degenerate π orbitals form inter-ring bonding and antibonding combinations (17), and so two π bands, consisting of six orbitals each, arise. The energy spread of

the orbitals, i.e., the widths of the bands, is determined by the inter-ring overlap. The band, based on the combination of benzene orbitals with most weight at the linking carbon atoms consisting of the three highest anti-bonding and the three lowest bonding orbitals, has the highest overlap between benzene rings and energy spread and will be called the delocalized band. The other benzene π orbital has lower inter-ring overlap, and consequently the six orbitals arising from it in 6P have lower energy dispersion. These intermediate-energy "nonbonding" orbitals (18) will be referred to as the localized band. The degree of inter-ring overlap is naturally dependent on the molecules torsional angle, and the energy dispersion of these bands will be lowest in twisted gas phase molecules.

The band structure, $E(k)$ versus k, of an isolated 6P molecule is illustrated schematically in Fig. 1C. In the manner of Hoffmann (19), sacrificing precision for clarity, the 6P orbitals are best conceptualized as a linear combination of the benzene orbitals

$$\Psi_k = \Sigma_n e^{ikna} \chi_n$$

where a is the interring spacing and χ_n the benzene orbital of the nth ring. For the delocalized band at $k = 0$, $\Psi_0 = \Sigma_n \chi_n$ is the most antibonding orbital [the highest occupied molecular orbital (HOMO)], whereas at $k = \pi/a$, $\Psi_{\pi/a} = \Sigma_n (-1)^n \chi_n$ is the most bonding orbital (HOMO-11). This band decreases in energy from Γ ($k = 0$)

to the first Brillouin zone boundary. In contrast, at $k = 0$, the orbital of the localized band is bonding, and this band will increase in energy from the Γ point. In the schematic, the orbitals at the extremes of the bands are depicted (all orbitals can be found in fig. S1). These have been calculated by first principles density functional theory and differ from expectations from a simplistic linear combination of benzene orbitals because of the finite dimension of the chain, with the electron density tailing off toward the ends of the molecule.

A set of valence band photoemission spectra from the π orbitals, measured as a function of electron emission angle (θ) in the direction along the molecular axis, is shown in Fig. 2A. The orbital emissions exhibit distinct maxima at discrete θ values because different takeoff angles probe different momenta. After converting θ to momentum, the π band map of sexiphenyl [$E(k_x)$] is obtained (Fig. 2B). The density of states, derived from integrating the data over k_x, is included on the side, and the orbitals of the delocalized π band are labeled, starting with the HOMO.

The emission intensities of the molecular orbitals are clearly not homogeneously distributed in k_x, and distinct maxima are observed. If the crystalline periodicity of 54.6 Å in this direction were dominant, the Brillouin zone would be small (0.12 Å^{-1}). Such a small k-space periodicity would yield a more or less constant intensity over the 3 Å^{-1} k range recorded (15), which is not evident in the data. At first glance, the data

Fig. 1. (A) Representation of a sexiphenyl (20-3) oriented crystal. The spacings (in Å) in the three orthogonal directions explored are indicated. **(B)** STM image of the sexiphenyl monolayer template on which the 6P(20-3) crystallites grow. The 2D unit cell (11.1 Å by 54.6 Å) indicated is compressed in the y direction relative to that of the (20-3) plane in the bulk 6P. **(C)** Schematic of the π band structure of an isolated planar 6P molecule, showing a sequence of orbitals defining bands derived from the two degenerate HOMOs of benzene. In the antibonding π orbitals, at the top of each band, the two degenerate π orbitals of benzene, from which they originate, are well expressed.
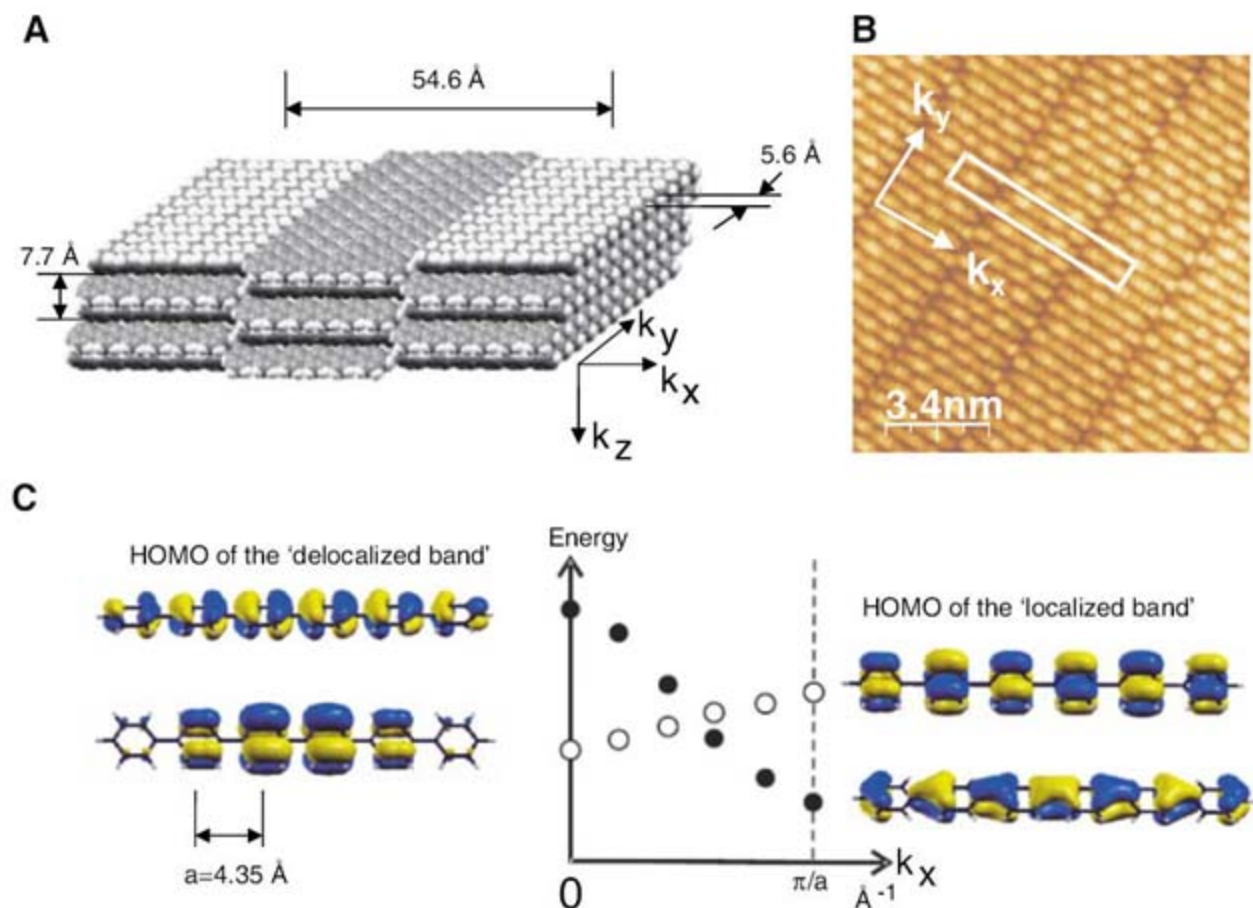
are very similar to that expected for an isolated molecule expressed in Fig. 1C. The six orbitals of the delocalized band are seen running down from the Brillouin zone center ($k_x = 0$) to $k_x = \pi/a$, and the observed k-space periodicity of 1.4 $Å^{-1}$ relates well to the inter-ring spacing within the molecule of $a = 4.35$ Å. Note that these orbital emissions are much stronger running up from $k = \pi/a$ to $2\pi/a$, which will be discussed with the Fourier analysis.

However, more features are seen than would be expected for the band of the planar molecule, in particular the intensity around π/a for the HOMO and the HOMO-1. The observed periodicity in reciprocal space is not $2\pi/a$ but rather $2\pi/2a$, indicating that the periodicity within the molecule is not the monomer spacing but the dimer spacing, which leads to a folding back of the band. This periodicity can be rationalized by the molecule having a twisted conformation, at least in the near-surface region probed by ARPES. We have introduced the possibility of such a twisted conformation for 6P in the solid state in earlier work from ionization energy considerations (20, 21). From a band structure point of view, the delocalized band should rather be interpreted in terms of two minibands created by the folding back: an antibonding band consisting of HOMO, HOMO-1, and HOMO-2 and a bonding band containing HOMO-9, HOMO-10, and HOMO-11, with the quasi–Brillouin zone boundary at $\pi/2a$.

Although the number of orbitals in a band is determined by the number of unit cells, the k-space widths of each orbital is reciprocally related to its spatial extent and thus the finite size of the system; an infinitely long polyparaphenylene chain would result in a band consisting of an infinite number of orbitals that are infinitely sharp in k. Thus, the Fourier transform of each orbital should reflect its k space spread (1, 22). In Fig. 2, the results of the Fourier transform of the six delocalized π orbitals calculated for a twisted 6P molecule are overlaid on the experimental band map. The agreement with experiment is remarkable, with the positions, the k widths, and the relative intensities being fully reproduced. Of particular note is the precise agreement of both position and relative intensities for the HOMO and the HOMO-1, which are energetically well resolved from other bands. In fig. S2, the experimental intensity line scans at the respective orbital energies are shown in comparison to the Fourier transforms of the calculated orbitals for both planar and twisted 6P. Again, the better explanation of the data by twisted 6P is emphasized.

A surprising aspect of the comparison of the Fourier transforms with experiment is that the observed high intensities in the second Brillouin zone are reproduced. Photoemission intensities can be determined by the transition matrix within Fermi's Golden Rule and are generally difficult to calculate. However, the mathematics of the Fourier transform of the orbitals is equivalent to a calculation for the transition matrix from the initial state orbital to a plane wave final state (8). This analysis naturally neglects phase shift and diffraction effects of the outgoing photo-

electron; such scattering effects by each atomic potential and a reciprocal lattice vector would enhance the intensity of the HOMO at Γ, which is not reproduced in the Fourier transform.

As well as the distinct features associated with these delocalized π orbitals, the nonbonding πs appear as an almost-continuous intensity background in the region around 4.25 eV, that is, roughly between the two minibands. Close inspection suggests that this localized band does indeed run up from the Γ point with a dispersion of about 0.2 eV. The orbitals of this band are near degenerate, as expected if the molecule is twisted, but, given the uncertainty arising from the experimental resolution and the proximity in energy of HOMO-9, no strong conclusion will be drawn from it.

Such unambiguous observation of such intramolecular orbital dispersion has been difficult to obtain. For relatively long alkyl chains, which pack vertically in films, the bands from normal emission experiments have been plotted, but, because of the necessarily large number of repeat units, the discrete orbitals could not be observed (4, 6, 23). Similar measurements on films of upright 6P itself (1) could not resolve these features because, in the 6P(001) orientation, the molecules are actually at 17° from normal.

We now consider the angular behavior of the orbital emissions in the direction perpendicular to the molecular axis. In this direction, the molecules present themselves as relatively densely packed π stacks with a periodicity of 5.6 Å (Fig. 1A), the closest interplanar spacing for the molecules in a 6P crystal. Any intermolecular over-
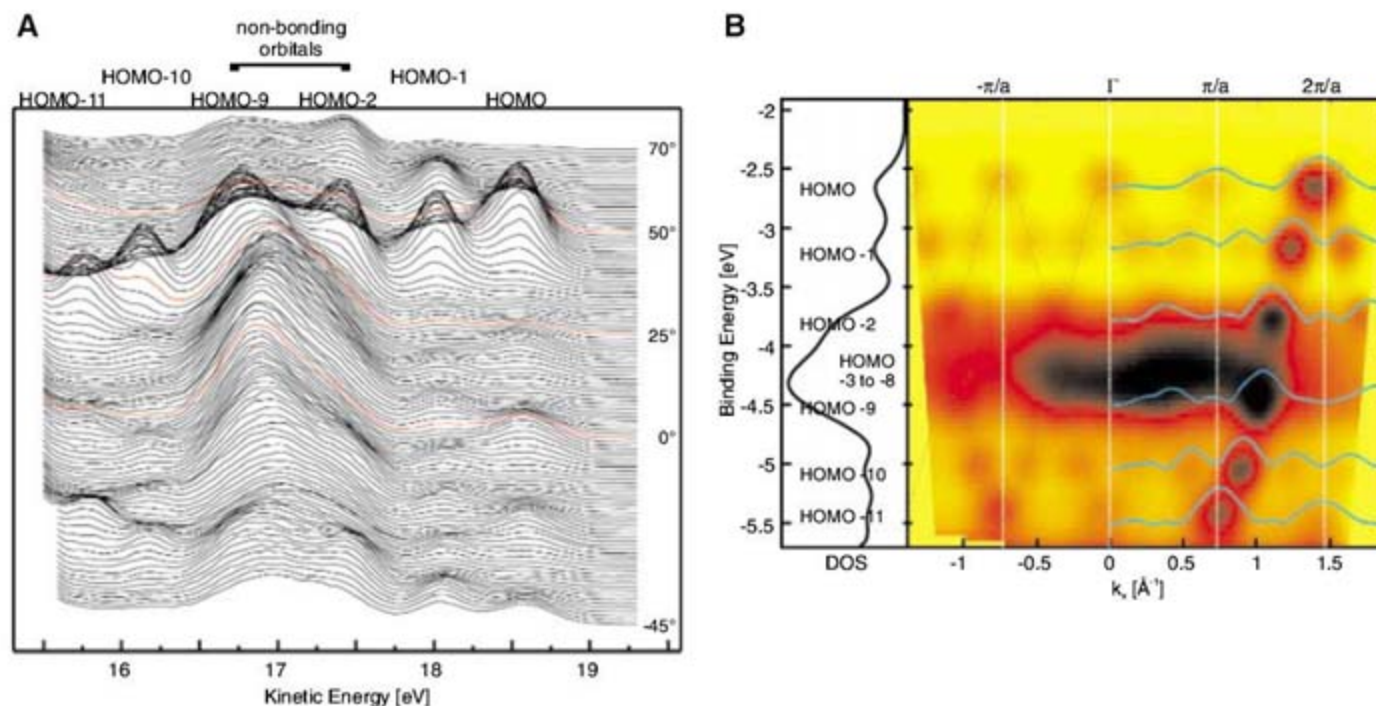
Fig. 2. (**A**) The set of He I photoemission spectra of the 6P π bands measured for electron emission angles from −45° to 70° in the plane containing the long molecular axis and the surface normal. (**B**) The set of photoemission data presented as a contour map. The color scale is linear with highest intensity dark. The energy scale is referred to the Fermi level of the substrate, whereas the momentum (k_x) derived from the electron emission angle θ, $k_x = [2m_e E_{kin}/\hbar^2]^{1/2}\sin\theta$, is given in $Å^{-1}$. The density of states (DOS) is on the left with all orbitals enumerated. The Fourier spectra from the DFT-calculated orbitals of an isolated twisted 6P molecule are overlaid on the experimental band map. A reciprocal lattice vector (G) of ∼π/a rather than $2\pi/a$ is observed. The two dotted sinusoids on the left guide the reader's eye to the two minibands.

lap, and thus any considerable intermolecular dispersion, would be expected to be in this direction. In the photoemission data over a 60° range of takeoff angle, the delocalized π orbitals are weak, and the π band emissions are dominated by the localized band [nonbonding orbitals (fig. S3)]. In contrast to the k_x data, the k_y data show very little intensity variation with angle, and the major change is in the energy position of the nonbonding feature. The data are presented in an intensity map in Fig. 3 after conversion from θ to k_y. The only delocalized orbitals of the molecule that can be truly distinguished are HOMO and HOMO-1. Their intensities are spread almost uniformly in k_y, with a barely discernable energy dispersion. Such flat bands imply these orbitals are localized to the molecules. These orbitals have little overlap between molecules in the crystal and are unlikely to be directly involved in so-called band transport. In the $E(k_y)$ map, the energy changes in the nonbonding orbitals are visibly periodic in k. This band runs up from Γ to a zone boundary at ~0.56 Å^{-1}, which implies a real space lattice periodicity of 5.6 Å, which is the same as the molecular spacing of the bulk crystal in this direction.

This intermolecular band has a dispersion of ~0.7 eV, which is very large for a film with a single component (5). Such a large dispersion implies that these nonbonding orbitals are de-

localized throughout the 6P molecular crystal. The direction in which the band dispersion runs also reveals packing information. If the molecules were stacked face-on, this band would run down from Γ. That it disperses up is a result of tilt of the molecular plane inherent in the herringbone structure (fig. S4).

The results of the band structure calculations for the crystal of planar 6P molecules in this direction are overlaid on the experimental data of Fig. 3. Each molecular orbital of the isolated molecule gives rise to two near-degenerate bands because there are two 6P molecules per unit cell in the crystal. The predicted dispersion of the delocalized πs HOMO and HOMO-1 is ~0.1 eV, which is of the order of the experimental resolution at room temperature and can be barely discerned in the experiment. For the localized band, all defining parameters, that is, the direction, periodicity, and size of the dispersion, are in good agreement with experiment. At the Γ point, the band is experimentally sharper in energy than the calculation. This discrepancy between theory and experiment arises presumably because the molecules are in fact not planar (24). A twist in the molecules leads to a collapse to near degeneracy for the localized orbitals.

We have also investigated the band structure perpendicular to the surface plane [$E(k_z)$] by recording the photoemission spectra in normal

emission as a function of photon energy [40 to 110 eV (fig. S5)]. The results are qualitatively similar to the y direction discussed above, in that the orbitals of the delocalized π band are weak with little intensity variation. The dominating nonbonding orbitals display a smaller dispersion of 0.35 eV. The observed periodicity is 0.7 Å^{-1} and reflects the interplanar distance of 3.8 Å rather than 7.6 Å and is in agreement with band structure calculations in this direction.

Controlled film growth has allowed both the intra- and intermolecular band structure of a prototypical π conjugated system to be directly determined. Perpendicular to the molecules, the observed band dispersion reflects the lattice spacing of the crystal. Interestingly, the orbitals delocalized over the molecule are seen to be localized on the molecule in the crystal, whereas the orbitals localized on the phenyl building blocks of the molecule are delocalized in the crystal and form strongly dispersing bands. In the direction parallel to the molecules, the intermolecular overlap is seen to be negligible, and the result reflects the formation of the band structure of an isolated molecule out of individual orbitals. In this case, the individual orbitals constituting the band are resolvable, and it can be concluded that the molecules in fact adopt a twisted conformation.

The results are also important for organic thin film fabrication, where, for example, the effects on the electronic structure of structural phase transitions or different thin film polymorph structures, common in the organics, are as yet to be explored. The challenge is to control the organic thin film growth, as done here, to achieve highly oriented molecular films with a single crystalline orientation.
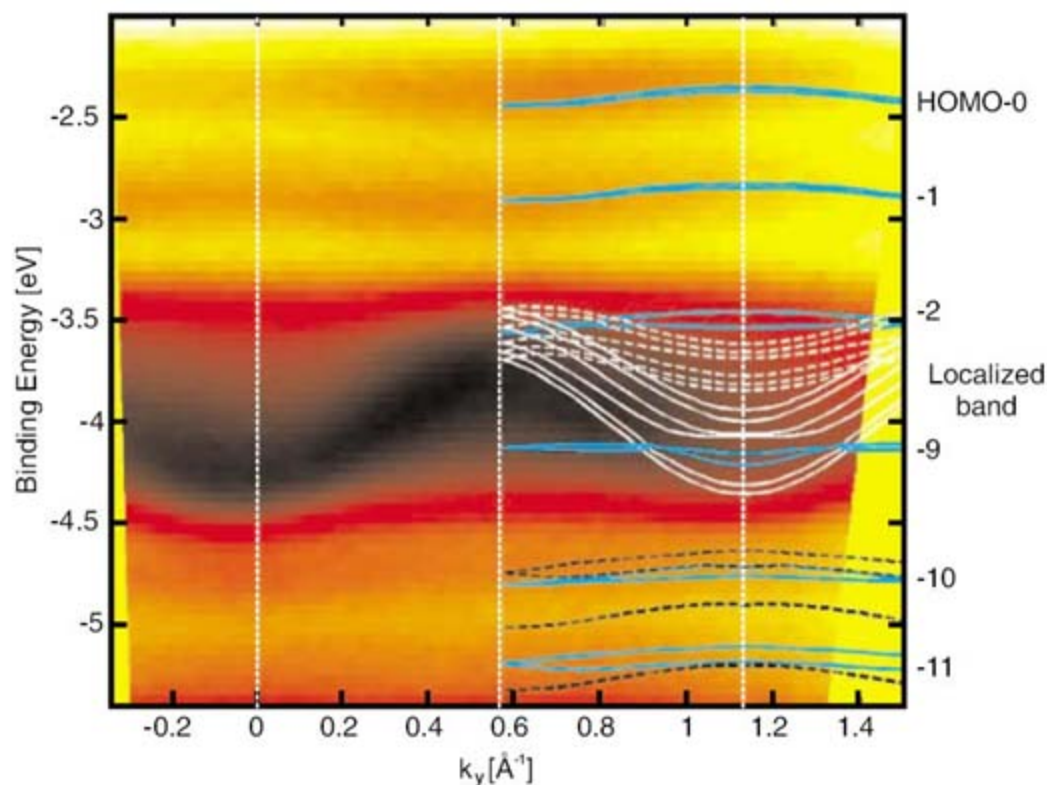
Fig. 3. The band map as measured perpendicular to the molecular axes. The momentum k_y is given in Å^{-1}, and the expected Brillouin zone boundary for $b = 5.6$ Å (0.56 Å^{-1}) is indicated. The band structure in this direction calculated from the bulk structure of 6P is superimposed on the data for the second Brillouin zone. The theoretical result fits the experiment well, reproducing not only the very weak dispersion in the bands derived from the orbitals delocalized (blue lines) over the molecule (HOMO and HOMO-1), but also the strong dispersion of the orbitals localized (white lines) on the phenyl rings in the isolated molecule.

References and Notes
1. S. Narioka et al., Phys. Rev. B **52**, 2362 (1995).
2. H. Yamane et al., Phys. Rev. B **68**, 033102 (2003).
3. C. Rojas, J. Caro, M. Grioni, J. Fraxedas, Surf. Sci. **482–485**, 546 (2001).
4. D. Yoshimura et al., Phys. Rev. B **60**, 9046 (1999).
5. X. Crispin et al., J. Am. Chem. Soc. **126**, 11889 (2004).
6. K. Seki, U. Karlsson, R. Engelhardt, E. E. Koch, Chem. Phys. Lett. **103**, 343 (1984).
7. S. Hasegawa et al., J. Chem. Phys. **100**, 6969 (1994).
8. Information on materials and methods is available on Science Online.
9. G. Koller et al., Adv. Mater. **16**, 2159 (2004).
10. S. Berkebile et al., Surf. Sci. Lett. **600**, L313 (2006).
11. G. Koller et al., Nano Lett. **6**, 1207 (2006).
12. M. Oehzelt et al., Adv. Mater. **18**, 2466 (2006).
13. M. Oehzelt et al., Chem. Phys. Chem., in press; available online at http://dx.doi.org/10.1002/cphc.200700357.
14. Band structure calculations are generally presented in high symmetry directions of the bulk crystal, which are not necessarily the important directions, for example, to charge transport, or the experimentally accessible directions. In this case, the calculations are for the measured directions parallel and perpendicular to the molecular axis.
15. P. Puschnig, C. Ambrosch-Draxl, Phys. Rev. B **60**, 7891 (1999).
16. K. N. Baker et al., Polymer **34**, 1571 (1993).

17. M. G. Ramsey, D. Steinmüller, M. Schatzmayr, M. Kiskinova, F. P. Netzer, *Chem. Phys.* **177**, 349 (1993).
18. J. P. Maier, D. W. Turner, *Faraday Discuss. Chem. Soc.* **54**, 149 (1972).
19. R. Hoffmann, *Solids and Surfaces: A Chemist's View of Bonding in Extended Structures* (Wiley-VCH, New York, 1988).
20. J. Ivanco, B. Winter, F. P. Netzer, M. G. Ramsey, *Adv. Mater.* **15**, 1812 (2003).
21. B. Winter *et al.*, *Appl. Phys. Lett.* **88**, 253111 (2006).
22. E. L. Shirley, L. J. Terminello, S. Santoni, F. J. Himpsel, *Phys. Rev. B* **51**, 13614 (1995).
23. D. Yoshimura *et al.*, *J. Chem. Phys.* **120**, 10753 (2004).
24. Whereas structural studies have concluded that 6P is "on average planar" in the solid state, our measurements on numerous films on a variety of substrates always yield the ionization potential (IP) of the twisted conformation when the molecules are oriented parallel to the substrate. In contrast, films of upright molecules [6P(001)] yield a higher IP, in keeping with a planar conformation. The observed twist, we believe, is the result of a novel surface reconstruction of these molecular crystals, lowering the total energy.
25. This work was supported by the Austrian Science Funds (FWF).

Spontaneous Superlattice Formation in Nanorods Through Partial Cation Exchange

Richard D. Robinson,[1] Bryce Sadtler,[2]* Denis O. Demchenko,[3]* Can K. Erdonmez,[2] Lin-Wang Wang,[3] A. Paul Alivisatos[1,2]†

Lattice-mismatch strains are widely known to control nanoscale pattern formation in heteroepitaxy, but such effects have not been exploited in colloidal nanocrystal growth. We demonstrate a colloidal route to synthesizing CdS-Ag$_2$S nanorod superlattices through partial cation exchange. Strain induces the spontaneous formation of periodic structures. Ab initio calculations of the interfacial energy and modeling of strain energies show that these forces drive the self-organization of the superlattices. The nanorod superlattices exhibit high stability against ripening and phase mixing. These materials are tunable near-infrared emitters with potential applications as nanometer-scale optoelectronic devices.

The ability to pattern on the nanoscale has led to a wide range of advanced artificial materials with controllable quantum energy levels. Structures such as quantum-dot arrays and nanowire heterostructures can be fabricated by vacuum- and vapor-deposition techniques such as molecular beam epitaxy (MBE) and vapor-liquid-solid (VLS) processes, resulting in quantum-confined units that are attached to a substrate or embedded in a solid medium (*1–5*). A target of colloidal nanocrystal research is to create these same structures while leveraging the advantages of solution-phase fabrication, such as low-cost synthesis and compatibility in disparate environments [e.g., for use in biological labeling (*6, 7*) and solution-processed light-emitting diodes (*8*) and solar cells (*9*)]. One key difference between quantum dots epitaxially grown on a substrate and free-standing colloidal quantum dots is the presence of strain. In epitaxially grown systems, the interface between the substrate crystal and the quantum dot creates a region of strain surrounding the dot. Ingeniously, this local strain has been used to create an energy of interaction between closely spaced dots; this use of "strain engineering" has led, in turn, to quantum-dot arrays that are spatially patterned in two (and even three) dimensions (*2–4*). We demonstrate the application of strain engineering in a colloidal quantum-dot system by introducing a method that spontaneously creates a regularly spaced arrangement of quantum dots within a colloidal quantum rod.

A linear array of quantum dots within a nanorod effectively creates a one-dimensional (1D)

[1]Materials Science Division, Lawrence Berkeley National Laboratory, Berkeley, CA 94720, USA. [2]Department of Chemistry, University of California, Berkeley, CA 94720, USA. [3]Computational Research Division, Lawrence Berkeley National Laboratory, Berkeley, CA 94720, USA.

*These authors contributed equally to this work.
†To whom correspondence should be addressed. E-mail: alivis@berkeley.edu
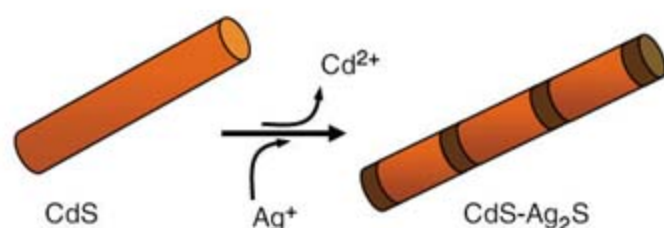
Fig. 1. TEM images of superlattices formed through partial cation exchange. (**A**) The original 4.8–by–64-nm CdS nanorods. (**B** and **C**) Transformed CdS-Ag$_2$S superlattices. (Inset) Histogram of Ag$_2$S segment spacing (center-to-center). The average spacing is 13.8 ± 3.8 nm. The sample set for the histogram was greater than 250 spacings.
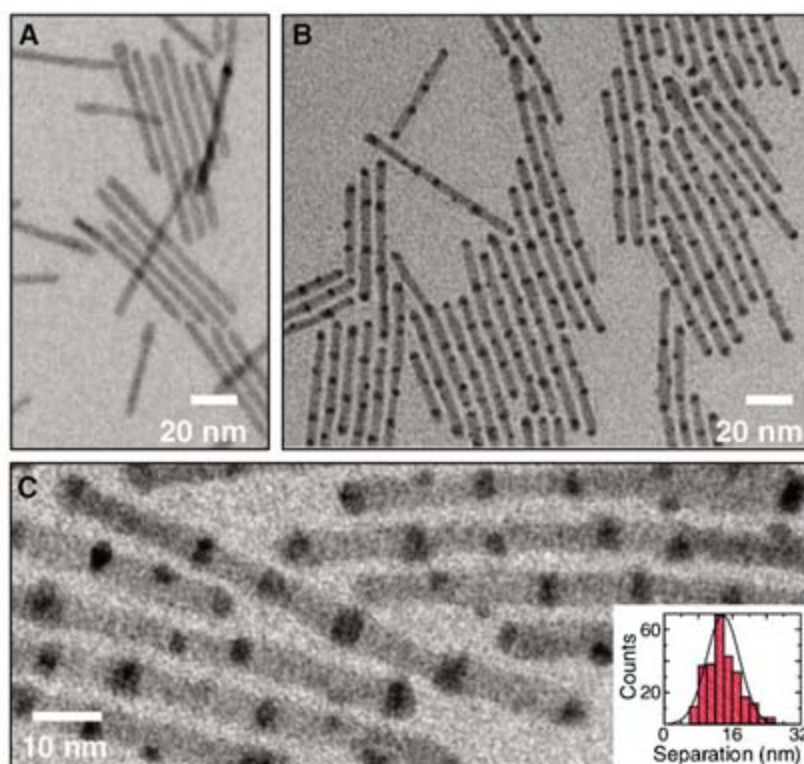
superlattice, a promising new generation of materials (*10, 11*). Such 1D superlattices exhibit confinement effects and are unusual because of their ability to tolerate large amounts of lattice mismatch without forming dislocations and degrading device performance (*12, 13*). Strong coupling of electronic states makes them interesting for optical systems and good candidates for photonic applications. One-dimensional superlattices are also of interest for thermoelectric devices and the study of ionic transport in 1D systems. VLS growth has demonstrated the formation of extended nanowire superlattices (e.g., alternating Si-Ge or InAs-InP) containing hundreds of repeat units (*14–16*). To achieve this, the precursors are alternated for the growth of each layer. The formation of 1D superlattices by this same time-dependent variation of precursor concentration is out of reach for present colloidal growth techniques. The largest number of alternating layers produced so far is three, and yet the sequence of purifications required in that instance was already taxing to implement (*17*).

Cation exchange provides a facile method for systematically varying the proportion of two chemical compositions within a single nanocrystal. We have previously shown that cation exchange can be used to fully (and reversibly) convert CdSe, CdS, and CdTe nanocrystals to the corresponding Ag-chalcogenide nanocrystal by a complete replacement reaction of the Cd^{2+} cations for Ag^+ cations (*18*). The resultant material is the Ag-anion analog of the starting material (i.e., Ag_2Se, Ag_2S, and Ag_2Te). The size and shape of the nanocrystal are preserved when the nanocrystal has minimum dimensions greater than 4 nm (*18*). The high mobility of cations in the CdS(Se,Te) lattice suggests that partial cation exchange may lead to interesting patterns of segregated domains of Ag chalcogenide within a Cd-chalcogenide nanorod. This led us to investigate the possibility of converting a previously formed nanorod of a single chemical composition into a striped pattern by a single-step partial chemical transformation. In the case explored here, a linear arrangement of regularly spaced Ag_2S dots contained within a CdS rod forms spontaneously at ~36% cation exchange. The near-infrared (NIR) band gap of the Ag_2S dots is embedded within the larger gap of the CdS, creating a type I heterostructure with interesting optical properties.

Studies of partial cation exchange for 4.8–by–64-nm CdS to CdS-Ag_2S nanorods are shown in transmission electron microscopy (TEM) images in Fig. 1. In these experiments, the initial CdS nanorods (Fig. 1A) were exceptionally smooth and the rod diameter was tightly controlled (SD = 10%), whereas the length varied between 30 and 100 nm. The CdS colloidal nanorods were added to a solution of toluene, $AgNO_3$, and methanol at –66°C in air (*19*). The concentration of $AgNO_3$ was a controlled fraction of the concentration of Cd^{2+} ions present in the starting material. In the presence of excess Ag^+, the rods are completely

converted to Ag_2S (*18*). However, when the Ag^+ ions are limited to yield approximately 36% exchange, the resulting nanorods displayed a periodic pattern of light- and dark-contrast regions (Fig. 1, B and C). The average spacing between the dark regions is 13.8 nm, with a standard deviation of 28% (Fig. 1C, inset). The spacing between periodic segments can be controlled by the diameter of the initial CdS rod (fig. S1).

Examination of these regions shows that the light- and dark-contrast regions are CdS and

Ag_2S, respectively. Energy-dispersive x-ray spectroscopy (EDS) indicates that the striped rods alternate between Cd-S– and Ag-S–rich regions (Fig. 2A) (*20*). Powder x-ray diffraction (XRD) data confirms the presence of wurtzite CdS and monoclinic acanthite Ag_2S (Fig. 2B) (*21*). Peaks appearing in the original CdS rods can be indexed to wurtzite CdS [Joint Committee on Powder Diffraction Standards (JCPDS) #41-1049], and those in the fully exchanged rods can be indexed to acanthite (JCPDS #14-0072). Peaks visible in the striped rods can be attributed

Fig. 2. Characterization of CdS-Ag_2S heterostructures. (**A**) EDS spectra of the striped rods at the (top) light- and (bottom) dark-contrast regions, corresponding to Cd-S– and Ag-S–rich regions, respectively. a.u., arbitrary units. (**B**) XRD spectra of CdS rods (black line), striped rods (blue line), and fully exchanged Ag_2S rods (green line). Spectra from the striped rods show new peaks corresponding to Ag_2S and a modified (002) peak, indicating interruption of the CdS lattice along the rod axis.
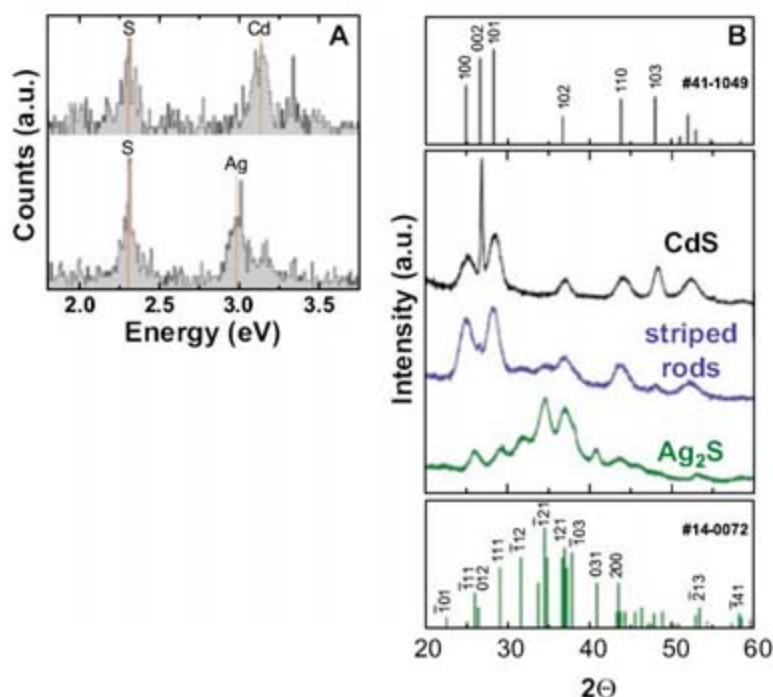
Fig. 3. Effects of increasing $AgNO_3$ concentration. (**A** and **B**) TEM images. (A) Low concentration (Ag^+/Cd^{2+} ~0.2). (B) Intermediate concentration that produced the nanorod superlattices (Ag^+/Cd^{2+} ~0.9). Scale bar (A and B), 20 nm. (**C** and **D**) Histograms of the number of Ag_2S regions per rod. (C) Low and (D) intermediate concentration. More than 250 nanorods were examined for each histogram. (**E** and **F**) Pair-distribution histograms for Ag_2S regions on individual CdS-Ag_2S nanorods. (E) Low and (F) intermediate concentration. Intrarod distances between each Ag_2S region, measured for 200 nanorods in each of the sample sets shown in (A) and (B). Spacings were normalized by the number of Ag_2S regions and the length of the rod. Low concentration (E) shows no correlation beyond the nearest-neighbor spacing. Intermediate concentration (F) shows a periodicity, which extends over several nearest neighbors.
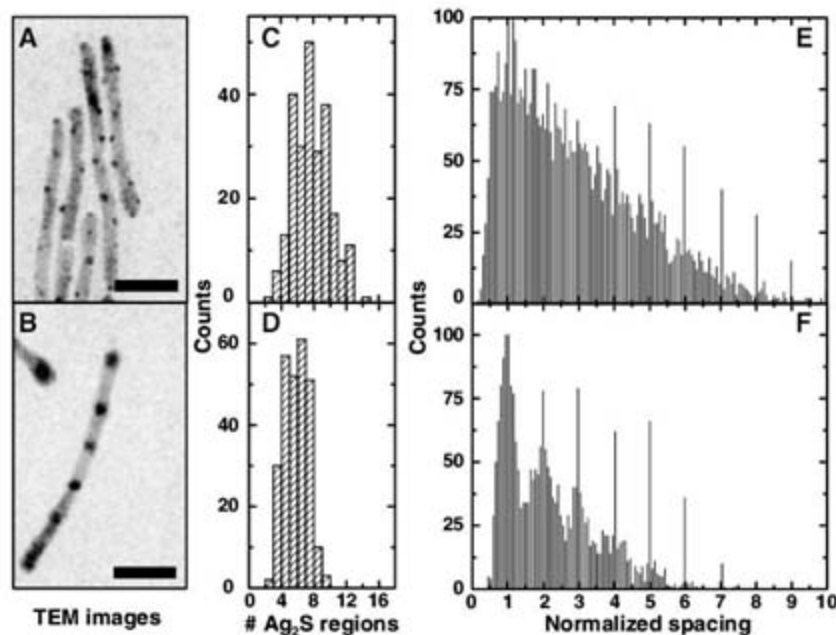
purely to a combination of these two phases. No Ag peaks are present. Furthermore, a simulation of the XRD pattern for a mixture of Ag_2S and CdS crystalline domains with dimensions matching those of the sample agrees qualitatively with the experimental patterns, in terms of the relative intensities of Ag_2S peaks to CdS peaks, supporting the extent of the conversion observed in TEM images (fig. S2). In our experimental XRD patterns, the CdS (002) peak is broader and weaker for the striped rods than for the initial CdS sample. This indicates a decreased CdS crystallite size along <001> [the growth axis of the rods (22)] after the partial ion exchange. Debye-Scherrer analysis of peak widths for several striped-rod samples indicates that the CdS grain size along the axis has decreased from >30 nm to 12 to 16 nm for the striped rods. The decrease in grain size along this direction is attributed to the interruption of the {001} planes by the Ag_2S material, because the shorter length is consistent with the average spacing in this striped-rod sample. TEM images show that the Ag_2S regions, which have a broad range of separations at low concentrations (Fig. 3A), become increasingly ordered at slightly higher concentrations (Figs. 1, B and C, and 3B). The change in the number and periodicity (spacing) of the Ag_2S regions suggest a systematic organization as the volume fraction of Ag_2S increases (Fig. 3, C to F). Intrarod Ag_2S spacings were correlated through a pair-distribution function in which the distances between each Ag_2S region and all other Ag_2S regions on a rod were measured. The organization of the Ag_2S regions into superlattices is seen in the periodicity of the histogram (Fig. 3F), extending over several nearest-neighbor distances. In the superlattices, the Ag_2S regions are spaced evenly along the rod, whereas no periodicity is seen for the lower Ag^+ concentration (Fig. 3E).

The mechanism by which the initial arrangement of randomly distributed small islands of Ag_2S evolves into a periodic, 1D pattern is of particular interest. Because there exists a positive CdS-Ag_2S interface formation energy (~1.68 eV per Cd-Ag-S elementary interface unit, from our ab initio calculations), it is energetically favorable to merge small Ag_2S islands into larger Ag_2S segments. The fast diffusion of cations leads to a situation where Ostwald ripening between the initially formed islands of Ag_2S can occur, so that larger islands grow at the expense of nearby smaller ones. Diffusion of the cations is allowed because both Ag^+ and Cd^{2+} are considered fast diffusers (23–25). Also, Ag chalcogenides exhibit superionic conductivity in their high-temperature phases (25). A critical juncture occurs when the regions of Ag_2S grow to the point where they span the diameter of the rod. At this point, further Ostwald ripening is kinetically prohibited, because an atom-by-atom exchange of Ag^+ among segments will not reduce the total interfacial area. This leads to Ag_2S segments of nearly equal size (fig. S3). The rod is in a

metastable state; i.e., the complete joining of two Ag_2S regions is always a lower-energy configuration, but one that cannot readily be accessed by simple atomic-exchange events.

A second factor that promotes the regular spacing of the stripe pattern is the elastic repulsion between two Ag_2S segments because of the strain in the intervening CdS region. A model for the coherent atomic connection between the two materials is shown in Fig. 4A (26). To match the basal lattice constant for CdS (4.3 Å), the Ag_2S body-centered–cubic lattice in the plane of interface has to expand by 4% in one direction and contract by 15% along the perpendicular direction. There is a repulsive elastic force between segments of like material because of the resulting strain fields. Results from valence force field (VFF) modeling (27) show that the elastic energy stored in the rod increases markedly as two Ag_2S segments approach each other (Fig. 4B). Bond strain in

the z direction (axial) is responsible for the repulsive elastic interaction (Fig. 4C). CdS atoms are pushed away from the closest Ag_2S segment, forming convex-shaped atomic layers. For two Ag_2S segments approaching each other, the z displacements in the CdS are in opposite directions, leading to an interaction term between the fields that gives higher strain energy at smaller separations (28). The model is consistent with the experimental finding that increasing the rod diameter increases the spacing between segments (fig. S1). Similar effects of spontaneous ordering of quantum dots in two dimensions produced by MBE growth have been explained with corresponding arguments [e.g., (3)]. However, the 1D geometry explored here imposes a stronger constraint on ripening processes, leading to an especially robust path to stable, regularly spaced quantum dots within a rod.

The importance of strain in attaining the superlattice pattern can be illustrated by examining
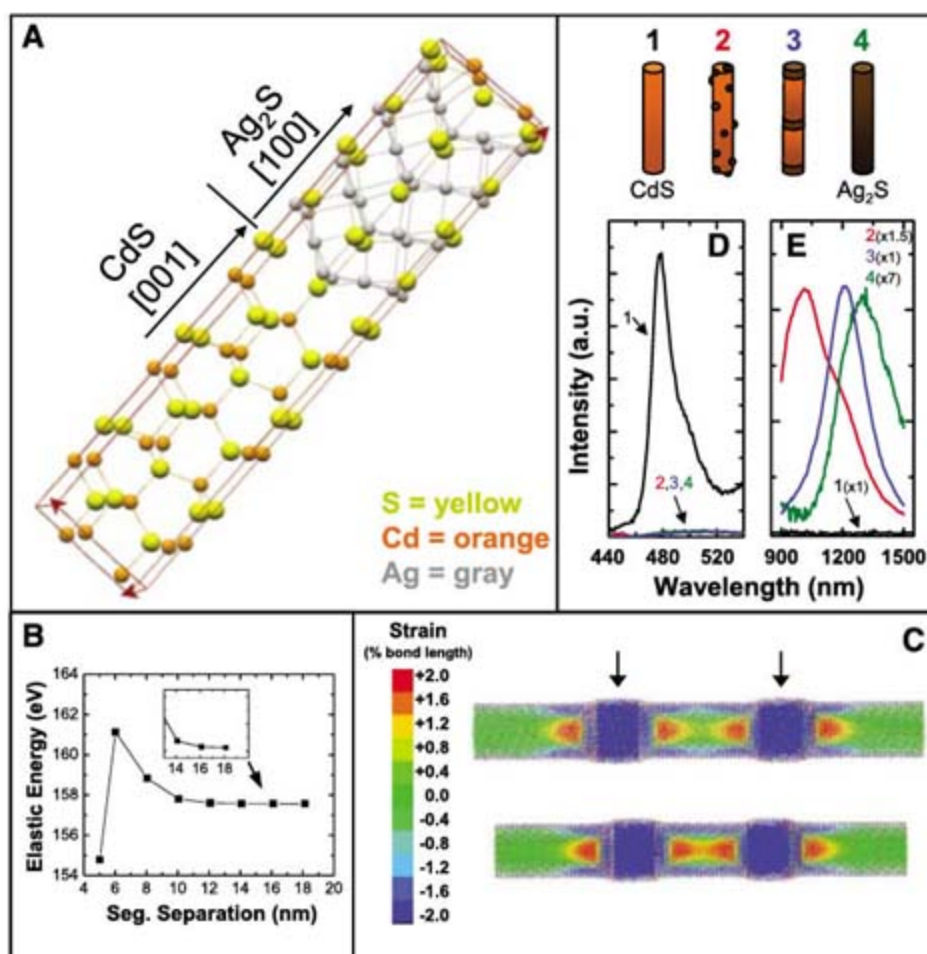
Fig. 4. Theoretical modeling and experimental optical characterization. (**A**) Cubic-cutout representation of cells used for ab initio energy calculations. A distorted monoclinic Ag_2S (100) plane connects with the wurtzite CdS (001) plane. (**B**) Elastic energy of the rod as a function of segment separation (center-to-center). (**C**) Z-axis strain for the case of two mismatched segments at a center-to-center separation distance of 14.1 nm (top) and 12.1 nm (bottom). The elastic interaction between segments is greatly reduced for separations >12.1 nm. Arrows show the placement of mismatched segments. The CdS rods used for VFF calculations (B and C) were 4.8 nm in diameter, with two 4.8–by–4.0-nm lattice-mismatched segments. Effective elastic constants for the mismatched segments were from ab initio calculations for monoclinic Ag_2S. (**D**) Visible and (**E**) NIR PL spectra at λ = 400- and 550-nm excitation, respectively. Coupling between the CdS and Ag_2S is evident by the complete quenching of the visible PL (D) in the heterostructures. The shift in NIR PL (E) is due to quantum confinement of the Ag_2S.

similar studies of metal ions reacting with semiconductor nanocrystals. Mokari et al. and Saunders et al. have created interesting metal-semiconductor nanocrystal heterostructures by reducing Au^{3+} ions onto InAs quantum dots (29) and CdS/Se nanorods (30, 31). Because Au^{3+} has a much greater electron affinity than Ag^+, reduction of the ion takes place rather than an exchange reaction. The positive interfacial energy between the two materials drives a phase segregation, similar to our Ag_2S-CdS system, leading to Ostwald ripening. However, epitaxial strain does not play a major role in the Au growth, and these heterostructures continue to ripen into single-metal domains, either at the tip of the rod (CdS/Se), or inside the quantum dot (InAs). In contrast, the epitaxial relationship between the two phases in the Ag_2S-CdS superlattice structures results in strain fields from the lattice mismatch, which cause like segments to repel each other, preventing further ripening.

The resulting striped rods display properties expected of a type I array of Ag_2S quantum dots separated by confining regions of CdS, in agreement with our ab initio calculations of the band structure. The visible CdS photoluminescence (PL) is quenched, indicating coupling between materials at the heterojunction (32), and NIR PL from the Ag_2S segments is observed (Fig. 4, D and E). The band gap of the Ag_2S segments depends on their size, matching the bulk value (33) for fully converted nanorods and shifting to higher energy in smaller dots because of quantum confinement (Fig. 4E). In the present configuration, the Ag_2S quantum dots are only very weakly coupled to each other, because the CdS segments are large. Such structures are of interest for colloidal quantum-dot solar cells, where the sparse density of electronic states within a dot may lead to multiple-exciton generation (34). The formation of nanorod superlattices through partial cation exchange can also be applied to other pairs of semiconductors, yielding a broader class of quantum-confined structures. Cation-exchange reactions have already been reported in HgS, Ag_2S, SnS_2, CdS, ZnS, Cu_2S, Bi_2S_3, and Sb_2S_3 (35–37). Two-component combinations of these compounds can produce materials with functional properties ranging from type I (e.g., ZnS-Ag_2S) and type II (e.g., Cu_2S-CdS) band alignments to thermoelectric-power junctions (e.g., CdS-Bi_2S_3).

References and Notes

1. S. Guha, A. Madhukar, K. C. Rajikumar, Appl. Phys. Lett. 57, 2110 (1990).
2. M. S. Miller et al., J. Appl. Phys. 80, 3360 (1996).
3. V. A. Shchukin, D. Bimberg, Rev. Mod. Phys. 71, 1125 (1999).
4. R. Notzel, Semicond. Sci. Technol. 11, 1365 (1996).
5. M. Law, J. Goldberger, P. D. Yang, Annu. Rev. Mater. Res. 34, 83 (2004).
6. M. Bruchez Jr., M. Moronne, P. Gin, S. Weiss, A. P. Alivisatos, Science 281, 2013 (1998).
7. W. C. W. Chan, S. Nie, Science 281, 2016 (1998).
8. M. Achermann et al., Nature 429, 642 (2004).
9. I. Gur, N. A. Fromer, M. L. Geier, A. P. Alivisatos, Science 310, 462 (2005).
10. D. Y. Li, Y. Wu, R. Fan, P. D. Yang, A. Majumdar, Appl. Phys. Lett. 83, 3186 (2003).
11. M. S. Dresselhaus et al., Phys. Solid State 41, 679 (1999).
12. G. Kästner, U. Gösele, Philos. Mag. 84, 3803 (2004).
13. E. Ertekin, P. A. Greaney, D. C. Chrzan, T. D. Sands, J. Appl. Phys. 97, 114325 (2005).
14. Y. Y. Wu, R. Fan, P. D. Yang, Nano Lett. 2, 83 (2002).
15. M. S. Gudiksen, L. J. Lauhon, J. Wang, D. C. Smith, C. M. Lieber, Nature 415, 617 (2002).
16. M. T. Bjork et al., Nano Lett. 2, 87 (2002).
17. D. J. Milliron et al., Nature 430, 190 (2004).
18. D. H. Son, S. M. Hughes, Y. Yin, A. P. Alivisatos, Science 306, 1009 (2004).
19. Materials and methods are available as supporting material on Science Online.
20. A minority of segments are Ag-rich with little or no S, probably due to the decomposition of Ag-S compounds by the electron beam (38). This beam damage also distorted the phase and prevented accurate images from being acquired with high-resolution TEM.
21. For these experiments, TEM images show that the original CdS rods were 5.3 by 50 nm, and the striped rods made from these had 5.3–by–11-nm CdS grains.
22. X. Peng et al., Nature 404, 59 (2000).
23. T. D. Dzhafarov, M. Serin, D. Oren, B. Sungu, M. S. Sadigov, J. Phys. D Appl. Phys. 32, L5 (1999).
24. H. H. Woodbury, Phys. Rev. 134, A492 (1964).
25. M. Kobayashi, Solid State Ionics 39, 121 (1990).
26. In both common polymorphs of Ag_2S (cubic and monoclinic), the anion sublattice assumes a body-centered–cubic structure with only slight distortions in the monoclinic phase (39). Several epitaxial relationships were considered, and the epitaxial connection with minimal lattice distortion to the (001) CdS face is the body-centered–cubic (110) face [monoclinic (100) face].
27. A. J. Williamson, L. W. Wang, A. Zunger, Phys. Rev. B 62, 12963 (2000).
28. When the segments are very close to each other, however, the elastic energy is actually lowered. With only three atomic layers separating the segments (leftmost point in Fig. 4B), the number of distorted layers in the z direction is small, which results in a smaller repulsive interaction. Additionally, the interaction of the radial distortions from the two segments is cooperative (unlike the z-direction distortions), because they pull the atoms in the same direction. The overall result is a lowering of the elastic energy.
29. T. Mokari, A. Aharoni, I. Popov, U. Banin, Angew. Chem. Int. Ed. 45, 8001 (2006).
30. T. Mokari, E. Rothenberg, I. Popov, R. Costi, U. Banin, Science 304, 1787 (2004).
31. A. E. Saunders, I. Popov, U. Banin, J. Phys. Chem. B 110, 25421 (2006).
32. D. Battaglia, B. Blackman, X. Peng, J. Am. Chem. Soc. 127, 10889 (2005).
33. P. Junod, H. Hediger, B. Kilchor, J. Wullschleger, Philos. Mag. 36, 941 (1977).
34. V. I. Klimov, J. Phys. Chem. B 110, 16827 (2006).
35. A. Mews, A. Eychmuller, M. Giersig, D. Schooss, H. Weller, J. Phys. Chem. 98, 934 (1994).
36. C. D. Lokhande, V. V. Bhad, S. S. Dhumure, J. Phys. D Appl. Phys. 25, 315 (1992).
37. L. Dloczik, R. Koenenkamp, J. Solid State Electrochem. 8, 142 (2004).
38. L. Motte, J. Urban, J. Phys. Chem. B 109, 21499 (2005).
39. H. Schmalzried, Prog. Solid State Chem. 13, 119 (1980).
40. This work was supported by the U.S. Department of Energy under contract no. DE-AC02-05CH11231. We thank C. Nelson, C. Kisielowski, the National Center for Electron Microscopy at Lawrence Berkeley National Laboratory. We also thank D. Talapin, T. Teague, and D.-H. Son. R.D.R. thanks the Lawrence Berkeley National Laboratory for the Lawrence Postdoctoral Fellowship.

A Late Triassic Dinosauromorph Assemblage from New Mexico and the Rise of Dinosaurs

Randall B. Irmis,[1]* Sterling J. Nesbitt,[2,3]* Kevin Padian,[1] Nathan D. Smith,[4,5] Alan H. Turner,[3] Daniel Woody,[6] Alex Downs[7]

It has generally been thought that the first dinosaurs quickly replaced more archaic Late Triassic faunas, either by outcompeting them or when the more archaic faunas suddenly became extinct. Fossils from the Hayden Quarry, in the Upper Triassic Chinle Formation of New Mexico, and an analysis of other regional Upper Triassic assemblages instead imply that the transition was gradual. Some dinosaur relatives preserved in this Chinle assemblage belong to groups previously known only from the Middle and lowermost Upper Triassic outside North America. Thus, the transition may have extended for 15 to 20 million years and was probably diachronous at different paleolatitudes.

Dinosaurs originated in the Late Triassic Period (1, 2) (Carnian-Norian stages, about 230 to 200 million years ago), when they replaced faunas dominated by a variety of basal archosaurs and other amniotes (3, 4). Archosaurs are divided into two primary lineages: the Pseudosuchia, which include phytosaurs, aetosaurs, "rauisuchians," and crocodylomorphs, and the Ornithodira, which include pterosaurs, basal dinosauromorphs such as

Lagerpeton and *Marasuchus*, and dinosaurs (*5*, *6*). By the beginning of the Jurassic, all of these clades except the dinosaurs, pterosaurs, and crocodylomorphs became extinct (*7*). The pace of this faunal turnover is poorly understood, even though Late Triassic skeletal and footprint assemblages are distributed worldwide (*8*). Most evidence has supported the hypothesis that dinosaurs diversified in the Late Triassic after the more archaic faunas were eliminated, either by rapidly outcompeting the archaic forms or replacing them quickly and opportunistically after they died out for other reasons (*1*, *2*, *6*, *9*, *10*), rather than by more gradual processes of ecological replacement.

Until recently, the only evidence of dinosaur precursors was from the Middle Triassic (Ladinian) terrestrial Chañares Formation of Argentina (*11–13*). Without evidence from other continents, the South American fossil record suggested that the Middle Triassic basal dinosauromorphs gave way to the earliest dinosaurs relatively abruptly at the beginning of the Late Triassic. This understanding of early dinosaur evolution began to change with several new discoveries: *Silesaurus opolensis* (*14*) demonstrated that basal dinosauriforms survived into the Late Triassic; a reappraisal of the North American dinosaur record suggested that Triassic dinosaurs were less diverse and rarer than previously thought (*15*); and a reevaluation of putative Triassic ornithischian dinosaurs showed that most were misidentified (*16*). Here we describe fossils from the upper Chinle Formation (Upper Triassic) Hayden Quarry (HQ) in New Mexico demonstrating that early dinosaur faunal replacement was neither abrupt nor as simple as previously thought and also that much of it occurred in North America.

The HQ was opened to large-scale excavation in 2006, and since then our field crew has collected and cataloged nearly 1300 vertebrate specimens. Stratigraphically, the HQ lies approximately 65 m below the famous Ghost Ranch *Coelophysis* Quarry, 15 m below the Snyder Quarry, and 12 m below the Canjilon Quarry (Fig. 1) (*17*). These four quarries lie within several kilometers of each other and preserve different but partially overlapping assemblages (Table 1). The HQ assemblage includes pseudopalatine phytosaurs and the aetosaurs *Typothorax coccinarum*

and *Rioarribasuchus chamaensis*, indicative of a Norian age (*17–19*).

The HQ has a diverse tetrapod assemblage; in addition to various representatives of phytosaurs, aetosaurs, "rauisuchians," and other archosauromorphs, the HQ preserves several dinosaur taxa, including the basal saurischian *Chindesaurus bryansmalli* and coelophysoid theropods. The sauropodomorph and ornithischian dinosaurs known from high-paleolatitude sites of Europe and Gondwana are absent, as they are from all other North American Triassic assemblages (*15*, *16*). The HQ also contains the remains of non-dinosaurian relatives of dinosaurs: a basal dinosauriform similar to *Silesaurus* and a new non-dinosauriform dinosauromorph similar to *Lagerpeton* (a taxon known only from the Middle Triassic of Argentina) (*11*), which we describe here.

Archosauria Cope 1869 *sensu* Gauthier and Padian 1985; Dinosauromorpha Benton 1985 *sensu* Sereno 1991; *Dromomeron romeri*, gen. et sp. nov.

Etymology. *Dromomeron*, from *dromas* (Greek word for running) and *meros* (Greek word for femur); *romeri*, for Alfred Sherwood Romer, who first described the dinosaur precursors from Argentina, including *Lagerpeton*.

Holotype. Complete left femur, specimen number GR 218 (Fig. 2, A to D), reposited in the collections of the Ghost Ranch Ruth Hall Museum of Paleontology (GR).

Paratypes. Additional specimens were found within several feet of the holotype. A right femur, GR 219, and a left tibia, GR 220, may belong to the same individual as the holotype. Additional material includes GR 221, a partial left femur; GR 222, a complete left tibia (Fig. 2, E to H); GR 223, a complete astragalocalcaneum (Fig. 2, I- to K); and GR 234, a nearly complete right femur.

Referred material. New Mexico Museum of Natural History (NMMNH) P-35379, a complete astragalocalcaneum.

Locality and horizon. Site 3, HQ, Ghost Ranch, Rio Arriba County, New Mexico, USA. The HQ is in the lower portion of the Petrified Forest Member of the Upper Triassic Chinle Formation. The referred NMMNH specimen is from the nearby Snyder Quarry (*20*), also within the Petrified Forest Member. The Petrified Forest Member in this area is of Norian age, according to fossil pollen and vertebrate biostratigraphy (*17–19*, *21*, *22*).

Diagnosis. Differs from all other dinosauromorphs except *Lagerpeton chanarensis* in possessing a hook-shaped femoral head (Fig. 2A), a lateral emargination ventral to the femoral head (Fig. 2A), an enlarged posteromedial tuber on the proximal portion of the femur (Fig. 2, B and C), an enlarged crista tibiofibularis on the distal end of the femur (Fig. 2D), a posteromedial crest on the distal end of the tibia (Fig. 2H), and an astragalus with a posterior ascending process (Fig. 2, I

[1]Museum of Paleontology and Department of Integrative Biology, University of California, Berkeley, CA 94720-4780, USA. [2]Lamont-Doherty Earth Observatory, Columbia University, Palisades, NY 10964, USA. [3]Division of Paleontology, American Museum of Natural History, New York, NY 10024, USA. [4]Committee on Evolutionary Biology, University of Chicago, Chicago, IL 60637, USA. [5]Geology Department, Field Museum of Natural History, Chicago, IL 60605, USA. [6]Department of Geological Sciences, University of Colorado, Boulder, CO 80309-0399, USA. [7]Ruth Hall Museum of Paleontology, Ghost Ranch Conference Center, Abiquiu, NM 87510-9601, USA.

*To whom correspondence should be addressed. E-mail: irmis@berkeley.edu (R.B.I.); snesbitt@ldeo.columbia.edu (S.J.N.)

Fig. 1. Stratigraphic position of the HQ and related assemblages. SS, sandstone.

to K); differs from *Lagerpeton* in possessing a much larger crista tibiofibularis; and differs from all other basal dinosauromorphs in the absence of a fourth trochanter (Fig. 2, A and B), the presence of a sharp ridge on the antero-medial edge of the distal end of the femur (Fig. 2D), and a large crest on the anteromedial edge of the astragalus (Fig. 2I) (autapomorphies).

Phylogenetic analyses consistently place *Lagerpeton chanarensis* closer to dinosaurs than to pterosaurs and pseudosuchians (6, 11, 23) (Fig. 3). The referred tibiae of *Dromomeron* share two synapomorphies with *Lagerpeton*: a distal end with a posteromedial crest (Fig. 2H) and a posterolateral concavity for the reception of the posterior ascending process of the astragalus. The distal end of the tibia of *Dromomeron* also possesses an anteromedial concavity for the reception of the enlarged anteromedial crest of the astragalus, creating an anteromedial-posterolateral groove in the distal end of the tibia (Fig. 2, E and H). The astragalus overlaps the calcaneum dorsally (Fig. 2K). The calcaneum is triangular in dorsal view, widening anteriorly and narrowing posteriorly (Fig. 2I). Our phylogenetic analysis places *Dromomeron* as the sister taxon to *Lagerpeton* and recovers this clade as the sister taxon to all other dinosauromorphs (Fig. 3) (17).

Although most of the HQ material is disarticulated, several diagnostic elements of each taxon have been recovered. Material of the *Silesaurus*-like dinosauriform includes a partial tooth-bearing dentary (GR 224) (Fig. 2L), an ilium (GR 225) (Fig. 2M), and a proximal femur (GR 195) (Fig. 2, N to O). This material may be

Table 1. Tetrapods from Chinle Formation quarries in the Chama Basin, New Mexico. Hayden Quarry, HQ; Canjilon Quarry, CN; Snyder Quarry, SQ; *Coelophysis* Quarry, CO; Petrified Forest Member at Petrified Forest National Park, Arizona, PF. See supporting online material (17) for voucher specimen numbers.

Taxon	HQ	CN	SQ	CO	PF
Metoposauridae	X	X	X		X
Drepanosauridae	X			X	
Vancleavea	X	X		X	X
Pseudopalatus spp.	X	X	X		X
Typothorax coccinarum	X	X	X		X
Rioarribasuchus chamaensis	X		X		X
"Rauisuchia"	X	X	X	X	X
Shuvosaurus-like taxon	X			X	X
Crocodylomorpha	X			X	X
Dromomeron romeri	X		X		
Silesaurus-like taxon	X				
Chindesaurus bryansmalli	X				X
Coelophysoidea	X	X	X	X	X

Fig. 2. Dinosauromorphs from the HQ. (**A** to **D**) Femur of *D. romeri* (GR 218) gen. et sp. nov. in anterior (A), posterior (B), proximal (C), and distal (D) view. (**E** to **H**) Tibia of *D. romeri* (GR 222) in anterior (E), lateral (F), proximal (G), and distal (H) view. (**I** to **K**) Astragalocalcaneum of *D. romeri* (GR 223) in proximal (I), anterior (J), and posterior (K) view. (**L** to **O**) *Silesaurus*-like dentary (GR 224) in medial view (L), ilium (GR 225) in lateral view (M), and proximal femur (GR 195) in proximal (N) and posterior (O) view. (**P**) *Chindesaurus bryansmalli* femur (GR 226) in posterior view; and (**Q**) coelophysoid theropod fused tibia, fibula, and astragalocalcaneum (GR 227) in anterior view. Abbreviations are as follows: anteromedial crest (amc), anteromedial process (amp), anteromedial ridge (amr), brevis fossa (bf), calcaneum (ca), cnemial crest (cn), crista tibiofibularis (ct), groove (gr), lateral emargination (le), meckelian groove (mg), notch (n), posterior ascending process (pap), posteromedial crest (pmc), posteromedial tuber (pmt). Scale bars, 1 cm.
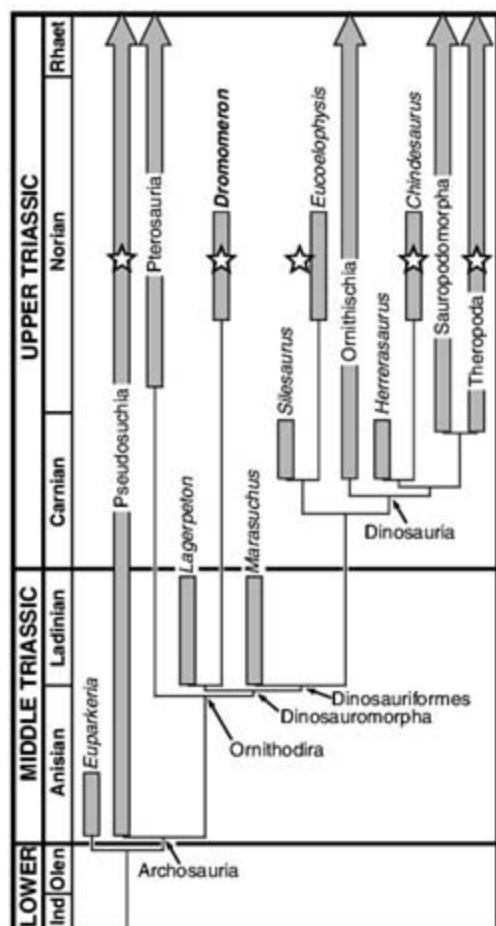
Fig. 3. Phylogenetic position of *D. romeri* gen. et sp. nov. among archosaurs. A single most-parsimonious tree was recovered from a parsimony analysis of 26 taxa and 127 characters (*17*). Pseudosuchia, Ornithischia, Sauropodomorpha, and Theropoda have been collapsed for brevity. Stars indicate taxa present in the HQ. For lineages that do not extend into the Jurassic, the length of the gray bar indicates stratigraphic imprecision. Ind, Induan; Olen, Olenekian; Rhaet, Rhaetian.

referable to *Eucoelophysis baldwini*, a *Silesaurus*-like dinosauriform known from the same stratigraphic unit (*15*, *17*). The dentary shares two synapomorphies with *Silesaurus*: striated tooth bases that partially fuse to the jaw (unlike ornithischian dinosaurs) and a Meckelian groove near the ventral border of the dentary that extends to the anterior tip (Fig. 2L). The teeth are subtriangular with enlarged denticles, a labial basal swelling of the crown, and a distinct narrowing at the base of the crown similar to the herbivorouslike teeth of other archosaurs (*16*, *24*). They lack the distinct striations found toward the tip of *Silesaurus* teeth (*14*). The ilium shares with *Silesaurus* an enlarged brevis fossa and shelf, which is open laterally (Fig. 2M). The femoral head is triangular in proximal view (Fig. 2N) and bears a small notch ventrally (Fig. 2O); both of these characters are found in *Silesaurus*, *Eucoelophysis*, and *Pseudolagosuchus* (*15*).

A complete femur (GR 226) displays an autapomorphy of *Chindesaurus bryansmalli*: an elongate, subrectangular femoral head with a flat proximal surface (*15*) (Fig. 2P). One example of recovered coelophysoid material is a fused tibia, fibula, and astragalocalcaneum (GR 227) (Fig. 2Q); the fusion of these elements is present in coelophysoid and neoceratosaur theropods (*25*), and a specimen from the nearby Snyder Quarry also displays this character (*16*, *26*). An unambiguous coelophysoid synapomorphy present in GR 227 is a small anteromedial process on the distal fibula that overlaps the ascending process of the astragalus (Fig. 2Q) (*25*).

The HQ assemblage changes our picture of the early evolution of dinosaurian faunas in several ways. First, it documents that a mixed assemblage of true dinosaurs and their basal dinosauromorph relatives lived together along with other typical Triassic tetrapods in the Norian. Our investigations have found the same co-occurrences in several other Chinle Formation and Dockum Group localities in Arizona, New Mexico, and Texas (*15*, *17*). Therefore, the HQ assemblage cannot be explained by time-averaging of sedimentation or redeposition of earlier fossils [which is confirmed by our sedimentological and stratigraphic analysis of HQ (*17*)]. The HQ assemblage also reinforces the pattern that low-paleolatitude faunas of southern North America differ from the high-paleolatitude faunas of Europe, Greenland, South America, and South Africa in lacking basal sauropodomorph and rare ornithischian dinosaurs. This biogeographic disparity may reflect a real large-scale climatic or latitudinal effect (*27*), smaller-scale community or ecological differences, or merely facies-dependent sampling biases.

The HQ assemblage and others of western North America and Europe document the persistence of basal dinosauromorphs well into the Late Triassic. In Argentina, *Lagerpeton*, *Marasuchus*, and *Pseudolagosuchus* are confined to the Middle Triassic (Ladinian) Chañares Formation and never occur with dinosaurs (*1*, *3*). However, the Late Triassic (Carnian and Norian) forms differ from their Middle Triassic relatives, indicating a continued diversification of these groups. The age range of the HQ fossils and our assessment of other assemblages and their ages in North American museum collections imply that these dinosaurs and non-dinosaurian dinosauromorphs coexisted for at least 15 to 20 million years. There are too few radiometric dates of Late Triassic localities to permit a more precise time calibration, but it is nonetheless clear that the Late Triassic faunal replacement was not abrupt. Rather, it was protracted and possibly diachronous, as evidenced by paleolatitudinal faunal differences across Late Triassic Pangaea. The appearance of the first dinosaurs in the Ischigualasto assemblage (*1*), along with the late occurrences of basal dinosauromorphs from the HQ assemblage, extends the transition time from assemblages of dinosaur precursors to assemblages exclusively of dinosaurs and indicates that models of rapid competitive or fortuitous replacement are not correct.

References and Notes

1. R. R. Rogers, C. C. Swisher III, P. C. Sereno, C. A. Forster, A. M. Monetta, *Science* **260**, 794 (1993).
2. P. C. Sereno, *Annu. Rev. Earth Planet. Sci.* **25**, 435 (1997).
3. J. F. Bonaparte, *J. Vertebr. Paleontol.* **2**, 362 (1982).
4. N. Fraser, *Dawn of the Dinosaurs* (Indiana University Press, Bloomington, IN, 2006).
5. M. J. Benton, J. M. Clark, in *The Phylogeny and Classification of the Tetrapods*, M. J. Benton, Ed. (Clarendon Press, Oxford, 1988), vol. 1, chap. 8.
6. M. J. Benton, in *The Dinosauria*, D. B. Weishampel, P. Dodson, H. Osmólska, Eds. (Univ. of California Press, Berkeley, CA, ed. 2, 2004), pp. 7–19.
7. K. Padian, in *Dawn of the Age of Dinosaurs in the American Southwest*, S. G. Lucas, A. P. Hunt, Eds. (New Mexico Museum of Natural History, Albuquerque, NM, 1989), pp. 401–414.
8. P. E. Olsen et al., *Science* **296**, 1305 (2002).
9. M. J. Benton, *Q. Rev. Biol.* **58**, 29 (1983).
10. M. J. Benton, *Science* **260**, 769 (1993).
11. P. C. Sereno, A. B. Arcucci, *J. Vertebr. Paleontol.* **13**, 385 (1993).
12. P. C. Sereno, A. B. Arcucci, *J. Vertebr. Paleontol.* **14**, 53 (1994).
13. A. Arcucci, *Ameghiniana* **24**, 89 (1987).
14. J. Dzik, *J. Vertebr. Paleontol.* **23**, 556 (2003).
15. S. J. Nesbitt, R. B. Irmis, W. G. Parker, *J. Syst. Palaeontol.* **5**, 209 (2007).
16. R. B. Irmis, W. G. Parker, S. J. Nesbitt, J. Liu, *Hist. Biol.* **19**, 3 (2007).
17. See supporting material on *Science* Online.
18. S. G. Lucas, *Palaeogeogr. Palaeoclimatol. Palaeoecol.* **143**, 347 (1998).
19. W. G. Parker, *Mus. N. Ariz. Bull.* **62**, 46 (2006).
20. K. E. Zeigler, A. B. Heckert, S. G. Lucas, *N. M. Mus. Nat. Hist. Sci. Bull.* **24**, 1 (2003).
21. R. J. Litwin, A. Traverse, S. R. Ash, *Rev. Paleobot. Palynol.* **68**, 269 (1991).
22. A. B. Heckert, S. G. Lucas, R. M. Sullivan, A. P. Hunt, J. A. Spielmann, *N. M. Geol. Soc. Guidebook* **56**, 302 (2005).
23. F. E. Novas, *J. Vertebr. Paleontol.* **16**, 723 (1996).
24. W. G. Parker, R. B. Irmis, S. J. Nesbitt, J. W. Martz, L. S. Browne, *Proc. R. Soc. London Ser. B* **272**, 963 (2005).
25. R. S. Tykoski, T. Rowe, in *The Dinosauria*, D. B. Weishampel, P. Dodson, H. Osmólska, Eds. (Univ. of California Press, Berkeley, CA, ed. 2, 2004), pp. 47–70.
26. A. B. Heckert, K. E. Zeigler, S. G. Lucas, L. F. Rinehart, *N. M. Mus. Nat. Hist. Sci. Bull.* **24**, 127 (2003).
27. C. A. Sidor et al., *Nature* **434**, 886 (2005).
28. Fieldwork and research were funded by the National Geographic Society (grant no. 8014-06) (to K.P.), David Clark Inc., the Theodore Roosevelt Memorial Fund (to R.B.I.), the Jurassic Foundation (to S.J.N.), a Bryan Patterson Memorial Grant (to R.B.I.), an NSF Graduate Fellowship (to R.B.I. and S.J.N.), and the UC-Berkeley Department of Integrative Biology (to R.B.I.). We thank the staff and paleontology seminar participants at Ghost Ranch, A. Balanoff, G. Bever, M. Cohen, W. G. Parker, M. Brown, and M. Stocker for assistance with fieldwork. Ghost Ranch, the University of California Museum of Paleontology (UCMP), American Museum of Natural History, and Field Museum of Natural History all facilitated the preparation of specimens. This is UCMP contribution no. 1949.

Genetic Diversity in Honey Bee Colonies Enhances Productivity and Fitness

Heather R. Mattila* and Thomas D. Seeley

Honey bee queens mate with many males, creating numerous patrilines within colonies that are genetically distinct. The effects of genetic diversity on colony productivity and long-term fitness are unknown. We show that swarms from genetically diverse colonies (15 patrilines per colony) founded new colonies faster than swarms from genetically uniform colonies (1 patriline per colony). Accumulated differences in foraging rates, food storage, and population growth led to impressive boosts in the fitness (i.e., drone production and winter survival) of genetically diverse colonies. These results further our understanding of the origins of polyandry in honey bees and its benefits for colony performance.

One of the central challenges for understanding the evolution of sociality in bees, ants, and wasps (Order Hymenoptera) is the phenomenon of polyandry, or multiple mating with different males by queens (*1*). Selection for polyandry is unexpected because it generates intracolonial genetic diversity, which erodes high levels of relatedness among female offspring, thereby hindering the evolution of altruistic behavior toward kin. Nevertheless, polyandry occurs repeatedly in social insects (*2*) and to an extreme degree in every species of honey bee (genus *Apis*) (*3*). Several hypotheses have been proposed to explain how the benefits of a genetically diverse work force could outweigh the costs of reduced altruism resulting from low within-colony relatedness (*4*). A popular hypothesis suggests that genetically diverse work forces may operate more efficiently (*5*) and, consequently, produce colonies with a fitness advantage over those with uniform gene pools. However, there is conflicting evidence that genetically diverse colonies perform tasks better as a collective than genetically uniform colonies do (*6–10*) and, furthermore, enhanced productivity of the work force has never been linked explicitly with colony-level fitness gains.

A honey bee colony propagates its genes in two ways: by producing reproductive males (drones) and by producing swarms, when a reproductive female (queen) and several thousand infertile females (workers) leave and establish a new nest. Swarming is costly and perilous; with limited resources and labor, a swarm must construct new comb, build a food reserve, and begin rearing workers to replace the aging work force. In temperate climates, newly founded colonies must operate efficiently because there is limited time to acquire the resources to support these activities. Colony founding is so difficult that only 20% of swarms survive their first year (*11*); most do not gather adequate food to fuel the colony throughout the winter and die of starvation.

With the challenges of successful colony founding in mind, we conducted a long-term study to compare the development of genetically diverse and genetically uniform colonies after a swarming event. Each genetically diverse colony ($n = 12$) had a queen that was instrumentally inseminated with sperm from a unique set of fifteen drones and each genetically uniform colony ($n = 9$) had a queen inseminated with a similar volume of sperm from a single drone. Drones were selected at random from a pool of over 1000 individuals collected from 11 drone-source colonies. To replicate the experience of feral colonies, swarms were created by forcing a queen and 1 kg of her worker offspring (~7700 bees) to cluster in a screened cage for three days, where they were fed sucrose solution ad libitum to simulate preswarming engorgement on honey. Each swarm was subsequently relocated to a combless hive that was similar to that preferred by colonies naturally (*12*). Colonies were founded on 11 June 2006, during the region's swarming season (*13*). Once swarms were in their new nest sites, we documented colony development by measuring comb construction, brood rearing, foraging activity, food storage, population size, and weight gain at regular intervals (*14*). Intracolonial genetic diversity improves disease resistance (*15*), therefore colonies were medicated throughout the study so that we could examine the effects of multiple patrilines on productivity and fitness with minimal interference from the effects of enhanced resistance to disease.

There were notable differences in the progress of genetically diverse and genetically uniform colonies during the early stages of colony founding. Colonies with genetically diverse worker populations built ~30% more comb than colonies with genetically uniform populations before construction leveled off after 2 weeks [(Fig. 1); repeated measures ANOVA; $F(1,19) = 25.7$, $P < 0.0001$ (colony type); $F(19,342) = 126.9$, $P < 0.0001$ (time); $F(19,342) = 31.8$, $P < 0.0001$ (interaction)]. During the second week of colony founding, we compared foraging rates (number of workers returning to hive per minute for all workers and for only those carrying pollen) between different combinations of randomly paired colonies (one colony from each treatment, $n = 50$ pairs per day) throughout five consecutive mornings. Genetically diverse colonies maintained foraging levels that were 27 to 78% higher than genetically uniform colonies on three of five mornings [(Fig. 2); paired *t* tests with Bonferroni adjustment; 20 June: $t(49) = 4.1$, $P = 0.0001$ and $t(49) = 5.7$, $P < 0.0001$; 21 June: $t(49) = 3.2$, $P = 0.002$ and $t(49) = 5.5$, $P < 0.0001$; 22 June: $t(49) = 5.2$, $P < 0.0001$ and $t(49) = 5.8$, $P < 0.0001$]. Moreover, after 2 weeks in their new nest site, genetically diverse colonies stockpiled 39% more food than genetically uniform colonies [mean 1390 ± 120 versus 990 ± 145 cm^2 comb per colony filled with food; *t* test; $t(19) = 2.1$, $P = 0.045$]. This difference was not because some colonies lacked space (genetically diverse and uniform colonies had mean $61 \pm 1.1\%$ and $66 \pm 3.2\%$ of comb empty, respectively); instead, it was likely a consequence of increased foraging activity in genetically diverse colonies. The magnitude of these differences in growth during the initial 2 weeks after colony founding is impressive, considering that work forces in genetical-
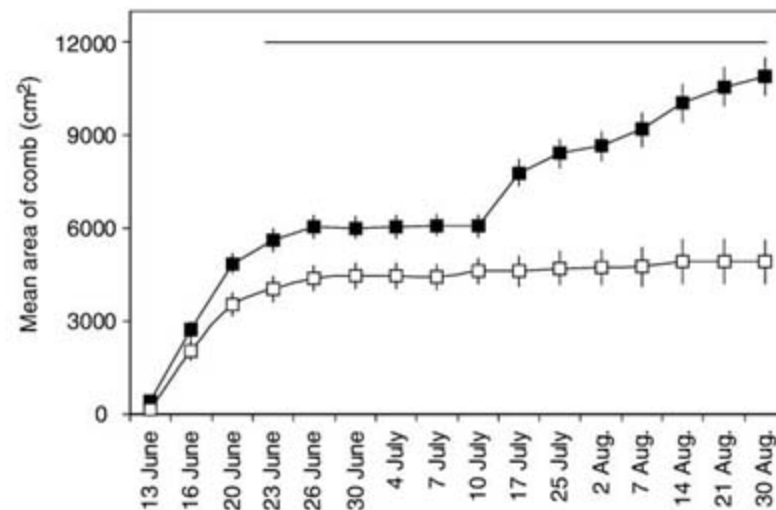
Fig. 1. Area of comb (means ± SEM) constructed by genetically diverse (■) and genetically uniform (□) colonies after occupying new nest sites on 11 June. Dates when groups differed significantly in comb area are indicated by a horizontal line (top).

Department of Neurobiology and Behavior, Cornell University, Ithaca, NY 14853, USA.

*To whom correspondence should be addressed. E-mail: hrm24@cornell.edu

ly diverse and genetically uniform colonies were still similarly sized 1 month after founding [9 July comparison of worker populations; t test; $t(19) = 1.6$, $P = 0.12$].

One month after "swarming," there was an isolated and brief period when abundant forage became available (~9 to 21 July). At the start of this honey flow, genetically diverse colonies were already twice as heavy as genetically uniform colonies [(Fig. 3); repeated measures ANOVA; $F(1,19) = 39.9$, $P < 0.0001$ (colony type); $F(86,1373) = 237.0$, $P < 0.0001$ (time); $F(82,1373) = 17.4$, $P < 0.0001$ (interaction)]. Throughout the flow, genetically diverse colo-

nies gained an average of 0.3 ± 0.05 kg/day per colony and increased their higher initial colony weight by 305%, whereas genetically uniform colonies gained only 0.09 ± 0.01 kg/day per colony and increased their lower colony weight by only 163% before resources waned (Fig. 3; comparison of mean daily weight gain during flow; paired t test; $t(11) = 3.9$, $P = 0.0007$). The influx of food sparked a resurgence in comb construction in genetically diverse colonies, however, comb area remained unchanged in genetically uniform colonies (Fig. 1).

Production of new workers in genetically diverse colonies surpassed that of genetically uniform colonies within the first month of colony development [(Fig. 4); repeated measures ANOVA; $F(1,19) = 63.5$, $P < 0.0001$ (colony type); $F(11,174) = 37.4$, $P < 0.0001$ (time); $F(11,174) = 16.0$, $P < 0.0001$ (interaction)]. Brood rearing by workers increased continually in genetically diverse colonies until the end of August, whereas genetically uniform colonies produced consistently low numbers of workers over the same period (Fig. 4). Consequently, genetically diverse colonies had far larger worker populations by the end of August [mean $26,700 \pm 1830$ versus 5300 ± 2400 individuals per colony; t test; $t(17) = 7.1$, $P < 0.0001$]. These differences in post-founding development likely resulted from a combination of an enhanced capacity of multiple-patriline colonies to construct nest materials, to rear brood, and to acquire food (given comparable worker populations) and the momentum that this lent to the pace of colony growth, a pace that single-patriline colonies were not able to match despite having similar opportunities after a "swarming" event.

Colony size is closely tied to fitness; larger colonies produce more drones, have higher winter survival, and issue more swarms (16–18). Here, intracolonial genetic diversity resulted in considerably more populous and resource-rich colonies, which in turn affected their fitness. Genetically diverse colonies reared significantly more drones than genetically uniform colonies before brood rearing declined in September: mean 1910 ± 384 versus 240 ± 109 drones per colony [Fig. 4; t test; $t(19) = 3.7$, $P = 0.002$]. The larger, genetically diverse colonies also collected and stored more food than genetically uniform colonies and all survived a late-August cold period that starved and killed 50% of genetically uniform colonies (Fig. 3). The remaining genetically uniform colonies exhausted their food reserve and died by mid-December, whereas 25% of genetically diverse colonies survived to May (Fig. 3).

We have demonstrated that the productivity and fitness of honey bee colonies is enhanced by intracolonial genetic diversity. Our data confirm and extend trends toward increased growth reported in short-term studies of polyandrous colonies with low (≤6) numbers of patrilines (6, 7). The benefits of a genetically diverse worker population are especially evident during colony founding when survival depends critically on

Fig. 2. Foraging rates (means ± SEM) of genetically diverse (■: all returning workers; ●: only workers carrying pollen) and genetically uniform (□: all returning workers; ○: only workers carrying pollen) colonies. Asterisks mark days when daily foraging rates differed significantly between groups.
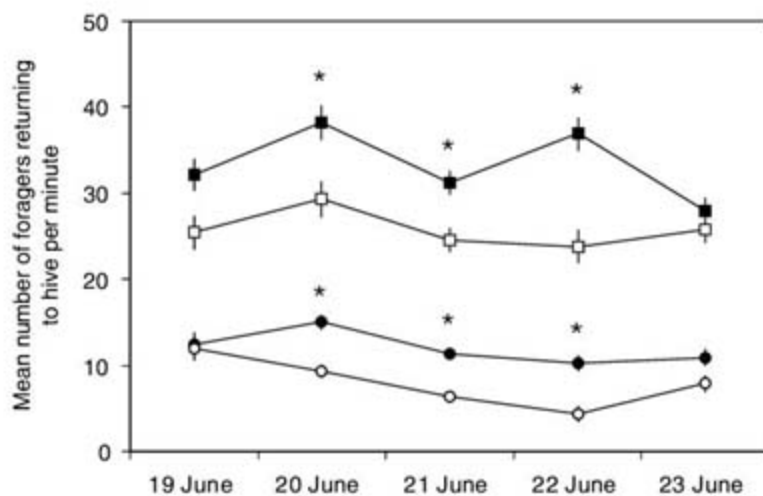
Fig. 3. Weight (means ± SEM) of genetically diverse (solid line) ($n = 12$) and genetically uniform (dashed line) ($n = 9$) colonies after occupying new nest sites on 11 June. Dates when groups differed significantly in weight are indicated by a horizontal line (top). Each arrow marks the death of a colony.
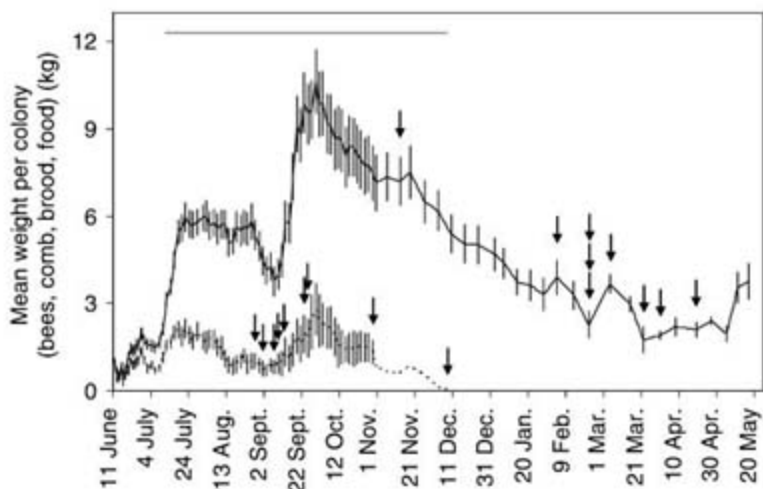
Fig. 4. Number (means ±SEM) of workers (solid lines) and drones (dashed lines) produced by genetically diverse (workers: ■; drones: ●) and genetically uniform (workers: □; drones: ○) colonies. A census of individuals in capped-pupae cells was made on each date; pupae counted at this time emerged as adults during the interval between that census and the next (14). Horizontal lines (workers: single line; drones: double line) mark periods when brood rearing differed significantly between groups.
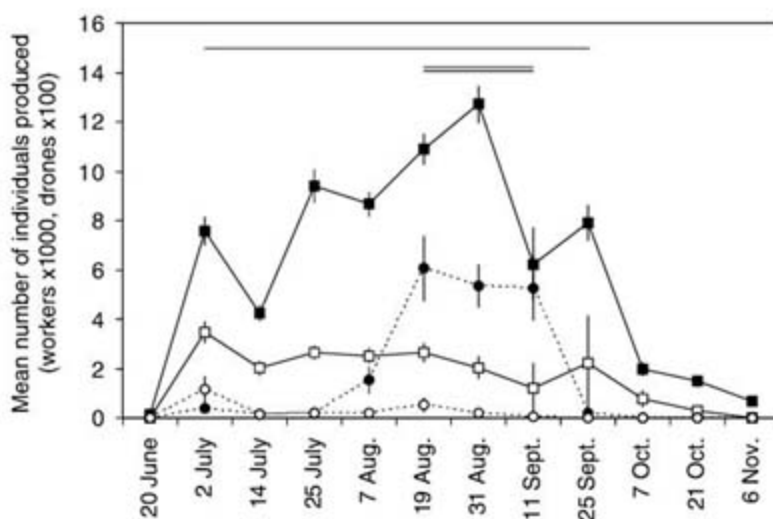
successfully accomplishing a variety of pressing tasks. Given similar numbers of workers, environmental conditions, and need, newly founded colonies built comb faster, foraged more, and stored greater amounts of food when their work forces were comprised of many genetically distinct patrilines. Initial differences in labor productivity amplified growth rates over time and led to dramatic fitness gains for genetically diverse colonies (i.e., production of drones, colony growth, and survival). Thus, we expect intense selection favoring polyandry because intracolonial genetic diversity improves the productivity of the work force and increases colony fitness during the risky process of colony founding.

Higher collective productivity of genetically diverse colonies may be rooted in a broader or more sensitive response from worker populations to changing conditions. The probability that a worker will engage in a task has been linked repeatedly to genotype [e.g. (5, 8, 19)]. Consequently, colonies with multiple patrilines would be expected to have worker populations that are able to respond to a broad range of task-specific stimuli and, as a group, should be able to provide appropriate, incremental responses to changes in these stimuli (5). The observation that intracolonial genetic diversity improved productivity in colonies is consistent with predictions made by models of division of labor that rely on genotypic differences in response thresholds among workers (20). Nevertheless, the extent to which genetically uniform colonies lagged behind genetically diverse colonies in the early stages of colony development was surprising, considering that colonies initially lacked comb and food reserves, and presumably, stimuli reflecting these needs could not have been greater. Actual response thresholds of workers are not well documented (20), and it is difficult to know how they are related to the productivity of individuals and the colony as a whole. For example, workers may vary genetically in the rate at which they perform a task once their response threshold is reached or they may not be "good" at tasks for which they have high thresholds (i.e., they lack physiological apparatuses or experience). Alternatively, thresholds may be so high for some tasks that behaviors are effectively missing from a worker's repertoire, thus multiple patrilines would contribute to the diversity of labor in a colony, rather than division of labor among workers.

A key advantage of intracolonial genetic diversity was revealed during infrequent periods when food resources were plentiful (~33 days during our study). Genetically diverse colonies gained weight at rates that far exceeded those of genetically uniform colonies (Fig. 3), whose sluggish foraging rates suggest that intracolonial genetic diversity enhances the discovery and exploitation of food resources by work forces, especially during periods when resources become suddenly and abundantly available. Intracolonial genetic diversity would result in more rapid mobilization of forager work forces if, by

broadening the range of response thresholds in colonies, it increased the probability of having sufficient workers functioning as foragers and/or broadened the range of conditions over which foragers inspected, scouted, recruited to or were recruited/reactivated to food resources. Selection for polyandry would be strong if the genetic diversity that it bestows on colonies enhances the sophisticated mechanisms of honey bees for recruiting nest mates to food. Because successful colony founding by honey bees depends so heavily on rallying foragers and the swift accumulation of resources, this could explain, in concert with other benefits unrelated to worker productivity (15, 21), the widespread occurrence of extreme polyandry in all honey bee species.

References and Notes

1. R. H. Crozier, P. Pamilo, *Evolution of Social Insect Colonies* (Oxford Univ. Press, Oxford, 1996).
2. J. Strassmann, *Insectes Soc.* **48**, 1 (2001).
3. D. R. Tarpy, D. I. Nielsen, *Ann. Entomol. Soc. Am.* **95**, 513 (2002).
4. R. H. Crozier, E. J. Fjerdingstad, *Ann. Zool. Fennici* **38**, 267 (2001).
5. G. E. Robinson, R. E. Page Jr., in *Genetics of Social Evolution*, M. D. Breed, R. E. Page Jr., Eds. (Westview Press, Boulder, CO, 1989), pp. 61–80.
6. B. P. Oldroyd, T. E. Rinderer, J. R. Harbo, S. M. Buco, *Ann. Entomol. Soc. Am.* **85**, 335 (1992).
7. S. Fuchs, V. Schade, *Apidologie* **25**, 155 (1994).
8. J. C. Jones, M. R. Myerscough, S. Graham, B. P. Oldroyd, *Science* **305**, 402 (2004).
9. R. E. Page Jr., G. E. Robinson, M. K. Fondrk, M. E. Nasr, *Behav. Ecol. Sociobiol.* **36**, 387 (1995).
10. P. Neumann, R. F. A. Moritz, *Insectes Soc.* **47**, 271 (2000).
11. T. D. Seeley, *Oecologia* **32**, 109 (1978).
12. T. D. Seeley, R. A. Morse, *Insectes Soc.* **25**, 323 (1978).
13. R. D. Fell et al., *J. Apic. Res.* **16**, 170 (1977).
14. Materials, methods, and statistical analyses are available on *Science* Online.
15. T. D. Seeley, D. R. Tarpy, *Proc. R. Soc. Lond. B. Biol. Sci.* **274**, 67 (2007).
16. J. B. Free, P. A. Racey, *Entomol. Exp. Appl.* **11**, 241 (1968).
17. T. D. Seeley, P. K. Visscher, *Ecol. Entomol.* **10**, 81 (1985).
18. P. C. Lee, M. L. Winston, *Ecol. Entomol.* **12**, 187 (1987).
19. G. Arnold, B. Quenet, C. Papin, C. Masson, W. H. Kirchner, *Ethology* **108**, 751 (2002).
20. S. N. Beshers, J. H. Fewell, *Annu. Rev. Entomol.* **46**, 413 (2001).
21. D. R. Tarpy, R. E. Page Jr., *Behav. Ecol. Sociobiol.* **52**, 143 (2002).
22. We thank K. Burke for field assistance, T. and S. Glenn for rearing queens, and P. Barclay, M. Kirkland, and two anonymous reviewers for comments on the manuscript. Funded by a Postdoctoral Fellowship (H.R.M.) from Natural Sciences and Engineering Research Council (Canada) and a grant from the National Research Initiative of the U.S. Department of Agriculture Cooperative State Research, Education, and Extension Service (T.D.S.) (no. 2003-35302-13387).

PDZ Domain Binding Selectivity Is Optimized Across the Mouse Proteome

Michael A. Stiffler,[1]* Jiunn R. Chen,[2]* Viara P. Grantcharova,[1]† Ying Lei,[1] Daniel Fuchs,[1] John E. Allen,[1] Lioudmila A. Zaslavskaia,[1]‡ Gavin MacBeath[1]§

PDZ domains have long been thought to cluster into discrete functional classes defined by their peptide-binding preferences. We used protein microarrays and quantitative fluorescence polarization to characterize the binding selectivity of 157 mouse PDZ domains with respect to 217 genome-encoded peptides. We then trained a multidomain selectivity model to predict PDZ domain–peptide interactions across the mouse proteome with an accuracy that exceeds many large-scale, experimental investigations of protein-protein interactions. Contrary to the current paradigm, PDZ domains do not fall into discrete classes; instead, they are evenly distributed throughout selectivity space, which suggests that they have been optimized across the proteome to minimize cross-reactivity. We predict that focusing on families of interaction domains, which facilitates the integration of experimentation and modeling, will play an increasingly important role in future investigations of protein function.

Eukaryotic proteins are modular by nature, comprising both interaction and catalytic domains (1, 2). One of the most frequently encountered interaction domains, the PDZ domain, mediates protein-protein interactions by binding to the C termini of its target proteins (3–6). Previous studies of peptide-binding selectivity have placed PDZ domains into discrete functional categories: Class I domains recognize the consensus sequence Ser/Thr-X-ψ-COOH, where X is any amino acid and ψ is hydrophobic; class II domains prefer ψ-X-ψ-COOH; and class III

domains prefer Asp/Glu-X-ψ-COOH (5, 7). More recent information has suggested that these designations are too restrictive and so additional classes have been proposed (8, 9). The idea that domains fall into discrete categories, however, raises questions about functional overlap: Domains within the same class are more likely to cross-react with each other's ligands. To resolve this issue, we characterized and modeled PDZ domain selectivity on a genome-wide scale.

We began by cloning, expressing, and purifying most of the known PDZ domains encoded in

the mouse genome (*10–12*) (table S1). Soluble protein of the correct molecular weight was obtained for 157 PDZ domains (fig. S1). Whereas previous efforts to characterize the selectivity of PDZ domains have relied on collections of peptides with randomized sequences (*7, 9, 13, 14*), our goal was to focus on genome-encoded sequences. We therefore synthesized and purified fluorescently labeled peptides derived from the 10 C-terminal residues of mouse proteins. In total, we synthesized 217 such peptides, which we termed our "training set" (table S2) (*15*). Although our training set is not guaranteed to contain ligands for every PDZ domain, it permitted us to obtain a broad view of binding selectivity.

To investigate biophysical interactions between the 157 well-behaved PDZ domains and each of the 217 fluorescent peptides, we devised a strategy that combines the throughput of protein microarrays and the fidelity of fluorescence polarization (FP) with predictive modeling (Fig. 1A). Microarrays of PDZ domains were prepared within individual wells of microtiter plates and probed, in triplicate, with a 1 μM solution of each peptide (Fig. 1B) (*16*). Interactions with a mean fluorescence that was at least three times the median fluorescence on the array were scored as "array positives" (*17*). This process yielded 1301 putative interactions involving 127 PDZ domains. Little can be concluded about the 30 domains for which no array positives were found. For domains that bound at least one peptide, however, the inability to bind other peptides provides important information: These noninteractions were scored as "array negatives."

As with any high-throughput method, there are error rates associated with identifying both positives and negatives. To eliminate array false positives, we retested and quantified every array positive with a solution-phase FP assay (Fig. 1C), which served as our "gold standard" (*17*). By measuring FP at 12 concentrations of PDZ domain, we determined the dissociation constant (K_d) for each of the 1301 array positives (table S3). Interactions that showed saturation binding (*18*) with a $K_d < 100$ μM were considered "positives"; those that did not were considered "negatives." On the basis of these criteria, 85 PDZ domains bound at least one peptide in the training set. Although our K_d cutoff was high, ~90% of the interactions had a $K_d < 50$ μM, and ~60% of interactions had a $K_d < 20$ μM (fig. S2). In addition, FP assays revealed the false-

negative rate of the protein microarray assay to be 6.6% (*19*).

To extract from our data the rules that govern the peptide-binding selectivity of PDZ domains, we built a model that predicts the PDZ domains to which a peptide will bind, given its sequence. Peptide recognition is often modeled with a position-specific scoring matrix (PSSM), $\Theta =$

$\{\theta_{p,q}\}$, where $\theta_{p,q}$ is defined as the probability of observing amino acid q at position p in the subset of peptides that bind to that domain (*20*). This scoring approach is useful for predicting peptides that bind to a single domain, but it is not ideally suited to our purpose for two reasons. First, our peptide sequences are derived from the genome and thus are not random. Second, our goal is to
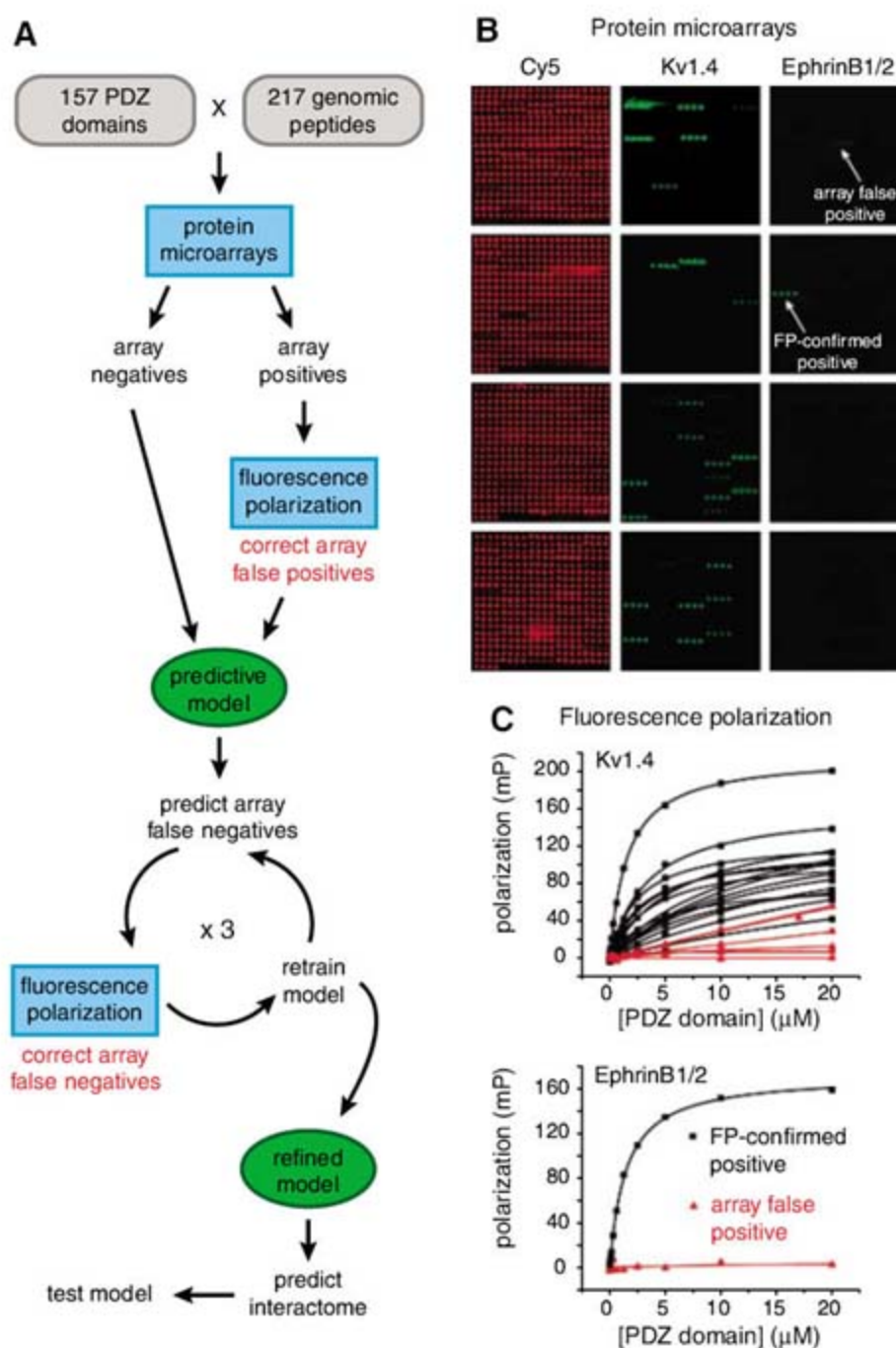
Fig. 1. (**A**) Strategy for constructing a multidomain selectivity model for mouse PDZ domains. Protein microarrays were used to test all possible interactions between 157 mouse PDZ domains and 217 genome-encoded peptides. Array positives were retested and quantified by FP, thereby correcting array false positives. The resulting data were used to train a predictive model of PDZ domain selectivity. The model highlighted putative array false negatives, which were tested by FP, and the corrected data were used to retrain the model. After three cycles of prediction, testing, and retraining, the refined model was used to predict PDZ domain–protein interactions across the mouse proteome. (**B**) Representative images of protein microarrays, probed with fluorescently labeled peptides. PDZ domains were spotted in quadruplicate in individual wells of 96-well microtiter plates. (Four wells were required to accommodate all of the domains.) The red images (Cy5) show the location of the PDZ domain spots. The green images show arrays probed with a promiscuous peptide derived from Kv1.4 (left) and a selective peptide derived from ephrin B1/2 (right). (**C**) FP titration curves obtained for the array positives identified in (**B**).

[1]Department of Chemistry and Chemical Biology, Harvard University, 12 Oxford Street, Cambridge, MA 02138, USA. [2]Department of Molecular and Cellular Biology, Harvard University, 12 Oxford Street, Cambridge, MA 02138, USA.

*These authors contributed equally to this work.
†Present address: Merrimack Pharmaceuticals, 1 Kendall Square, Building 700, Cambridge, MA 02139, USA.
‡Present address: Tepnel Lifecodes Corporation, 550 West Avenue, Stamford, CT 06902, USA.
§To whom correspondence should be addressed. E-mail: macbeath@chemistry.harvard.edu

learn how one domain differs from another, (i.e., how selectivity is achieved). This information is not captured in a traditional PSSM because peptide residues that contribute strongly to binding affinity, such as the C-terminal residue, dominate the model, even if they are not important in distinguishing one domain from another.

To construct a single model that includes many PDZ domains, we developed a variation of a PSSM in which a peptide is predicted to bind to PDZ domain i if

$$\varphi_i = \sum_{p,q} A_{p,q} \theta_{i,p,q} > \tau_i \qquad (1)$$

where φ is a binding score, A is an indicator of peptide sequence, ($A_{p,q} = 1$ if the amino acid at position p of the peptide is q and $A_{p,q} = 0$ otherwise), and τ_i is a scoring threshold, specific to each domain. To ensure that our model focuses on PDZ domain selectivity, we constrained $\sum_i \theta_{i,p,q}$ to be 0 for every position p and every amino acid q. Thus, $\theta_{i,p,q}$ is positive if PDZ domain i prefers amino acid q at position p more than the other PDZ domains, negative if it prefers it less, and 0 if it has no bias relative to the other domains. To tailor the threshold appropriately for each domain, we defined τ_i to be the mth percentile of φ_i's for all of the peptides in our training set that bound to PDZ domain i. Empirically, we found that setting $m = 5$ provides a good balance between false-positive predictions and false-negative predictions. Because this model is designed to highlight selectivity across many members of a domain family, we refer to it as a multidomain selectivity model (MDSM).

Our model takes into account the five C-terminal residues of the peptide ligand: positions –4, –3, –2, –1, and 0. Even with 217 data points for each domain, there is insufficient information to train such a high-dimensional model. To avoid overfitting, we implemented a smoothing technique. If two PDZ domains bind a similar subset of peptides, it is reasonable to expect that their $\theta_{p,q}$'s are also similar, unless the data suggest otherwise. Likewise, if two amino acids have similar physicochemical properties, it is reasonable to expect that their $\theta_{i,p}$'s will be similar. Smoothing requires a quantitative measure of pairwise distance. With PDZ domains, distance was defined as the Hamming distance of their binding vectors across the training-set peptides. With amino acids, we relied on previously reported "z scales" to capture their physicochemical properties, where z_1 is considered a descriptor of hydrophilicity, z_2 is a descriptor of molecular weight and surface area, and z_3 is a descriptor of polarity and charge (21). We reduced the equivalent degrees of freedom in our model by smoothing over PDZ domains and over amino acids with a Gaussian kernel during regression (22).

We were able to model 74 of the 85 PDZ domains, which suggests that the majority of

PDZ domains (87%) conform to the assumption that the contribution of each peptide position to selective binding is additive. Having trained the MDSM, we used it to predict false negatives in our microarray data (Fig. 1A). Predicted array false negatives were assayed experimentally by quantitative FP, and the MDSM was retrained using the updated information. This cycle of prediction, experimentation, and retraining was performed three times. In total, we tested 303 predicted array false negatives, of which 133 (44%) were found to be positives, yielding a high-quality, quantitative interaction matrix for mouse PDZ domains (Fig. 2A and table S3). Overall, we found that the average binding affinity of the array false negatives was slightly lower than that of the array true positives. The distributions of binding affinities, however, overlapped considerably (fig. S3).

The refined model performs well on the updated data set, with a true-positive rate of 96% (it correctly identifies 515 of 536 FP-confirmed positives) and a false-positive rate of 15% (it predicts an interaction for 186 of 1229 FP-confirmed negatives) when m is set to 5 (Fig. 2B). The parameters of the MDSM are depicted as a heat map in Fig. 2C and are provided in table S4. As anticipated, position 0 does not contribute strongly to discriminative binding, but the four other positions contribute substantially (Fig. 2C).

To extract biophysical modules out of the resulting interaction network, we designed a modified version of the Markov cluster algorithm (23), tailored to the special situation of a bipartite network (22). The algorithm simulates a random walk on the graph and is based on the observation that random walks tend to be confined within "tight clusters" of nodes. The algorithm identified four tight clusters of PDZ domains and their binding partners (Fig. 2D). For example, the claudins (tight junction proteins) cluster with ZO-1 and ZO-2, whereas the N-methyl-D-aspartic acid (NMDA) receptor subunit isoforms NMDAR2A and NMDAR2B, as well as several voltage-gated potassium channels, cluster with PSD-95, SAP-97, Magi-1, Magi-2, and Magi-3.

Encouraged by the close agreement of our model with the training-set data, we used the MDSM to predict to which proteins in the mouse proteome each of the 74 PDZ domains are able to bind. In total, we surveyed 31,302 peptide sequences corresponding to the C termini of all translated open reading frames (24). We have previously shown that our domain-based in vitro strategy faithfully captures ~85% of the previously reported interactions involving PDZ domains (17). We therefore provide these predictions (18,149 PDZ domain–peptide interactions) as supplemental information (table S5) to help guide future biological investigations (25). We note, however, that not all interactions that are observed in vitro necessarily occur in vivo.

To further assess the accuracy of our model, we selected a "test set" of 48 proteins from the mouse proteome that were predicted to be highly

connected to PDZ domains (table S6). We synthesized fluorescently labeled peptides corresponding to their C termini and assayed them for binding to the 74 PDZ domains in our MDSM with the use of a single-point FP assay (26). These peptides were not included in the training set and so offer a stringent test of our model. In total, 493 new interactions and 3059 noninteractions were identified. Our model predicted 48% (237) of the new interactions and 88% (2680) of the noninteractions when m was set to 5 (Fig. 2E), with a true-positive/false-positive (TP/FP) ratio of 0.63 (237/379). The TP/FP ratio of our model predictions exceeds by a factor of more than 20 the TP/FP ratio of a Bayesian model that integrates information from two large-scale yeast two-hybrid experiments and two large-scale in vivo pull-down experiments in *Saccharomyces cerevisiae*, while maintaining the same true-positive rate (27). We attribute the accuracy of our MDSM to its focus on a related family of domains, rather than on a broad collection of proteins with disparate properties. This argues strongly for a systematic but segmented effort to uncover protein-protein interactions by focusing on families of interaction modules.

We also observed a positive correlation between the model output (φ_i) and binding affinity (fig. S5). We found that smoothing over both PDZ domains and amino acids substantially contributes to the accuracy of the model, boosting the TP/FP ratio by 44% over the model constructed without smoothing, while maintaining the true-positive rate essentially the same (Fig. 2E). Most of the effect was derived from smoothing over PDZ domains, but smoothing over amino acids was also beneficial. To exclude the possibility that the model performance was due to chance correlation, we performed a Y-randomization test (28) in which the interaction data were shuffled. The resulting receiver operating characteristic (ROC) curve was indistinguishable from the no-discrimination line (fig. S6), indicating the effectiveness of our training and test sets.

Having established that the model accurately captures information about the binding selectivity of PDZ domains, we asked which physicochemical properties each domain uses at each position to define its selectivity. For example, if we look at the amino acid preferences of Dlgh3 (1/1) at position –4, we find that the 20 θ's are positively correlated with z_1 but are not correlated with z_2 or z_3 (Fig. 3A). In contrast, z_2, but not z_1 or z_3, correlates with discriminative binding at position –4 for Magi-1 (4/6) (Fig. 3B), whereas z_3, but not z_1 or z_2, correlates with discriminative binding at position –4 for MUPP1 (10/13) (Fig. 3C). These three examples are extremes; in general, PDZ domains rely on all three z scales for discriminative binding. To capture this information for all PDZ domains at all positions, we constructed a correlation matrix between the model parameters and the first three z scales of amino acids (Fig. 3D). Because the contribution to discriminative binding at position 0 is weak, we omitted this

position from our analysis to avoid biasing our results with artificially amplified effects.

To understand the organization of peptide-binding selectivity on a global level, we deconvoluted the correlation matrix through singular-value decomposition and found that the distribution of

PDZ domain binding preferences can be largely explained by three principal axes. The space defined by these axes can be thought of as "PDZ domain selectivity space." Each of the first two axes explains ~30% of the variance in the correlation matrix, whereas the third axis ex-

plains ~14% (Fig. 3E). The first axis (Fig. 3F) can distinguish canonical class I PDZ domains, which are preferred by peptides with a small, hydrophilic residue at position –2, from canonical class II domains, which are preferred by peptides with a large, hydrophobic residue at posi-
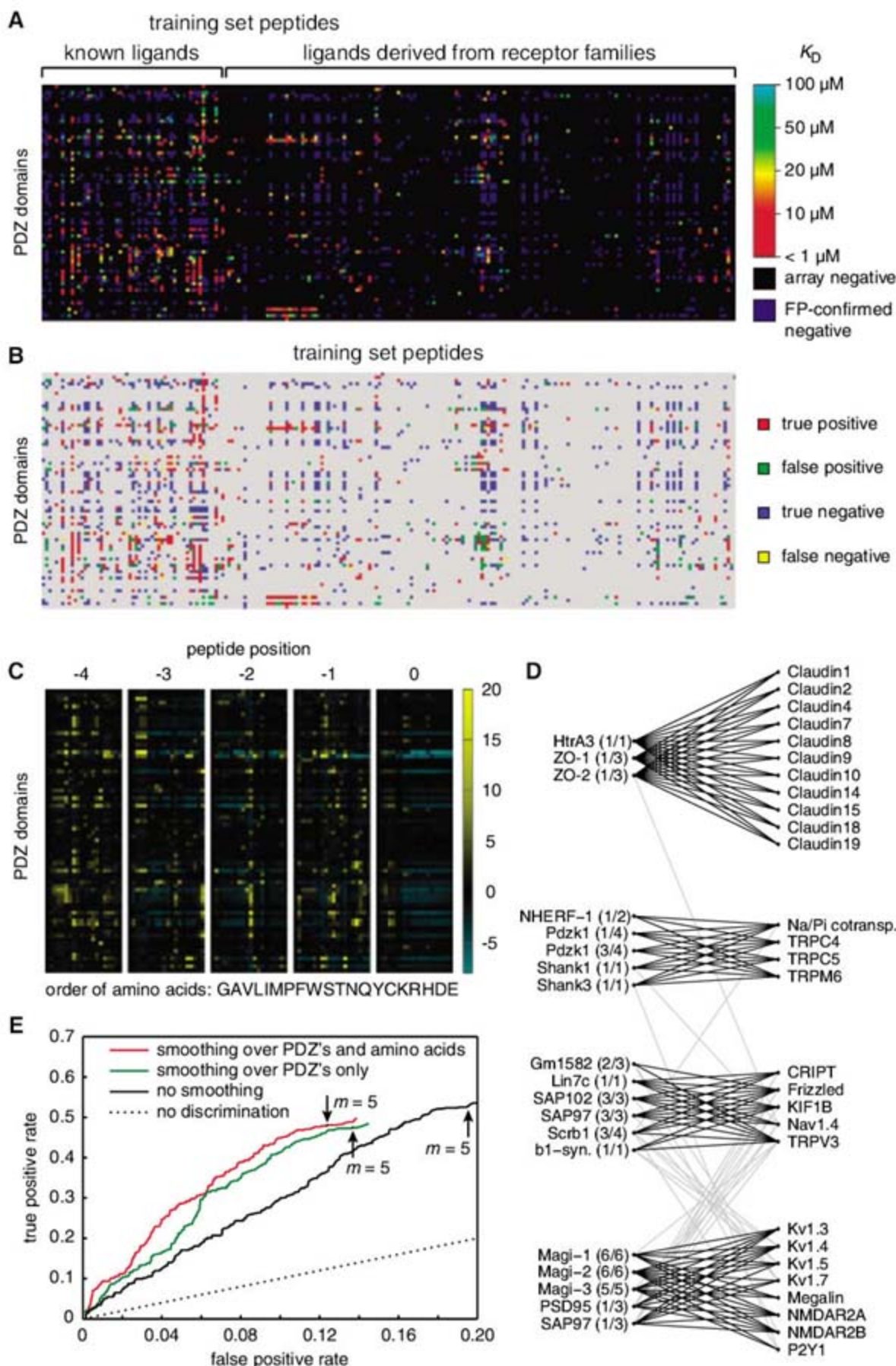
Fig. 2. (A) Graphical view of the training-set data. K_d's of FP-confirmed positives are represented by colors, ranging from high affinity (red) to low affinity (light blue). Array negatives are shown in black, and FP-confirmed negatives are shown in dark blue. Numerical values are provided in table S3. **(B)** Performance of the MDSM on the training set, with m set to 5. True positives are shown in red, false positives in green, true negatives in blue, and false negatives in yellow. **(C)** Graphical representation of the MDSM parameters, $\theta_{i,p,q}$. Positive contributions to discriminative binding are graded from black to yellow, and negative contributions are graded from black to light blue. Numerical values are provided in table S4. Single-letter abbreviations for the amino acid residues are as follows: A, Ala; C, Cys; D, Asp; E, Glu; F, Phe; G, Gly; H, His; I, Ile; K, Lys; L, Leu; M, Met; N, Asn; P, Pro; Q, Gln; R, Arg; S, Ser; T, Thr; V, Val; W, Trp; and Y, Tyr. **(D)** Tight clusters embedded in the bipartite interaction network between the 74 PDZ domains and the 217 training-set peptides. **(E)** ROC curves for three versions of the MDSM, obtained with the test set of 48 peptides. The best performance was obtained after smoothing over both PDZ domains and amino acids. The performance of each version of the MDSM with m set to 5 is indicated with an arrow.

tion –2. Thus, the class I domains PSD-95 (1/3) and Shank3 (1/1) lie at the negative end of the first principal axis (Fig. 3G), whereas the class II domains PDZ-RGS3 (1/1) and Grip1 (6/7) lie at the positive end. Erbin (1/1), which has been shown to bind both class I and class II peptides (28–31), lies between the two extremes. The second and third principal axes (Fig. 3F) add further resolution. In particular, the third axis distinguishes class III domains, such as neuronal nitric oxide synthase (nNOS) (1/1) (preferred by peptides with a negatively charged residue at position –2), from the other PDZ domains. The closer a PDZ domain lies to the positive end of

the third principal axis, the more it falls into the class III designation.

There are, however, two important differences between the standard view of PDZ domain selectivity and the view that emerges from our broad investigation. First, positions –4, –3, –2, and –1 all contribute substantially to the definition of our three principal axes (Fig. 3F). This implies that selectivity is derived from interactions throughout the binding pocket, whereas peptide library screens have shown that affinity is derived largely from the recognition of amino acids at positions –2 and 0 (7). Second, and more importantly, PDZ domains do not fall into

discrete classes but instead lie on a continuum. Indeed, the canonical classes lie only in select portions of this continuum (i.e., at the extremes of the first and third principal axes). Moreover, the PDZ domains represented in our model are evenly distributed throughout selectivity space (Fig. 3G). Zarrinpar et al. previously showed that the 23 Src homology 3 domains in S. cerevisiae are optimized to avoid cross-reactivity with the mitogen-activated protein kinase signaling protein Pbs2 (32). Here, we find on a much broader scale that a similar principle is in effect among mouse PDZ domains and their ligands. Although the selectivity of protein-protein interactions
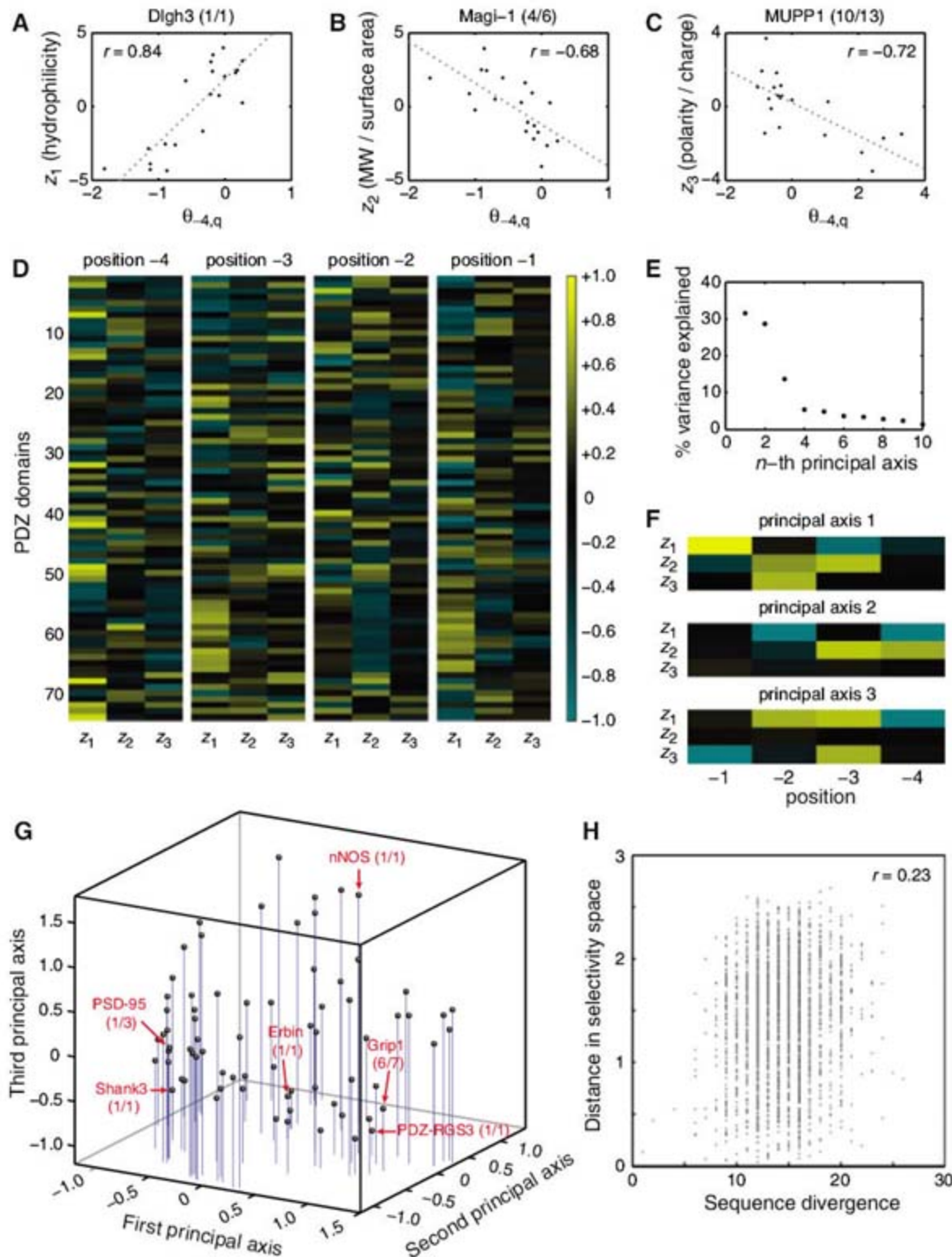
Fig. 3. (**A** to **C**) Correlations between z scales and model parameters at position –4 for three PDZ domains. (**A**) z_1 positively correlates with $\theta_{-4,q}$ for Dlgh3 (1/1). (**B**) z_2 negatively correlates with $\theta_{-4,q}$ for Magi-1 (4/6). (**C**) z_3 negatively correlates with $\theta_{-4,q}$ for MUPP1 (10/13). (**D**) Correlation matrix between the model parameters for all 74 PDZ domains at positions –4, –3, –2, and –1 and the first three z scales of the amino acids. (**E**) Percentage of variance in the correlation matrix that is explained by the 12 principal axes identified through singular-value decomposition. (**F**) Graphical representation of the first three principal axes, used to define PDZ domain selectivity space. (**G**) Distribution of the 74 PDZ domains in selectivity space. Selected PDZ domains are shown, representing class I domains [PSD-95 (1/3) and Shank3 (1/1)], class II domains [Grip1 (6/7) and PDZ-RGS3 (1/1)], and class III domains [nNOS (1/1)]. Erbin (1/1), which has been described as a dual-specificity domain, lies between the class I and class II domains. (**H**) Correlation between pairwise sequence divergence of PDZ domains and their pairwise distances in selectivity space. Sequence divergence was obtained from pairwise alignments performed with Vector NTI version 8 (InforMax, Invitrogen Life Science Software, Frederick, Maryland), using the blosum62mt2 matrix. Pairwise distances in selectivity space are Euclidean distances obtained from the three-dimensional plot in (G).

could, in a multicellular organism, be controlled at the level of gene coexpression and protein colocalization, our results indicate that the intrinsic selectivity of PDZ domains is tuned across the mouse proteome to minimize cross-reactivity.

Finally, we observed only a weak correlation (correlation coefficient $r = 0.23$) between the pairwise sequence divergence of PDZ domains and their distances in selectivity space (Fig. 3H). Similarity at the overall sequence level is thus a poor predictor of PDZ domain function. This low correlation suggests that most of the sequence variation among PDZ domains is neutral with respect to peptide-binding selectivity and that only a subset of residues—presumably in the binding pocket of the PDZ domain—is responsible for the distribution of PDZ domains in selectivity space.

References and Notes

1. T. Pawson, Nature 373, 573 (1995).
2. T. Pawson, P. Nash, Science 300, 445 (2003).
3. E. Kim, M. Niethammer, A. Rothschild, Y. N. Jan, M. Sheng, Nature 378, 85 (1995).
4. H. C. Kornau, L. T. Schenker, M. B. Kennedy, P. H. Seeburg, Science 269, 1737 (1995).
5. C. Nourry, S. G. N. Grant, J.-P. Borg, Sci. STKE 2003, re7 (2003).
6. B. Z. Harris, F. W. Lau, N. Fujii, R. K. Guy, W. A. Lim, Biochemistry 42, 2797 (2003).
7. Z. Songyang et al., Science 275, 73 (1997).
8. I. Bezprozvanny, A. Maximov, FEBS Lett. 509, 457 (2001).
9. E. Song et al., Mol. Cell. Proteomics 5, 1368 (2006).
10. I. Letunic et al., Nucleic Acids Res. 34, D257 (2006).
11. J. Schultz, F. Milpetz, P. Bork, C. P. Ponting, Proc. Natl. Acad. Sci. U.S.A. 95, 5857 (1998).
12. The "genomic" mode of the Simple Modular Architecture Research Tool (SMART) database (10, 11) currently lists 240 PDZ domains identified from the mouse genome sequence. We obtained sequence-verified clones for 203 of them. In addition, we cloned 18 PDZ domains that are listed only in the "normal" mode of the SMART database.

Each domain was purified in a single step from a large-scale bacterial culture, its purity was assessed by SDS–polyacrylamide gel electrophoresis (fig. S1), and its aggregation state was assessed by analytical gel filtration (table S1). Soluble protein of the correct molecular weight was obtained for 157 PDZ domains. Of these, 151 were monomeric, 4 were dimeric, and 2 were a mixture of monomers and dimers (table S1).

13. G. Fuh et al., J. Biol. Chem. 275, 21486 (2000).
14. Y. Zhang et al., J. Biol. Chem. 281, 22299 (2006).
15. We derived 57 of the training-set peptides from proteins that had previously been shown to interact with PDZ domains. To allow for the possibility of discovering sequences that fall outside the established view of peptide-binding selectivity, we derived the other peptides from different members of 13 families of membrane proteins, regardless of whether their C termini feature canonical PDZ domain binding motifs (table S2).
16. R. B. Jones, A. Gordus, J. A. Krall, G. MacBeath, Nature 439, 168 (2006).
17. M. A. Stiffler, V. P. Grantcharova, M. Sevecka, G. MacBeath, J. Am. Chem. Soc. 128, 5913 (2006).
18. Data for each PDZ-peptide combination [FP, recorded as millipolarization (mP) units] were fit to an equation that describes saturation binding, as previously noted (17). Interactions were scored as "positive" if all three of the following criteria were met: (i) The data fit well to the equation ($r^2 > 0.95$); (ii) the difference between FP at 20 µM PDZ domain and FP at 0 µM PDZ domain was >15 mP units; and (iii) the K_d was <100 µM.
19. To estimate the false-negative rate of our microarray assay, we randomly selected 32 PDZ domains and 32 peptides. We then screened all 1024 possible interactions with the use of a single-point FP assay and determined the K_d for all positive interactions. A comparison of the resulting interaction matrix with the microarray data showed a false-negative rate of 6.6%.
20. J. C. Obenauer, L. C. Cantley, M. B. Yaffe, Nucleic Acids Res. 31, 3635 (2003).
21. M. Sandberg, L. Eriksson, J. Jonsson, M. Sjostrom, S. Wold, J. Med. Chem. 41, 2481 (1998).
22. Materials and methods are available as supporting material on Science Online.
23. S. van Dongen, thesis, University of Utrecht, Netherlands (2000).
24. Full-length sequences of 31,302 unique mouse proteins (including splicing variants) were downloaded with

BioMart from data set NCBIM36 (Mus musculus genes) of Ensembl 44. The C-terminal sequence of each entry was extracted using a Python script.
25. Interactions in table S5 are model predictions with m set to 20. On the basis of the results of our model validation efforts, we estimate these predictions to have a true-positive rate of 35%, a false-positive rate of 7%, and a TP/FP ratio of 0.83.
26. This single-point assay measures the difference between FP at 20 nM peptide, 20 µM PDZ domain and FP at 20 nM peptide, 0 µM PDZ domain. An analysis of 1710 FP titration curves shows that applying a threshold of 40 mP units to this single-point assay correctly identifies 91% of the positives and 96% of the negatives (fig. S3). Thus, instead of performing an additional 1170 titration curves, we used this single-point assay with a threshold of 40 mP units to evaluate interactions between the 48 test peptides and the 74 PDZ domains in the MDSM.
27. R. Jansen et al., Science 302, 449 (2003).
28. A. Tropsha, Annu. Rep. Comput. Chem. 2, 113 (2006).
29. G. Birrane, J. Chung, J. A. Ladias, J. Biol. Chem. 278, 1399 (2003).
30. F. Jaulin-Bastard et al., J. Biol. Chem. 277, 2869 (2002).
31. F. Jaulin-Bastard et al., J. Biol. Chem. 276, 15256 (2001).
32. A. Zarrinpar, S. H. Park, W. A. Lim, Nature 426, 676 (2003).
33. We thank A. Tropsha for valuable suggestions and the Faculty of Arts and Sciences Center for Systems Biology for support with instrumentation and automation. This work was supported by awards from the Smith Family Foundation, the Arnold and Mabel Beckman Foundation, and the W. M. Keck Foundation and by a grant from the NIH (1 RO1 GM072872-01). M.A.S. was supported in part by the NIH Molecular, Cellular, and Chemical Biology Training Grant (5 T32 GM07598-25), and J.R.C. was the recipient of a Corning CoStar fellowship.

Brain IRS2 Signaling Coordinates Life Span and Nutrient Homeostasis

Akiko Taguchi, Lynn M. Wartschow, Morris F. White*

Reduced insulin-like signaling extends the life span of Caenorhabditis elegans and Drosophila. Here, we show that, in mice, less insulin receptor substrate–2 (Irs2) signaling throughout the body or just in the brain extended life span up to 18%. At 22 months of age, brain-specific Irs2 knockout mice were overweight, hyperinsulinemic, and glucose intolerant; however, compared with control mice, they were more active and displayed greater glucose oxidation, and during meals they displayed stable superoxide dismutase–2 concentrations in the hypothalamus. Thus, less Irs2 signaling in aging brains can promote healthy metabolism, attenuate meal-induced oxidative stress, and extend the life span of overweight and insulin-resistant mice.

Reaching old age in good health is not just good luck but the result of a favorable balance between hundreds of disease-causing and longevity-promoting genes; regardless, some common mechanisms that influence life span have emerged (1). First, calorie restriction reliably increases animal longevity, and second, reduced insulin-like signaling extends life span in Caenorhabditis elegans and

Drosophila melanogaster (2, 3). Calorie restriction and reduced insulin-like signaling might be linked because fasting reduces the intensity and duration of insulin secretion required for glucose homeostasis, and reduced insulin-like signaling promotes the expression of antioxidant enzymes that are associated with longevity (3–5). Adapting these principles to humans is challenging because calorie restriction is difficult and because reduced

insulin-like signaling can be associated with small stature, metabolic disease, and diabetes.

Insulin and insulin-like growth factor-1 (IGF1) bind to receptors on the surface of all cells that phosphorylate tyrosyl residues on the insulin receptor substrates (IRSs)—chico in Drosophila and Irs1, -2, -3, and -4 in mammals. This signaling cascade activates the phosphoinositide-3-kinase (Pik3C) and the thymoma viral proto-oncogene Akt, which regulates many cellular processes, including the inactivation of forkhead box O1 (FoxO1) transcription factor (6). Reduced chico expression decreases brain and body growth while increasing life span up to 50%, which is related to the increased activity of dFOXO in Drosophila (7, 8). In mice, the deletion of Irs1 reduces body growth and causes hyperinsulinemia, whereas the deletion of Irs2 ($Irs2^{-/-}$ mice) reduces brain growth and causes

Howard Hughes Medical Institute, Division of Endocrinology, Children's Hospital Boston, Harvard Medical School, Boston, MA 02115, USA.

*To whom correspondence should be addressed. E-mail: morris.white@childrens.harvard.edu

fatal diabetes by 3 months of age because of pancreatic β cell failure (9). By comparison, young (2-months-old) $Irs2^{+/-}$ mice display normal metabolic phenotypes (10). Old (22½-months-old) $Irs2^{+/-}$ mice were slightly heavier than wild-type (WT) mice, although young and old WT and $Irs2^{+/-}$ mice consumed the same amount of food each day (Fig. 1, A and B). In addition, old $Irs2^{+/-}$ mice were more insulin sensitive than old WT mice (Fig. 1C) because their fasting insulin and glucose concentrations were lower (fig. S1, A and B).

Because insulin sensitivity is associated with longevity (3), we compared the life spans of WT and $Irs2^{+/-}$ mice. Inspection of the results suggested that the date of birth (DOB), paternal (PID) and maternal (MID) identity, and sex influenced life span (table S1); therefore, we used semiparametric (Cox) and parametric regression to control the covariates and evaluate the effect of Irs2 (11). Cox regression revealed a 48-fold ($P < 10^{-9}$) reduced risk of death for $Irs2^{+/-}$ mice compared with WT controls (Fig. 1D and table S3). By using parametric analysis, we found that the median life span for $Irs2^{+/-}$ mice was 17% longer [for WT, median = 789 days and 95% confidence interval (CI) 755 to 769; for $Irs2^{+/-}$, median = 925 days and 95% CI 887 to 940; $P = 0.01$] (table S4). The maximum life span, estimated at the 90th percentile, increased similarly (for WT, 837 days and 95% CI 801 to 845; for $Irs2^{+/-}$, 982 days and 95% CI 935 to 998) (Fig. 1D and table S4).

Irs2 is expressed throughout the body (Fig. 2A) and many regions of the brain, including the cerebrum, the cerebellum, and the arcuate and paraventricular nuclei of the hypothalamus (fig. S2) (12, 13). Reduced insulin-like signaling in neurons increases the life span of *C. elegans* and *Drosophila*, so it is possible that reduced neuronal Irs2 could extend mouse life span (3, 14, 15). To test this hypothesis, we deleted one ($bIrs2^{+/-}$) or both ($bIrs2^{-/-}$) loxP-flanked Irs2 alleles ($fIrs2$-alleles) in the brain by intercrossing $fIrs2$ mice with nestin-cre transgenic mice (13). Polymerase chain reaction (PCR) analysis confirmed that *Irs2* RNA was retained in all tested tissues of the $bIrs2^{-/-}$ mice except for the brain (Fig. 2A). Quantitative reverse transcription PCR (RT-PCR) confirmed that *Irs2* RNA was reduced about 50% in $bIrs2^{+/-}$ brains and more than 90% in $bIrs2^{-/-}$ brains compared with that of control $fIrs2$ mice (Fig. 2A). By contrast, *Irs2* RNA increased in the pancreas of $bIrs2^{+/-}$ and $bIrs2^{-/-}$ mice, confirming that nestin-cre expression did not take place in pancreatic β cells (Fig. 2A).

Crosses between $bIrs2^{+/-}$ mice produced offspring at a normal frequency, whereas crosses between $bIrs2^{+/-}$ and $bIrs2^{-/-}$ mice produced fewer offspring; offspring were never produced by crossing $bIrs2^{-/-}$ mice (fig. S3A). Old male and female $bIrs2^{-/-}$ mice consumed the most food each day by comparison to the other mice (Fig. 2B). However, by 22 months the $bIrs2^{+/-}$ and $bIrs2^{-/-}$ mice were about 10 g heavier than controls, owing in part to increased adiposity (fig. S3, B and C). The

$bIrs2^{-/-}$ mice were 10% longer, and their brains were 30% smaller than those of $fIrs2$ or $bIrs2^{+/-}$ mice (fig. S3, D and E). These results support previous conclusions that brain Irs2 signaling promotes embryonic brain growth, central nutrient homeostasis, melanocortin 4 receptor signaling (body length), and fertility (13, 16–18).

Control $fIrs2$ mice developed insulin resistance between 2 and 22 months of age (Fig. 2C). Unlike old $Irs2^{+/-}$ mice (Fig. 1), old $bIrs2^{+/-}$ mice and young and old $bIrs2^{-/-}$ mice were insulin resistant (Fig. 2C). All the insulin-resistant mice displayed mild glucose intolerance (Fig. 2D). However, diabetes did not develop in these mice because insulin concentrations increased to compensate for peripheral resistance, reaching the highest amount in old male $bIrs2^{+/-}$ and $bIrs2^{-/-}$ mice (Fig. 2E). Consistent with the observed hyperinsulinemia, pancreatic islets were larger in old male $bIrs2^{+/-}$ and $bIrs2^{-/-}$ mice than in old controls (Fig. 2F).

Next, we compared the life spans of $fIrs2$, $bIrs2^{+/-}$, and $bIrs2^{-/-}$ mice by using semiparametric (Cox) and parametric regression to control for the covariates (table S2). Although $bIrs2^{+/-}$ and $bIrs2^{-/-}$ mice displayed metabolic changes usually associated with a shorter life span, their risk of death determined by Cox regression was

significantly reduced compared with that of controls (for $bIrs2^{+/-}$, a 14-fold reduction, $P < 10^{-11}$; for $bIrs2^{-/-}$, a sixfold reduction, $P < 10^{-5}$) (Fig. 3A and table S3). With parametric regression, we found that the median life spans for $bIrs2^{+/-}$ and $bIrs2^{-/-}$ mice were 18% and 14% longer, respectively, than life spans for controls (for $fIrs2$, median = 791 days and 95% CI 731 to 796; for $bIrs2^{+/-}$, median = 936 days and 95% CI 923 to 945; for $bIrs2^{-/-}$, median = 901 days and 95% CI 888 to 919); the maximum life spans (90th percentile) increased similarly (Fig. 3A and table S4).

To determine whether brain Irs2 affects systemic metabolism, we studied young and old mice in a comprehensive lab animal monitoring system (CLAMS). Young control ($fIrs2$) mice were more active and consumed more oxygen than did young $bIrs2^{+/-}$ or $bIrs2^{-/-}$ mice (Fig. 3, B and C). Oxygen consumption by old $fIrs2$ and $bIrs2^{+/-}$ mice declined to the same amount, whereas the $bIrs2^{-/-}$ mice consumed slightly less oxygen (Fig. 3B). All the mice were less active at 22 months; however, the old $bIrs2^{+/-}$ and $bIrs2^{-/-}$ mice were about twice as active as the old controls (Fig. 3C).

Next we determined the respiratory quotient ($R_q = VCO_2/VO_2$, where V is volume) to estimate the daily transition between fat ($R_q = 0.7$) and carbohydrate ($R_q = 1$) oxidation (19). The R_q for
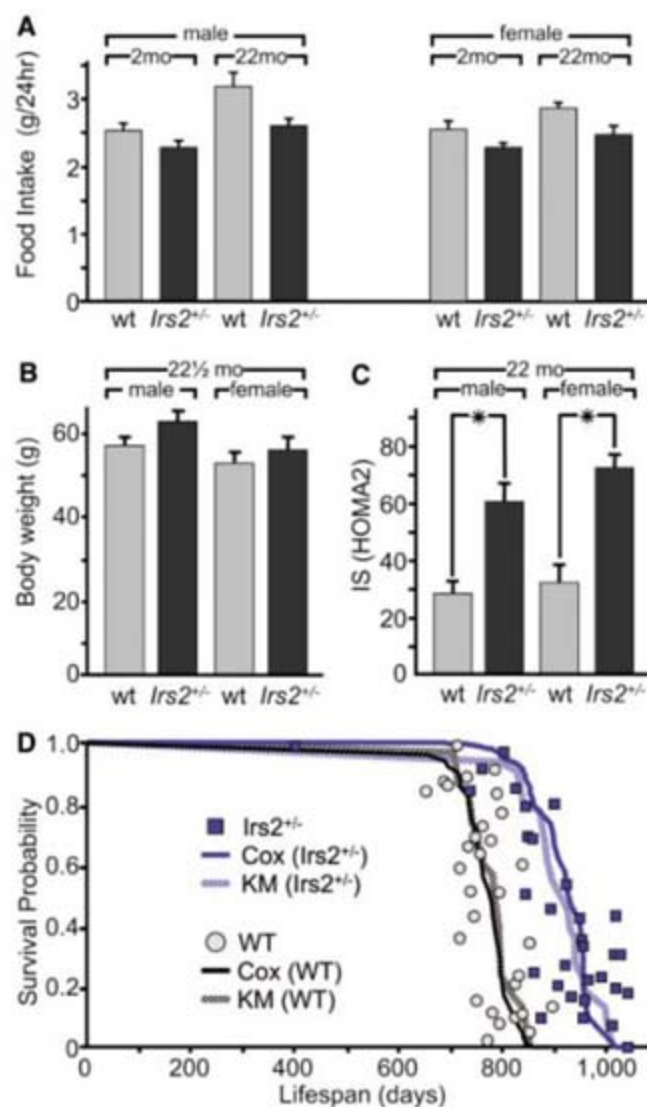
Fig. 1. Metabolism and life span of $Irs2^{+/-}$ mice. (**A**) Food intake [average (g/24 hour) ± SEM, n = 6 mice] in male or female mice at 2 and 22 months of age. (**B**) Body weight [average (g) ± SEM, n = 6] at 22½ months. (**C**) HOMA2 (homeostatic model assessment) of insulin sensitivity (IS) (average ± SEM, n = 8, *P < 0.05). (**D**) Survival probability was determined by Cox regression for each WT (●) and $Irs2^{+/-}$ (■, blue) mouse. Solid lines indicate the Cox survival probability of WT and $Irs2^{+/-}$ mice controlled for other covariates (see table S3 for details). Hatched lines correspond to Kaplan-Meier (KM) estimates obtained by parametric regression (see table S4 for details).
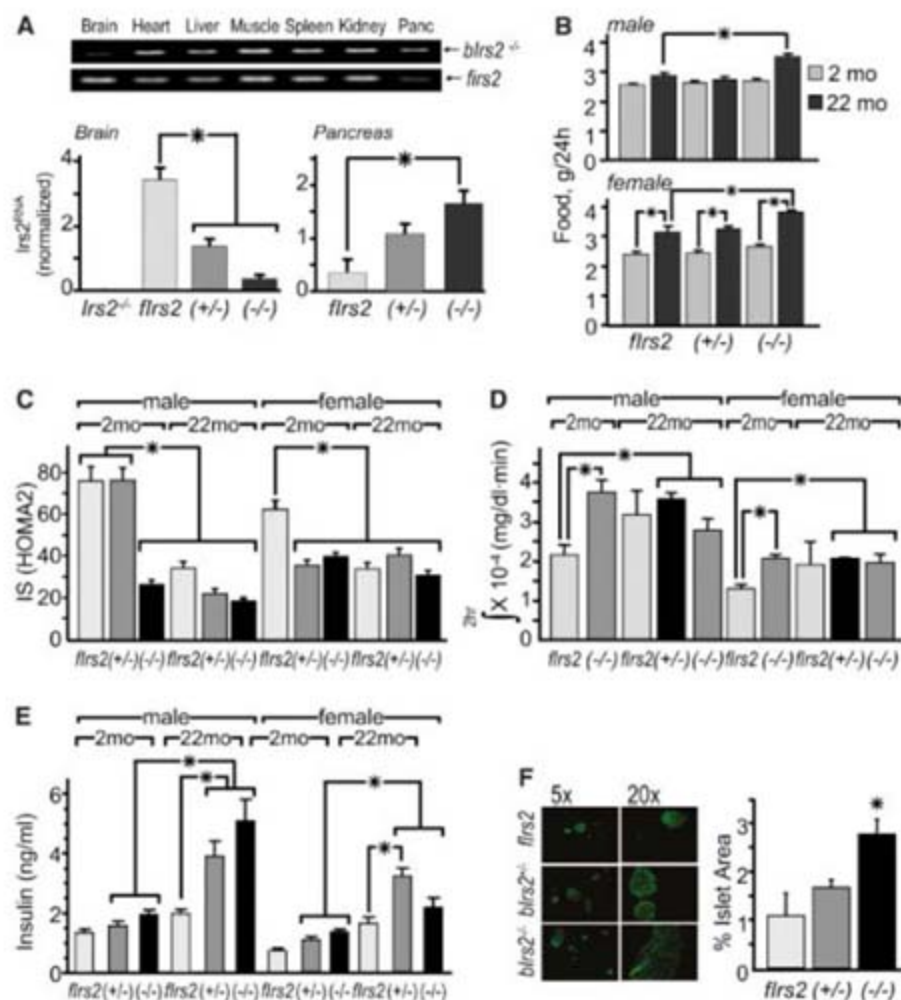
Fig. 2. Reduced neuronal Irs2 causes peripheral insulin resistance. (**A**) (Top) RT-PCR of *Irs2* RNA in mouse tissues and (bottom) quantitative RT-PCR (normalized ± SEM; $n = 5$; *$P < 0.05$) in brain and pancreas ($Irs2^{-/-}$ indicates systemic $Irs2^{-/-}$ mice). (**B**) Food intake [average (g/24 hour) ± SEM; $n = 6$; *$P < 0.05$] at 2 months and 22 months of age. (**C**) HOMA2 of IS (average ± SEM, $n = 8$; *$P < 0.05$). (**D**) Average area (±SEM; $n = 6$; *$P < 0.05$) under the blood glucose clearance curve. (**E**) Fasted insulin concentrations (±SEM; $n = 14$ to 16; *$P < 0.05$). (**F**) (Left) Pancreas sections from 22-month-old mice were immunostained with antibody against insulin (green) or glucagon (red), and (right) the amount of islet β cell area (average ± SEM, $n = 6$ sections; *$P < 0.05$).

all the young mice displayed the usual diurnal rhythm, which approached the maximum value during the dark cycle (Fig. 3D). By contrast, old *fIrs2* mice lost the diurnal rhythm; the R_q was indistinguishable between light and dark cycles (Fig. 3D). However, the R_q for old $bIrs2^{+/-}$ and $bIrs2^{-/-}$ mice increased significantly during the dark cycle, revealing a more youthful transition between fat and carbohydrate oxidation (Fig. 3D). Indeed, healthy long-lived humans also display a higher R_q that is closer to the value of healthy middle-aged adults (*20*).

Oxidative stress is associated with a reduced life span, and many enzymes protect cells from oxidative stress, especially superoxide dismutase (Sod) (*3, 4, 21*). In mice, FoxO1 promotes the expression of Sod2, so we investigated whether reduced neuronal Irs2 might help maintain brain Sod2 concentrations during feeding. Sod2 and FoxO1 protein was measured by immunoblotting hypothalamic lysates from young and old mice before and 2 hours after feeding (Fig. 4A). The Sod2 concentrations were not changed by feeding the young mice; however, Sod2 decreased at least 50% in the old fed control mice (Fig. 4, A and B). By contrast, Sod2 was not reduced by feeding old $bIrs2^{+/-}$ and $bIrs2^{-/-}$ mice (Fig. 4, A and B). A similar pattern was observed for FoxO1 levels in young and old hypothalamic tissues (Fig. 4, A and C). Thus, hypothalamic Sod2 reveals a more youthful response to feeding in mice with reduced brain Irs2.

Together, our results show that reduced Irs2 signaling in all tissues ($Irs2^{+/-}$) or just in the brain ($bIrs2^{+/-}$) increases the life spans of mice maintained on a high-energy diet about 5 months and about 4 months in $bIrs2^{-/-}$ mice (table S4). Some studies show that calorie restriction, reduced body size, and increased peripheral insulin sensitivity extend mammalian life span (*5, 22*).
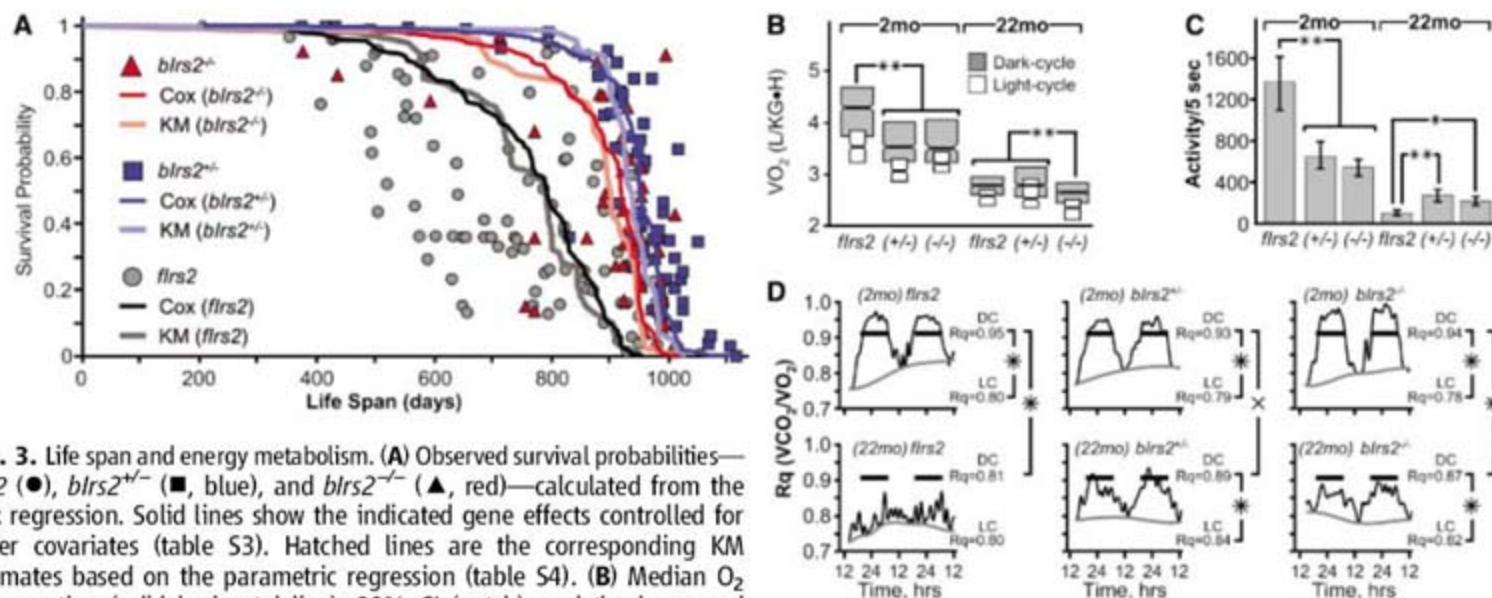
Fig. 3. Life span and energy metabolism. (**A**) Observed survival probabilities—*fIrs2* (●), $bIrs2^{+/-}$ (■, blue), and $bIrs2^{-/-}$ (▲, red)—calculated from the Cox regression. Solid lines show the indicated gene effects controlled for other covariates (table S3). Hatched lines are the corresponding KM estimates based on the parametric regression (table S4). (**B**) Median O_2 consumption (solid horizontal line), 99% CI (notch), and the lower and upper quartiles ($n = 425$ for each genotype, **$P < 0.0001$) by male mice in dark (shaded boxes) and light cycles (open boxes). (**C**) Median voluntary movement (±95% CI) for male mice measured during a 5-s interval in the dark cycle ($n = 425$ for each genotype, *$P < 0.02$, **$P < 0.0001$). (**D**) Average R_q (VCO_2/VO_2) determined during 48 hours from six male mice of the indicated age and genotype. Median R_q determined in dark (DC, black bar) and light (LC) cycles (Kruskal-Wallis nonparametric test: *$P < 0.0001$; ×$P = 0.03$).

Fig. 4. Loss of brain Irs2 stabilizes Sod2 in the postprandial brain. **(A)** Hypothalamic lysates were prepared from pairs of male siblings of the indicated genotype before (Fast) or after 2-hour feeding (Fed), resolved by SDS polyacrylamide gel electrophoresis, and immunoblotted with antibodies against Sod2 or FoxO1 (two independent experiments are shown). β-tubulin (shown for one experiment) was immunoblotted for all the experiments to confirm equivalent loading. Autoradiographs were quantified, and the ratio of intensities (Fed/Fast) for **(B)** Sod2 ($n = 5$) or **(C)** FoxO1 ($n = 4$) was calculated. Boxes show the median ratio (solid horizontal line) and the lower and upper quartiles; the Kruskal-Wallis nonparametric test was used to compare the groups across all genotypes (*$P < 0.05$).

References and Notes

1. K. A. Hughes, R. M. Reynolds, *Annu. Rev. Entomol.* **50**, 421 (2005).
2. R. A. Miller, *J. Am. Geriatr. Soc.* **53**, S284 (2005).
3. C. Kenyon, *Cell* **120**, 449 (2005).
4. D. A. Sinclair, L. Guarente, *Sci. Am.* **294**, 48 (2006).
5. M. S. Bonkowski, J. S. Rocha, M. M. Masternak, K. A. Al Regaiey, A. Bartke, *Proc. Natl. Acad. Sci. U.S.A.* **103**, 7901 (2006).
6. M. F. White, *Science* **302**, 1710 (2003).
7. D. J. Clancy et al., *Science* **292**, 104 (2001).
8. D. S. Hwangbo, B. Gershman, M. P. Tu, M. Palmer, M. Tatar, *Nature* **429**, 562 (2004).
9. D. J. Withers et al., *Nature* **391**, 900 (1998).
10. D. J. Withers et al., *Nat. Genet.* **23**, 32 (1999).
11. D. W. Hosmer Jr., S. Lemeshow, *Applied Survival Analysis* (Wiley, New York, 1999).
12. R. W. Gelling et al., *Cell Metab.* **3**, 67 (2006).
13. X. Lin et al., *J. Clin. Investig.* **114**, 908 (2004).
14. T. L. Parkes et al., *Nat. Genet.* **19**, 171 (1998).
15. C. A. Wolkow, K. D. Kimura, M.-S. Lee, G. Ruvkum, *Science* **290**, 147 (2000).
16. D. J. Burks et al., *Nature* **407**, 377 (2000).
17. A. I. Choudhury et al., *J. Clin. Investig.* **115**, 940 (2005).
18. M. Schubert et al., *J. Neurosci.* **23**, 7084 (2003).
19. Y. Wang et al., *Physiol. Genomics* **27**, 131 (2006).
20. M. R. Rizzo et al., *J. Clin. Endocrinol. Metab.* **90**, 409 (2005).
21. H. Kabil, L. Partridge, L. G. Harshman, *Biogerontology* **8**, 201 (2007).
22. R. A. Miller, J. M. Harper, A. Galecki, D. T. Burke, *Aging Cell* **1**, 22 (2002).
23. M. Barbieri et al., *Exp. Gerontol.* **38**, 137 (2003).
24. We thank R. Leshan, K. Martin, C. Aubin, N. Fujii, and V. Petkovana for technical assistance and C. Lee, J. Elmquist, M. Anderson, and H. Feldman for helpful advice. This work was supported by NIH (grants DK55326 and DK38712 to M.F.W.), the Japan Society for the Promotion of Science (A.T.), and the Yamada Science Foundation (A.T.). M.F.W. is an investigator at the Howard Hughes Medical Institute.

However, our long-lived mice are slightly larger and consume about the same or slightly more food than the short-lived controls. Indeed, long-lived systemic $Irs2^{+/-}$ mice are more insulin sensitive and glucose tolerant than WT mice; however, long-lived brain-specific $bIrs2^{+/-}$ and $bIrs2^{-/-}$ mice are insulin resistant, hyperinsulinemic, and glucose intolerant. The mechanism responsible for this disparity is unknown. Regardless, our results point to the brain as the site where reduced insulin-like signaling can have a consistent effect to extend mammalian life span—as it does in *C. elegans* and *D. melanogaster* (*1, 3*).

As mammals age, compensatory hyperinsulinemia usually develops to maintain glucose homeostasis and prevent the progression toward life-threatening type 2 diabetes (*6*); however, increased circulating insulin might have negative effects on the brain that can reduce life span (*4, 21, 23*). By directly attenuating brain Irs2 signaling, an aging brain can be shielded from the negative effects of hyperinsulinemia that ordinarily develop with overweight and advancing age. Consistent with this hypothesis, moderate daily exercise, calorie restriction, and weight loss—which reduce circulating insulin—might increase life span by attenuating Irs2 signaling in the brain. Other strategies that improve peripheral insulin sensitivity, such as reduced growth hormone signaling, could have the same effect (*5*). Indeed, human centenarians display increased peripheral insulin sensitivity and reduced circulating insulin concentrations (*23*). Hence, we suggest that the Irs2 signaling cascade in the brain integrates the effects of peripheral nutrient homeostasis with life span.

Patched1 Regulates Hedgehog Signaling at the Primary Cilium

Rajat Rohatgi,[1,2]* Ljiljana Milenkovic,[1]* Matthew P. Scott[1]†

Primary cilia are essential for transduction of the Hedgehog (Hh) signal in mammals. We investigated the role of primary cilia in regulation of Patched1 (Ptc1), the receptor for Sonic Hedgehog (Shh). Ptc1 localized to cilia and inhibited Smoothened (Smo) by preventing its accumulation within cilia. When Shh bound to Ptc1, Ptc1 left the cilia, leading to accumulation of Smo and activation of signaling. Thus, primary cilia sense Shh and transduce signals that play critical roles in development, carcinogenesis, and stem cell function.

The Hedgehog (Hh) signaling pathway plays an important role both in embryonic development and in adult stem cell function (*1, 2*). Dysregulation of the pathway causes birth defects and human cancer (*2*). Despite the importance of Hh signaling in mammals, there are gaps in our understanding of early events in this pathway. In the absence of signal, the transmembrane protein Patched1 (Ptc1) keeps the pathway turned off by inhibiting the function of a second transmembrane protein, Smoothened (Smo). The secreted protein Sonic Hedgehog (Shh) binds and inactivates Ptc1, allowing activation of Smo. Smo then triggers target gene transcription through the Gli family of transcription factors. The mechanism by which Shh inhibits Ptc1 and Ptc1 inhibits Smo is not understood in mammals.

In *Drosophila*, Ptc inhibits the movement of Smo to the plasma membrane. Binding of Hh causes the internalization of Ptc from the plasma

[1]Departments of Developmental Biology, Genetics, and Bioengineering and Howard Hughes Medical Institute, Stanford University School of Medicine, Stanford, CA 94305, USA. [2]Department of Oncology, Stanford University School of Medicine, Stanford, CA 94305, USA.

*These authors contributed equally to this work.
†To whom correspondence should be addressed. E-mail: mscott@stanford.edu

membrane to vesicles, allowing Smo to translocate to the plasma membrane and activate downstream signaling (3, 4). The discovery that protein components of primary cilia are required for Hh signaling suggested that subcellular localization has an important role in mammalian Hh signaling (5). Primary cilia are cell surface projections found on most vertebrate cells that function as sensory "antennae" for signals (6). Several components of the Hh pathway, including Smo and the Gli proteins, accumulate in primary cilia, and Smo is enriched in cilia upon stimulation with Shh (7, 8).

We examined the dynamic subcellular localization of Ptc1 and Smo in mammalian cells with the use of novel antibodies to the two proteins (fig. S1). These antibodies allowed detection of endogenous Ptc1 and Smo in cultured mouse fibroblasts (NIH 3T3 cells) and mouse embryonic fibroblasts (MEFs), two Hh-responsive cell types (9). Hh signaling was activated in NIH 3T3 cells by treatment with either Shh or SAG (Shh-agonist),

a small molecule that directly binds and activates Smo (10). Because *ptc1* is itself a transcriptional target of Hh signaling, increases in Ptc1 protein levels can serve as a metric for pathway activation. Ptc1 protein levels began to rise by 4 hours and continued to increase until 24 hours after addition of Shh (Fig. 1A). After stimulation of cells with Shh or SAG, endogenous Smo was enriched in primary cilia (Fig. 1B). The mean fluorescence intensity of Smo in cilia began to increase as early as 1 hour after stimulation of cells with Shh or SAG (Fig. 1C and fig. S2). This likely represented relocalization from a cytoplasmic pool, because the total amount of Smo protein did not increase at this time point (Fig. 1A).

To determine whether Ptc1 regulates the localization of Smo, we examined Smo localization in MEFs from *ptc1*$^{-/-}$ mice (9). These cells showed constitutive activation of Hh target gene transcription (fig. S3). Consistent with a role of Ptc1 in regulating Smo trafficking, Smo was constitutively localized to primary cilia in

these cells even in the absence of Shh or SAG (Fig. 1, D and E). Reintroduction of Ptc1 into these cells by means of a retrovirus suppressed Hh-pathway activity (fig. S3) and prevented Smo accumulation in primary cilia (Fig. 1, D and E). Thus, the regulation of Smo localization by Ptc1 is conserved from flies to mammals.

To understand how Ptc1 may regulate entry of Smo into the cilium, we examined the localization of Ptc1 in MEFs and mouse embryos. Endogenous Ptc1 was present in small amounts in MEFs, near the limit of detection by immunofluorescence. We therefore increased the amounts of Ptc1 protein by stimulating cells with SAG. Under these conditions, Ptc1 was highly enriched in primary cilia (Fig. 2A). The ciliary localization of Ptc1 was confirmed in three additional ways. First, Ptc1 fused to yellow fluorescent protein (Ptc1-YFP) was found around the base and in the shaft of cilia in unstimulated *ptc1*$^{-/-}$ cells infected with a retrovirus encoding Ptc1-YFP (Figs. 2B and fig. S12). Second, Ptc1-YFP overproduced

Fig. 1. Rapid localization of Smo in primary cilia after activation of the Hh pathway and regulation by Ptc1. (**A**) Immunoblots with antibodies to Ptc1, Smo, and actin were used to assess amounts of endogenous proteins in extracts from NIH 3T3 cells treated with Shh or SAG (100 nM). (**B**) Enrichment of Smo in primary cilia of NIH 3T3 cells left untreated (control) or treated with Shh or SAG (100 nM) for 24 hours. (**C**) Mean intensity of Smo fluorescence in cilia of NIH 3T3 cells treated with Shh or SAG (100 nM). Each point shows the mean ± SEM of fluorescence from 10 to 20 cilia. (**D** and **E**) Constitutive presence of Smo in the cilia of unstimulated *ptc1*$^{-/-}$ MEFs and reversal by retrovirally transduced Ptc1-YFP. In (B) and (D), confocal images of the ciliary marker acetylated tubulin (red) and Smo (green) were detected by immunofluorescence; nuclei (blue) were stained with 4′,6′-diamidino-2-phenylindole (DAPI).

in $ptc1^{-/-}$ cells by transfection showed clear ciliary localization in both live and fixed cells (Fig. 3A and figs. S10 and S14). Third and most important, endogenous Ptc1 was found in the cilia of mouse embryo mesoderm cells responsive to Shh (Fig. 2D and figs. S4 and S5) (*1*).

Ptc1 staining in cross sections of embryonic day 9.5 (E9.5) embryos was detected in cells of the ventral neural tube, notochord, splanchnic mesoderm, and paraxial mesoderm, precisely the regions where Hh signaling is known to be active and Shh target genes such as *ptc1* are highly expressed (Fig. 2C and fig. S4B) (*1*). We focused on mesoderm cells because they are likely the cells that gave rise to the MEFs that we have analyzed in culture. Endogenous Ptc1 showed asymmetric localization to a domain surrounding the base of the cilium and in particles along the shaft of the cilium (Fig. 2D and figs. S4C and S5). This localization pattern around the base and in a particulate pattern along the shaft of the cilium is similar to that seen in cultured fibroblasts (compare Fig. 2D and fig. S12). In embryo cells, there was more variability in the amount of Ptc1 in the shaft of cilia, a finding likely related to differences in the amount of Shh signal received by cells in the complex milieu of embryonic tissue. The concentration of Ptc1 at the base of primary cilia suggests a mechanism for how it may inhibit Smo activation. Transport of proteins in and out of primary cilia is thought to be regulated at their base, and Ptc1 could function at this location to inhibit a protein-trafficking step critical for Smo activation (*11*).

Shh could inactivate Ptc1 by binding to it at the cilium and inducing its internalization, degradation, or movement to other regions of the plasma membrane. To determine whether Ptc1 at the cilium can bind to Shh, we produced a fluorescently labeled version of the N-terminal signaling fragment of Shh (ShhN-A594). Minute amounts of ShhN-A594, one-hundredth of those required to activate signaling, were added to live $ptc1^{-/-}$ cells transfected with Ptc1-YFP and a marker for cilia, inversin fused to cyan fluorescent protein (inversin-CFP) (*12*). Live cells were used because the interaction between Shh and Ptc1 does not survive fixation. ShhN-A594 concentrated at cilia containing Ptc1-YFP and colocalized with puncta of Ptc1-YFP (Fig. 3A and fig. S7). $Ptc1^{-/-}$ cells expressing inversin-CFP alone did not bind ShhN-A594, and an excess of unlabeled ShhN prevented binding of ShhN-A594 (fig. S7).

We next asked whether the interaction of Shh with Ptc1 influences the localization of Ptc1. Ptc1 was concentrated at cilia after treatment of cells with SAG alone but not after treatment with Shh or a combination of Shh and SAG (Fig. 3B). This suggested that Shh binding might trigger the removal of the Ptc1-Shh complex from the cilium, or that new Ptc1 produced in response to Shh was not localized in the cilium. To distinguish these possibilities, we induced the production of large amounts of Ptc1 in the cilia of NIH 3T3 cells with SAG treatment and then
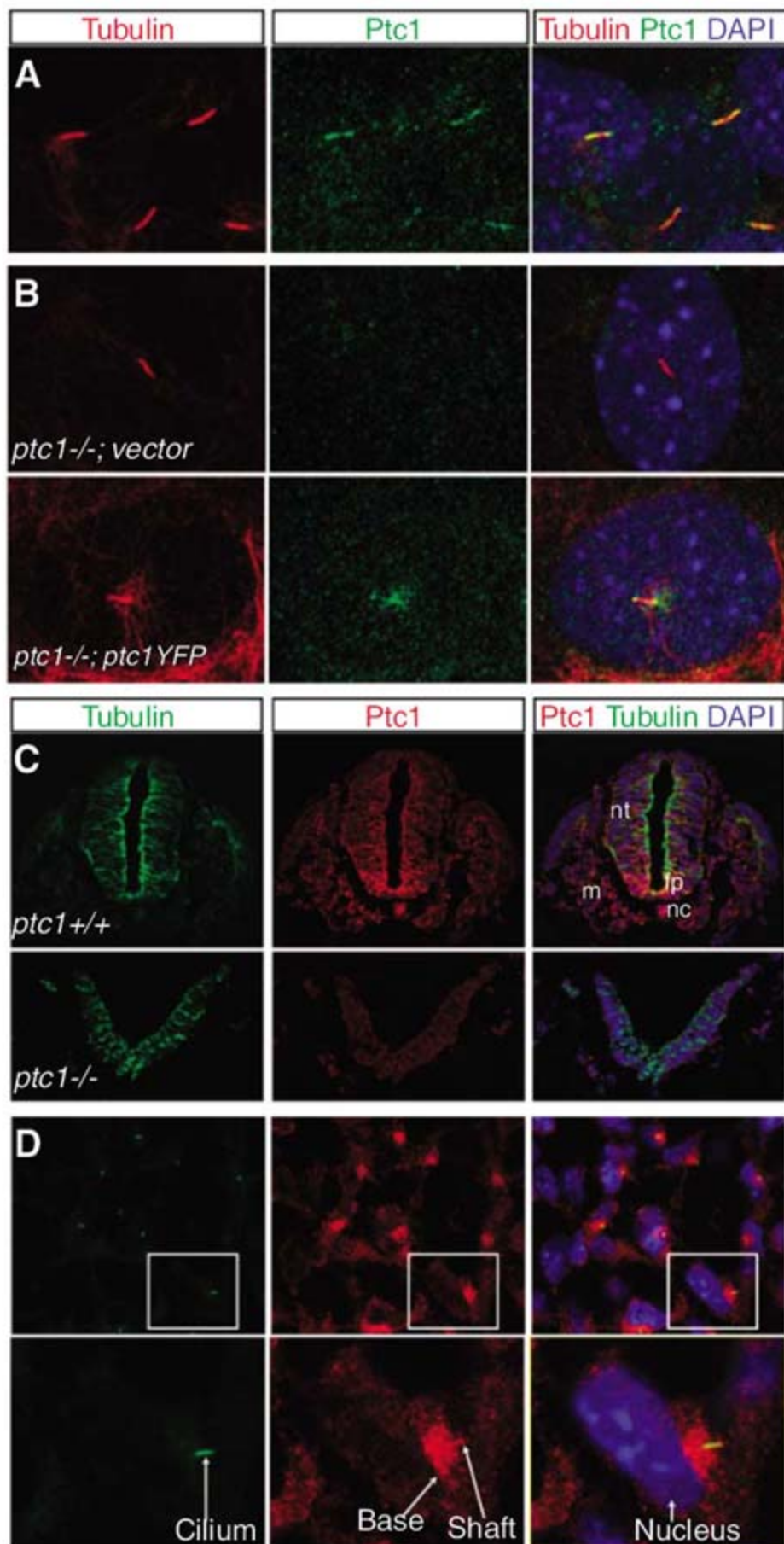
Fig. 2. Localization of Ptc1 in primary cilia. (**A**) Concentration of endogenous Ptc1 in cilia of NIH 3T3 cells stimulated with 100 nM SAG. (**B**) Localization of Ptc1-YFP in $ptc1^{-/-}$ MEFs infected with a retrovirus carrying an empty vector or the *ptc1-YFP* coding sequence. In (A) and (B), cilia (red) and Ptc1 (green) were visualized by immunofluorescence; nuclei (blue) were stained with DAPI. (**C**) Ptc1 staining in Shh-responsive cells of the neural tube (nt), notochord (nc), floor plate (fp), and paraxial mesoderm (m). Cross sections of wild-type (top row) or control $ptc1^{-/-}$ (bottom row) mouse embryos (E9.5) were imaged with a 40× objective. (**D**) Asymmetric, ciliary localization of Ptc1 in paraxial mesoderm cells. The cell boxed in white is magnified in the bottom panel; arrows indicate Ptc1 staining (red) around the base and in the shaft of cilia (green).
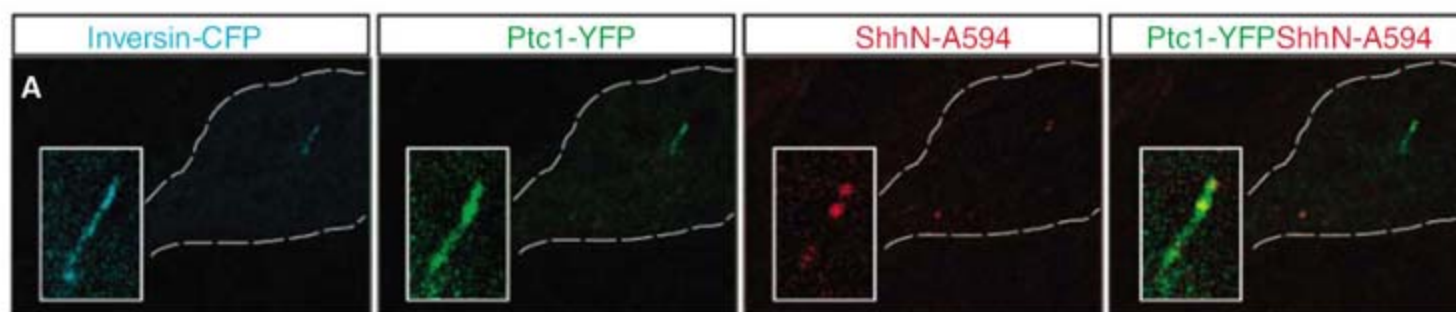
Fig. 3. Interactions between Shh and Ptc1 at primary cilia. (**A**) Colocalization of Shh and Ptc1 at the cilium shown in a confocal image of a live *ptc1*$^{-/-}$ cell transfected with Ptc1-YFP (green) and incubated with ShhN-A594 (red, 300 ng/ml) for 45 min. Inversin-CFP (cyan) marks the cilium, the dotted line demarcates the cell border, and insets show magnified views of the cilia. (**B**) Mean Ptc1 fluorescence in cilia of NIH 3T3 cells treated with SAG (100 nM), Shh, or both. (**C**) Disappearance of Ptc1 from primary cilia after Shh treatment. NIH 3T3 cells preincubated with SAG for 24 hours were switched to control medium (untreated) or into Shh-containing medium. The red dashed baseline shows the amount of ciliary Ptc1 in cells treated with Shh for 4 hours without a 24-hour SAG pulse.
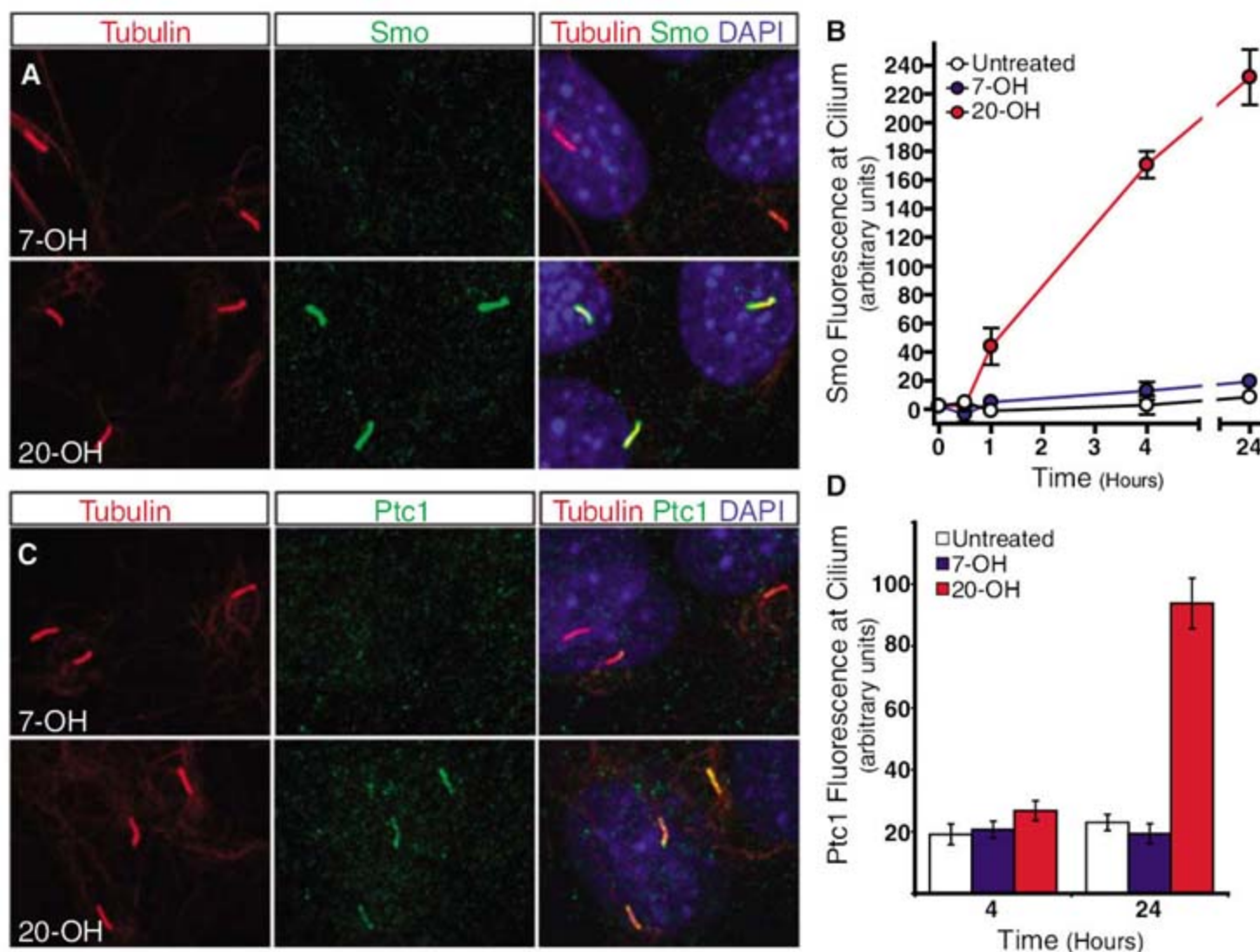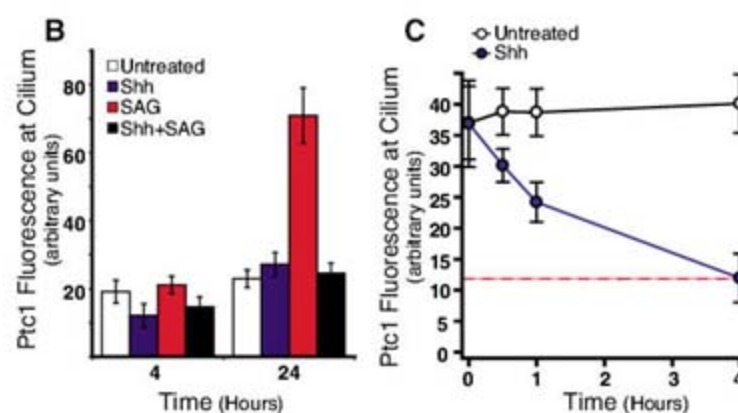
Fig. 4. Accumulation of Smo and Ptc1 at cilia of NIH 3T3 cells exposed to 20α-hydroxycholesterol. (**A** and **C**) Localization of cilia (red) and Smo or Ptc1 (green) in cells treated with 10 μM 20α-hydroxycholesterol or 7α-hydroxycholesterol for 24 hours. (**B**) Time course of Smo accumulation at the primary cilium in NIH 3T3 cells treated with 20α-hydroxycholesterol. (**D**) Increase in Ptc1 fluorescence in primary cilia after treatment with 20α-hydroxycholesterol. In (**B**) and (**D**), each point shows the mean ± SEM of fluorescence from 10 to 20 cilia.

switched the cells to control medium or medium containing Shh (Fig. 3C). Ptc1 levels in the cilium remained stable in the control, but Shh treatment caused a time-dependent disappearance of Ptc1 from the primary cilium (Fig. 3C and fig. S8). The loss of Ptc1 from cilia was not associated with a decrease in total Ptc1 protein levels (fig. S11) and thus implied movement of Ptc1 from cilia to another location in the cell. This delocalization was only evident with the endogenous protein and not upon examination of transfected Ptc1-YFP, a far more abundant protein (fig. S7B).

We measured Ptc1 and Smo localization (Figs. 1 and 3) in the same experiment. Because the localization changes for Ptc1 and Smo described above were each seen in >80% of the cilia visualized, the levels of Ptc1 and Smo in cilia were inversely correlated. The reciprocal time courses of Ptc1 disappearance and Smo appearance at cilia after Shh addition (Figs. 1C and 3C) support a model in which Shh triggers the removal of Ptc1 from the cilium, allowing Smo to enter and activate signaling. Consistent with this idea, cells of the ventral neural tube and floor plate, which receive large amounts of Shh, showed high levels of Smo and low levels of Ptc1 in cilia (fig. S13). The movement of Ptc1 and Smo at the cilium is analogous to the situation in *Drosophila*, where pathway activation is associated with Smo movement to the plasma membrane and movement of Ptc away (3).

Ptc1 may regulate Smo localization through a small molecule (13). Because Smo translocation to the primary cilium appears to be a critical step in its activation, a regulatory small molecule would be predicted to control this step. Naturally occurring oxysterols are good candidates for endogenous small molecules that regulate Smo function. Cellular sterol concentrations are important determinants of a cell's responsiveness to Shh, and oxysterols can activate Hh signaling (14–16). When we treated NIH 3T3 cells with activating concentrations of the oxysterol 20α-hydroxycholesterol, Smo rapidly translocated to the primary cilium with kinetics that were identical to those seen in cells treated with SAG or Shh (Fig. 4, A and B, and fig. S9). Treatment with 7β-hydroxycholesterol, an oxysterol that does not activate the Hh pathway, did not induce translocation of Smo. This result provides a specific molecular mechanism—Smo translocation to cilia—to explain how oxysterols regulate Hh signaling.

Cells treated with 20α-hydroxycholesterol also retained Ptc1 in cilia in a pattern similar to that seen in cells treated with SAG (Fig. 4, C and D). Thus, oxysterols appear to function not like Shh, by causing the removal of Ptc1 from cilia, but at a more downstream step to make Smo insensitive to the inhibitory effects of Ptc1. However, oxysterols function differently from SAG because they likely do not directly bind to Smo (16).

Our results suggest that Ptc1 localization to primary cilia inhibits the Hh pathway by excluding Smo and also allows cilia to function as chemosensors for the detection of extracellular Shh. Binding of Shh to Ptc1 at primary cilia is coupled to pathway activation by the reciprocal movement of Ptc1 out of the cilia and Smo into the cilia, a process that may be mediated by oxysterols. Elucidating the molecular machinery that controls Ptc1 and Smo trafficking at primary cilia will likely provide new targets for modulation of this important pathway.

References and Notes

1. P. W. Ingham, A. P. McMahon, *Genes Dev.* **15**, 3059 (2001).
2. P. A. Beachy, S. S. Karhadkar, D. M. Berman, *Nature* **432**, 324 (2004).
3. A. J. Zhu, L. Zheng, K. Suyama, M. P. Scott, *Genes Dev.* **17**, 1240 (2003).
4. N. Denef, D. Neubuser, L. Perez, S. M. Cohen, *Cell* **102**, 521 (2000).
5. D. Huangfu *et al.*, *Nature* **426**, 83 (2003).
6. V. Singla, J. F. Reiter, *Science* **313**, 629 (2006).
7. K. C. Corbit *et al.*, *Nature* **437**, 1018 (2005).
8. C. J. Haycraft *et al.*, *PLoS Genet.* **1**, e53 (2005).
9. J. Taipale *et al.*, *Nature* **406**, 1005 (2000).
10. J. K. Chen, J. Taipale, K. E. Young, T. Maiti, P. A. Beachy, *Proc. Natl. Acad. Sci. U.S.A.* **99**, 14071 (2002).
11. J. L. Rosenbaum, G. B. Witman, *Nat. Rev. Mol. Cell Biol.* **3**, 813 (2002).
12. D. Watanabe *et al.*, *Development* **130**, 1725 (2003).
13. J. Taipale, M. K. Cooper, T. Maiti, P. A. Beachy, *Nature* **418**, 892 (2002).
14. M. K. Cooper *et al.*, *Nat. Genet.* **33**, 508 (2003).
15. R. B. Corcoran, M. P. Scott, *Proc. Natl. Acad. Sci. U.S.A.* **103**, 8408 (2006).
16. J. R. Dwyer *et al.*, *J. Biol. Chem.* **282**, 8959 (2007).
17. M.P.S. is an investigator of the Howard Hughes Medical Institute and is supported by National Cancer Institute grant R01 CA088060. R.R. is a Robert Black Fellow of the Damon Runyon Cancer Research Fund (DRG 103-06). We thank R. Corcoran for discussions of oxysterol effects, P. Beachy for *smo*^{-/-} cells and for sharing results before publication, J. Chen for SAG, O. Brandman for image analysis advice, J. Hyman for microscopy advice, R. Johnson and K. Suyama for Ptc1 antiserum, H. Hamada for inversin constructs, D. Ko for the Ptc1-YFP construct, A. Salic for the Shh labeling strategy, and T. Hillman, C. Ho, A. Kumar, and A. Balmain for comments.

Host Immune System Gene Targeting by a Viral miRNA

Noam Stern-Ginossar,[1]* Naama Elefant,[2]* Albert Zimmermann,[3] Dana G. Wolf,[4] Nivin Saleh,[4] Moshe Biton,[1] Elad Horwitz,[1] Zafnat Prokocimer,[1] Mark Prichard,[5] Gabriele Hahn,[6]† Debra Goldman-Wohl,[7] Caryn Greenfield,[7] Simcha Yagel,[7] Hartmut Hengel,[3] Yael Altuvia,[2]‡ Hanah Margalit,[2]*‡ Ofer Mandelboim[1]*‡

Virally encoded microRNAs (miRNAs) have recently been discovered in herpesviruses. However, their biological roles are mostly unknown. We developed an algorithm for the prediction of miRNA targets and applied it to human cytomegalovirus miRNAs, resulting in the identification of the major histocompatibility complex class I–related chain B (MICB) gene as a top candidate target of hcmv-miR-UL112. MICB is a stress-induced ligand of the natural killer (NK) cell activating receptor NKG2D and is critical for the NK cell killing of virus-infected cells and tumor cells. We show that hcmv-miR-UL112 specifically down-regulates MICB expression during viral infection, leading to decreased binding of NKG2D and reduced killing by NK cells. Our results reveal a miRNA-based immunoevasion mechanism that appears to be exploited by human cytomegalovirus.

MiRNAs constitute a large family of small noncoding RNAs that regulate gene expression posttranscriptionally, affecting mRNA degradation and translation by base-pairing with the 3′ untranslated regions (3′UTRs) (1). The recent discovery of virally encoded miRNAs, mostly in herpesviruses, intriguingly suggests that miRNAs may function in interspecies regulation involving viral miRNAs and host genes (2–4). Human cytomegalovirus (HCMV) is known to have evolved effective immune evasion strategies, encoding many immunomodulatory proteins that manipulate the immune response (5, 6). It is thus conceivable that miRNAs encoded by HCMV (2) might be exploited during immune evasion. To test this hypothesis, we sought to identify potential human target genes of the HCMV miRNAs by using our newly developed target prediction algorithm,

[1]Lautenberg Center for General and Tumor Immunology, Hebrew University Hadassah Medical School, Jerusalem, Israel. [2]Department of Molecular Genetics and Biotechnology, Hebrew University Hadassah Medical School, Jerusalem, Israel. [3]Institute for Virology, Heinrich Heine University, D40225 Düsseldorf, Germany. [4]Department of Clinical Microbiology and Infectious Diseases, Hadassah University Hospital, Jerusalem, Israel. [5]Department of Pediatrics, University of Alabama, Birmingham, AL 35233, USA [6]Max von Pettenkofer Institut, Department of Virology, D80336 Munich, Germany. [7]Department of Obstetrics and Gynecology, Hadassah Hebrew University Hospital Mount Scopus, Jerusalem, Israel.

*These authors contributed equally to this work.
†Present address: Klinikum Ingolstadt, Institut für Laboratoriumsmedizin, D84049 Ingolstadt, Germany.
‡To whom correspondence should be addressed. E-mail: yaelal@md.huji.ac.il (Y.A.); hanahm@ekmd.huji.ac.il (H.M.); oferm@ekmd.huji.ac.il (O.M.)

RepTar (7). Briefly, RepTar has its basis in the observation that miRNA binding sites can repeat several times in the target's 3'UTR (1). It therefore searches for repetitive elements in each 3'UTR sequence and evaluates these elements as potential miRNA binding sites. A complementary module of the algorithm, cRepTar, screens for additional single binding sites by using the information obtained by RepTar (7). This algorithm, unlike most other algorithms (8), is independent of evolutionary conservation of the binding sites. Therefore, it is more suitable for predicting targets of the less evolutionary conserved viral miRNAs (2).

We applied RepTar and subsequently cRepTar to all human 3'UTRs, searching for potential binding sites of the 11 HCMV miRNAs listed in miRBase 7.0 (9). MICB, an immunorelated gene, was among the highest ranking predicted targets and the top prediction for hcmv-miR-UL112 (Fig. 1A). MICB is a stress-
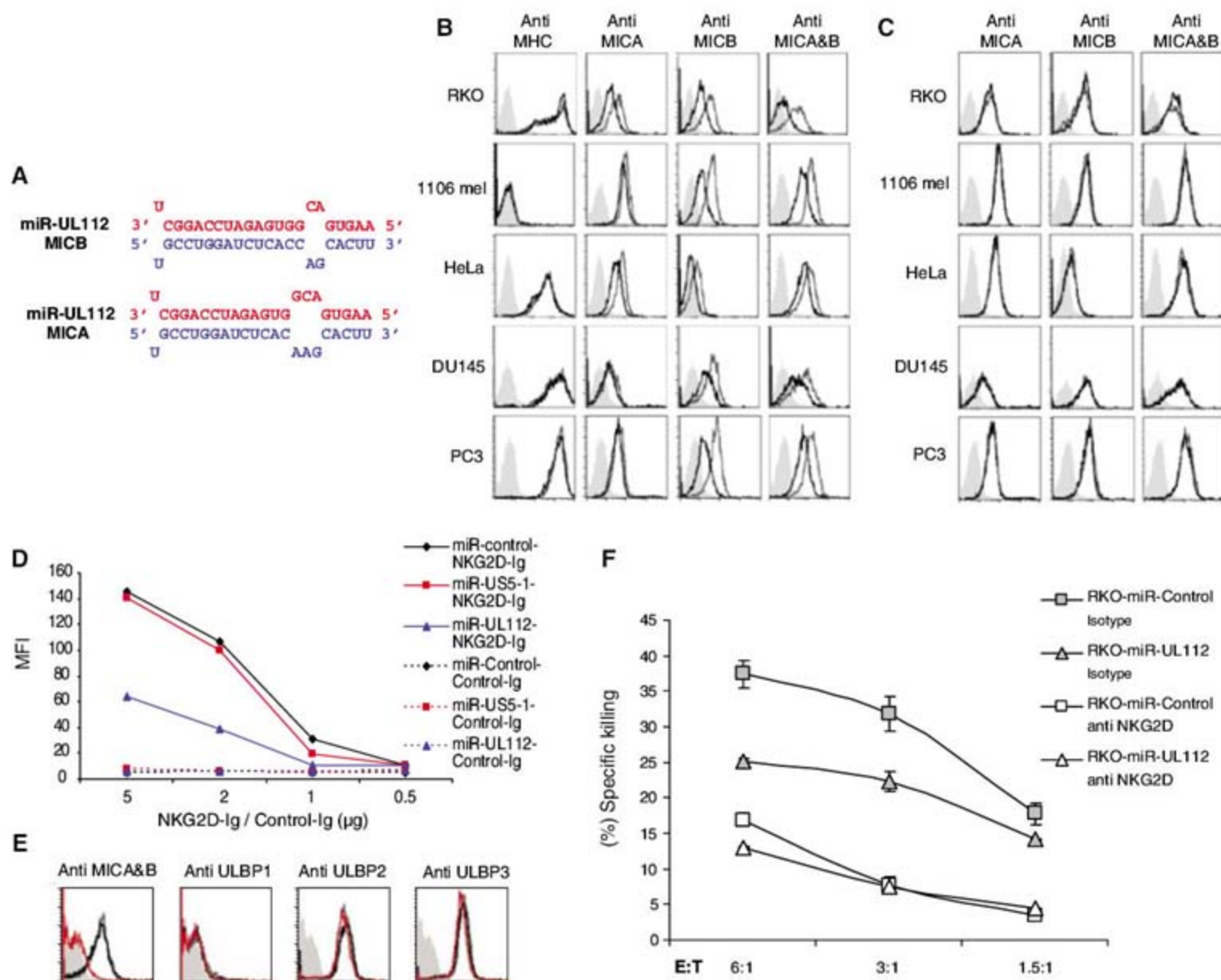
Fig. 1. hcmv-miR-UL112 specifically down-regulates MICB expression and reduces NK cytotoxicity. For all panels, one representative experiment is shown out of at least three performed. (**A**) The predicted duplex of hcmv-miR-UL112 (red) and its target site (blue) in the 3'UTR of MICB (top) and MICA (bottom). (**B**) Ectopic expression of hcmv-miR-UL112 down-regulates MICB expression. Various human cell lines were transduced with lentiviruses expressing GFP either with hcmv-miR-UL112 (black histogram) or miR-control (open gray histogram). Expression levels of MHC class I, MICA, and MICB were assessed by FACS. (**C**) Ectopic expression of hcmv-miR-US5-1 does not affect MICB expression. Human cell lines were transduced with lentiviruses expressing GFP and either hcmv-miR-US5-1 (black histogram) or miR-control (open gray histogram). The expression levels of MICA and MICB were assessed by FACS. The histogram plots of (B) and (C) were gated only on the GFP-positive cells. Background levels for (B) and (C) were measured by using only the secondary Cy5-conjugated Ab (gray solid histogram). (**D**) Reduced binding of NKG2D to cells expressing hcmv-miR-UL112. Binding of NKG2D-Ig to the RKO cells expressing miR-control, hcmv-miR-US5-1, or hcmv-miR-UL112 was assessed by FACS using NKG2D-Ig and the control CD99-Ig (Control-Ig) in various concentrations. (**E**) The reduced NKG2D-Ig binding is due to reduced MICB expression. The expression level of the various NKG2D ligands was assessed by FACS in RKO cells expressing hcmv-miR-UL112 (open red histogram), miR-control (open gray histogram), or hcmv-miR-US5-1 (open black histogram). The histogram plots are gated only on the GFP-positive cells. The background was measured as in (B) and (C) (solid gray histogram). (**F**) Reduced killing of RKO cells expressing hcmv-miR-UL112. Bulk NK cells were preincubated either with anti-NKG2D mAb (white) or with isotype-match control mAb (gray). Labeled RKO cells expressing miR-control or hcmv-miR-UL112 were then added and incubated for 5 hours at the indicated effector:target (E:T) ratios. The differences between the killing of the RKO cells expressing miR-control and those expressing hcmv-miR-UL112 in the presence of the isotype-matched control mAb were significant ($P < 0.01$, t test). Error bars represent standard deviation of replicates.

induced ligand of NKG2D, a natural killer (NK) activating receptor expressed on almost all human NK cells and activated cytotoxic T lymphocytes (CTLs) (*10*). The importance of MICB in the immune response against HCMV infection is substantiated by the specific down-regulation of MICB surface expression via the UL16 protein of HCMV (*11*, *12*). MICA, another stress-induced ligand of NKG2D, was also ranked among the top predicted targets of hcmv-miR-UL112 (Fig. 1A). The hcmv-miR-UL112 putative binding sites of both genes are almost identical and are located within a highly similar but not evolutionarily conserved (*7*) 150-nucleotide (nt) region of their 3′UTRs.

To assess the function of hcmv-miR-UL112, we expressed this miRNA in various human tumor cell lines that endogenously express MICA and MICB with the use of recombinant lentiviral vectors: hcmv-miR-UL112 and two control vectors, a non-miRNA sequence (miR-control) and hcmv-miR-US5-1. The expression of hcmv-miR-UL112 was confirmed by quantative real-time polymerase chain reaction (qPCR) (fig. S1). The vectors contained green fluorescent protein (GFP) for monitoring the infection efficiency (*7*). No difference in the transduction efficiency of the different lentiviral vectors was measured (fig. S2). Analysis of the various tumor cells transduced with hcmv-miR-UL112 revealed a specific and extensive reduction of MICB and little or no reduction of MICA (Fig. 1B). The down-regulation was specific to MICB and to hcmv-miR-UL112, because no change in the level of major histocompatibility complex (MHC) class I was observed (Fig. 1B) and transduction with hcmv-miR-US5-1 had no effect (Fig. 1C).

To study whether the observed changes in MICB protein levels affected its interaction with NK cell activating receptor NKG2D, we stained RKO cells expressing either miR-control, hcmv-miR-US5-1, or hcmv-miR-UL112 with NKG2D fused to immunoglobulin G1 (IgG1), as previously described (*11*). Fluorescence-activated cell sorting (FACS) analysis revealed a measurable decrease in NKG2D-Ig staining of cells expressing hcmv-miR-UL112 compared with those expressing hcmv-miR-US5-1 or miR-control (Fig. 1D). The reduction in NKG2D binding was specifically due to the reduced levels of MICB, because the expression of other NKG2D ligands was not affected by hcmv-miR-UL112 (Fig. 1E).

The functional implication of the hcmv-miR-UL112–mediated reduction in NKG2D binding was demonstrated by measuring NK lysis of RKO cells expressing hcmv-miR-UL112 or miR-control. Cells expressing hcmv-miR-UL112 were killed less efficiently than cells expressing miR-control (Fig. 1F). When NKG2D interactions were blocked with a monoclonal antibody (mAb) against NKG2D (anti-NKG2D), killing levels of both cells were similar (Fig. 1F), indicating that this reduced killing was explicitly due to reduced NKG2D recognition.

Direct binding of hcmv-miR-UL112 to the 3′UTR of MICA and MICB was studied by luciferase reporter assays in HeLa cells ectopically expressing either hcmv-miR-UL112 or miR-control. In agreement with the staining results (Fig. 1B), a measurable decrease in the activity of the luciferase reporter gene was observed only when it was fused to the 3′UTR of MICB and only in cells expressing hcmv-miR-UL112 (Fig. 2A). To demonstrate that the down-regulation of MICB by hcmv-miR-UL112 is

mediated through the predicted binding site, we generated two double substitution mutations, disrupting the predicted pairing between hcmv-miR-UL112 and the 3′UTR of MICB (Fig. 2B). Both mutations abolished the repression mediated by hcmv-miR-UL112 (Fig. 2A). The binding site in the 3′UTR of MICB has one additional putative paired nucleotide in comparison to MICA (Figs. 1A and 2B). To test whether the difference observed between MICA and MICB was due to the change in this single nucleotide, we generated
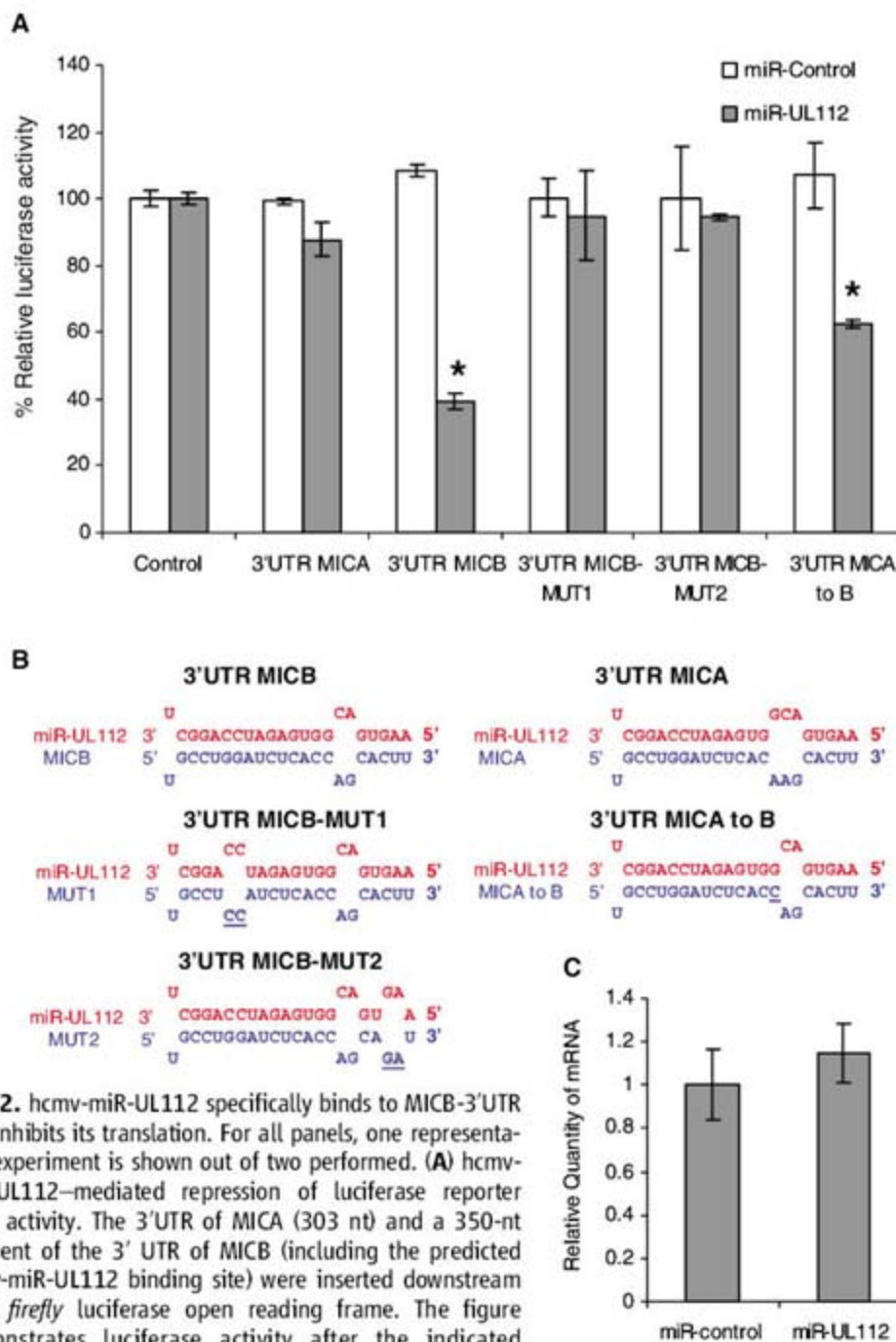
Fig. 2. hcmv-miR-UL112 specifically binds to MICB-3′UTR and inhibits its translation. For all panels, one representative experiment is shown out of two performed. (**A**) hcmv-miR-UL112—mediated repression of luciferase reporter gene activity. The 3′UTR of MICA (303 nt) and a 350-nt segment of the 3′ UTR of MICB (including the predicted hcmv-miR-UL112 binding site) were inserted downstream of a *firefly* luciferase open reading frame. The figure demonstrates luciferase activity after the indicated reporter plasmids were transfected into HeLa cells expressing either hcmv-miR-UL112 (gray) or miR-control (white). *Firefly* luciferase activity was normalized to *Renilla* luciferase activity and then normalized to the average activity of the control reporter. Values are mean ± SD for triplicate samples. *Statistically significant difference between cells expressing miR-control and those expressing hcmv-miR-UL112 ($P < 0.005$ by t test). (**B**) Schematic representation of the mutations made in MICB and MICA 3′UTRs (blue) and their base-pairings with hcmv-miR-UL112 (red). Mutated positions are underlined. (**C**) qPCR analysis of MICB. Experiments were performed with RKO cells expressing either miR-control or hcmv-miR-UL112. The levels of 18S ribosomal RNA were used as internal standard control. Values are mean ±SD for triplicate samples.

a point substitution that changed the MICA binding site to that of MICB (MICA to B, Fig. 2B). This mutation indeed caused a reduction in luciferase activity but not as substantial as that with the 3′UTR of MICB, supporting previous suggestions that additional factors are involved in the determination of a functional binding site (13).

To determine whether hcmv-miR-UL112 reduced MICB expression by influencing its mRNA degradation, we tested MICB mRNA levels in RKO cells expressing either miR-control or hcmv-miR-UL112 by using qPCR. No significant change in MICB mRNA level was observed (Fig. 2C), suggesting that the down-regulation of MICB was due to translation inhibition.

We next explored the function of hcmv-miR-UL112 during authentic HCMV infection with use of a wild-type HCMV-AD169 strain and a HCMV-AD169 mutant (14). In this mutant the UL114 gene is deleted, and therefore the hcmv-miR-UL112 gene that resides on the complementary strand is also absent. HCMV-AD169 laboratory strain is adapted to infect primary fibroblasts and a limited number of cell lines. Expression of MICB protein was not observed in several primary fibroblasts and cell lines, before or after infection (fig. S3). We used this to our benefit and expressed MICB with its 3′UTR (MICB-3′UTR)

or MICB without its 3′UTR (MICB) in primary human foreskin fibroblasts (HFF) cells. Ectopic expression of hcmv-miR-UL112 in these cells resulted in down-regulation of only MICB-3′UTR protein (fig. S4), indicating that these cells are adequate for testing the effect of viral hcmv-miR-UL112 on MICB expression.

We used the HFF cells expressing either MICB-3′UTR or MICB and infected them with the AD169-wild-type or with the AD169-mutated virus. The protein expressed by MICB-3′UTR was almost completely down-regulated on day 3 after infection in the AD169-wild-type–infected cells but not in the cells infected with the AD169-mutated virus (Fig. 3A). This is consistent with the accumulation of hcmv-miR-UL112 3 days after infection (fig. S5) (15). In contrast, MICB down-regulation in the absence of the 3′UTR (which was mediated by the UL16 protein) was similar in cells infected with the AD169-wild-type and mutated viruses (Fig. 3A). The effect of hcmv-miR-UL112 on MICB-3′UTR expression was specific, because the level of MHC class I [known to be down-regulated by the virus during infection (16)] was similarly reduced by both viruses (Fig. 3B).

To segregate the miRNA posttranscriptional regulation of MICB from the posttranslational

regulation mediated by HCMV UL16 protein, (12) we examined the effect of hcmv-miR-UL112 in HFF cells expressing either GFP, GFP fused to the 3′UTR of MICB, or GFP fused to the 3′UTR of MICA. Consistent with the observed MICB-3′UTR down-regulation (Fig. 3A) and the qPCR results (fig. S5), the most substantial reduction in GFP expression was observed on day 3, only when the cells were infected with the AD169-wild-type virus and only in those expressing the GFP fused to 3′UTR of MICB (Fig. 3C). No changes in the GFP levels were observed in cells carrying GFP alone or GFP fused to the 3′UTR of MICA (Fig. 3C and fig. S5).

To further demonstrate the biological relevance of hcmv-miR-UL112 and to exclude the possibility that the deletion of the UL114 protein-encoding gene affected MICB down-regulation, we constructed two new mutated viruses in the HCMV TB40 strain (17): a control virus in which UL114 is mutated but hcmv-miR-UL112 is intact (TB40-UL114P-mut) and a mutated UL114 virus in which hcmv-miR-UL112 was deleted (TB40-miR-UL112-mut). The HCMV TB40 strain is similar to clinical strains and infects endothelial cells, one of the natural targets of HCMV in vivo (17). Infection of human umbilical vein endothelial cells (HUVECs) that endogenously express
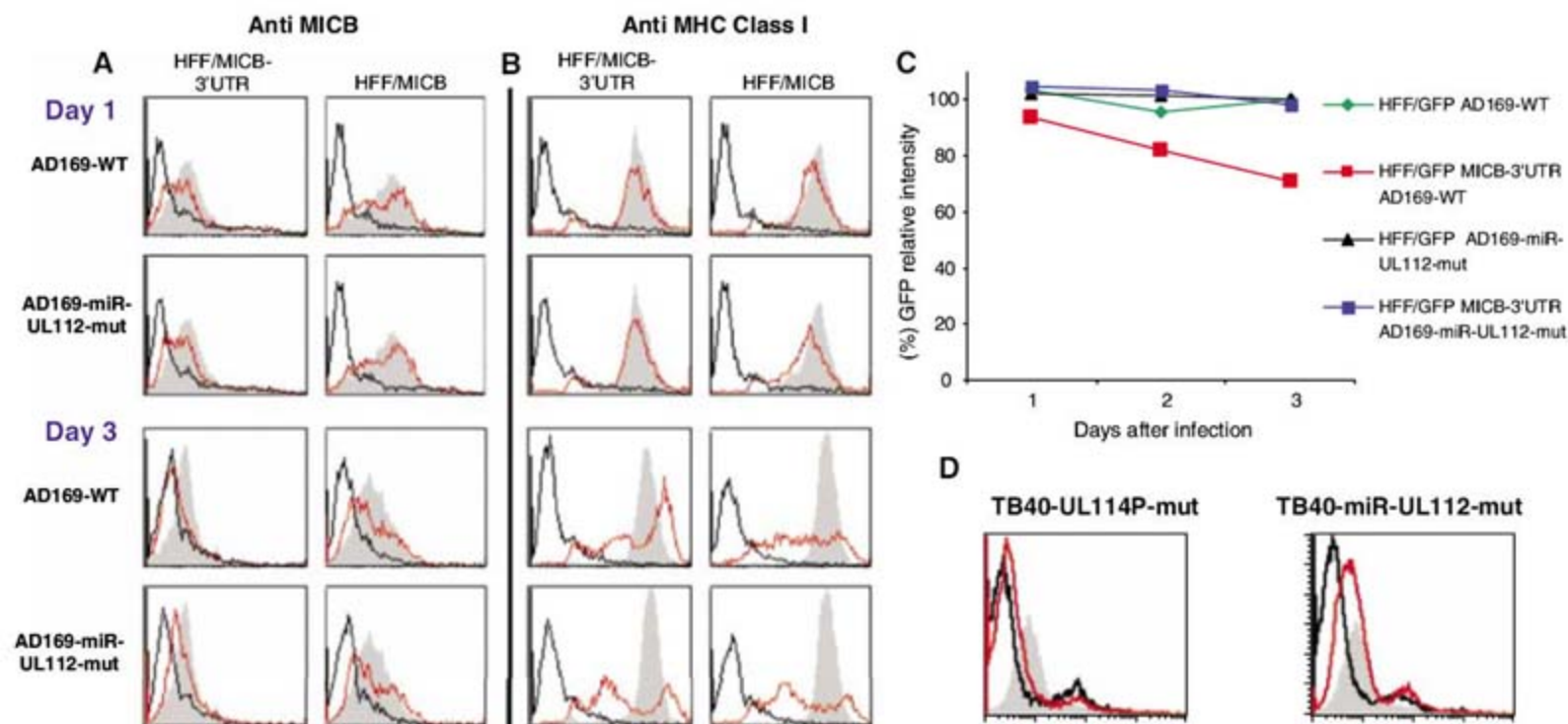
Fig. 3. hcmv-miR-UL112–mediated down-regulation of MICB during authentic viral infection. (**A** and **B**) Time course expression of MICB (A) and MHC class I (B) on HFF cells expressing either MICB-3′UTR or only MICB. Cells were infected with either the AD169-wild-type virus (AD169-WT) or the AD169-miR-UL112 mutant virus (AD169-miR-UL112-mut). The expression levels of MICB (A) and MHC class I (B) were assessed by FACS staining (red histograms). The gray histograms represent staining of the corresponding uninfected cells. Background levels (black histogram) are the secondary fluorescein isothiocyanate (FITC)–conjugated Abs. (**C**) HFF cells expressing GFP or GFP fused to the 3′UTR of MICB were infected with either AD169-wild-type or with AD169-miR-UL112-mut viruses, and the levels of GFP expression were measured along the course of infection. The symbols represent the percentage of GFP compared to the corresponding uninfected cells. For (A) to (C), one representative experiment is shown out of three performed. (**D**) HUVECs were infected with either TB40 UL114-mutant virus (TB40-UL114P mut) or with the TB40 hcmv-miR-UL112 mutant virus (TB40-miR-UL112 mut), and the expression of MICB was measured (red histograms). The gray histograms represent the staining of the corresponding uninfected cells. Background levels (black histogram) are the secondary FITC-conjugated Abs. Shown is one representative experiment out of two performed.

MICB with the TB40-UL114P-mut resulted in an almost complete down-regulation of MICB expression after 3 days, whereas MICB expression was still evident in cells infected with the TB40-miR-UL112-mut virus (Fig. 3D). The level of MHC class I was not reduced during viral infection, because the TB40 viruses we used lack the viral US2-US6 genes that mediate MHC class I down-regulation (7). This result suggests that, during clinical viral infection, endogenous MICB is down-regulated by hcmv-miR-UL112.

We next performed killing assays in parallel with the staining presented in Fig. 3, A, B, and D. On day 3 of the infection, the cells expressing MICB-3'UTR and infected with the AD169-mutant virus were killed more efficiently than those infected with the AD169-wild-type virus (Fig. 4, A and B). Similarly, HUVECs infected with the TB40-miR-UL112-mut virus were killed more efficiently than those infected with the TB40-UL114P-mut virus (Fig. 4C). Addition of anti-NKG2D mAb abolished those differences (Fig. 4, B and C). The killing levels of the infected HUVECs were low, even at higher effector:target ratios, probably because of the high levels of MHC class I molecules, which inhibit NK cytotoxicity. Thus, during authentic viral infection, hcmv-miR-UL112 down-regulates MICB, perturbing its binding with NKG2D and consequently aiding in NK attack evasion.

The discovery of viral miRNAs has raised the intriguing possibility of their involvement in immune evasion (4). The first direct evidence for an miRNA-related immunoevasion mechanism was discovered in the SV40 virus, where a viral miRNA targets a viral gene, resulting in CTL evasion (18). Our results demonstrate a novel miRNA-based evasion strategy used by HCMV, in which a viral miRNA directly down-regulates a host immune defense gene. HCMV is known to rely on several functionally redundant immunoevasive proteins that can cooperatively target the same process or even the same immune protein of the host (6). Our results expand this view, demonstrating a cooperative mechanism between a viral miRNA (hcmv-miR-UL112) and a viral protein [HCMV UL16 (12)], both targeting the host MICB protein. Down-regulation of host genes by interactions of their mRNAs with viral miRNAs has been also supported by recent findings in herpes simplex virus–1 (19). The advantages of a viral miRNA-based evasion mechanism are multiple. First, these molecules are small, nonimmunogenic, and specific (4). Second, from an evolutionary perspective it should be simpler to develop a regulatory antisense molecule rather than a regulatory protein. Lastly, the combination of protein-mediated and miRNA-mediated posttranscriptional regulation provides a tighter evasion strategy, which is more resistant to the host defense mechanisms because two immunomodulatory elements need to be impaired. The therapeutic implications of such a mechanism are intriguing, because targeting these viral miRNAs might constitute an antiviral therapy while mimicking their role could provide a means of immunosuppressive therapy.
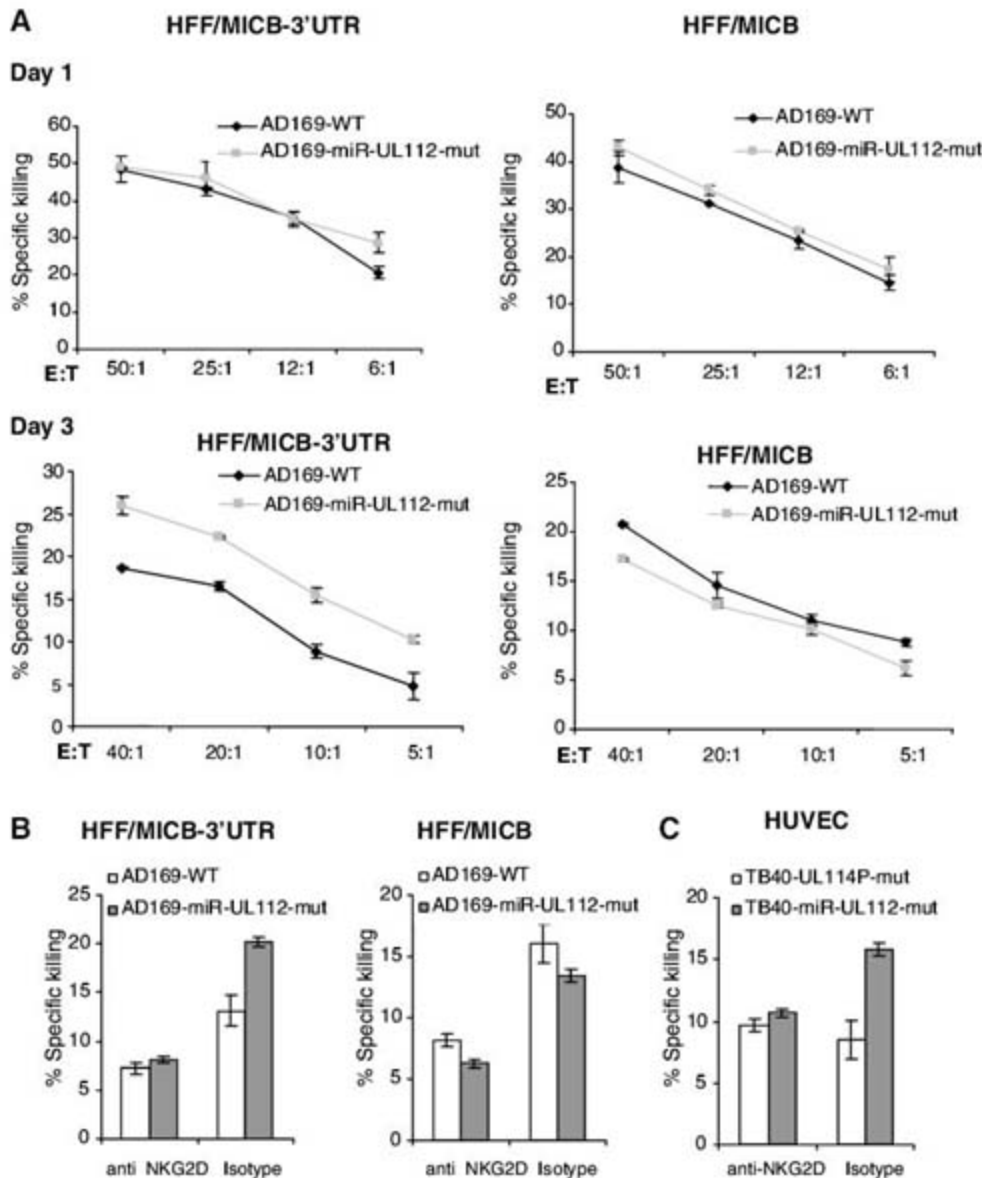
Fig. 4. hcmv-miR-UL112–mediated down-regulation of MICB during viral infection reduces NK cells cytotoxicity. Experiments were performed concomitantly with the FACS staining presented in Fig. 3. Error bars represent standard deviation of three replicates. Shown is one representative experiment out of two performed. (**A**) HFF cells expressing either MICB-3'UTR or MICB were infected with either AD169-WT (black) or with AD169-miR-UL112-mut viruses (gray) and incubated with bulk NK cells at the indicated effector:target (E:T) ratios. (**B** and **C**) Bulk NK cells were preincubated with either anti-NKG2D or with an isotype-match control mAb. In (B), HFF cells expressing either MICB-3'UTR or MICB that were infected for 3 days either with AD169-wild-type (white) or with AD169-miR-UL112-mut (gray) were then added at a final effector:target ratio of 20:1. In (C), HUVECs that were infected for 3 days either with TB40-UL114P mutant (white) or with TB40-miR-UL112 mutant (gray) were then added at a final effector:target ratio of 15:1.

References and Notes
1. D. P. Bartel, *Cell* **116**, 281 (2004).
2. S. Pfeffer *et al.*, *Nat. Methods* **2**, 269 (2005).
3. C. S. Sullivan, D. Ganem, *Mol. Cell* **20**, 3 (2005).
4. B. R. Cullen, *Nat. Genet.* **38** (suppl.), S25 (2006).
5. A. R. French, W. M. Yokoyama, *Curr. Opin. Immunol.* **15**, 45 (2003).
6. E. S. Mocarski Jr., *Cell. Microbiol.* **6**, 707 (2004).
7. Materials and methods are available as supporting material on *Science* Online.
8. N. Rajewsky, *Nat. Genet.* **38** (suppl. 1), S8 (2006).
9. S. Griffiths-Jones, R. J. Grocock, S. van Dongen, A. Bateman, A. J. Enright, *Nucleic Acids Res.* **34**, D140 (2006).
10. S. Bauer *et al.*, *Science* **285**, 727 (1999).
11. D. Cosman *et al.*, *Immunity* **14**, 123 (2001).
12. C. Dunn *et al.*, *J. Exp. Med.* **197**, 1427 (2003).
13. T. W. Nilsen, *Trends Genet.* **23**, 243 (2007).
14. M. N. Prichard, G. M. Duke, E. S. Mocarski, *J. Virol.* **70**, 3018 (1996).
15. F. Grey *et al.*, *J. Virol.* **79**, 12095 (2005).
16. E. S. Mocarski Jr., *Trends Microbiol.* **10**, 332 (2002).
17. C. Sinzger *et al.*, *J. Gen. Virol.* **80**, 2867 (1999).
18. C. S. Sullivan, A. T. Grundhoff, S. Tevethia, J. M. Pipas, D. Ganem, *Nature* **435**, 682 (2005).
19. A. Gupta, J. J. Gartner, P. Sethupathy, A. G. Hatzigeorgiou, N. W. Fraser, *Nature* **442**, 82 (2006).
20. We thank D. Cosman for the NKG2D-Ig and C. Sinzger for bacterial artificial chromosome plasmid pTB40 reagent; T. Tuschl, S. Altuvia, and D. M. Davis for useful discussions; R. Melnikov for technical support; and E. Akiva and G. Lithwick for their useful comments on the manuscript. This study was supported by grants from the

Mosaic Organization of Neural Stem Cells in the Adult Brain

Florian T. Merkle, Zaman Mirzadeh, Arturo Alvarez-Buylla*

The in vivo potential of neural stem cells in the postnatal mouse brain is not known, but because they produce many different types of neurons, they must be either very versatile or very diverse. By specifically targeting stem cells and following their progeny in vivo, we showed that postnatal stem cells in different regions produce different types of neurons, even when heterotopically grafted or grown in culture. This suggests that rather than being plastic and homogeneous, neural stem cells are a restricted and diverse population of progenitors.

Every day, thousands of new neurons are generated by astrocyte-like stem cells residing in the subventricular zone (SVZ), a thin but extensive layer of cells lining the lateral wall of the lateral ventricle in the adult mouse brain (1). These newly born neurons (neuroblasts) migrate to the olfactory bulb in a complex network of chains that eventually merge to form the rostral migratory stream (RMS). On reaching the olfactory bulb, neuroblasts integrate and mature into several distinct cell types (2). It is not known how this diversity of neurons is generated, largely because it is difficult to study individual stem cells in vivo. Indeed, our understanding of stem cells is strongly influenced by the in vitro techniques with which they were first isolated and later defined by their ability to be passaged (demonstrating self-renewal) and differentiated into astrocytes, neurons, and oligodendrocytes (demonstrating multipotency) (3, 4). These results led to the widely held assumption that neural stem cells are a homogeneous population of multipotent, plastic progenitors (Fig. 1A). Similarly, it was thought that neuroblasts born in the SVZ might be equivalent until they reach the olfactory bulb and begin to differentiate. However, recent evidence suggests that neuroblasts are heterogeneous before reaching the olfactory bulb (5, 6). We therefore hypothesized that stem cells are not equivalent and that they specify the fate of the neurons they produce (Fig. 1B). To test this hypothesis, we labeled stem cells in different regions and followed their progeny in vivo.

We have previously shown that adult neural stem cells are derived from radial glia present in

Department of Neurosurgery and Developmental and Stem Cell Biology Program, University of California, San Francisco, San Francisco, CA 94143–0525, USA.

*To whom correspondence should be addressed. E-mail: abuylla@stemcell.ucsf.edu

the neonatal (P0) mouse brain (7). Radial glia, which are now recognized as the principal stem cell of the embryonic and early postnatal mouse brain (8, 9), have a unique morphology that allows them to be targeted specifically. Their cell bodies line the ventricles and they send a long, radial process to the brain surface. Adenoviruses readily infect these processes and are transported to the cell body. When an adenovirus expressing Cre recombinase (Ad:Cre) is injected into green fluorescent protein (GFP) reporter (Z/EG) mice (10), infected radial glia and their progeny become permanently labeled with GFP (7). Because adenoviruses do not diffuse readily in the brain, the localized injection of a small volume (20 nl) of Ad:Cre labels a spatially restricted patch of neural stem cells.

To label radial glia in a regionally specific manner, we developed a method to stereotaxically inject Ad:Cre in P0 mice (Fig. 1E) (11). Injections resulted in the reproducible labeling of spatially segregated patches of radial glia (Fig. 1, C and D) and the adult SVZ stem cells they generate (Fig. 1, F and G). In contrast, cells labeled locally at the injection site do not give rise to olfactory bulb neurons or neural stem cells (7). By systematically varying the injection location (Fig. 1H), we targeted 15 different populations of radial glial cells at six different rostrocaudal levels (i to vi) (11). We targeted the dorsal (D) or ventral (V) lateral wall of the lateral ventricle at four different rostrocaudal levels (ii to v) and the entire dorsoventral extent of the lateral wall at level vi. We also targeted the RMS (i), the medial (septal) wall (iiM), and the cortical wall of the lateral ventricle (iiC to vC) because these regions have been suggested to contain neural progenitors (1, 4, 12, 13). When we analyzed the brains of mice 4 weeks after Ad:Cre injection, we observed a patch of labeled cells in the same anatomical location as the targeted radial glial cell bodies, indicating that neural stem cells do

not disperse tangentially (fig. S1). Figure 1, F and G, show examples of SVZ labeling after neonatal targeting of dorsal and ventral SVZ radial glia, respectively.

We then examined the mature GFP-labeled neurons in the olfactory bulb. The two principal types of adult-born olfactory neurons, periglomerular cells and granule cells, are interneurons that modulate the activity of neurons that project to olfactory cortex. Periglomerular cells can be subdivided into three nonoverlapping populations of cells: calretinin- (CalR+) and calbindin-expressing (CalB+) cells, and tyrosine hydroxylase-expressing (TH+) dopaminergic cells (14). Granule cells include deep, superficial, and CalR+ cells (Fig. 2A) (15, 16). These subtypes are thought to be distinct functional elements of the olfactory bulb circuitry (14, 15, 17).

Olfactory bulb interneurons were produced from all labeled regions including regions i, iiM, and iiC to vC, which extend beyond the lateral wall of the lateral ventricle, the accepted boundary of the neurogenic adult SVZ. Notably, each region gave rise to only a very specific subset of interneuron subtypes. Anterior and dorsal regions produced periglomerular cells (Fig. 2B and fig. S2, A to D). Interestingly, the highest percentage was produced in region iiM (Fig. 2B and fig. S2, A and B). Periglomerular cell subtypes were also produced in a region-specific manner. Dorsal regions (iiC to vC) produced the highest percentage of TH+ cells (Fig. 2C and fig. S3, A to C), whereas CalB+ cells were produced mainly ventrally, in regions iiV and iiiV (Fig. 2D and fig. S3, D to F). CalR+ periglomerular cells were less frequently observed when these regions were targeted, but were frequently labeled with targeting of regions i and iiM (Fig. 2E and fig. S3, G to I). Each targeted region produced granule cells (Fig. 2F), though region iiM produced relatively few (Fig. 2B and fig. S2, A and B). Dorsal regions (iiC to vC, iiD, iiiD) tended to produce superficial granule cells, whereas ventral regions (iiV to vV) produced mostly deep granule cells (Fig. 2F and fig. S2, E and H). CalR+ granule cells were produced mostly from the anterior regions (i and iiM) that also produced many CalR+ periglomerular cells (Fig. 2G and fig. S3, J to L). This is consistent with a recent study showing that CalR+ olfactory bulb neurons are derived from SP8+ cells, which are found embryonically in regions i and iiM (18).

Each neonatally targeted region continued to produce neuroblasts in the adult brain, suggesting the continued presence of a neural stem cell (fig. S2, B, D, F, and H). Neonatal radial glia convert into SVZ astrocytes that express glial fibrillary

acidic protein (GFAP) and function as the adult neural stem cells (*1, 7, 19*). To test whether adult neural stem cells were also regionally specified, we constructed an adenovirus that expresses Cre under the control of the murine GFAP promoter (Ad:GFAP-Cre). This virus induces recombination in GFAP-expressing cells including adult neural stem cells, but not the more differentiated cells they give rise to (fig. S4, A to C) (*11*). We injected P60 Z/EG mice with Ad:GFAP-Cre in regions i, iiiD, iiiV, and vC (fig. S4, D to G) and killed the animals 28 days later to examine the olfactory bulb cell types produced. Each targeted region produced olfactory bulb neurons and neuroblasts (Fig. 3, A to D), suggesting that they contain long-lived GFAP+ neurogenic progenitors. This finding agrees with previous work suggesting the presence of a neurogenic progenitor in the adult RMS (*5, 20, 21*) and subcallosal zone (regions ivC and vC) (*12*). Furthermore, these labeled cells produced superficial and deep granule cells (Fig. 3, A to E), as well as TH+, CalB+, and CalR+ cells (Fig. 3F) in virtually the same region-specific pattern obtained from neonatal labeling. A recent study suggests that the potential of progenitors to produce different types of periglomerular cells changes over development (*22*). This study might have inadvertently examined progenitors and tangentially migrating neuroblasts from different regions at different ages, whereas our technique targets only primary progenitors. The apparent maintenance of stem cell potential over postnatal development suggests that the factors specifying neural progenitors in the SVZ are maintained throughout development in a regionally specific manner.

These factors could be either environmental or intrinsic to stem cells. To distinguish between these two possibilities, we challenged neonatal stem cells by heterotopic transplantation (*11*). If environmental factors specify the fate of newborn neurons, grafted (donor) stem cells and their progeny should respond to these factors and make cell types produced in the host region. To obtain labeled neural stem cells, neonatal radial glia were infected with Ad:Cre as described above, microdissected after 2 hours, dissociated to a single-cell suspension, and homotopically or heterotopically grafted into the littermates of donor animals (fig. S5A). We then analyzed the olfactory bulb cell types produced 40 days after grafting and found that labeled radial glia continued to produce the cell types appropriate to their region of origin (fig. S5, B and C). To determine if progenitors would maintain their region-specific potential in the absence of any environmental cues, we cultured anterior, dorsal, or ventral progenitors under adherent conditions that recapitulate postnatal SVZ neurogenesis (*23*). Cultures were expanded, differentiated (fig. S5D), and immunostained for cell type–specific markers (fig. S6). Despite being removed from their complex environment and exposed to a cocktail of growth factors, neural stem cells maintained their region-specific potential (fig.

S5E). We confirmed this result by targeting dorsal or ventral radial glia, culturing them for 2 weeks, and grafting them heterotopically into wild-type neonatal mice (fig. S5F). Again, grafted cells produced cell types appropriate to their region of origin, not their grafted location (fig. S5G).

The above experiments suggest that neural stem cells are not readily respecified by environmental factors present in the postnatal brain, but we cannot eliminate the possibility that unlabeled cells grafted alongside labeled stem cells could be carrying factors from the donor environment into the host graft site. Therefore, we microdissected progenitors from different regions of neonatal wild-type or ActB-GFP mice

(*24*) and cultured them for three passages over 2 weeks. To ensure that grafted cells were surrounded by foreign environmental cues, we mixed GFP+ cells from the donor region with a 10:1 excess of unlabeled wild-type cells from the host region before grafting them into wild-type neonatal mice (Fig. 4A). Four weeks later, grafted brains contained labeled astrocyte-like cells at the graft site (fig. S7, A, C, E, and G) and mature neurons in the olfactory bulbs (fig. S7, B, D, F, and H). Because grafted cells continued to produce neuroblasts as efficiently as directly targeted primary progenitors (fig. S8), grafted cells were most likely stem cells and not intermediate progenitors. Again, heterotopically grafted stem cells produced neuronal subtypes
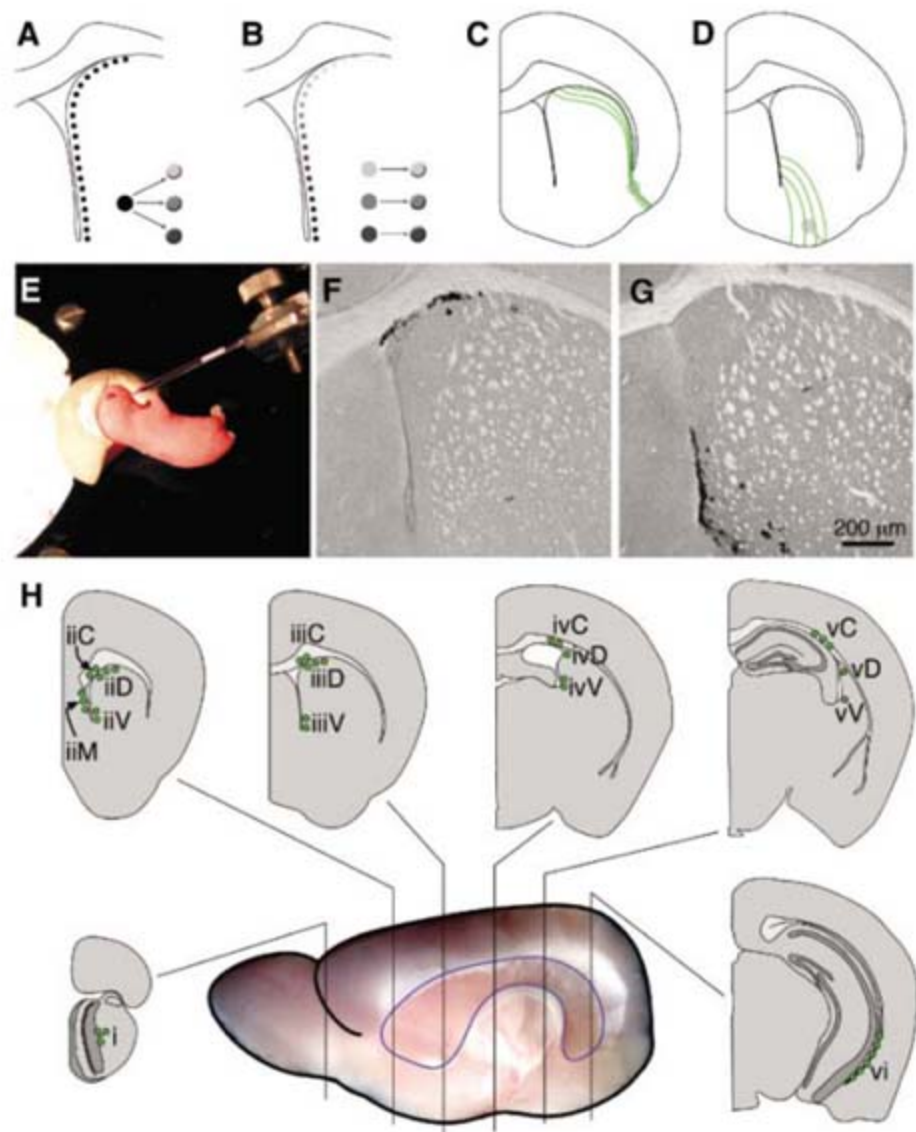
Fig. 1. Specific regional targeting of neural stem cells. (**A** and **B**) In the traditional model of SVZ stem cell potential (A), equivalent stem cells (black dots) generate multiple neuron types, which are produced by a diverse stem cell population in the proposed model (B). (**C** and **D**) Diagram of a neonatal mouse brain showing targeting of dorsal (C) or ventral (D) radial glia (green) with virus deposited at the injection site and along the needle tract (gray circle and bar). (**E**) Stereotaxic setup showing an acrylic model of a neonatal pup positioned in a customized head mold for viral injection parallel to radial glial processes. (**F** and **G**) Photomicrograph of a P28 Z/EG brain injected at P0 to target dorsal (F) or ventral (G) radial glia, visualized with immunoperoxidase staining for GFP. (**H**) Diagram of brain regions targeted. Representative frontal sections of the right hemisphere traced from the adult brain are shown relative to a photomicrograph of an adult lateral ventricular wall whole mount outlined in blue (*30*). Targeted regions, indicated by green dots, are named for their anterior-posterior level (i to vi) followed by the location within that level, where C is cortical, M is medial, D is dorsal, and V is ventral.

Fig. 2. Regional production of postnatally born interneuron subtypes. (**A**) Color-coded camera lucida traces of analyzed interneuron subtypes superimposed over a photomicrograph of the olfactory bulb. EPL, external plexiform layer; IPL, internal plexiform layer; GC, granule cell; GL, glomerular layer; GRL, granule cell layer; PGC, periglomerular cell. (**B**) Percentage of labeled (GFP+) olfactory bulb neurons that are periglomerular cells. All analysis was performed 28 days after stem cell labeling, and targeted regions are named as in Fig.

1H. (**C** to **E**) Percentage of labeled periglomerular cells immunopositive for TH (C), CalB (D), or CalR (E). (**F**) Position of labeled granule cells within the GRL. Cell distributions that could not be definitively classified as superficial (green) or deep (blue) are indicated in teal. (**G**) Percentage of labeled granule cells immunopositive for CalR. Error bars represent the SD of the mean, except in (F), where they represent the SEM.
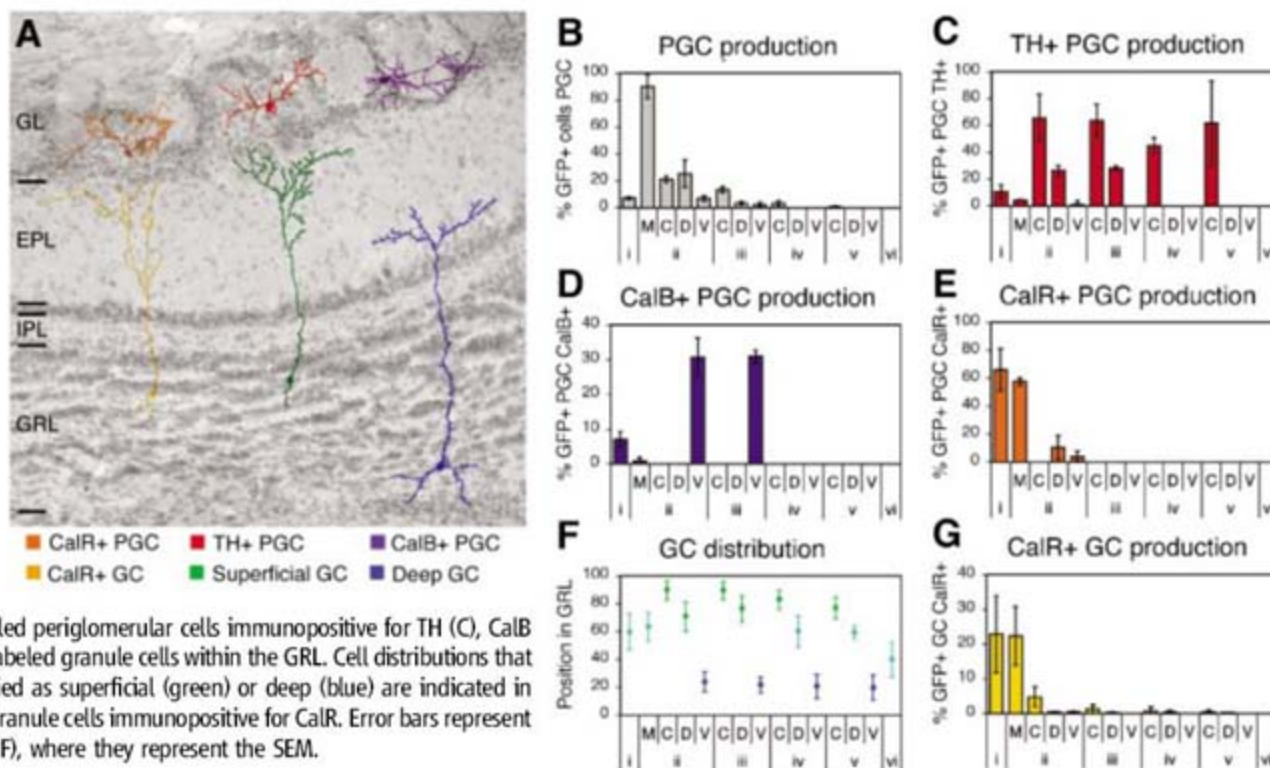
Fig. 3. The potential of neural stem cells is maintained in the adult. (**A** to **D**) Photomicrographs of olfactory bulbs of Z/EG mice injected with Ad:GFAP-Cre 28 days earlier at P60 in region i (A), iiiD (B), iiiV (C), or vC (D), with cells visualized by immunoperoxidase staining for GFP. The distribution of granule cells within the granule cell layer (GRL) and the continued presence of neuroblasts in the olfactory bulb core (arrowheads) are indicated. (**E** and **F**) Quantification of labeled granule cell position in the GRL (E) and TH+ (red), CalB+ (purple), and CalR+ (gold) cell production (F) 28 days after radial glial (P0) or adult (P60) stem cell targeting.
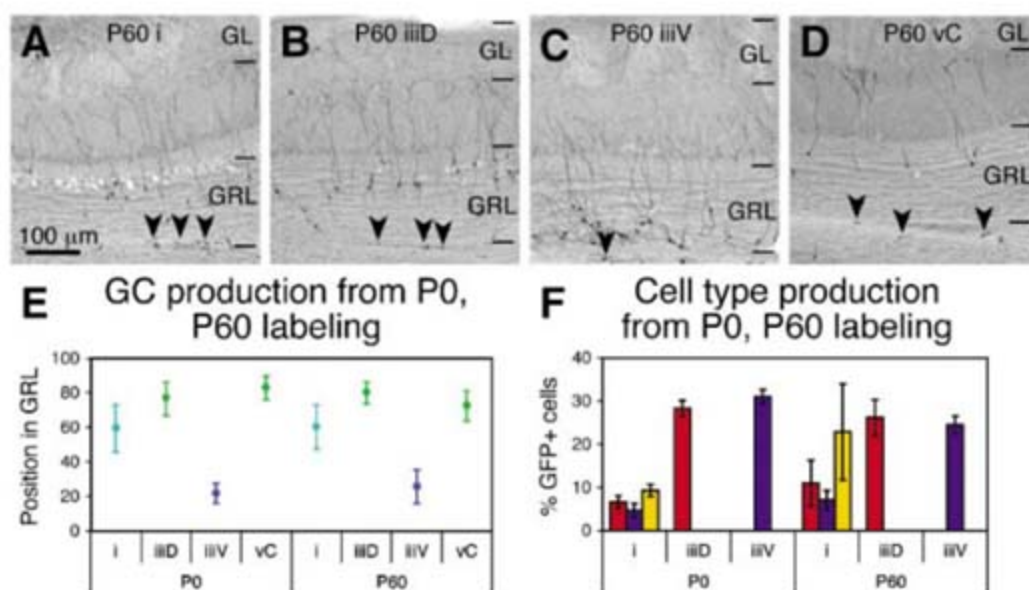
with the same regional specificity observed by in vivo lineage tracing (Fig. 4, B to E). The lack of evidence for even partial respecification indicates that grafted cells behaved like a single population that was resistant to respecification. However, we cannot discard the possibility that some environmental factors were not totally eliminated in our experiments. Neural stem cell potential could also be altered by factors not included in our culture conditions or after extended periods of time ex vivo. Previous studies have suggested that adult hippocampal or spinal cord progenitors might be respecified when heterotopically grafted (25, 26). Our findings suggest that although SVZ neural stem cells retain the potential to produce astrocytes, oligodendrocytes, and neurons, they are restricted in the types of neurons they can generate. We conclude that postnatal neural stem cells are diverse and are organized in an intricate mosaic in the postnatal germinal zone.

These findings suggest that, as during embryonic brain development (27–29), the potential of postnatal neural stem cells is determined by a spatial code, supporting the model shown in Fig. 1B. Stem cells do not appear to migrate tangentially as they mature from radial glia into astrocyte-like adult cells and must have integrated positional information at some point in development. We suggest that this positional information becomes encoded in the progenitors, perhaps by expression of a transcription factor code, and maintained into adulthood. This insight is a key step toward understanding the molecular mechanisms of neural stem cell potential and for future efforts to use these cells for brain repair. The mosaic distribution of progenitors also raises the possibility that the activity of stem cells is regionally modulated in order to regulate the production of different types of neurons. This may provide a mechanism for the brain to dynamically fine tune the olfactory bulb circuitry.

References and Notes
1. F. Doetsch, I. Caille, D. A. Lim, J. M. García-Verdugo, A. Alvarez-Buylla, *Cell* **97**, 703 (1999).
2. F. H. Gage, *Science* **287**, 1433 (2000).
3. B. A. Reynolds, S. Weiss, *Science* **255**, 1707 (1992).
4. C. M. Morshead et al., *Neuron* **13**, 1071 (1994).
5. M. A. Hack et al., *Nat. Neurosci.* (2005).
6. M. Kohwi, N. Osumi, J. L. Rubenstein, A. Alvarez-Buylla, *J. Neurosci.* **25**, 6997 (2005).
7. F. T. Merkle, A. D. Tramontin, J. M. Garcia-Verdugo, A. Alvarez-Buylla, *Proc. Natl. Acad. Sci. U.S.A.* **101**, 17528 (2004).
8. S. C. Noctor et al., *J. Neurosci.* **22**, 3161 (2002).
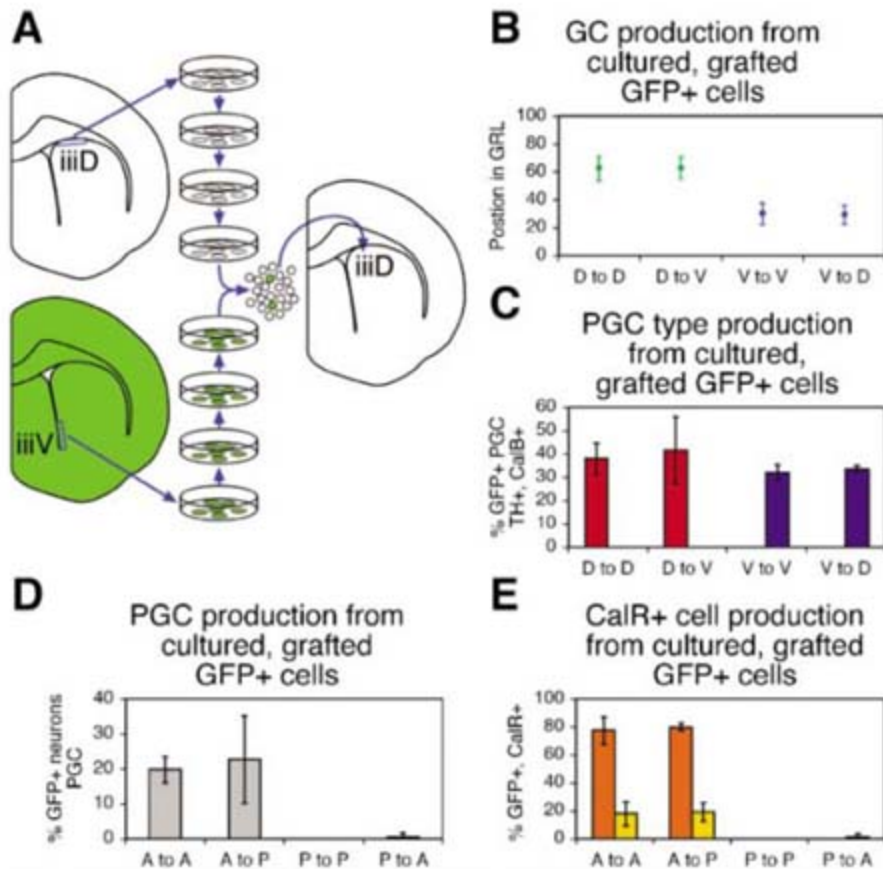
Fig. 4. Neural stem cell potential is cell-intrinsic. (**A**) Neonatal SVZ progenitors from GFP+ and wild-type mice are cultured for multiple passages, mixed 1:10, and grafted into the SVZ of a wild-type P0 host. (**B** and **C**) Quantification of granule cell distribution in the granule cell layer (B) and of TH+ (red) or CalB+ (purple) periglomerular cell production (C) by GFP+ cells from dorsal or ventral regions grafted hetero- or homotopically. (**D** and **E**) Quantification of periglomerular cell production (D) or CalR+ periglomerular (orange) and granule cell (gold) production (E) by GFP+ cells from anterior or posterior regions grafted hetero- or homotopically.

9. T. E. Anthony, C. Klein, G. Fishell, N. Heintz, *Neuron* **41**, 881 (2004).
10. A. Novak, C. Guo, W. Yang, A. Nagy, C. G. Lobe, *Genesis* **28**, 147 (2000).
11. Materials and methods are available as supporting material on *Science* Online.
12. B. Seri *et al.*, *Cereb. Cortex* **16** (suppl. 1), i103 (2006).
13. R. E. Ventura, J. E. Goldman, *J. Neurosci.* **27**, 4297 (2007).
14. K. Kosaka *et al.*, *Neurosci. Res.* **23**, 73 (1995).
15. J. L. Price, T. P. S. Powell, *J. Cell Sci.* **7**, 125 (1970).
16. D. M. Jacobowitz, L. Winsky, *J. Comp. Neurol.* **304**, 198 (1991).
17. G. M. Shepherd, C. A. Greer, in *The Synaptic Organization of the Brain*, G. M. Shepherd, Ed. (Oxford Univ. Press, New York, 1998).
18. R. R. Waclaw *et al.*, *Neuron* **49**, 503 (2006).
19. T. Imura, H. I. Kornblum, M. V. Sofroniew, *J. Neurosci.* **23**, 2824 (2003).
20. A. Gritti *et al.*, *J. Neurosci.* **22**, 437 (2002).
21. N. Fukushima, K. Yokouchi, K. Kawagishi, T. Moriizumi, *Neurosci. Res.* **44**, 467 (2002).
22. S. De Marchis *et al.*, *J. Neurosci.* **27**, 657 (2007).
23. B. Scheffler *et al.*, *Proc. Natl. Acad. Sci. U.S.A.* **102**, 9353 (2005).
24. A. K. Hadjantonakis, M. Gertsenstein, M. Ikawa, M. Okabe, A. Nagy, *Mech. Dev.* **76**, 79 (1998).
25. J. O. Suhonen, D. A. Peterson, J. Ray, F. H. Gage, *Nature* **383**, 624 (1996).
26. L. S. Shihabuddin, P. J. Horner, J. Ray, F. H. Gage, *J. Neurosci.* **20**, 8727 (2000).
27. J. L. R. Rubenstein, P. A. Beachy, *Curr. Opin. Neurobiol.* **8**, 18 (1998).
28. K. Campbell, *Curr. Opin. Neurobiol.* **13**, 50 (2003).
29. F. Guillemot, *Curr. Opin. Cell Biol.* **17**, 639 (2005).
30. F. Doetsch, A. Alvarez-Buylla, *Proc. Natl. Acad. Sci. U.S.A.* **93**, 14895 (1996).
31. We thank C. Lois for supplying Ad:Cre virus and C. Yaschine and R. Romero for assistance with cell culture and tissue processing. This work was supported by grants from the NIH and by a fellowship from the NSF for F.T.M.

Queen Pheromone Blocks Aversive Learning in Young Worker Bees

Vanina Vergoz, Haley A. Schreurs, Alison R. Mercer*

Queen mandibular pheromone (QMP) has profound effects on dopamine signaling in the brain of young worker honey bees. As dopamine in insects has been strongly implicated in aversive learning, we examined QMP's impact on associative olfactory learning in bees. We found that QMP blocks aversive learning in young workers, but leaves appetitive learning intact. We postulate that QMP's effects on aversive learning enhance the likelihood that young workers remain in close contact with their queen by preventing them from forming an aversion to their mother's pheromone bouquet. The results provide an interesting twist to a story of success and survival.

To advertise her presence in the colony and to exert influence over its members, a honey bee queen produces a complex blend of substances known as queen mandibular pheromone (QMP) (*1*). Young workers, attracted to the queen by QMP are enticed not only to feed her, but also to lick and to antennate her body. As they do so, they gather samples of QMP, which they distribute to other members of the colony (*2*, *3*). At the colony level, QMP inhibits the rearing of new queens (*4*), influences comb-building activities (*5*), helps prevent the development of worker ovaries (*6*), and modulates the behavioral development of workers (*7*, *8*).

We recently showed that brain dopamine levels, levels of dopamine receptor gene expression, and brain tissue responses to this amine are altered significantly in young workers exposed to QMP (*9*). Among its many functions, dopamine contributes to cellular events underlying learning and memory. In insects, dopamine signaling is essential for aversion learning (*10–12*), which raises an interesting question: Does QMP, through its actions on brain dopamine function in young workers, alter their ability to establish aversive olfactory memories?

We examined QMP's impact on associative olfactory learning in bees exposed to QMP from the time of adult emergence. Bees of the same age maintained under identical conditions but without exposure to QMP were used as controls. To begin, we examined QMP's effects on aversive learning in young (6-day-old) bees. A differential conditioning paradigm was used to train bees to extend their sting to an odorant paired

Department of Zoology, University of Otago, Dunedin, New Zealand.

*To whom correspondence should be addressed. E-mail: alison.mercer@stonebow.otago.ac.nz

with an aversive stimulus (mild electric shock) and not to respond to a nonreinforced odorant (*12*, *13*). Over successive conditioning trials, the percentage of control (untreated) bees responding with sting extension to the reinforced odorant (CS+) increased significantly (Fig. 1A, i), whereas the percentage of bees exhibiting sting extension in response to the nonreinforced odorant (CS–) declined [Fig. 1A, i, and supporting online material (SOM) text]. Comparison of the response curves shows that bees in the control group clearly differentiate between the two odorants (Fig. 1A, i). In a retention test performed 1 hour after the last conditioning trial, the bees responded significantly more to CS+ than to CS– (Fig. 1A, ii), which demonstrated that an aversive memory was established. In contrast, bees exposed to QMP failed to show aversive learning. There was no significant change in responsiveness to the reinforced odorant over

successive conditioning trials (SOM text) and no difference between the response curves obtained for the two odorants (Fig. 1B, i). There was also no significant difference in QMP-treated bees between the levels of responses to the two odorants 1 hour after the last conditioning trial (Fig. 1B, ii).

How selective are these effects? In *Drosophila*, synaptic output from dopamine neurons is important for aversive learning, but is not required for appetitive learning (*10*). On the basis of these findings, we predicted that, if QMP targets dopamine pathways selectively (*9*), appetitive learning in young bees should not be affected by QMP. We thus compared the ability of young QMP-treated bees and controls to associate an odorant stimulus with a sucrose reward. Appetitive learning was examined using the proboscis extension reflex (*13*, *14*). QMP-treated bees and control (untreated) bees were

trained to differentiate between an odorant stimulus paired with sucrose (CS+) and an odorant stimulus that was not reinforced (CS–). Over successive conditioning trials, the percentage of bees exhibiting proboscis extension in response to the reinforced odorant (CS+) increased significantly (controls, Fig. 2A, i; QMP-treated, Fig. 2B, i), whereas responses to the nonreinforced odorant (CS–) showed no significant change (controls, Fig. 2A, i; QMP-treated, Fig. 2B, i, and SOM text). The response curves show that bees in both groups clearly differentiate CS+ from CS– (Fig. 2). Moreover, in retention tests performed 1 hour after the last conditioning trial, both groups responded significantly more to CS+ than to CS– (controls, Fig. 2A, ii; QMP-treated, Fig. 2B, ii). These results are consistent with evidence that the reinforcing capacity of sucrose in associative olfactory discrimination tasks is mediated not by dopamine, but by octopamine (*10*, *15*, *16*), an amine that is not affected by the presence or absence of queen pheromone (*17*).

What is responsible for mediating the QMP effects on aversive learning in young workers? The aromatic compound, 4-hydroxy-3-methoxyphenylethanol (homovanillyl alcohol, HVA) is a major contributor to QMP's effects on dopamine signaling in the brain (*9*). To examine HVA's contribution to QMP's effects on aversive learning, we treated newly emerged adults with HVA alone (*13*). Two control groups were included for comparison: untreated bees and bees treated with the QMP component, methyl *p*-hydroxybenzoate (HOB) (*1*). In contrast to HVA, HOB does not modulate brain dopamine function in young worker bees (*9*).

We found clear evidence of aversive learning in both untreated bees (fig. S1) and bees treated with HOB. As a result of conditioning, the percentage of bees responding with sting extension to the reinforced odorant increased significantly, whereas responses to the nonreinforced odorant decreased (Fig. 3A, i, and SOM text). In both groups, bees clearly differentiated between CS+ and CS– (controls, fig. S1; HOB-treated, Fig. 3A, i), and the level of responses to CS+ was still significantly higher than the level of responses to CS– 1 hour after the last conditioning trial (controls, fig. S1; HOB-treated, Fig. 3A, ii).

In bees treated with HVA, learning was impaired. Over successive conditioning trials, the percentage of HVA-treated bees responding to CS+ declined, mirroring responses to CS– (Fig. 3B, i, and SOM text). Comparison of the response curves for CS+ and CS– revealed no significant difference between the levels of responses to the two odorants (Fig. 3B, i). One hour after the last conditioning trial, the level of responses to CS+ was significantly higher than to CS– (Fig. 3B, ii), which suggested that in some HVA-treated bees an aversive memory was established. However, the percentage of HVA-treated bees exhibiting a conditioned response was significantly lower than that of controls (Fig. 3B, ii).
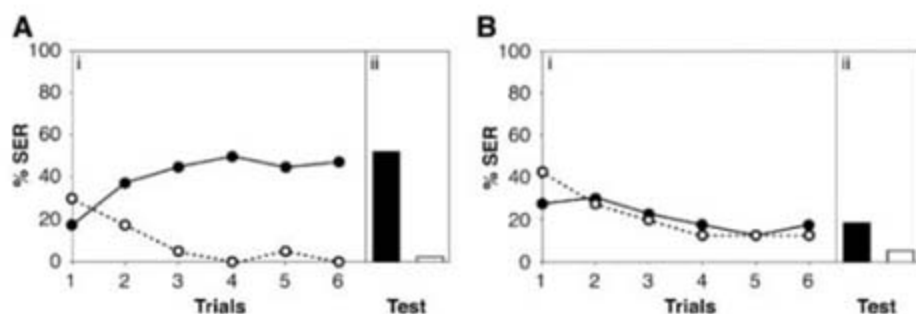
Fig. 1. Effects of QMP on aversive learning in 6-day-old workers. Associative olfactory conditioning of the sting extension response (SER) was used to compare aversive learning in (**A**) control bees and (**B**) bees treated with QMP. Bees were trained to discriminate between an odorant paired with electric shock (CS+, filled circles) and an odorant that was not reinforced (CS–, open circles). (A) (i) After 12 conditioning trials (6 with CS+ and 6 with CS–), control bees clearly discriminated between the two odorants [$F(1,78) = 31.86$, $P < 0.0001$]. (A) (ii) One hour after the last conditioning trial, a significantly higher percentage of controls responded with sting extension to the odorant associated with electric shock (black bar) than to the nonreinforced odorant (white bar) ($\chi^2 = 18.05$; $P < 0.0001$). (B) (i) QMP-treated bees did not learn to discriminate between the two odorants as a result of conditioning [$F(1,78) < 0.0001$, not significant (n.s.)]. (B) (ii) One hour after the last conditioning trial, the percentage of bees responding to the two odorants was similar ($\chi^2 = 3.2$, n.s.).
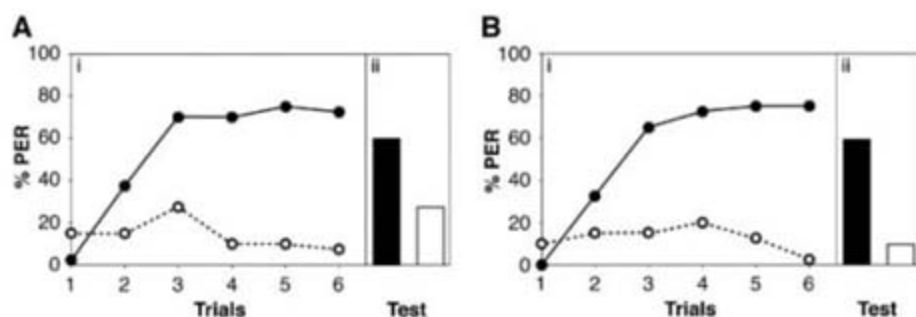
Fig. 2. Effects of QMP on appetitive learning in 6-day-old workers. Associative olfactory conditioning of the proboscis extension response (PER) was used to compare appetitive learning in (**A**) controls and (**B**) bees treated with QMP. Bees were trained to discriminate between an odorant paired with sucrose (CS+, filled circles) and a nonreinforced odorant (CS–, open circles). (A) (i) After 12 conditioning trials (6 with CS+ and 6 with CS–), control bees clearly discriminated between the two odorants [$F(1,78) = 48.51$, $P < 0.0001$]. (A) (ii) One hour after the last conditioning trial, a significantly higher percentage of controls responded with proboscis extension to the odorant associated with sucrose (black bar) than to the nonreinforced odorant (white bar) ($\chi^2 = 13.47$, $P = 0.0002$). (B) (i) QMP-treated bees learned to discriminate between the two odorants [$F(1,78) = 44.6$, $P < 0.0001$]. (B) (ii) One hour after the last conditioning trial, the percentage of bees responding to the reinforced odorant (black bar) was significantly higher than the percentage of bees responding to the nonreinforced odorant (white bar) ($\chi^2 = 7.83$, $P = 0.005$).
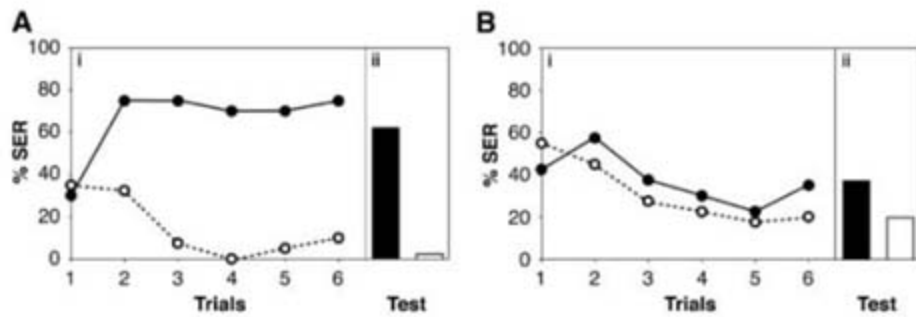
Fig. 3. Effects of (**A**) HOB and (**B**) HVA on aversive learning in 4-day-old workers. Bees were trained to discriminate between an odorant paired with an electric shock (CS+, filled circles) and a nonreinforced odorant (CS−, open circles). (A) (i) HOB-treated bees clearly discriminate between the two odorants [$F(1,78) = 84.61$, $P < 0.0001$]. (A) (ii) One hour after the last conditioning trial, a higher percentage of bees responded with sting extension to the odorant paired with electric shock (black bar) than to the nonreinforced odorant (white bar) ($\chi^2 = 24$, $P < 0.0001$). (B) (i) Comparison of the response curves for CS+ and CS− revealed no significant difference between the levels of responses to the two odorants in HVA-treated bees [$F(1,78) = 0.83$, n.s.]. (B) (ii) One hour after the last conditioning trial, a higher percentage of HVA-treated bees responded with sting extension to the reinforced odorant (black bar) than to the nonreinforced odorant (white bar) ($\chi^2 = 4$, $P = 0.045$). However, the percentage of bees exhibiting conditioned responses is significantly lower in HVA-treated bees than in HOB-treated bees ($\chi^2 = 9.26$, $P = 0.002$).
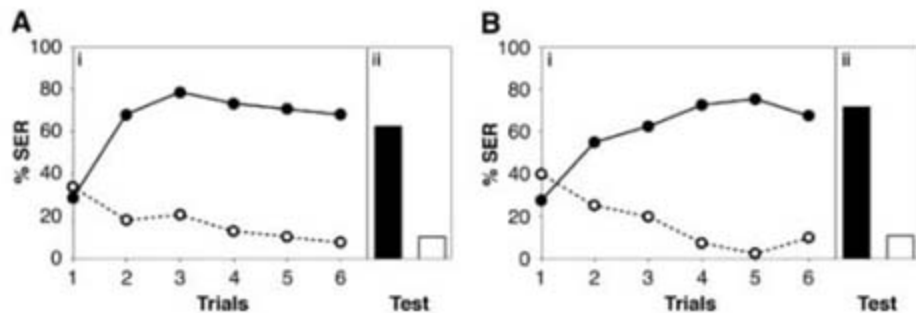
Fig. 4. Effects of QMP on aversive learning in 15-day-old workers. Associative olfactory conditioning of the SER was used to compare aversive learning in (**A**) control bees and (**B**) bees treated for 15 days with QMP. Bees were trained to discriminate between an odorant paired with electric shock (CS+, filled circles) and an odorant that was not reinforced (CS−, open circles). After conditioning, bees in both groups clearly discriminated between the two odorants [(A) (i) $F(1,78) = 53.7$, $P < 0.0001$; (B) (i) QMP-treated bees $F(1,78) = 47.96$, $P < 0.0001$]. One hour after the last conditioning trial, a significantly higher percentage of bees responded with sting extension to the odorant associated with electric shock (black bar) than to the nonreinforced odorant (white bar); [(A) (ii) $\chi^2 = 18.05$, $P < 0.0001$; (B) (ii) QMP-treated, $\chi^2 = 20.05$, $P < 0.0001$].

Despite being exposed to queen pheromone, forager bees show aversion learning (*12*). How can this be explained? Some QMP effects, including QMP's ability to elicit retinue behavior, are age-dependent (*2*, *3*). We examined aversion learning in bees exposed to QMP for 15 days (Fig. 4) (*13*) and found that both QMP-treated bees (Fig. 4A) and controls (Fig. 4B) showed robust aversion learning. These results indicate that QMP's effects on associative olfactory learning and, presumably, also those of HVA alone, depend on worker age.

HVA has recently been identified as the pheromone most important for increasing queen survival (*18*). This suggests that HVA blocking of aversive learning in young workers is somehow advantageous to the queen. One possibility is that high dosages of QMP experienced by workers attending the queen have unpleasant side effects. Previous reports have shown, for example, that QMP in high concentrations can be repellent to workers (*19*, *20*) and can elicit aggression (*21*, *22*), behaviors that could jeopardize the survival of the queen. By blocking the establishment of aversive memories, young bees would be prevented from forming an association between QMP and any unpleasant side effects induced by high dosages of this pheromone. This would confer significant benefit, as it would increase the likelihood of workers' remaining in attendance of the queen. Retinue behavior not only ensures that the queen is constantly fed, groomed, and antennated by young workers (*1–3*), but also, that the queen's attendants facilitate the distribution of QMP throughout the colony (*23*). It is noteworthy that, for reasons that remain unclear, QMP's effects on aversive learning are age-dependent. Even in the presence of queen pheromone, older workers exhibit robust aversion learning. This is also significant, as it ensures that this important survival tool can benefit workers and contribute ultimately to the survival of the colony as a whole.

References and Notes

1. K. N. Slessor, L.-A. Kaminski, G. G. King, J. H. Borden, M. L. Winston, *Nature* **332**, 354 (1988).
2. M. L. Winston, *The Biology of the Honeybee* (Harvard Univ. Press, Cambridge, MA, 1987).
3. K. N. Slessor, M. L. Winston, Y. Le Conte, *J. Chem. Ecol.* **31**, 2731 (2005).
4. M. L. Winston, H. A. High, S. J. Colley, T. Pankiw, K. N. Slessor, *Ann. Entomol. Soc. Am.* **84**, 234 (1991).
5. M. N. Ledoux, M. L. Winston, C. I. Keeling, K. N. Slessor, Y. Le Conte, *Insectes Soc.* **48**, 14 (2001).
6. S. E. Hoover, C. I. Keeling, M. L. Winston, K. N. Slessor, *Naturwissenschaften* **90**, 477 (2003).
7. T. Pankiw, Z. Huang, M. L. Winston, G. E. Robinson, *J. Insect Physiol.* **44**, 685 (1998).
8. H. Kaatz, H. Hildebrandt, W. Engels, *J. Comp. Physiol. B* **162**, 588 (1992).
9. K. T. Beggs *et al.*, *Proc. Natl. Acad. Sci. U.S.A.* **104**, 2460 (2007).
10. M. Schwaerzel *et al.*, *J. Neurosci.* **23**, 10495 (2003).
11. S. Unoki, Y. Matsumoto, M. Mizunami, *Eur. J. Neurosci.* **22**, 1409 (2005).
12. V. Vergoz, E. Roussel, J.-C. Sandoz, M. Giurfa, *PLoS ONE* **2**, e288 (2007).
13. Materials and methods are available as supporting material on *Science* Online.
14. R. Menzel, U. Müller, *Annu. Rev. Neurosci.* **19**, 379 (1996).
15. M. Hammer, *Nature* **366**, 59 (1993).
16. M. Hammer, R. Menzel, *J. Neurosci.* **15**, 1617 (1995).
17. J. W. Harris, J. Woodring, *Comp. Biochem. Physiol.* **111C**, 271 (1995).
18. J. Rhodes, D. Somerville, *Introduction and Early Performance of Queen Bees* (Publication no. 03/049, ISBN 0642 58497 4, Rural Industries Research and Development Corporation, Australian Government, Kingston, ACT, Australia, 2003).
19. J. S. Pettis, M. L. Winston, K. N. Slessor, *Entomol. Soc. Am.* **88**, 580 (1995).
20. R. F. A. Moritz, R. M. Crewe, H. R. Hepburn, *Ethology* **107**, 465 (2001).
21. M. N. Pham, B. Roger, J. Pain, *Apidologie* **13**, 143 (1982).
22. G. Vaitkevičiené, A. Budriené, *Pheromones* **6**, 39 (1999).
23. K. Naumann, M. L. Winston, K. N. Slessor, G. D. Prestwich, F. X. Webster, *Behav. Ecol. Sociobiol.* **29**, 321 (1991).
24. We thank K. Garrett for maintaining the honey bee colonies and K. Miller for assisting with the formatting of the figures. We are also grateful to K. Beggs, L. Crosbie and J. McQuillan for their very helpful comments during the preparation of this manuscript. This research was supported by a grant from the Royal Society of New Zealand, Marsden Fund to ARM (UOO312).

Oscillating Diamond Knife

The Diatome UltraSonic Oscillating Diamond Knife produces ultrathin sections free from compression. The patented knife overcomes the problems of compression even in room temperature sections, which can be as much as 20 percent with conventional sectioners.

Diatome U.S. For information 215-412-8390 www.emsdiasum.com

PCR Reagents

The TaqMan Gene Expression Master Mix and TaqMan Genotyping Master Mix reagents are formulated for exceptional sensitivity and reproducibility for both routine and challenging real-time polymerase chain reaction (PCR) applications. When used as part of TaqMan-based quantitative real-time PCR protocols, the TaqMan Gene Expression Master Mix helps researchers to detect low expressed genes, perform duplex PCR of a target and reference gene, and distinguish between similar DNA or RNA sequences. When included as part of TaqMan-based single nucleotide polymorphism genotyping protocols, the TaqMan Genotyping Master Mix generates high-quality genotyping data with distinct, well-separated clusters of alleles.

Applied Biosystems For information 800-327-3002 www.appliedbiosystems.com/taqman

Custom DNA–Peptide Conjugates

A new synthesis service for custom DNA–peptide conjugates features the native chemical ligation approach involving linking a cysteine in one moiety (either peptide or DNA) to an activated thioester terminus in the others. Customers can provide their own DNA or peptide for conjugation or Activotec can synthesize the DNA and peptide to be conjugated.

Activotec For information +44 1223 260008 www.activotec.com

Aequorin Option for Screening System

A new aequorin option for the FLIPR Tetra fluorometric imaging plate reader includes a uniquely designed camera that can detect both fluorescence and aequorin luminescence. It also includes a cell suspension option. Both the camera and cell suspension option are optimized to enable researchers to expand their calcium mobilization assays to include aequorin luminescence measurements. The new option enables cell suspension assays, thereby minimizing cell preparation time and reducing assay costs.

Molecular Devices For information 408-747-3514 www.moleculardevices.com

Methyltransferase Assay

SAM (S-Adenosylmethionine) Methyltransferase Assay is a continuous enzyme-coupled assay for the measurement of methyltransferase activity. The assay can be used for a large family of enzymes that use SAM as a substrate. The assay does not require radioactively labeled samples or endpoint measurement with ultraviolet detection.

Genotech/G-Biosciences For information 800-628-7730 www.GBiosciences.com

Single-Stranded DNA

CircLigase ssDNA Ligase efficiently catalyzes the circularization of single-stranded DNA (ssDNA) of greater than 30 bases without the need for oligonucleotide "bridges." Virtually no linear or circular concatamers are produced. This ligase is suitable for preparing circular ssDNA for rolling circle replication or rolling circle transcription assays.

Epicentre Biotechnologies For information 800-284-8474 www.epibio.com/CircLigase.asp

Long Wavelength UV Plates

Krystal-UV plates are a range of clear-bottomed microplates designed for performance in the long wavelength ultraviolet (UV) range. They are available in 24-well, 96-well, and 384-well formats and in black or white polystyrene. They offer excellent photometric performance down to 325 nm. Wavelengths below 350 nm are particularly useful for a variety of fluorescent assays such as HNK-1 and thioguanine, as well as many absorbance assays, including vitamin A, retinol and retinyl acetate, caspase, acid phosphatase, and hydroxyproline.

Porvair Sciences For information +44 1932 240255 www.porvair-sciences.com

DLS Microplate Instrument

The HorizonDLS is a dynamic light scattering (DLS) instrument that features patented single mode fiber optical detection, dual attention technology, and independent temperature control of microplate and sample. The HorizonDLS delivers sensitivity on ultra-low sample volumes automatically from the entire plate or selected wells, with no user interaction required. After the prepared microplate is manually or robotically placed in the temperature-controlled instrument, intuitive software automatically makes the measurements according to the user-programmed acquisition sequence. The results are displayed in seconds. A complete size distribution of an entire microplate can be automatically accomplished in just minutes. The instrument's applications include screening of aggregates prior to protein crystallization, monitoring size and aggregation as a function of varying solution conditions, buffer optimization, and characterization and screening of biotherapeutics for self-association.

Viscotek Europe For information +44 1344 467180 www.viscotek.com

Newly offered instrumentation, apparatus, and laboratory materials of interest to researchers in all disciplines in academic, industrial, and government organizations are featured in this space. Emphasis is given to purpose, chief characteristics, and availability of products and materials. Endorsement by *Science* or AAAS of any products or materials mentioned is not implied. Additional information may be obtained from the manufacturer or supplier.

POSITIONS OPEN

TENURE-TRACK FACULTY POSITION
Infectious Diseases

The Department of Veterinary Microbiology and Pathology, College of Veterinary Medicine, Washington State University (WSU), invites applications for a full-time, tenure-track position in infectious diseases. This position will be defined as 50 to 60 percent research and 40 to 50 percent teaching, depending on the goals of the individual who fills it. The anticipated start date is May 1, 2008, or before. The faculty member will be expected to develop and maintain an independent extramurally funded research program that interfaces with active research programs within the College of Veterinary Medicine. The Department is extremely collaborative. Active, funded research groups are focused on the immunology, pathogenesis, epidemiology, and genomics of infectious organisms that produce disease in animals and/or are zoonotic in nature. Zoonotic agents include food- and water-borne pathogens for which animals are important hosts. The Department's research programs are enhanced by NIH-funded training grants and are located in excellent facilities on the WSU campus. Preference will be given to candidates with demonstrated abilities in attracting funding, conducting and publishing the results of hypothesis-based research, and interest in high-quality graduate education. A Ph.D. and D.V.M. or equivalent degree is required, as well as a research focus on infectious disease and a commitment to excellent teaching in a clinically relevant context. The teaching responsibility includes teaching and directing veterinary bacteriology, a core course in WSU's professional veterinary medicine curriculum. The successful candidate will also be expected to work closely with other teaching faculty in the Department, and be actively involved in the Department's collaborative teaching efforts. The position is anticipated to be at the level of **ASSISTANT or ASSOCIATE PROFESSOR.** Applicants for an Associate Professor level position must have a strong publication record, current extramural funding, and excellent teaching credentials. Review of applications will begin July 20, 2007. Submit letter of application, curriculum vitae, and names and addresses of three references to: **Dr. Stephen Hines, c/o Ms. Sue Zumwalt, College of Veterinary Medicine, Washington State University, P.O. Box 647040, Pullman, WA 99164-7040.** The application letter should indicate the applicant's short and long-term goals regarding both research and teaching. It should also outline his/her qualifications for the position described. Protected group members are encouraged to apply. For more information see **website: http://www.vetmed.wsu. edu/employment/.** *WSU is an Equal Employment Opportunity/Affirmative Action Employer.*

EVOLUTIONARY BIOLOGY

The University of Oregon Center for Ecology and Evolutionary Biology (CEEB; **website: http:// evolution.uoregon.edu/**) and the Department of Biology invite applications for a tenure-track position (**ASSISTANT PROFESSOR**) in evolutionary biology. We are particularly interested in candidates studying the evolution of biological processes at the molecular level in order to address fundamental questions in evolutionary biology. The successful candidate will have an outstanding research program and a commitment to excellence in teaching. Ph.D. required. Applicants should submit curriculum vitae, statement of research interests, statement of teaching philosophy, and three letters of recommendation to: **Evolution Search Committee, Department of Biology, 1210 University of Oregon, Eugene, OR 97403-1210.** To ensure full consideration, applications should be received by September 5, 2007.

The University of Oregon is an Equal Opportunity/ Affirmative Action Institution committed to cultural diversity and compliance with the Americans with Disabilities Act. Women and minorities are encouraged to apply. We invite applications from qualified applicants who share our commitment to diversity.

POSITIONS OPEN

Texas A&M University, Chemistry. Nominations of renowned leaders in any area of chemistry are solicited for the **DOHERTY-WELCH CHAIR** and the **BARTON-WELCH CHAIR** in the Department of Chemistry at Texas A&M University. Nominations and inquiries should be made to: **David H. Russell, Head; Department of Chemistry; Texas A&M University; College Station, TX 77843-3255** (telephone: 979-845-9829; e-mail: chemhead@ mail.chem.tamu.edu).

This search is part of an extraordinary hiring program in all areas and ranks. *We strongly encourage applications from women, minorities, dual career couples, veterans, and individuals with disabilities.*

TWO TENURE-TRACK FACULTY POSITIONS
Infectious Diseases/Microbial Immunology

The Department of Veterinary Microbiology and Pathology in the Washington State University, College of Veterinary Medicine invites applications for two full-time (12-month) tenure-track positions in infectious diseases. The positions will be at the **ASSISTANT PROFESSOR** level and are defined as approximately 85 percent research and 15 percent teaching. A Ph.D. or clinical Doctorate (D.V.M., M.D.) with a minimum of two years of postdoctoral experience is required. The successful candidates will have evidence of conducting and publishing high-quality results from hypothesis-based research, potential for attracting extramural funding, interest in high-quality graduate education, and commitment to mentoring undergraduate and professional students in research. The faculty member will be expected to teach graduate level courses and develop and maintain an independent extramurally funded research program that interfaces with ongoing infectious diseases research within the Department, College, and University. Active, well-funded research groups are focused on the immunology, pathogenesis, epidemiology, and genomics of animal pathogens and zoonotic agents. Research training at the undergraduate, graduate, and postdoctoral levels are supported by NIH training programs, and the faculty member is expected to actively participate in these programs at all levels. Review of applications will begin August 15, 2007. Submit the letter of application, curriculum vitae, and letters of support from three references to: **Dr. Guy Palmer, c/o Ms. Sue Zumwalt** by e-mail: szumwalt@vetmed.wsu.edu, **College of Veterinary Medicine, Washington State University, P.O. Box 647040, Pullman, WA 99164-7040.** For more information see **website: http://www.vetmed. wsu.edu/employment/.** *WSU is an Equal Employment Opportunity/Affirmative Action Employer. Protected group members are encouraged to apply.*

The School of Forest Resources and Environmental Science at Michigan Technological University invites applications for a tenure-track, nine-month faculty position in the area of wetland science at the **ASSISTANT PROFESSOR** level. Candidates must possess a Ph.D. at the time of appointment. Preference will be given to candidates with research and teaching experience in wetland ecology, biogeochemistry, soils, or hydrology. Responsibilities include teaching three courses per academic year and development of a vigorous, extramurally funded research program supporting Master's and doctoral students. For additional information see **website: http://forest.mtu.edu/faculty/openings/.**

To apply, send curriculum vitae, copies of transcripts, names of three references, a one-page statement of research interests, and a one-page statement of teaching philosophy to: **Dr. Blair Orr, Wetland Scientist Search Committee, School of Forest Resources and Environmental Science, Michigan Technological University, 1400 Townsend Drive, Houghton, MI 49931-1295.** Review of applications will begin October 1, 2007, and will continue until the position is filled.

Michigan Technological University is an Equal Opportunity Education Institution/Equal Opportunity Employer.

OFFICE OF PORTFOLIO ANALYSIS AND STRATEGIC INITATIVES
DIRECTOR, DIVISION OF STRATEGIC COORDINATION

The Office of the Director, National Institutes of Health (NIH) in Bethesda, Maryland, is seeking a Director of the Division of Strategic Coordination (DSC) within the Office of Portfolio Analysis and Strategic Initiatives (OPASI). If you are an exceptional candidate with an M.D. and/or Ph.D., we encourage your application.

The OPASI's primary objective is to develop: a transparent process of planning and priority-setting characterized by a defined scope of review with broad input from the scientific community and the public; valid and reliable information resources and tools, including uniform disease coding and accurate, current and comprehensive information on burden of disease; an institutionalized process of regularly scheduled evaluations based on current best practices; the ability to weigh scientific opportunity against public health urgency; a method of assessing outcomes to enhance accountability; and a system for identifying areas of scientific and health improvement opportunities and supporting regular trans-NIH scientific planning and initiatives.

As the DSC Director, you will be responsible for integrating information and developing recommendations to inform the priority-setting and decision-making processes of the NIH in formulating NIH-wide strategic initiatives. These initiatives will address exceptional scientific opportunities and emerging public health needs (akin to the Roadmap, Obesity, and Neuroscience Blueprint initiatives). You will also be responsible for providing the NIH Director with the information needed to allocate resources effectively for trans-NIH efforts.

Salary is commensurate with experience and includes a full benefits package. A detailed vacancy announcement with the mandatory qualifications and application procedures can be obtained on **USAJOBS at www.usajobs.gov (announcement number OD-07-172844-T42) and the NIH Web Site at http://www.jobs.nih.gov**. Questions on the application procedures may be addressed to **Brian Harper on 301-594-5332**. Applications must be received by midnight eastern standard time on **August 10, 2007.**

OFFICE OF PORTFOLIO ANALYSIS AND STRATEGIC INITATIVES
DIRECTOR, DIVISION OF EVALUATION AND SYSTEMIC ASSESSMENTS

The Office of the Director, National Institutes of Health (NIH) in Bethesda, Maryland, is seeking a Director of the Division of Evaluation and Systemic Assessments (DESA) within the Office of Portfolio Analysis and Strategic Initiatives (OPASI). If you are an exceptional candidate with an M.D. and/or Ph.D. and the vision and ability to integrate evaluation systems and programs across multiple disciplines and organizations, we encourage your application.

The OPASI's primary objective is to develop: a transparent process of planning and priority-setting characterized by a defined scope of review with broad input from the scientific community and the public; valid and reliable information resources and tools, including uniform disease coding and accurate, current and comprehensive information on burden of disease; an institutionalized process of regularly scheduled evaluations based on current best practices; the ability to weigh scientific opportunity against public health urgency; a method of assessing outcomes to enhance accountability; and a system for identifying areas of scientific and health improvement opportunities and supporting regular trans-NIH scientific planning and initiatives.

As the DESA Director, you will be responsible for planning, conducting, supporting, and coordinating, specific program evaluations and projects of NIH Institutes and Centers such as the Roadmap, Obesity, and Neuroscience Blueprint initiatives. In addition, you will serve as the liaison for conducting governmentally required assessments according to the Government Performance and Results Act (GPRA) and OMB Program Assessment Rating Tool (PART). You will also serve as a member of the OPASI Steering Committee involved in oversight of institution-wide planning and analysis.

Salary is commensurate with experience and includes a full benefits package. A detailed vacancy announcement with the mandatory qualifications and application procedures can be obtained on **USAJOBS at www.usajobs.gov (announcement number OD-07-172847-T42) and the NIH Web Site at http://www.jobs.nih.gov**. Questions on the application procedures may be addressed to **Brian Harper on 301-594-5332**. Applications must be received by midnight eastern standard time on **August 10, 2007**.

OFFICE OF PORTFOLIO ANALYSIS AND STRATEGIC INITATIVES
DIRECTOR, DIVISION OF RESOURCE DEVELOPMENT AND ANALYSIS

The Office of the Director, National Institutes of Health (NIH) in Bethesda, Maryland, is seeking a Director of the Division of Resource Development and Analysis (DRDA) within the Office of Portfolio Analysis and Strategic Initiatives (OPASI). If you are an exceptional candidate with an M.D. and/or Ph.D., we encourage your application.

The OPASI's primary objective is to develop: a transparent process of planning and priority-setting characterized by a defined scope of review with broad input from the scientific community and the public; valid and reliable information resources and tools, including uniform disease coding and accurate, current and comprehensive information on burden of disease; an institutionalized process of regularly scheduled evaluations based on current best practices; the ability to weigh scientific opportunity against public health urgency; a method of assessing outcomes to enhance accountability; and a system for identifying areas of scientific and health improvement opportunities and supporting regular trans-NIH scientific planning and initiatives.

As the DRDA Director, you will be responsible for employing resources (databases, analytic tools, and methodologies) and developing specifications for new resources, when needed, in order to conduct assessments based on NIH-owned and other databases in support of portfolio analyses and priority setting in scientific areas of interest across NIH.

Salary is commensurate with experience and includes a full benefits package. A detailed vacancy announcement with the mandatory qualifications and application procedures can be obtained on **USAJOBS at www..usajobs.gov (OD-07-172841-T42) and the NIH Web Site at http://www. jobs.nih.gov**. Questions on the application procedures may be addressed to **Brian Harper on 301-594-5332**. Applications must be received by midnight eastern standard time on **August 10, 2007**.

NIDDK
Post-doctoral Fellowship Positions
National Institute of Diabetes and Digestive and Kidney Diseases

Post-doctoral fellowship positions are available starting September 1, 2007 in the Diabetes Branch of the National Institute of Diabetes, Digestive and Kidney Diseases (NIDDK), National Institutes of Health (NIH). Research will focus on elucidating the roles of cell cycle regulators in the pathogenesis of diabetes and obesity. Projects involve generation and characterization of genetically engineered mouse models. Candidates with a strong background in molecular biology, experience in pancreatic islet beta cell/adipocyte biology fields and familiarity with ex vivo and in vivo models of diabetes/obesity are especially encouraged to apply. Applicants should have received their Ph.D. within the past five years and be eligible for an appropriate US visa, if necessary. A current C.V, a statement describing research interests and career goals, and three letters of reference should be sent to:

Sushil G. Rane, Ph.D.
Regenerative Biology Section, Diabetes Branch
National Institute of Diabetes & Digestive and Kidney Diseases
National Institutes of Health
Building 10, Clinical Research Center, West Laboratories
5-5940 South Drive and Old Georgetown Road
Bethesda, MD 20892

E.mail: ranes@mail.nih.gov; Tel: 301-451-9834

INFLAMMATION AND CANCER
TENURE TRACK POSITION
LABORATORY OF HUMAN CARCINOGENESIS

The Laboratory of Human Carcinogenesis (LHC), Center for Cancer Research, National Cancer Institute, has a long tradition of excellence in the investigation of the molecular carcinogenesis and epidemiology of human cancer. The Laboratory now invites applications for a tenure track position to study the role of chronic inflammation in human cancer. The applicant should have previous postdoctoral experience; a substantive record of publications in quality, peer-reviewed journals; and the potential to develop an independent research program that utilizes basic research discoveries and their translation to investigate the role of chronic inflammation in the molecular pathogenesis and progression of human cancer. Previous translational studies of cancer-prone chronic inflammatory diseases in animal models and humans and/or molecular epidemiological studies are recommended.

This position is available for a Ph.D. or M.D. with a salary commensurate with education and experience. The position is available to U.S. citizens and foreign nationals. A one or two-page statement of research interests and goals should be submitted in addition to three letters of recommendation and a curriculum vitae to:

Ms. Shirley Swindell, Laboratory Program Specialist, LHC, CCR, NCI, Building 37, Room 3060C, Bethesda, MD 20892-4258, Phone: 301-496-2048, Fax: 301-496-0497, email: swindels@mail.nih.gov.

Applications must be postmarked by **October 1, 2007**.

U.S. Department of Energy
Associate Director
Office of Science for
Biological and Environmental Research
Announcement # SES-SC-HQ-014 (kd)

The U.S. Department of Energy's (DOE's) Office of Science is seeking qualified candidates to lead its Biological and Environmental Research (BER) Program. With an annual budget of more than $500 million, the BER Program is the nation's leading program devoted to applications of biology to bio-energy production and use and to environmental remediation. The BER Program supports major research programs in genomics, proteomics, systems biology, and environmental remediation. The Program is also one of the nation's leading contributors to understanding the effects of greenhouse gas emissions, aerosols, and atmospheric particulates on global climate change.

The Director of Biological and Environmental Research is responsible for all strategic program planning in the BER Program; budget formulation and execution; management of the BER office including a federal workforce of more than 30 technical and administrative staff; program integration with other Office of Science activities and with the DOE technology offices; and interagency integration. The position is within the ranks of the U.S. government's Senior Executive Service (SES); members of the SES serve in key positions just below the top Presidential appointees. For more information on the program please go to **http://www.sc.doe.gov/ober/**.

For further information about this position and the instructions on how to apply and submit an application, please go to the following website: **http://jobsearch.usajobs.opm.gov/getjob.asp?JobID=58520806&AVSDM=2007%2D06%2D06+13%3A44%3A02&Logo=0&q=SES-SC-HQ-014+(kd)&FedEmp=N&sort=rv&vw=d&brd=3876&ss=0&FedPub=Y&SUBMIT1.x=47&SUBMIT1.y=18**. To be considered for this position you must apply online. It is important that you follow the instructions as stated on the announcement **SES-SC-HQ-014 (kd)** located at the website above.

Professor and Co-Director
Redox Biology Center and Department of Biochemistry
University of Nebraska-Lincoln (UNL)

The Redox Biology Center (RBC) at UNL, funded as a Center of Biomedical Research Excellence by the National Institutes of Health, invites nominations and applications from established investigators for a **tenured Full Professor** position in the Department of Biochemistry and **Co-Director of the Center**. The RBC is a major focus group for research in redox biology, incorporating various investigators at UNL and the University of Nebraska Medical Center in Omaha. Areas such as thiol-based redox signaling and gene regulation, redox control of neurodegenerative diseases and cancer, biochemistry of redox-active trace elements, structural biology, proteomics/metabolomics, microbial pathogenesis and redox homeostasis are all current targets of investigation. The Center also operates mass-spectrometry and spectroscopy core research facilities. The successful applicant will be expected to lead an internationally recognized, federally funded research program and contribute to the development and leadership of the Center.

The position will be housed in the state-of-the-art George W. Beadle Center, and carries with it a 12-month, state-funded appointment. This senior hire is the first of several new positions that the RBC will fill in various areas of redox biology during the next four years. To learn more about the Center and the Department, please visit **http://www.unl.edu/RedoxBiologyCenter** and **http://biochem.unl.edu**.

Applicants should go to **www.employment.unl.edu** and search for position **#070421**. Complete the faculty academic/administrative information form. Applicants should submit letter of application, curriculum vitae, a succinct statement of research interests, and three letters of reference sent to: **Dr. Vadim Gladyshev, Redox Biology Center Director, University of Nebraska, N118 Beadle Center, Lincoln, NE 68588-0662, USA** (email: **redox2@unl.edu**). Review of applications will begin on **September 4, 2007** and continue until the position is filled.

The University of Nebraska is committed to a pluralistic campus community through Affirmative Action and Equal Opportunity and is responsive to the needs of dual career couples. We assure accommodation under the Americans with Disabilities Act; contact Sheila Hayes at 402-472-4742 for assistance.

Scientific Curator

Professional positions are available as Scientific Curators with the Mouse Genome Informatics Program at The Jackson Laboratory. Successful candidates will be primarily responsible for data acquisition and analysis, evaluating and annotating data to be incorporated into the database, integrating information from disparate sources, and interacting with research laboratories and genome centers to facilitate data transfer. In addition, Curators take part in database and interface design by contributing biological perspectives to new data content and displays. Currently we are recruiting for curators for the KOMP (Knockout Mouse Project), the Mouse Genome Database, and the Mouse Tumor Biology Database. Preferred areas of expertise are gene annotation and analysis based on biological data; mammalian phenotypes and genetic engineering; and cancer biology, respectively. Other desirable attributes include excellent writing/communication skills and the ability to work effectively in a team environment. Ph.D. degree in Life Sciences required, postdoctoral experience preferred.

A cover letter should be submitted with your resume. Interested individuals should apply on-line on the internet (**www.jax.org**), refer to job requisition **#SC-05**. Please submit cover letter and resume as one document.

The Jackson Laboratory is one of the world's foremost centers for mammalian genetics research. Located in Bar Harbor, Maine, the lab is adjacent to Acadia National Park. Mountains, ocean, forests, lakes, and trails are all within walking distance.

If you love high tech challenges but you're looking for a more natural environment, this could be the opportunity you've been searching for.

SOUTHWESTERN
THE UNIVERSITY OF TEXAS
SOUTHWESTERN MEDICAL CENTER
AT DALLAS
Faculty Positions in Infectious Diseases

The Division of Infectious Diseases in the Department of Internal Medicine at the University of Texas Southwestern (UTSW) Medical Center at Dallas is seeking new faculty members at the Assistant Professor, Associate Professor, or Professor levels. Faculty will be expected to develop independent and externally funded independent research programs that focus on understanding the molecular pathogenesis of infectious diseases and/or host defense mechanisms. Preference will be given to applicants performing "cutting-edge" research on medically important pathogens, emerging pathogens, and/or agents of potential biothreat. Excellent opportunities exist for collaborations with faculty members in Infectious Diseases, the Department of Microbiology, and the Department of Immunology at UTSW and with the Regional Center of Excellence (RCE) for Biodefense and Emerging Infectious Diseases. UTSW is an outstanding scientific environment with established strengths in structural biology, biochemistry, molecular biology, genetics, and numerous other areas. Candidates will be expected to contribute to the teaching and research training of Infectious Diseases fellows. The positions offer attractive start-up packages and laboratory space. Candidates should have an M.D. and/or a Ph.D. degree with at least two years of postdoctoral experience and an outstanding publication record.

To apply, submit a C.V., three letters of reference, and a description of research interests to: **Dr. Beth Levine, Chief, Division of Infectious Diseases, UT Southwestern Medical Center, 5323 Harry Hines Blvd, Dallas, TX 75390-9113.** E-mail: Cindy.Jozefiak@UTSouthwestern.edu.

UT Southwestern is an Equal Opportunity/Affirmative Action Employer.

Chair of Biomedical Engineering Department

BU College of Engineering

The College of Engineering is seeking a dynamic, innovative leader for the position of Chair of the Biomedical Engineering Department. The Chair is responsible for overall departmental leadership and administration and reports to the Dean of Engineering. The individual should be an active researcher with a strong history of external funding in addition to being recognized for distinguished contributions to biomedical engineering or a related field. The individual will be expected to attract, lead, and mentor high quality faculty.

The Biomedical Engineering Department is the only department in the nation to have received both a Whitaker Foundation Leadership Award and a Coulter Foundation Translational Research Partnership Award. The department also has an NIH Pre-doctoral training grant in Quantitative Biology and Physiology and it maintains new cutting-edge core facilities in micro and nano biofabrication, micro and nano imaging, biointerface technologies, biomedical computing, and teaching laboratories. The department attracts about $18 million per year in external funding with research strengths including systems and synthetic biology, cell and tissue engineering, drug delivery and biomaterials, neuroengineering and sensory systems, multi-scale bioimaging, cardiopulmonary engineering, and orthopedics among others. The department is currently ranked 6th in *US News and World Report*.

The BME department is poised to impact the major biological-thru-biomedical challenges of the next few decades. The next chair will have a mandate for faculty growth in areas that sustain world-class research and education in cross-cutting areas.

One of four departments within the College of Engineering, the Biomedical Engineering Department consists of 28 primary faculty members, 16 secondary faculty members, 4 research faculty members, 21 staff members, 150 graduate students and 350 undergraduates. Department faculty play key roles in many of the College and University research centers, including the BioMolecular Engineering Research Center, the Center for Advanced Biotechnology, the Center for Advanced Genomic Technology, the Center for BioDynamics, the Hearing Research Center, the Neuromuscular Research Center, the Center for Nanoscience and Nanobiotechnology, and the Photonics Center. For additional information about the department, please visit **www.bu.edu/bme**.

Persons interested in being considered for this position should submit a brief letter of interest, a vision statement for the field of Biomedical Engineering, and a current curriculum vitae. The search will be open until a suitable candidate is found. Please send applications and nominations to: **Jim Collins, Biomedical Engineering Search Committee Chair, College of Engineering, 44 Cummington Street, Boston, MA 02215** or by email (pdf or text documents) to **bmechairsearch@bu.edu**.

BOSTON UNIVERSITY

Boston University is an Affirmative Action, Equal Opportunity Employer. Women and minority candidates are encouraged to apply.

Research Professor (Division Chief)
Microbiology and Immunology
Yerkes National Primate Research Center at Emory

The Yerkes National Primate Research Center (YNPRC) at Emory University seeks a new Chief for its Division of Microbiology and Immunology. The successful candidate will have an established and internationally recognized research program in the areas of vaccine development or microbial pathogenesis and will have clear leadership skills. The Chief will be designated as a Core Scientist of the YNPRC and, as such, will be expected to have a role in the leadership of the Center as well as be expected to promote an open exchange of ideas, interdepartmental and interdisciplinary collaborations, and publication of fundamental discoveries and to espouse the highest standards of scientific integrity.

The Division of Microbiology and Immunology and the associated Emory Vaccine Center have established research programs focusing on HIV, malaria, HCV, and biodefense; all have as their foundation a strong commitment to world-class basic science in the immunology and pathogenesis of microbial infections. The Chief of the Division of Microbiology and Immunology will have an academic appointment in an appropriate Department within Emory University's School of Medicine and will also be a Member of the Emory Vaccine Center. The Emory Vaccine Center is a partner in a new State-wide Initiative launched by the Georgia Research Alliance to develop and deploy next generation vaccines and therapeutics. The selected candidate will play a major role in this Vaccine Initiative. Applications should be submitted by **September 30, 2007** and should be addressed to: **Dr. Rafi Ahmed ra@microbio.emory.edu; 1510 Clifton Road, Atlanta, GA 30322**.

Please reference job requisition **#1269BR** on the Emory employment website: **http://emory.hr.emory.edu/careers/index.html**

Emory University is an EEO/AA Employer.

From life on Mars to life sciences

For careers in science, turn to *Science*

www.ScienceCareers.org

- Search Jobs
- Career Advice
- Job Alerts
- Resume/CV Database
- Career Forum
- Graduate Programs

All of these features are FREE to job seekers.

Science Careers
From the journal *Science* ⬛AAAS

INSTITUT PASTEUR KOREA

Institut Pasteur Korea (IP-K) is a translational research institute, linking cell based disease models to therapy development. Using a chemical genomics approach, IP-K's technological platform relies on computer-aided visualization in conjunction with high throughput live cell imaging. The institute integrates all steps from basic cell biological research on disease models, to screening and pharmacology, medicinal chemistry as well as automated visual target ID and systems biology. It focuses on both chronic and infectious diseases. Institut Pasteur-Korea is an international institute, currently of 130 employees (30% foreign); the institute is to quickly grow and move into a newly constructed campus by the beginning of 2009. For more information, visit our website at **www.ip-korea.org**.

Head of Scientific Affairs & International Relations

Institut Pasteur Korea is inviting applications for the position of 'Head of Scientific Affairs and International Relations'. The main focus of this position is to plan, integrate, and focus the scientific efforts within the institute and to foster collaboration with a network of international partners in Asia, Europe and the US. A Ph.D. in life sciences and editorial experience are ideal qualifications for this position, and good communications skills are essential. Based in Seoul in the cultural heart of dynamic Korea, the position comes with a highly attractive salary and benefits package.

Applications including a CV and brief letter of intent should be submitted electronically to: **recruit@ip-korea.org**.

Group Leader of Hepatitis C Virus Biology

Institut Pasteur Korea also seeks an accomplished scientist to lead a research group in HCV biology and infection. During our current expansion we seek an outstanding researcher with a strong interest in the molecular basis of host virus interaction during HCV replication. The applicant's research program should make use of our high content visual platform technology, allowing for large scale chemical screening. Research groups within IP-K pursue a basic science research agenda in coordination with drug discovery efforts.

Candidates should have post-doctoral experience and a proven track record in research. Group leaders receive initial appointments of up to five years. Salaries will be commensurate with experience and achievements. The allocated research budget (including equipment) and size of the supported staff will be in accordance with the activity.

Letters of intent describing your proposed research program (in English, 3 pages max.), a detailed CV, a description of past activities, as well as contact information of three references should be submitted electronically to: **recruit@ip-korea.org**.

Science AAAS
EDITOR-IN-CHIEF

The American Association for the Advancement of Science (AAAS), publisher of *Science*, is initiating a search for **Editor-in-Chief**. The journal is published weekly with worldwide circulation to members of the AAAS and institutional subscribers, including libraries. *Science* serves as a forum for the presentation and discussion of important issues relating to the advancement of science, with particular emphasis on the interactions among science, technology, government, and society. It includes reviews and reports of research having interdisciplinary impact.

In selecting an editor-in-chief, the Board of Directors will attach special weight to evidence of significant achievement in scientific research, editorial experience and creativity, awareness of leading trends in the scientific disciplines, and managerial abilities.

Applications or nominations should be accompanied by complete curriculum vitae, including refereed publications, and should be sent to: **Gretchen Seiler, Executive Secretary, Search Committee, 1200 New York Avenue, NW, Washington, DC 20005**. Salary is negotiable based on qualifications and experience. Application materials should be sent by **August 15, 2007**.

The AAAS is an Equal Opportunity Employer.

Department of Health and Human Services
National Institutes of Health
National Institute on Aging
Intramural Research Program

TENURE TRACK - TRANSLATIONAL INVESTIGATOR

The Laboratory of Clinical Investigation (LCI) of the National Institute on Aging (NIA) is recruiting a translational scientist for a tenure-track position within its Intramural Research Program (IRP). This position is 100% research, includes an attractive set-up package and operating budget, and provides the unique and extensive resources of the NIH.

The successful individual must possess an M.D., M.D./Ph.D., or a Ph.D. degree with training and experience in translational research with a specific interest in stem cell biology, preferably in hematopoietic or cancer systems. The ideal candidate will have an established record of scientific accomplishment within the fields of clinical immunology/oncology and a strong publication record. The ultimate goal of the research should be innovative clinical trials for the treatment of human diseases.

Salary is commensurate with research experience and accomplishments, and a full Civil service package of benefits (including retirement, health, life and long term care insurance, Thrift Savings Plan participation, etc.) is available. Additional information regarding the NIA/IRP and the LCI are available at the following websites:

http://www.grc.nia.nih.gov
http://www.grc.nia.nih.gov/branches/INs./index.html

To apply: Please send a cover letter, curriculum vitae, bibliography, and statement of research interest to: Peggy Grothe, Intramural Program Specialist; Office of the Scientific Director (Box 09); Vacancy # **NIA-IRP-07-05**; National Institute on Aging, 5600 Nathan Shock Drive, Baltimore, MD 21224-6825. Applications must be received by **September 4, 2007**. If additional information is needed, please call 410-558-8012 or email **grothep@grc.nia.nih.gov**

DHHS and NIH are Equal Opportunity Employers

TENURE-TRACK POSITION
Department of Chemical Engineering and Materials Science
University of California, Davis

Applications are invited for a faculty position at the **ASSISTANT PROFESSOR** level in thermodynamics of materials with an experimental emphasis focusing on problems related to energy, nanomaterials, and complex materials. Commitment to cross-disciplinary undergraduate and graduate education is essential. A Ph.D. in materials science, chemical engineering, chemistry, or related discipline is required. (The successful applicant will have access to the **Peter A. Rock** Thermochemistry Laboratory which is a center of excellence in calorimetric measurements as well as to other characterization equipment in the departmental central facilities, the Nanomaterials in the Environment, Agriculture, and Technology Organized Research Unit **website: http://neat.ucda-vis.edu/** and elsewhere on campus.) Consult **website: http://www.chms.ucdavis.edu/employnent/** for our on-line application procedure and requirements.

The position is open until filled; but to assure full consideration, applications should be submitted no later than October 30, 2007, for a start date of July 1, 2008. *UC Davis is an Affirmative Action/Equal Opportunity Employer, and is dedicated to recruiting a diverse faculty community. We welcome all qualified applicants to apply, including women, minorities, individuals with disabilities, and veterans.*

THE UNIVERSITY of TEXAS SOUTHWESTERN MEDICAL CENTER at DALLAS

The Department of Internal Medicine, Division of Nephrology, seeks faculty at the **ASSISTANT/ASSOCIATE PROFESSOR** level who will develop independent research programs in kidney biology and disease. Individuals with expertise in human genetics or glomerular biology and who are eligible for Endowed Scholars or Disease-Oriented Clinical Scholars Programs are particularly encouraged to apply. Preference will be given to physician-scientists, but basic scientists will also be considered. Successful candidates will participate in our newly funded O'Brien Kidney Research Core Center. Applicant must have an M.D. or Ph.D. degree. Clinical duties, if applicable, include patient care activities in nephrology. Other responsibilities will include the teaching and training of medical students, graduate students, house staff, and fellows.

Visit our **website: http://www.utsouthwestern.edu/nephrology.** Send curriculum vitae, description of research, and three reference letters to: **Peter Igarashi, M.D., Chief of Nephrology, University of Texas Southwestern, 5323 Harry Hines Boulevard, Dallas, TX 75390-8856. E-mail: peter.igarashi@utsouthwestern.edu.** *UT Southwestern is an Equal Opportunity/Affirmative Action Employer.*

Two **POSTDOCTORAL POSITIONS** available immediately at the Vanderbilt-Ingram Cancer Center to investigate p120-catenin function in cell-cell adhesion and cancer. Seeking highly motivated and interactive individuals with keen interest in one of two areas. One involves p120 mechanism of action with respect to cadherin stability and Rho guanosine triphosphate activity; an interest in signaling and expertise in molecular and cellular biology is desirable. The other involves p120 ablation in vivo using a p120 conditional knockout mouse model; expertise in signal transduction and mouse modeling with interest in colon cancer is desirable. Candidates should have recent Ph.D., or be near completion of Ph.D., and have strong academic backgrounds in relevant technologies. Salaries are competitive. *Permanent U.S. residency is required.*

Please send by e-mail a brief cover letter with curriculum vitae and three references to **Dr. Al Reynolds, e-mail: al.reynolds@vanderbilt.edu.** For links to Reynolds Laboratory website and postdoctoral affairs at Vanderbilt, go to **website: http://bret.mc.vanderbilt.edu/bret/.** *Vanderbilt University is an Equal Opportunity Employer.*

THE UNIVERSITY of TEXAS SOUTHWESTERN MEDICAL CENTER at DALLAS

The Department of Internal Medicine/Division of Nephrology seeks an **ASSISTANT/ASSOCIATE PROFESSOR** for our expanding dialysis, transplantation, and clinical/translational research programs. Applicant must have an M.D. degree or equivalent from an approved Liaison Committee on Medical Education medical school and satisfactory completion of an internal medical residency and a nephrology fellowship from an Accreditation Council for Graduate Medical Education-accredited program. Level of appointment will be commensurate with experience. Candidate must be eligible for Texas medical licensure and be Board-certified/eligible in internal medicine. We are recruiting both **CLINICIANS and CLINICAL SCHOLARS.** Duties of Clinician will include patient care with emphasis on dialysis and transplantation; Clinical Scholars will be expected to develop independent research programs and participate in our newly funded O'Brien Kidney Research Core Center. Duties will also include the teaching and training of medical students, graduate students, house staff, and fellows. Individuals who are eligible for our Disease-Oriented Clinical Scholars (DOCS) Program are particularly encouraged to apply. Visit our **website: http://www.utsouthwestern.edu/nephrology.** Send curriculum vitae, description of research interests, and three reference letters to: **Robert Toto, M.D., Director of Clinical Nephrology, University of Texas Southwestern, 5323 Harry Hines Boulevard, Dallas, TX 75390-8856. E-mail: robert.toto@utsouthwestern.edu.** *UT Southwestern is an Equal Opportunity/Affirmative Action Employer.*

RESEARCH COLLABORATORY for STRUCTURAL BIOINFORMATICS SCIENTIFIC LEAD
University of California, San Diego (UCSD)
Location: La Jolla, California 92093

The Research Collaboratory for Structural Bioinformatics (RCSB) Protein Data Bank (PDB) site at the University of California San Diego (UCSD) is seeking an experienced **BIOLOGIST** for the position of Scientific Lead for the PDB Web development group. The incumbent will work with the PDB Director, Co-Director and scientific staff at both Rutgers and UCSD in defining the scientific objectives for the RCSB website, provide functional requirements, and participate in the design and development of data analysis tools. The Scientific Lead will have deep domain knowledge in structural biology, computational biology, or related discipline. The Scientific Lead will be skilled at working with scientists from diverse disciplines as well as IT development staff. The over arching goal for this individual will be to provide the PDB user community with relevant and creative tools with which to access and analyze the wealth of the PDB content to enhance their own research efforts. Qualified individuals will have the opportunity to pursue an academic research track.

Applicants should send a letter describing their interest in the position, complete curriculum vitae, and names of three references to **Professor Philip E. Bourne** at e-mail: **pbourne@ucsd.edu.**

Equal Opportunity/Affirmative Action Employer.

ABOUT MICROCHIP BIOTECHNOLOGIES

Microchip Biotechnologies Incorporated (MBI) is a privately-held startup company located in Dublin, California that is developing advanced nanofluidic sample preparation and analysis systems for the genomics, life sciences, and molecular diagnostics markets. These solutions are based on MBI's proprietary NanoBioProcessor platform and associated Microscale-on-Chip Valves (MOV) technology.

We are seeking highly qualified applicants who will thrive in a fast-moving startup environment for the following open positions: **SENIOR MICROFABRICATION ENGINEER, STAFF SYSTEM SCIENTIST, SENIOR SYSTEMS ENGINEER, MICROFABRICATION PROCESS ENGINEER.**

For more information on other open positions and on the company, please visit **website: http://www.microchipbiotech.com.**

FACULTY POSITION
Molecular Virology
Department of Microbiology and Immunology
University of Western Ontario

The Department of Microbiology and Immunology is seeking a position in the area of molecular virology. This position is for a probationary (tenure-track) faculty member at the level of **ASSISTANT PROFESSOR**. Outstanding candidates will also be considered at a higher rank.

The successful candidate will hold Ph.D., M.D., or equivalent degrees and is expected to establish an independent, externally funded research program and collaborations with others at the University, the J.P. Robarts Research Institute, and the Lawson Health Research Institute. Priority will be given to candidates with research interests and expertise in viral pathogenesis including virus-mediated immune modulation and vaccines and those who use a functional genomics approach, which will complement existing areas of research strength within the Department and initiatives on Functional and Genomics and Systems Biology at the Schulich School of Medicine and Dentistry. The successful candidate will be expected to participate in the teaching programs of the Department at the undergraduate and graduate levels.

Please send detailed curriculum vitae, a brief description of research accomplishments and future plans, copies of representative publications, and the names of three references to:

Miguel A. Valvano, Chair
Department of Microbiology and Immunology
Room 3014, Dental Sciences Building
The University of Western Ontario
London, Ontario, Canada
N6A 5C1

Applications will be accepted until the position is filled. Review of applications will begin after November 30, 2007.

These positions are subject to budget approval. *Applicants should have fluent written and oral communication skills in English. All qualified candidates are encouraged to apply; however, Canadian citizens and permanent residents will be given priority. The University of Western Ontario is committed to employment equity and welcomes applications from all qualified women and men, including visible minorities, aboriginal people, and persons with disabilities.*

ASSOCIATE DIRECTOR
Massachusetts Institute of Technology
Pharmaceutical Manufacturing Program

The Associate Director will work directly with the program director, an MIT professor, to run the daily operations of a multiyear program on pharmaceutical manufacturing based at MIT. This challenging program presently involves seven-plus MIT professors and will be ramped up to include thirty-plus graduate students and postdoctoral associates.

The objective of the program is to perform research directed at creating a new vision in pharmaceutical manufacturing. The Associate Director should be able to demonstrate technical creativity and innovational and out-of-the-box thinking. Will also need to possess proven technical and project management skills.

The position will involve coordinating and managing student and postdoctoral research projects in addition to facilitating communication between industrial sponsors and MIT staff and students. Position also involves working closely with suppliers, vendors, and external collaborators.

Requirements: a Ph.D. in chemical engineering, chemistry, or similar field and ten to fifteen-plus years of experience in pharmaceutical process development or manufacturing.

Interested candidates may apply online at **website: http://web.mit.edu.** Please reference job number mit-00004357 and include the names and contact information for three references.

MIT has a strong and continued commitment to diversity in engineering education, research, and practice and especially encourages applications from women and minorities. MIT is an Affirmative Action/Equal Opportunity Employer.

UNIVERSITY OF SOUTH CAROLINA

RESEARCH ASSISTANT PROFESSOR

Applications are invited for a Research Assistant Professor in cell signaling/immunology. Requires a Ph.D. in biomedical sciences with minimum three years of experience. Apply with curriculum vitae and three references to: **Dr. Mitzi Nagarkatti, Chair, Department of Pathology, Microbiology and Immunology, University of South Carolina School of Medicine, Columbia, SC 29208** or e-mail: mnagark@gw.med.sc.edu. *USC Columbia is an Equal Opportunity Affirmative Action Employer and encourages applications from women and minorities.*

ASSOCIATE DEAN for RESEARCH and GRADUATE PROGRAMS
Auburn University
Harrison School of Pharmacy

The Auburn University Harrison School of Pharmacy seeks applications and nominations for the newly created position of Associate Dean for Research and Graduate Programs, a tenure-track position.

Applicants must possess a terminal degree in pharmaceutical sciences or a related field, excellent communication and interpersonal skills, and demonstrated experience in leadership and management to ensure success in addressing the School's vision and mission. The ideal candidate should have academic credentials sufficient to meet tenure eligibility requirements, an outstanding scientific background in the area of drug-related sciences, an established and ongoing record of obtaining extramural funds, and editorial board or study section experience. Candidates should have proven abilities to foster an interdisciplinary approach to research to assist the School in achieving the next level of biomedical research. Salary will be competitive and commensurate with education and experience. *Candidates selected for this position must be able to meet eligibility requirements for work in the United States at the time the appointment begins and be able to communicate effectively in English.*

Nominations are invited. To assure full consideration, applications must include curriculum vitae, a letter of interest providing a summary of qualifications for the position, along with three letters of reference. Review of applications will begin August 1, 2007, and continue until the position is filled. Applications and nominations should be submitted to: **Harrison School of Pharmacy, Search Committee, Associate Dean for Research and Graduate Programs, 2316 Walker Building, Auburn, AL 36849-5501.** Applicants may contact **Ms. Brinda Lisano, Assistant to the Dean**, for further information at **telephone: 334-844-8348** or via **e-mail: lisanbp@auburn.edu.**

A full advertisement, including an overview of responsibilities, can be viewed at **website: http://pharmacy.auburn.edu/professionals/positions.htm.**

Women and minorities are encouraged to apply. Auburn University is an Equal Opportunity/Affirmative Action Employer.

QUANTITATIVE/THEORETICAL ECOLOGIST

The Department of Ecology and Evolution is seeking to fill a faculty position with an individual working at the interface of theory and data in ecology. Rank is open, with a preference for **ASSISTANT or ASSOCIATE PROFESSOR.** Interested applicants should submit curriculum vitae, selected reprints and preprints, statements of research and teaching interests, and the names and addresses of three references to **website: https://ecologysearch.uchicago.edu;** letters of reference can be submitted at this site as well. Applications will be accepted until the position is filled, but applications should be received before 15 September 2007, to ensure full consideration. *The University of Chicago is an Affirmative Action/Equal Opportunity Employer.*

FACULTY POSITION
Eukaryotic or Viral Pathogenesis
Department of Microbiology and Immunology
Dartmouth Medical School

The Department of Microbiology and Immunology at Dartmouth Medical School (DMS) invites applications from outstanding scientists studying the molecular basis of pathogenesis of eukaryotic pathogens or viruses, with a strong emphasis on interactions with the host. Candidates working on medically relevant fungi, protozoans, or viruses are particularly encouraged to apply. The intent is to recruit a tenure-track faculty member at the **ASSISTANT PROFESSOR** level (entry or experienced) who will expand our existing strengths in microbial pathogenesis and microbe-host interactions. The successful applicant will hold the M.D. and/or Ph.D. degree and have strong research and teaching credentials. Candidates will be expected to develop and/or expand upon a robust, independent yet collaborative, extramurally funded research program. Teaching expectations include participation in courses in medical microbiology/immunology/virology and graduate courses in the Molecular and Cellular Biology (MCB) Ph.D. Program. Opportunities also exist to participate in related undergraduate courses.

This position affords the opportunity to utilize the state-of-the-art facilities and resources associated with a major research and teaching institution and cancer center, while enjoying the high quality of life characteristic of the area of New England surrounding the Dartmouth community. For further information on the various programs at DMS see the listings at **websites: http://dms.dartmouth.edu/microbio/** and **http://www.dartmouth.edu/~molpath/.**

Applications should consist of curriculum vitae, a brief statement of research interests and plans, and three letters of reference. Direct the e-mail or hardcopy applications to: **George O'Toole, Ph.D. c/o Karen Thompson, e-mail: karen.l.thompson@dartmouth.edu, Administrative Assistant, Department of Microbiology and Immunology, Dartmouth Medical School, Vail Building HB7550, Hanover, NH 03755.** Review of applications will start September 15, 2007, and continue until the position is filled. *Dartmouth Medical School is an Affirmative Action/Equal Opportunity Employer and encourages applications from women and members of minority groups.*

HUMAN ANATOMY LECTURER, University of Kansas. Biological Sciences seeks applicants for term contract Lecturer position to teach four university-level courses/semester with primary emphasis on directing Human Anatomy Laboratories. Teaching of human anatomy dissection laboratories includes training/evaluating teaching assistants. Required: Ph.D. in biology or related discipline; demonstrated training in human anatomy dissection at the level of medical school anatomy with strong cadaver dissection component; demonstrated record of effective teaching. For a complete position description, refer to **website: https://www.kuub.ku.edu.** Contact: **Jan Elder, Biological Sciences, 1200 Sunnyside Avenue, University of Kansas, Lawrence, KS 66045-7534; e-mail: jelder@ku.edu; telephone: 785-864-5883.** Initial review of applications begins August 31, 2007, and will continue until position is filled.
Equal Opportunity/Affirmative Action Employer.

CAREER OPPORTUNITY

This unique program offers the candidate with an earned Doctorate in the life sciences the opportunity to obtain the Doctor of Optometry (O.D.) degree in 27 months (beginning in March of each year). Employment opportunities exist in research, education, industry, and private practice. Contact the **Admissions Office, telephone: 800-824-5526** at the **New England College of Optometry, 424 Beacon Street, Boston, MA 02115.** Additional information at **website: http://www.neco.edu,** e-mail: admissions@neco.edu.

Nagaoka University of Technology

長岡技術科学大学

Cultivation Center for Young Investigators through University-Industry Joint Research Program

Six Specialized Associate Professors and/or Lecturers

Applications are invited for 6 tenure-track positions at the ranks of Associate Professor and Lecturer in the areas specified below for a 5-year term, ending in March 2012.
Appointees will be provided with independent laboratories, startup budgets and research funds (altogether JPY 23,000,000 in the first year), as well as support staffs (post-doctoral fellows and RA's). Annual salary is over JPY 8,000,000 (US$ 64,000) and is fixed during the period of employment. Their promotion to tenured positions (employment guaranteed by the age of 65) with a minimum guaranteed annual salary will be determined through two reviews at the ends of their 2nd and 4th years after appointment.

The research areas of interest are as follows; 1) Information and Control Frontier, Creative Design and Production Engineering, Thermal and Fluid Engineering Frontier, and Creative Materials Engineering in the field of Mechanical Engineering, 2)Electronic Devices and Optical Electronics (Photonics-/Nano-Devices, etc.), Intelligent Control, Generation Actuator and Pulse Power, Information and Communication System Engineering, Intelligent and Knowledge-Based Information Engineering, and Integration and Creation Information Engineering in the field of Electrical Electronics and Information Engineering, 3) Materials Science, Ceramic Materials, Polymer Materials, Nano-scale Materials, Synthetic Organic Chemistry, Supramolecular Chemistry, and Materials Simulation in the field of Materials Science and Technology, 4) Environmental Chemistry, Environmental Materials Engineering, Environmental Energy Engineering, Environmental Information Engineering, and Environmental Preservation and Maintenance Engineering in the field of Environmental and Civil Engineering, 5) Life Science, System Biology, and Biotechnology in the field of Bioengineering, 6) Kansei Engineering (Affective Technology) and Intelligent Systems, and Environmental Symbiotic System Science on Society, Economy and Technology in the field of Management and Information Systems Science, and 7) Safety Technology, Safety Device, Safety Design, Risk Evaluation, Failure Analysis and Life Evaluation in the field of System Safety.

Applicants with their interest should visit at the website on http://www.nagaokaut.ac.jp/e/index.html for detailed information and way of application. For inquiry, please contact Prof. Keizo Uematsu, a secretariat for the Committee of Selection of Young Investigators, e-mail: toprun@vos.nagaokaut.ac.jp

---

TEXAS A&M HEALTH SCIENCE CENTER COLLEGE OF MEDICINE

Tenure-Track Faculty Positions
Neuroscience and Experimental Therapeutics

The Department of Neuroscience and Experimental Therapeutics (NExT) invites applications for multiple tenure-track faculty positions at the level of **ASSISTANT/ASSOCIATE PROFESSOR**. We are interested in outstanding scientists in the neurosciences or translational sciences with a strong record of research achievement and a commitment to graduate and medical education. Research in the NExT Department involves molecular, cellular and behavioral approaches to study brain function and disease processes including CNS development and aging, neuroendocrine and inflammatory processes, neural stem cells, mechanisms of drug abuse and ocular therapeutics (see **http://medicine.tamhsc.edu/basic-sciences/next/index.html**).

The College of Medicine also has strong research programs in infectious disease, virology, cardiovascular physiology and structural biochemistry. Faculty participate in the Interdisciplinary Faculty of Neuroscience and have collaborative ties in Biology/Psychology/Veterinary Medicine at Texas A&M University, the Texas Brain and Spine Institute as well as Psychiatry and Behavioral Science. Women and minorities are strongly encouraged to apply.

Review of applications will begin immediately and continue until the positions are filled. Applicants should submit a current curriculum vitae, a statement of research goals and names/addresses of four references by e-mail to: **Dr. Gerald D. Frye, Dept of Neuroscience and Experimental Therapeutics, Texas A&M Health Science Center, College of Medicine MS1114, 228 Reynolds Medical Building, College Station, TX 77843-1114 (gdfrye@medicine.tamhsc.edu)**.

The TAMHSC is an Affirmative Action/Equal Opportunity Employer. Women and minorities are strongly encouraged to apply.

Research and Tenure-Track Faculty Positions
NANOTECHNOLOGY CENTER
Bascom Palmer Eye Institute
Evelyn F. and William L. McKnight Vision Research Center
University of Miami Leonard M. Miller School of Medicine

Bascom Palmer Eye Institute is in the midst of renewing and expanding its research enterprise with the goal of capturing advanced technology for ophthalmic innovation. Through aggressive faculty recruitment over the past five years, we have established interactive, interdisciplinary programs in neuroscience, medical imaging, biomedical engineering, and clinical research. With additional wet lab space becoming available in early 2008, we now launch this new initiative in nanotechnology.

Ophthalmology is ripe for application of nanotechnology. The National Eye Institute is actively promoting nanotechnology funding initiatives, providing opportunity for program growth even in a time of NIH budgetary flat-lining.

Faculty recruitment for the nanotechnology initiative will encompass all ranks and include scientists and clinician-scientists. Generous start-up packages and competitive salaries will be offered for the right individuals. Endowed chairs are available for senior candidates, as well as the opportunity to recruit faculty colleagues. A current focus in ophthalmology is not required, only the flexibility to move in new directions, the willingness to be drawn into shared leadership projects, and an interest in clinical application.

Ranked as the #1 eye hospital in the nation by *US News and World Report*, Bascom Palmer Eye Institute provides an ideal environment for advancing medical innovation. A successful capital campaign and new senior leadership are transforming the University of Miami's research environment, making many new resources available.

To apply for these positions, please submit a CV with a cover letter describing qualifications and expectations to: **M. Elizabeth Fini, Ph.D, Professor and Scientific Director, efini@med.miami.edu**. For more information about us, please see our website at **www.bascompalmer.org**.

FACULTY POSITIONS, Virology.

The Department of Microbiology at University of Texas (U.T.) Southwestern Medical Center at Dallas is seeking new faculty in molecular virology at the **ASSISTANT PROFESSOR** (tenure track) level.

This will be a rolling search that continues until all positions are filled. Faculty will be expected to develop front-rank, competitive, independent research programs that focus on one or more aspects of the viral life cycle (host-pathogen interactions, viral pathogenesis, disruption of viral replication, command of host cell processes, viral immunology, et cetera) that will complement existing strengths in hepatitis C, poliovirus, West Nile virus, HIV/SIV, Kaposi's sarcoma-associated herpesvirus, and viral oncogenesis. Research on any virus of medical relevance or that may be a potential biothreat is of interest. The candidate also is expected to contribute to the teaching of medical and graduate students. Attractive startup packages, including a competitive salary and new laboratory space, are available to conduct research in an expanding, dynamic environment. For exceptional candidates, an Endowed Scholars Program offers startup funds of $700,000 (plus $300,000 towards salary support) over a four-year period. Candidates should have a Ph.D. and/or M.D. degree with at least three years of postdoctoral experience and an exceptional publication record. Candidates please forward curriculum vitae, three letters of recommendation, two or three representative publications, and a brief summary of future research to: **Dr. Michael V. Norgard, Chair, Department of Microbiology, University of Texas Southwestern Medical Center, 6000 Harry Hines Boulevard, Dallas, TX 75390-9048 (e-mail: michael.norgard@ utsouthwestern.edu).** *U.T. Southwestern is an Equal Opportunity/Affirmative Action Employer.*

FACULTY POSITION
Behavioral Neuroscience

The Department of Psychology at the University of Memphis invites applications for a tenure-track faculty position at the **ASSISTANT PROFESSOR** level. Candidates must possess a Ph.D. and postdoctoral experience. While the specific area of specialization within behavioral neuroscience is open, preference will be given to candidates who have a strong record of research publications, currently have or are likely to obtain external funding, and have had experience in successful collaborative research. The person who fills the position will also be expected to teach both undergraduate and graduate students and to periodically teach a course in research methods or statistics. Our Department currently includes 32 full-time faculty and offers Ph.D. degrees in experimental, clinical, and school psychology. Evaluation of candidates will begin on November 15, 2007, and may continue until position is filled. Send curriculum vitae, three letters of recommendation, and reprints/preprints to: **Guy Mittleman, Chair, Faculty Search Committee, Department of Psychology, The University of Memphis, Memphis, TN 38152.** *The University of Memphis is an Equal Opportunity Affirmative Action Employer and encourages applications from women, ethnic minorities, and persons with disabilities.*

FACULTY POSITIONS
EVOLUTIONARY BIOLOGIST
PHYSIOLOGIST-PROTEOMICS BIOLOGIST

Two tenure-track positions in the Department of Biological Sciences at California State University, Long Beach, starting fall 2008; **ASSISTANT PROFESSOR** preferred, **ASSOCIATE PROFESSOR** considered. See **websites: http://www.csulb.edu/ depts/biology** or **http://www.csulb.edu/ divisions/aa/personnel/jobs/cnsm** for application details and additional information. Application review begins on September 10, 2007. *CSULB is an Equal Opportunity Employer committed to excellence through diversity, and takes pride in its multicultural environment.*

COMMUNITY, ECOSYSTEM ECOLOGY

The Department of Ecology and Evolutionary Biology at the University of Toronto invites applications for a tenure-track position in community and/ or ecosystem ecology. The position is at the **ASSISTANT PROFESSOR** level with an expected start date of 1 July 2008. Details are at **website: http://link.library.utoronto.ca/academicjobs/ display_job_detail_public.cfm?job_id=2350.**

We are particularly interested in applications from individuals who use experimental and field approaches in research that addresses fundamental questions in ecology. The successful applicant will have a Ph.D., postdoctoral or equivalent experience, an outstanding academic record, and is expected to build an active, externally funded and internationally-recognized research program. The appointee will have the potential for excellence in teaching and contribute to the education and training of undergraduate and graduate students.

Applications will be accepted until 15 October 2007. Applicants should electronically submit curriculum vitae, statement of teaching philosophy and interests, and an outline of their proposed research to e-mail: **jhaugan@eeb.utoronto.ca.**

Applicants should arrange to have three confidential letters of recommendation sent on their behalf to: **Professor Robert Baker, Chair, Ecology and Evolutionary Biology, University of Toronto, 25 Willcocks Street, Toronto, Ontario, Canada.** *All qualified candidates are encouraged to apply; however, Canadian citizens and permanent residents will be given priority. The University of Toronto is strongly committed to diversity within its community and especially welcomes applications from visible minority group members, women, Aboriginal persons, persons with disabilities, members of sexual minority groups, and others who may contribute to the further diversification of ideas.*

ASSISTANT PROFESSOR
Insect Genomics/Proteomics/Bioinformatics
University of Kentucky

The Department of Entomology at the University of Kentucky invites applications for a tenure-track faculty position in insect genomics/proteomics/ bioinformatics. This is primarily a research position, with some teaching and advising responsibilities. Individual will develop a strong independent research program that will interact with and synergize existing departmental strengths. Applicants must have a Ph.D. in entomology, the biological sciences with a specialization in molecular biology, or in a closely related field. Postdoctoral experience in genomics/ proteomics/bioinformatics is highly desired. The full position description, qualifications, and application requirements are at **website: http://www. uky.edu/ Ag/Entomology.** Application deadline is September 1, 2007, or until a suitable applicant is identified.

Submit applications to: **Dr. Reddy Palli, Chair, Search Committee, University of Kentucky, Department of Entomology, S-225 Agricultural Science North, Lexington, KY 40546-0091 U.S.A. E-mail: rpalli@uky.edu. Website: http://www. uky.edu.**

The University of Kentucky is an Equal Opportunity Employer and encourages applications from minorities and females.

RESEARCH ASSISTANT.

Full-time, any level (B.S., M.S., Ph.D. in biochemistry-molecular biology or field related), available immediately, two-year minimum, NIH-funded, to study pre-tRNA 3' end maturation by tRNase Z. Research experience required. Curriculum vitae and contact information for academic/professional references to: **Dr. Louis Levinger, York College/City University of New York** in Jamaica, New York by e-mail:**louie@york. cuny.edu.** For more about research projects, see Zareen et al., *RNA* 12:1104, 2006; Yan et al., *J. Biol. Chem.* 281:3926, 2006. *Equal Opportunity Employer/Affirmative Action.*

LABORATORY MANAGER (Job Number 38464)
Laser Ablation-Inductively Coupled Plasma Mass Spectrometry Arizona LaserChron Center

The University of Arizona seeks a highly motivated scientist to serve as Manager of the Arizona LaserChron Center, which is a multi-user facility that focuses on U-Th-Pb geochronology by laser ablation-multicollector inductively coupled plasma mass spectrometry (ICPMS). Responsibilities would include: (1) directing installation of a new multi-collector ICPMS and Excimer laser, (2) developing new analytical techniques and applications using an existing multicollector ICPMS (GVI Isoprobe) and Excimer laser (DUV193), (3) performing minor maintenance and overseeing major repairs of these instruments, (4) supervising visits of research scientists, and (5) conducting independent research. The position is full-time and permanent. Applicants should have a M.S. or Ph.D. in earth science or chemistry, and have demonstrated experience with ICPMS instrumentation. Applications will be reviewed beginning 15 August 2007, and will continue until the position is filled. Applications should be submitted at **website: https://www.uacareertrack.com** for job number 38464. For additional information, please visit the Arizona LaserChron Center **website: http:// www.geo.arizona.edu/alc** and contact **George Gehrels (e-mail: ggehrels@e-mail.arizona.edu)** or **Joaquin Ruiz (e-mail: jruiz@e-mail.arizona.edu).** *The University of Arizona is an Equal Opportunity, Affirmative Action Organization.*

MULTIPLE POSITIONS
U.S. Army Research Laboratory

Multiple positions are available in the Sensors and Electron Devices Directorate (Optics Branch) of the U.S. Army Research Laboratory, Adelphi, Maryland. All positions involve the research and development of sensing technologies for a broad range of applications including chemical and biological hazard detection. A Master's or entry-level Ph.D./Postdoctoral Fellow in engineering, physical science, or life science disciplines is required. However, demonstrated skills in interdisciplinary problem solving and the ability to function as part of a multidisciplinary team are highly desired. Qualified candidates will also have experience in one or more of the following areas: Versatile knowledge of optical design and instrumentation development; biosensors, bioassays, and molecular recognition; explosives detection including point and/ or standoff sensing technologies; separations and microfluidics; in-depth expertise in optical/laser spectroscopy; bio/nanotechnology including characterization system engineering.

Interested candidates should submit curriculum vitae along with at least two to three references to e-mail: **arl-est@arl.army.mil.** Salary is commensurate with experience and qualifications. The positions will remain open until filled. *Although these are not civil service positions, U.S. citizenship is required.*

EDITORIAL ASSOCIATE
The National Academies, Washington, D.C.

The National Academies in Washington, D.C., is seeking an Editorial Associate to facilitate recruiting of original research submissions for the multidisciplinary research journal, the *Proceedings of the National Academy of Sciences* (PNAS) and related activities. A science-related Bachelor's degree, or equivalent knowledge with three years of related professional experience is required. A Ph.D. in a biological or physical science and publishing experience is highly desired. Superior communication skills and attention to detail are essential as well as a demonstrated ability to prioritize, multitask, and meet critical deadlines.

For additional information on this position and to apply online, please visit **website: http:// www. nationalacademies.org.** Under employment, view current opportunities by department, *Proceedings of the National Academy of Sciences*, requisition number 070143-6. *Equal Opportunity Employer, Minorities/ Females/Persons with Disabilities/Veterans.*

POSITIONS OPEN

The Department of Biological Sciences at Southeastern Louisiana University invites applicants for a tenure-track **ASSISTANT or ASSOCIATE PROFESSOR** position in molecular microbial ecology. Candidates should use modern methods of molecular biology and genetics to answer basic questions regarding the factors that influence the diversity and function of microorganisms in ecological systems.

The candidate will be an active participant in our Institute of Biodiversity and Interdisciplinary Studies. Candidates should have a Ph.D. in microbiology or a related field, postdoctoral experience, and a commitment to teaching and research. Applicants will be expected to establish an externally funded research program and will teach courses in microbial ecology, introductory microbiology, and other undergraduate/graduate courses in the biology curriculum. Applicants must be committed to working with diversity. To ensure review, application materials must be received by September 30, 2006.

Qualified applicants should send a letter of application, curriculum vitae, copies of both undergraduate and graduate transcripts (official transcript will be required of finalist), statement of teaching and research interest, and the names and contact information for three references to: **Dr. David M. Severs, Department Head, Department of Biological Sciences, Southeastern Louisiana University, SLU Box 10736, Hammond, LA 70402.** Information about the Department of Biological Sciences can be found at **website: http://www.selu.edu/Academics/Depts/Biology/.** *Southeastern is an Affirmative Action/ADA/Equal Employment Opportunity Employer.*

The Department of Medicine/Section of Cardiology is seeking qualified applicants for a full-time **RESEARCH ASSOCIATE (ASSISTANT/ASSOCIATE/PROFESSOR)** position to study the cardiovascular structure and function in small animals (using a 9.4T magnet) and humans. The position will be integrated into the small animal magnetic resonance program and will work on both animal models of pulmonary hypertension and on human right ventricular function in a shared imaging core for animals. The primary activity of the Research Associate (Assistant/Assocociate/Professor) is academic research in association with a faculty member or team. Qualified applicants are required to possess a Doctorate degree in engineering, biomedical engineering, or related fields. Applicants should possess excellent knowledge of cardiac imaging in humans and small animals. Three to five years of postdoctoral training is required. A demonstrated track record of publication and the potential to apply for peer reviewed funding is preferred. Compensation and level of appointment are dependent on qualifications. The University provides a generous package of fringe benefits. Interested applicants should submit cover letter, curriculum vitae, and three letters of reference via e-mail to: **Dr. Stephen Archer, e-mail: sarcher@medicine.bsd.uchicago.edu.** *The University of Chicago is an Affirmative Action/Equal Opportunity Employer.*

POSTDOCTORAL FELLOW
University of Cincinnati
Department of Molecular Genetics, Biochemistry, and Microbiology

We have an opening for a Postdoctoral Fellow in the area of gene regulation centered on both vascular and cardiac tissues. Much of the work will involve genes that maintain vascular integrity. The applicant should be experienced in gene regulation analysis and/or vascular or cardiac physiology. Resumes should be sent to: **Jerry B. Lingrel, Ph.D., Department of Molecular Genetics, University of Cincinnati, P.O. Box 670524, Cincinnati, OH 45267-0524** or to e-mail: **jerry.lingrel@uc.edu.** *The University of Cincinnati is an Affirmative Action/Equal Opportunity Employer.*

POSITIONS OPEN

ACADEMIC SUPPORT in BIOLOGY
Fall and Spring Semester 2007-2008

The St. Lawrence University (SLU) Biology Department seeks a full-time Academic Support person to work in their general biology course, Biology 101 (fall) and 102 (spring), during the 2007-2008 academic year. The Academic Support person will join a team of faculty and staff in implementing a dynamic, inquiry-based sequence of courses for both major and nonmajor students. Primary duties will include teaching two laboratory sections each week, attending all lectures, participating in a weekly team meeting, participating in a weekly teaching assistant training session, and assisting with course grading. Further, this particular support person will be in charge of working with the team to develop and manage a new, peer-based study component for the courses. Additional duties may include ordering supplies, making and disposing of reagents, maintenance of laboratory instrumentation, testing laboratory exercises, supervising and training student workers, and publishing the course laboratory manual.

Requiring approximately **40** hours per week, this position requires excellent organizational skills, computer skills, research and data analysis skills, and attention to detail. The candidate also needs excellent interpersonal skills to work with undergraduates, a departmental technician, and a team of instructors. A Master's degree (or equivalent course work) in biology or a related subdiscipline is preferred.

Interested candidates should submit a letter of application, current curriculum vitae, and have three letters of reference sent to: **Dr. Michael Temkin, Biology Department, St. Lawrence University, Romoda Drive, Canton, NY 13617.** Review of applications will begin immediately.

For more information please visit the Biology Department webpage at **website: http://it.stlawu.edu/~biology** and SLU's homepage at **website: http://www.stlawu.edu.** *St. Lawrence University is an Affirmative Action/Equal Employment Opportunity Employer. Women, minorities, veterans, and persons with disabilities are encouraged to apply.*

POSTDOCTORAL POSITION in cancer genetic epidemiology and genomics. Starting fall/winter 2007, a Postdoctoral position is available to perform whole genome association studies. The focus of this translational laboratory is on inherited susceptibility to cancers of the breast, ovary, colon, and prostate and lymphoma. Access to high-throughput genotyping platforms and a large number of research samples from a genetic isolate (Ashkenazi) is available. Methodology includes candidate gene association studies (see *Science* **297**:2013, 2002. *Cancer Res.* **66**:5104-10, 2006 and **64**:8891-900, 2004) and linage disequilibrium mapping (see *Genetic Epidemiology* **30**:48-61, 2006). Applicants will generally have a strong background in molecular genetics and statistical genetics. Send curriculum vitae and three letters of reference to: **Kenneth Offit, M.D., M.P.H., Clinical Genetics Service, P.O. Box 192, Memorial Sloan-Kettering Cancer Center, 1275 York Avenue, New York, NY 10021. Fax: 212-434-5166. E-mail: offitk@mskcc.org.** *Memorial Sloan-Kettering Cancer Center is an Equal Opportunity Employer with a strong commitment to enhancing the diversity of its faculty and staff. Women and applicants from diverse racial, ethnic and cultural backgrounds are encouraged to apply.*

POSTDOCTORAL POSITION

A Postdoctoral position is available to study cell/molecular and biology of complications of diabetes mellitus and kidney development. Potential candidates must have documented experience in this area of research and in cell and molecular biology techniques. Please send curriculum vitae with references to: **Yashpal S. Kanwar, M.D., Ph.D., Northwestern University Medical School, 303 E. Chicago Avenue, Chicago, IL 60611 U.S.A. E-mail: y-kanwar@northwestern.edu.**

POSITIONS OPEN

POSTDOCTORAL FELLOW
Membrane Transporters
University of Nebraska-Lincoln
Lincoln, Nebraska, U.S.A.

Postdoctoral Fellow positions funded by the NIH are available immediately at the Redox Biology Center and the Department of Biochemistry at the University of Nebraska-Lincoln. A Ph.D. in the field of biochemistry, cell biology, molecular biology, or a relevant discipline is required. The goal of the research project is to elucidate the function, mechanisms of action, and regulation of metal-ion transporters using yeast, mammalian cells, and genetically-modified mice. A multidisciplinary approach combining biochemistry, cell biology, genetics, and biophysics will be employed. For more information please see **website: http://www.unl.edu/RedoxBiologyCenter/; D. Sinani et al.,** *Proc. Natl. Acad. Sci.* **98**:6535, 2001; *J. Biol. Chem.* **282**:947, 2007 and **279**:17428, 2004, and in press. To apply, e-mail a cover letter, curriculum vitae, statement of research experience and career goals, and contact information of three references to **Dr. Jaekwon Lee, e-mail: jlee7@unlnotes.unl.edu.** *The University of Nebraska-Lincoln is an Equal Opportunity, Affirmative Action Employer.*

POSTDOCTORAL POSITION available immediately on a NIH-funded grant in the Department of Molecular Microbiology and Immunology at the Johns Hopkins University School of Public Health. Our laboratory is interested in the genomic/molecular mechanisms which control tissue-specific cytokine gene expression patterns. The successful candidate will be highly motivated, have Ph.D., and/or M.D., and a have strong background in molecular biology and immunology. Applicants with demonstrated experience in the latest techniques to analyze chromatin structure and gene regulation will be given preference. Experience with animal models is highly desirable. Please e-mail curriculum vitae and names and contact information of three references to **e-mail: jbream@jhsph.edu.** *Johns Hopkins University is an Equal Opportunity/Affirmative Action Employer.*

MARKETPLACE

LESS EFFORT.

MORE EASY EXTRACTION.

Eliminate steps. Enhance your cloning efficiency. All with the new E-Gel® CloneWell™ Gels, E-Gel® iBase,™ and E-Gel® Safe Imager™ Real-Time Transilluminator. Isolating DNA bands for cloning just got easier. Now you can retrieve DNA bands separated by agarose gel electrophoresis directly from the gel without slicing or additional purification steps. The extracted DNA is compatible with common cloning methods. It couldn't be safer or easier. See how at **www.invitrogen.com/clonewell**.

invitrogen™